

**Aeroservoelastic and Flight Dynamics Analysis
using Computational Fluid Dynamics**

**NASA Dryden University Consortium Cooperative Agreement
No. NAG4-154**

**Final research summary
For the Period: 31 APRIL 1998 - 31 APRIL 1999**

***NASA Technical Monitor:*
Dr. Kajal K. Gupta
NASA Dryden Flight Research Center
Edwards, CA**

***Principle Investigator:*
Dr. Andrew S. Arena, Jr.
School of Mechanical and Aerospace Engineering
Oklahoma State University
Stillwater, OK**

SUMMARY

This document in large part is based on the Masters Thesis of Cole Stephens. The document encompasses a variety of technical and practical issues involved when using the STARS codes for Aeroservoelastic analysis of vehicles. The document covers in great detail a number of technical issues and step-by-step details involved in the simulation of a system where aerodynamics, structures and controls are tightly coupled. Comparisons are made to a benchmark experimental program conducted at NASA Langley.

One of the significant advantages of the methodology detailed is that as a result of the technique used to accelerate the CFD-based simulation, a systems model is produced which is very useful for developing the control law strategy, and subsequent high-speed simulations.

In summary, the document details the following areas:

- Literature review of previous methods used for analysis
- A discussion and comparison of methods used for modeling surface deformations
- Details of the surface transpiration concept
- Summary of the appropriate STARS modules used
- Implementation of the benchmark test case including detailed discussion and sensitivity studies in the following areas:
 - Mode Shape calculation and definition
 - CFD geometry specification
 - Boundary condition specifications
 - Effects of dissipation parameters on the unsteady CFD solution
 - Steady-State solution convergence criteria
 - Uncertainty estimation
 - Time-step issues
 - Modal and system identification issues
 - Control law development
- Results including:
 - Steady State
 - Steady state with control surface deflections
 - Comparisons between actual deflection, simulated deflection using transpiration, and experimental results.
 - Aeroelastic results and comparisons with experiment
 - Aeroservoelastic results illustrating control law development and flutter suppression.

TABLE OF CONTENTS

Chapter	Page
1. INTRODUCTION	1
1.1 Background	1
1.2 Problem Definition.....	3
1.3 Research Objective	4
2. LITERATURE REVIEW	5
2.1 Structural Dynamics.....	5
2.2 Unsteady Aerodynamics Solver.....	6
2.2.1 Transonic Small Disturbance & Full Potential Equations	6
2.2.2 Euler and Navier-Stokes Equations	7
2.3 Modeling Surface Deformations.....	8
2.3.1 Body-Fitted Coordinate Systems	8
2.3.2 Dynamic Meshes.....	10
2.3.3 Re-Meshing.....	13
2.3.4 Surface Transpiration.....	14
2.4 Transpiration Concept.....	17
2.4.1 Origins of Transpiration.....	18
2.4.2 Application to Current Research.....	19
2.5 Benchmark Models Program	27
3. METHODOLOGY AND PROCEDURE	31
3.1 STARS Modules	31
3.1.1 SOLIDS Module	32
3.1.2 CFD Module	32
3.1.3 Aeroelastic and Aeroservoelastic Solver	34
3.2 Implementation of the BACT Model into STARS	35
3.2.1 BACT SOLIDS Model Development.....	36
3.2.1.1 Structural Mode Shape Definition	38
3.2.2 BACT CFD Model Development.....	43
3.2.2.1 BACT Geometry Specification in STARS	44
3.2.2.2 BACT Grid Specification in STARS	49
3.2.2.3 BACT Boundary Condition Specification in STARS	52
3.2.2.4 Effect of the Dissipation Parameters in STARS	53
3.2.2.5 Steady-State Solution Convergence Criteria	54

3.2.3	BACT Uncertainty Estimation.....	55
3.2.4	BACT Aeroelastic/Aeroservoelastic Development	61
3.2.4.1	Time-Step Definition in STARS.....	65
3.2.4.2	Modal Identification Technique.....	70
3.2.4.3	System Identification Technique	72
3.2.4.4	Control Law Development.....	75
4.	RESULTS	79
4.1	Steady Results Without Control Surface Deflections.....	79
4.2	Steady Results With Control Surface Deflections	84
4.2.1	Steady Solutions for Transpired and Actual Control Surface Deflections	85
4.2.2	Steady Solutions for Transpired Control Surface Deflections Compared With Experimental Data.....	90
4.3	Aeroelastic Results.....	96
4.3.1	Unsteady Data for the BACT and NACA 0012 Wings Tested at Langley	96
4.3.2	System Identification Parameters and Effectiveness	97
4.3.3	Flutter Prediction Using STARS	108
4.4	Aeroservoelastic Results.....	111
4.4.1	Control Law Development.....	112
4.4.2	Control Implementation into STARS	113
4.4.3	Flutter Suppression for the BACT Wing Using STARS	115
5.	CONCLUSIONS AND RECOMMENDATIONS	124
5.1	Conclusions.....	124
5.2	Recommendations.....	126
	BIBLIOGRAPHY.....	128
	APPENDICES	131
	APPENDIX A.....	131
A-1	STARS-SOLIDS Data File (<i>NOPAPA.DAT</i>)	131
A-2	STARS-SOLIDS Generalized Mode 1 Displacement Definition (Plunge)	137
A-3	STARS-SOLIDS Generalized Mode 2 Displacement Definition (Pitch).....	143
A-4	STARS-SOLIDS Generalized Mode 3 Displacement Definition (Control Mode).....	149
A-5	Program to Write Nodal Displacement Data into STARS- SOLIDS Format.....	155
	APPENDIX B	157
B-1	STARS-CFD Geometry Data File (<i>BACT.DAT</i>)	157
B-2	STARS-CFD Background Mesh Data File (<i>BACT.BAC</i>).....	186

B-3	STARS-CFD Boundary Condition File (<i>BACT.BCO</i>)	188
B-4	STARS-CFD Parameter Control File (<i>BACT.CONU</i>).....	189
B-5	STARS-Unsteady Scalars File (<i>BACT.SCALARS</i>)	190
B-6	Portion of STARS-Unsteady Arrays File (<i>BACT.ARRAYS</i>)	191

LIST OF TABLES

Table	Page
Table 3-1: Spreadsheet Layout for Manual Input of a Structural Mode.....	39
Table 3-2: Actual and Suggested Number of Mesh Nodes for STARS Volume.....	51
Table 3-3: Experimental Measurements in Structural Parameters	57
Table 3-4: Experimental Measurements in Structural Parameters	57
Table 3-5: BACT Model Parameters in STARS.....	65
Table 4-1: Nominal and Actual Parameters for Mach 0.77, $\alpha=0^\circ$, $\delta=2^\circ$	90
Table 4-2: Nominal and Actual Parameters for Mach 0.77, $\alpha=0^\circ$, $\delta=5^\circ$	90
Table 4-3: Nominal and Actual Parameters for Mach 0.77, $\alpha=0^\circ$, $\delta=10^\circ$	91
Table 4-4: Nominal and Actual Parameters for Mach 0.82, $\alpha=0^\circ$, $\delta=2^\circ$	93
Table 4-5: Nominal and Actual Parameters for Mach 0.82, $\alpha=0^\circ$, $\delta=5^\circ$	93
Table 4-6: Nominal and Actual Parameters for Mach 0.82, $\alpha=0^\circ$, $\delta=10^\circ$	93
Table 4-7: Model Orders and Associated RMS Errors at Various Mach Numbers.....	98
Table 4-8: Sensitivity to x_{cg} for the NACA 0012 & BACT Wings in STARS.....	109
Table 4-9: Percent Change in $q_{flutter}$ for a 0.9% Shift in x_{cg} (8.028" \Rightarrow 8.10")	109

LIST OF FIGURES

Figure	Page
Figure 2-1: Physical Coordinate System.....	9
Figure 2-2: Computational Coordinate System	9
Figure 2-3: Reference Grid for Deforming Mesh Algorithm	11
Figure 2-4: Maximum Pitch Angle ($\alpha=15^\circ$) Using a Deforming Mesh Algorithm	12
Figure 2-5: Minimum Pitch Angle ($\alpha=-15^\circ$) Using a Deforming Mesh Algorithm.....	12
Figure 2-6: Slight Surface Element Rotation.....	15
Figure 2-7: Illustration of the Transpiration Concept	16
Figure 2-8: 2×1 Plate CFD Mesh.....	19
Figure 2-9: Actual 2×1 Plate Deformation	19
Figure 2-10: Steady Pressure Contours on the Deformed 2×1 Plate at Mach 0.95	20
Figure 2-11: AGARD 445.6 Wing, Undelected and Deflected CFD Meshes.....	21
Figure 2-12: Steady Pressure Contours for the AGARD Wing at Mach 0.678.....	22
Figure 2-13: Variable Wing-Flap Intersection Example	23
Figure 2-14: Desired Flap Deflection	25
Figure 2-15: Mesh-Shearing Example	26
Figure 2-16: Equivalent Mesh for Transpiration	26
Figure 2-17: BACT Wing Model Dimensions.....	28
Figure 2-18: BACT Model on Flexible PAPA Mount	29
Figure 3-1: Stages of Advancing Front Technique.....	33
Figure 3-2: Block Diagram of Time-Marching Approach.....	35

Figure 3-3: Finite Element Solids Mesh for BACT Wing.....	37
Figure 3-4: Rigid Body Pitch Mode Definition Example.....	40
Figure 3-5: Structural Deformation Opposite Original Definition.....	41
Figure 3-6: Implemented Rotational Mode Shape for STARS.....	42
Figure 3-7: CFD Computational Volume Specification.....	45
Figure 3-8: Wing Geometry Specification.....	46
Figure 3-9: Close-Up of Deflected Flap Geometry Definition.....	47
Figure 3-10: Views Showing Tetrahedral Surface Mesh on the BACT Wing.....	50
Figure 3-11: Effect of Dissipation Constants on C_p in STARS CFD Solution.....	53
Figure 3-12: Solution Convergence Using Residuals and Maximum Mach Number.....	55
Figure 3-13: Effect of K_h , K_α and x_{cg} Location on Flutter Prediction.....	59
Figure 3-14: Effect of Time-Step at Two Different Values of $ncycl$ on the Lift Evolution for an Impulsively Started NACA 0012 Airfoil at Mach 0.3, $\alpha=5^\circ$	68
Figure 3-15: Effect of $ncycl$ with at Two Different Time-Steps on the Lift Evolution for an Impulsively Started NACA 0012 Airfoil at Mach 0.3, $\alpha=5^\circ$	69
Figure 3-16: Abbreviated Time-History of BACT Wing in STARS.....	71
Figure 3-17: Complete 5000-Step Time-History of BACT Wing in STARS.....	71
Figure 3-18: Multi-Step Sequence for the BACT Wing (3-Modes).....	73
Figure 3-19: Modeled and Actual Response to Multi-Step Input.....	74
Figure 3-20: MATLAB/SIMULINK® Model of BACT with Control.....	75
Figure 4-1: Steady Chordwise Pressure at Mach 0.51, $\alpha=0^\circ$, $\delta=0^\circ$, 60% Span.....	81
Figure 4-2: Steady Chordwise Pressure at Mach 0.67, $\alpha=0^\circ$, $\delta=0^\circ$, 60% Span.....	81
Figure 4-3: Steady Chordwise Pressure at Mach 0.71, $\alpha=0^\circ$, $\delta=0^\circ$, 60% Span.....	82
Figure 4-4: Steady Chordwise Pressure at Mach 0.77, $\alpha=0^\circ$, $\delta=0^\circ$, 60% Span.....	82
Figure 4-5: Steady Chordwise Pressure at Mach 0.80, $\alpha=0^\circ$, $\delta=0^\circ$, 60% Span.....	83
Figure 4-6: Steady Chordwise Pressure at Mach 0.82, $\alpha=0^\circ$, $\delta=0^\circ$, 60% Span.....	83

Figure 4-7: Comparison of Actual and Simulated 10° Control Surface Deflections.....	85
Figure 4-8: Surface Pressure Contours at Mach 0.77, 10° Control Surface Deflection ...	86
Figure 4-9: Comparison of Predicted Pressure Distributions for an Actual and Simulated 10° Control Surface Deflection at Mach 0.77, 0° α	86
Figure 4-10: Pressure Contours at Mach 0.82, 10° Control Surface Deflection.....	87
Figure 4-11: Comparison of Predicted Pressure Distributions for an Actual and Simulated 10° Control Surface Deflection at Mach 0.82, 0° α	88
Figure 4-12: Cross-Flow Velocity Vectors at the Trailing Edge of the BACT Wing With an Actual and Simulated 10° Control Surface Deflection.....	89
Figure 4-13: Comparison of Predicted and Experimental Chordwise Pressure Distributions at Mach 0.77, $\alpha=0^\circ$, $\delta=2^\circ$	91
Figure 4-14: Comparison of Predicted and Experimental Chordwise Pressure Distributions at Mach 0.77, $\alpha=0^\circ$, $\delta=5^\circ$	92
Figure 4-15: Comparison of Predicted and Experimental Chordwise Pressure Distributions at Mach 0.77, $\alpha=0^\circ$, $\delta=10^\circ$	92
Figure 4-16: Comparison of Predicted and Experimental Chordwise Pressure Distributions at Mach 0.82, $\alpha=0^\circ$, $\delta=2^\circ$	94
Figure 4-17: Comparison of Predicted and Experimental Chordwise Pressure Distributions at Mach 0.82, $\alpha=0^\circ$, $\delta=5^\circ$	95
Figure 4-18: Comparison of Predicted and Experimental Chordwise Pressure Distributions at Mach 0.82, $\alpha=0^\circ$, $\delta=10^\circ$	95
Figure 4-19: Flutter Boundary Comparison Between 2 Geometrically Similar Wings: NACA 0012 Wing (Air) & BACT Wing (R-12).....	96
Figure 4-20: Training Data at Mach 0.51, $q=141.8$ psf	100
Figure 4-21: Training Data at Mach 0.67, $q=146.5$ psf	101
Figure 4-22: Training Data at Mach 0.71, $q=146.9$ psf	102
Figure 4-23: Training Data at Mach 0.77, $q=144.2$ psf	103
Figure 4-24: Training Data at Mach 0.80, $q=147.2$ psf	104
Figure 4-25: Training Data at Mach 0.82, $q=159.9$ psf	105

Figure 4-26: Model Validation for STARS CFD/ASE: Model at Mach 0.82 for Plunge Displacement (in).....	106
Figure 4-27: Model Validation for STARS CFD/ASE: Model at Mach 0.82 for Pitch Displacement (deg).....	106
Figure 4-28: Model Validation for STARS CFD/ASE: Model at Mach 0.82 for Plunge Velocity (in/sec).....	107
Figure 4-29: Model Validation for STARS CFD/ASE: Model at Mach 0.82 for Pitch Velocity (deg/sec).....	107
Figure 4-30: Flutter Boundary Prediction for Different x_{cg} Locations	108
Figure 4-31: STARS Flutter Prediction Compared with Experimental Results from the NACA 0012 Wing and the BACT Wing.....	110
Figure 4-32: MATLAB [®] Flutter Suppression Example	112
Figure 4-33: Block Diagram of Control Implemented into STARS.....	113
Figure 4-34: Modified Multi-Step Sequence Used for ASE.....	116
Figure 4-35: Multi-Step Response for Model and Euler Solutions	117
Figure 4-36: Aeroservoelastic Response at Mach 0.51	119
Figure 4-37: Aeroservoelastic Response at Mach 0.77	120
Figure 4-38: MATLAB [®] Model Comparison Using a Similar Control Law at Mach 0.77	120
Figure 4-39: Aeroservoelastic Response at Mach 0.82	121
Figure 4-40: Euler Validation of the Modeled Aeroservoelastic Response at Mach 0.77	122

NOMENCLATURE

CFD	Computational Fluid Dynamics
ASE	Aeroservoelasticity
CG	Center of Gravity
EA	Elastic Axis
α	Angle of Attack ($^{\circ}$)
δ	Flap Deflection Angle ($^{\circ}$)
M	Mach Number
a	Speed of Sound (in/s)
q	Dynamic Pressure (psi, psf)
q_f	Dynamic Pressure at Flutter (psi, psf)
ρ	Air Density (slinch/in ³)
γ	Ratio of Specific Heats (1.4 Air, 1.148 R-12)
v	Fluid Velocity (in/s)
ω	Structural Natural Frequency (rad/s, Hz)
ϕ	Structural Mode Shape
ω_h	Plunge Frequency (rad/s, Hz)
ω_{α}	Pitch Frequency (rad/s, Hz)
ω_{δ}	Control Surface Frequency (rad/s, Hz)
K_h	Plunge Stiffness (in lb)

K_{α}	Pitch Stiffness (in·lb/rad)
m	Mass (slinch)
I_{α}	Pitch Mass Moment of Inertia (slinch·in ²)
I_{δ}	Control Surface Mass Moment of Inertia (slinch·in ²)
x_{cg}	Location of CG Relative to EA, Positive Aft (in)
$S_{h,\alpha}$	Plunge-Pitch Coupling (slinch·in)
$S_{h,\delta}$	Plunge-Control Surface Coupling (slinch·in)
$S_{\alpha,\delta}$	Pitch-Control Surface Coupling (slinch·in ²)

CHAPTER 1

INTRODUCTION

1.1 Background

An efficient method of predicting the aeroservoelastic characteristics of modern high-speed aircraft is crucial to aircraft design and flight testing. It is therefore essential that the flight envelope be well defined prior to flight test operations. Without accurate insight into an aircraft's aeroelastic tendencies, flight testing becomes a serious threat both for the aircraft and its pilot.

Aeroelastic solutions are characterized by two main disciplines: structural dynamics and computational fluid dynamics. Aeroservoelastic solutions include the additional complexities introduced by forced control surface deflections during the simulation. The structural dynamics portion of the code predicts a structure's natural response, or mode shapes. Any arbitrary deflection can therefore be described as a superposition of a number of these natural mode shapes [Dowell, 1995]. Given an arbitrary applied load, an aerodynamic load for example, the structural dynamics and resulting deformations can be determined. The CFD solver uses the resulting displacements and velocities that arise from the elastic structure and deflecting control surfaces, and calculates new aerodynamic loads.

In the case of an aerodynamic body, these deflections have a great impact on the flow field surrounding the body. Changes in this flow impact the lift, drag, and moment experienced. This variation in loading is accompanied by a corresponding change in structural deflections, which cause aerodynamic changes, which cause structural deformations, and the cycle is repeated until one of two possibilities occur. One possibility is that the changing aerodynamic loads and structural vibrations will peacefully coexist and not result in a structural instability. The other possibility is that the loads and deflections will coalesce and produce an unstable fluid-structure interaction, also known as aerodynamic flutter. It is this flutter phenomenon that poses the greatest threat to aircraft traveling at speeds ranging from high subsonic to hypersonic. Allowed to progress, flutter has the definite possibility of causing structural failure, and has the distinct probability of seriously injuring its pilot.

As described above, in the absence of forced control inputs, the classical aeroelastic system simply reacts to the unsteady aerodynamics. In general, however, aeroservoelastic systems have control surfaces such as ailerons and flaps that complicate an aeroelastic analysis. Deflecting an aileron, for example, not only produces the differential lift required to roll an aircraft, but also alters the twist of the wing itself. This twist causes an effective increase or decrease, depending on how the aileron is deflected, in the effective angle of attack seen by the entire wing. As a result, the effectiveness of a deflected control surface decreases with increasing Mach number until the resulting change in angle of attack exactly counteracts the increase or decrease in lift produced by the aileron such that the aircraft does not roll. This aeroservoelastic phenomenon is known as control surface reversal. In the case of flutter, control surfaces can serve as a

the case of flutter, control surfaces can serve as a means by which to actively control aeroelastic response, falling under the category of active flutter suppression.

Application of these solution techniques in an operational environment means that the time it takes to complete a complete aeroelastic or aeroservoelastic simulation be kept to a minimum without sacrificing solution accuracy. The structural solver requires far less time, by several orders of magnitude, than does the CFD solution. Emphasis should be given, therefore, to those means which improve the speed and efficiency of the CFD solution.

1.2 Problem Definition

For current research, the STARS computer programs developed at NASA Dryden Flight Research Center have been the primary means of a full ASE prediction [Gupta, 1997]. STARS is an highly integrated, finite-element based code for multidisciplinary analysis of flight vehicles including static and structural dynamics, computational fluid dynamics, heat transfer, and aeroservoelasticity capability.

Mentioned earlier, it is the CFD portion of the total simulation that requires the vast majority of the solution time. Within each time step, structural deflections are determined due to the predicted aerodynamic loads. Compared to the solution time required by the CFD module, determination of the structural dynamics is essentially instantaneous. This means that at each intermittent time step, it is the structural dynamics solver that ends up *waiting* for the aerodynamic loads from the CFD portion of the code. This computational time is substantially increased if the solution must be paused at each time step to deform the mesh based on a structural change due to modified aerodynamic loads. Further difficulty is encountered if the mesh must be deformed in such a way as to

account for discontinuous motions such as leading and trailing edge control surface deflections. Accounting for these control surface deflections in a CFD grid presents particular difficulty due to the very close proximity of the control surface and adjacent wing surfaces. In most cases, control surface deflections result in the exposure of surfaces not previously seen by the CFD solver. These overlapping surfaces prove to be a significant hindrance to flow computation.

1.3 Research Objective

In practical transonic and supersonic aeroservoelastic applications, thin, lightweight wings and control surfaces lend themselves to the susceptibility of flutter. Along with continuing improvements in computational speed, there are more sophisticated solution algorithms that take advantage of the additional speed and memory capabilities. These advances in solution techniques continue to push the limits of even the most powerful computers. In order to more fully appreciate advances in the state-of-the-art, ASE simulations must incorporate means which reduce the amount of computational effort required to produce an accurate prediction. With the computational overhead involved with time-dependent deforming meshes, it is necessary to cultivate an efficient means by which continuous surface deformations as well as control surface deflections are accounted for in the ASE simulation as a means of actively controlling the response of a system.

CHAPTER 2

LITERATURE REVIEW

Regardless of the solution methodology used, a full ASE simulation requires a means of coping with the structural dynamics and the determination of the natural mode shapes, the unsteady aerodynamics, control inputs, and a means of incorporating these structural and control surface deformations onto the CFD grid. Certainly, there will be other differences within each simulation method, but at a minimum, the above items will be common to virtually all ASE solutions.

2.1 Structural Dynamics

For the types of problems that are commonly encountered, the structural dynamics portion of the solution is already much faster than the aerodynamics. The determination of the structural mode shapes are generally determined one of two ways. First, the mode shapes, pitch and plunge for example, could be known prior to the ASE simulation and specified throughout the solution. A more general ASE simulation uses some sort of structural dynamics solver, finite elements etc, to determine the structural characteristics of the system. This type of solver computes arbitrary structural displacements based on the aerodynamic loads. However, no matter how one chooses to solve for the structural dynamics of the system, a significant amount of forethought must be given as to how these structural deformations are related to a corresponding CFD grid. This point is

discussed in more detail later. STARS incorporates the finite element method to solve for the structural response of the system.

2.2 Unsteady Aerodynamics Solver

The next issue is still the subject of a great many research papers. The question of exactly how to model the unsteady aerodynamics is very often subject to computational availability, time, and personal preference. Possibilities include, but are not limited to, transonic small disturbance (TSD), and full potential equations (FPE), and more recently Euler and Navier-Stokes equations. Historically, TSD and the full potential method were most commonly used due to their compatibility with the computers of the time. With advances in computer speed and memory, higher equation models such as the Euler and Navier-Stokes have become more tractable.

2.2.1 Transonic Small Disturbance & Full Potential Equations

For three dimensional configurations, the transonic small disturbance equations have been a popular choice for aeroelastic analysis and flutter prediction. The transonic speed range is of primary interest because the flutter dynamic pressure is typically lower there [Cunningham, Batina, & Bennett, 1988]. For the computational capability of the day, the TSD and FPE equations were a popular choice because of their relatively low computational cost and ease of implementation. Migration to more sophisticated models is due mainly to the fact that these equations are not adequate in the presence of strong shocks [Ruo & Sankar, 1987].

2.2.2 Euler and Navier-Stokes Equations

Advances in computational speed and memory have allowed the practical implementation of Euler and Navier-Stokes solution algorithms to complex two and three dimensional problems. These equations allow for the analysis of a wider variety of problems at broader Mach number range than can be done with TSD or FPE equations. The Navier-Stokes equations, with an adequate choice of turbulence model, are limited only by the assumption that the fluid is a continuum. Take the viscous terms out of the Navier-Stokes equations, and the Euler equations are obtained. For sufficiently high Reynolds numbers, the inviscid flow assumption makes good physical sense, as is shown by the following equation:

$$\text{Re}_L = \frac{\rho UL}{\mu} = \frac{\rho U^2}{\mu U/L} \quad (2-1)$$

The above equation expresses the Reynolds number as a ratio of the inertial forces to viscous forces. It is apparent, therefore, that as the Reynolds number increases, inertial forces become more dominant than the viscous terms. The dominance of the inertial terms in high-speed flows, such as those encountered during flutter, show that the inviscid flow assumption made in the Euler equations are a valid means of aerodynamic prediction. As one would expect, the Euler solutions are more limited in solutions where there are significant boundary layer effects, boundary-layer/shock-interactions, and regions of separated flow.

Substantial work has demonstrated the effectiveness of the Euler solution for problems of practical interest. Free from the burden of determining a turbulence model and constructing a mesh capable of resolving the boundary layer, an Euler solution is an

extremely attractive alternative to a code using the Navier-Stokes equations. Introduced in section 1.2, STARS makes use of the Euler equations on an unstructured mesh for its CFD prediction.

2.3 Modeling Surface Deformations

As with the choice of flow solvers, there are several popular methods of applying a resulting surface deflection to a CFD grid. Many mesh deformation techniques use a body-fitted mesh which generally requires that the mesh move rigidly or shear as the body deforms. These assumptions consequently limit the ASE analysis to rigid-body or small amplitude motions [Batina, 1989]. Again, not an exhaustive collection of methods, but a presentation of a few practical grid deformation techniques follows in the next few sections.

2.3.1 Body-Fitted Coordinate Systems

One popular method of accounting for structural deformations in the CFD mesh is the use of a body-fitted coordinate system. With this coordinate system, the wing surface becomes a coordinate surface. This method involves a coordinate map from this physical space to computational space [Malone, Sankar, & Sotomayer, 1984]. The relationship between the physical and computational coordinate system can be visualized by *unwrapping* the physical grid about a line, or axis, which lies within the wing surface. Then, in the computational grid, the wing surface, as well as any assumed wake shape, becomes a coordinate surface [Malone & Sankar, 1985]. Figure 2-1 shows the body fitted coordinate system in the physical coordinate system. Note that key points are

labeled with letters. Figure 2-2 shows the transformed physical coordinate system in the computational coordinate system.

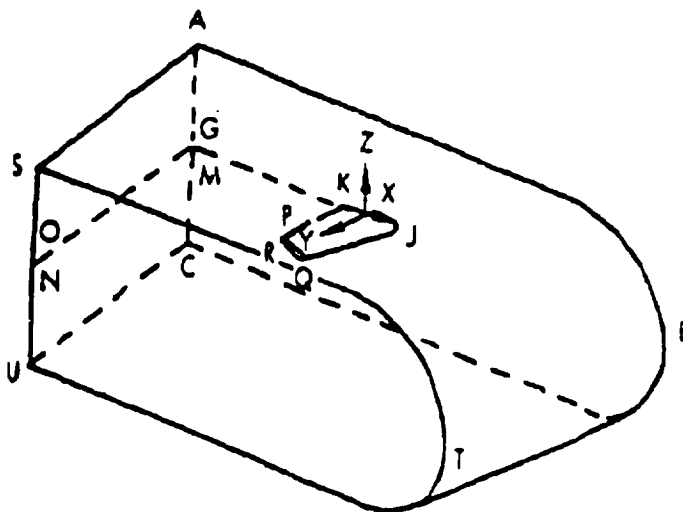


Figure 2-1: Physical Coordinate System

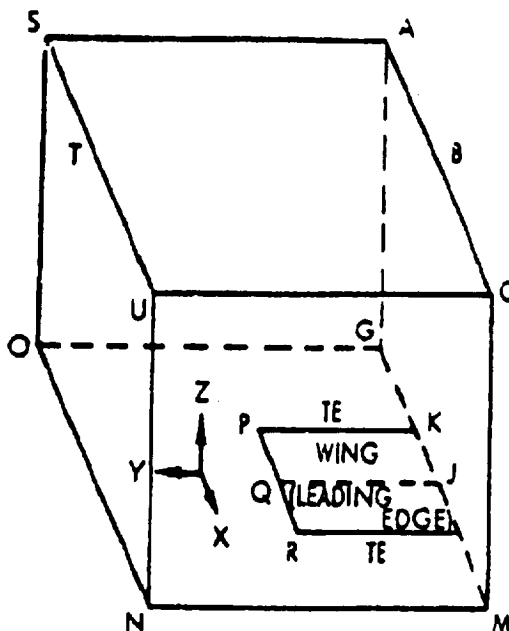


Figure 2-2: Computational Coordinate System

The above figures were obtained from a paper on the unsteady modeling of a fighter wing in transonic flow [Malone, Sankar, & Sotomayer, 1984].

Resulting surface deformations must be related from physical to computational space through a series of matrix transformations. These matrix transformations must be calculated and implemented at each time step in an ASE solution. Although implementation presents relatively few problems, the computational expense of these transformations can be significant on complicated three-dimensional geometries. Additionally, this author has not seen this method implemented on a case involving a discontinuous surface deflection such as those due to flaps or ailerons. As was discussed earlier, the use of these meshes often require the assumption of small-amplitude, rigid-body deformations.

2.3.2 Dynamic Meshes

Possibly the most intuitive of methods is the concept of a moving mesh. It simply makes sense that one could deform the mesh in accordance to that predicted by a structural dynamics solver. Work done by Batina has demonstrated the effectiveness of such a method using an unstructured finite-difference mesh with an Euler solver [Batina, 1989].

Though the concept is simple, implementation comes at a price. What this type of mesh boils down to is a large network of nodes connected by a series of springs whose stiffness is inversely proportional to the length of its edge. At each time step, specified boundary nodes are displaced by an amount corresponding to that of the aeroelastic response of the body. The displacement of the rest of the computational domain is therefore solved iteratively using static equilibrium equations in the x and y directions.

This results in x and y displacements for each of the interior nodes inside the computational domain. This iterative procedure is accomplished by a predictor-corrector method that first predicts the displacements due to linear extrapolation and corrects these displacements with several Jacobi iterations of the static equilibrium equations.

Given in Figure 2-3, Figure 2-4, and Figure 2-5 are the original reference grid, the deformed grid at maximum α and the deformed grid at minimum α , respectively, for a wing oscillating about its quarter chord.

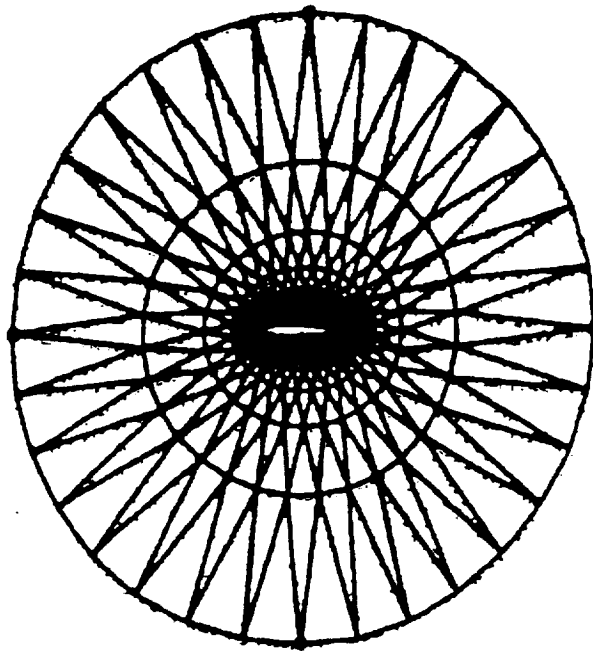


Figure 2-3: Reference Grid for Deforming Mesh Algorithm

Mentioned previously, the grid points on the outer boundary are fixed and the grid points on the airfoil are fixed relative to the airfoil. From a maximum pitch oscillation of 15° to a minimum pitch angle of -15° , the mesh smoothly transitions from one state to another using the procedure described above.

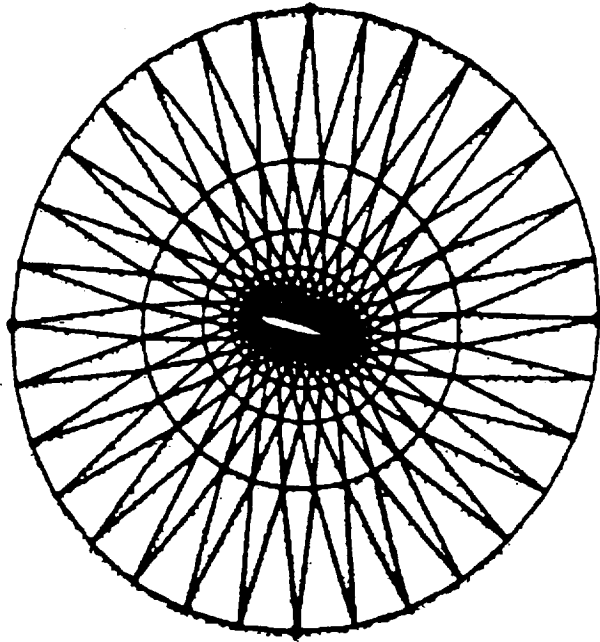


Figure 2-4: Maximum Pitch Angle ($\alpha=15^\circ$) Using a Deforming Mesh Algorithm

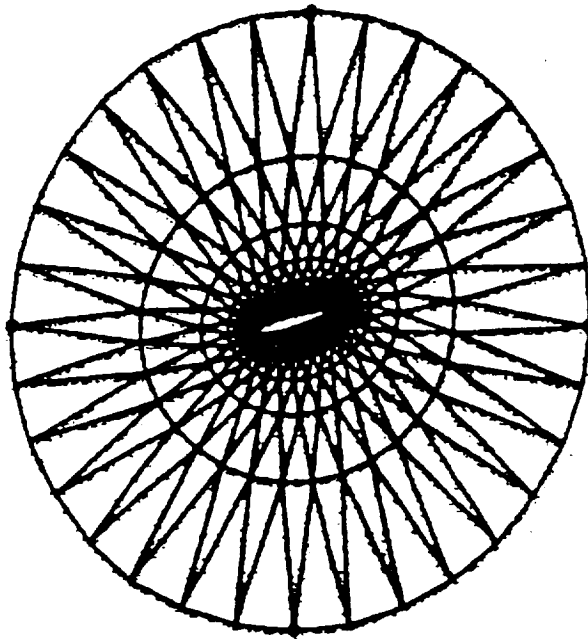


Figure 2-5: Minimum Pitch Angle ($\alpha=-15^\circ$) Using a Deforming Mesh Algorithm

The above figures were taken from a paper by J. T. Batina [Batina, 1989].

As one can imagine, the use of this type of mesh results in elements that have been deformed from their original shape. These deformations lead to volumetric changes within each element inside the computational domain. It is therefore necessary to add a geometric conservation law to account for the changing cell areas at each time step. As will be discussed later, deforming meshes also encounter difficulty in areas of surface discontinuities.

Recently, an improved spring analogy was presented as an alternative to the method proposed by Batina [Farhat, Degand, Koobus, and Lesoinne, 1998]. In addition to the linear springs between nodes, torsional springs at each node were also included to further deal with the difficulties involved with volumetric changes during mesh deformation. Results were presented for a wing with a full-length flap. Although related to the problem of discontinuous surface deformations, the full-length flap is more amiable to this type of problem since moving surfaces never separate from one another. Common to any dynamic mesh algorithm, substantial computational effort was involved with deforming the mesh at each time-step. An estimate was made that the computational overhead involved in the implementation of this dynamic mesh accounted for roughly 20% of the CPU time involved in a complete solution.

2.3.3 Re-Meshing

Perhaps the most versatile option is the re-meshing approach. Using this method, the entire computational domain is re-meshed at each time-step to account for structural deformations and velocities. This method does not involve a complicated mesh-deforming algorithm, it simply re-defines the surface geometry and generates a new

computational mesh. Of course, with current hardware, the re-meshing approach is still by far the most computationally expensive.

The problem with discontinuous surface deformations still exists with this method. Even though the grid is re-defined at each step and there is no mesh-shearing to speak of, the varying intersection points at the interface of the wing and control surface must still be calculated in order to model the geometry exactly. This calculation involves specific knowledge about the geometry and would be difficult to implement in a general-purpose CFD code. Often, when a mesh is re-generated to account for control surface deflections, additional surfaces are required to fill structural voids resulting from the displacement. In an unsteady ASE simulation where the solution involves both wing and control surface deflections, maintaining these varying intersection points would be complicated at best and would most likely involve a substantial amount of user intervention. This point is further illustrated in section 2.4.2.

2.3.4 Surface Transpiration

Though both the body fitted coordinate system and the dynamic mesh algorithms have demonstrated their efficacy for solving aeroelastic problems, both require a substantial amount of computational effort in between mesh deformations. As was seen with the body fitted coordinate system, the resulting deformed grid must be mapped to a computational system at each intermediate time-step. Even more so with the dynamic mesh algorithms, consequential structural deformations result in a modification of the entire computational domain.

In an environment where speed, without sacrificed accuracy, is of primary concern, surface transpiration has shown itself as a viable tool to the aeroelastician. The

concept of surface transpiration is simple. With known structural displacements and velocities, a simple modification to the nodal boundary conditions on the existing CFD grid is capable of altering the displacements and velocities used in the flow solver.

With this method, no modifications are made to the existing CFD grid except for a slight boundary condition modification to nodes on a deformable surface. As was encountered with the previously discussed methods of grid modification, there are no other complications associated with the transpiration method. With the transpiration method there is no mapping from one coordinate system to another, no relative nodal displacements, no elemental volume changes, no changes to the computational domain, no need to iteratively solve for new nodal boundary conditions, etc. Stated again, the only changes necessary are to nodal boundary conditions on deformable surfaces. Unlike previous methods, deformations are accounted for only on those surfaces that require it.

What exactly is this change in *existing boundary conditions*? Generally it is quite simply a change in the flow tangency boundary condition on an element. To attain the no-flow normal to the surface boundary condition, the flow solver computes a surface normal for each surface element. Observe Figure 2-6 below.

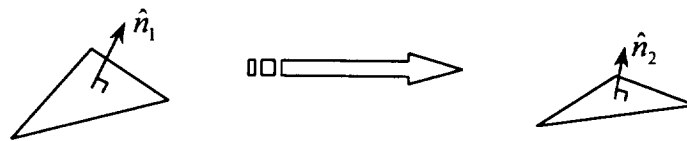


Figure 2-6: Slight Surface Element Rotation

This figure shows an arbitrary surface element undergoing a *slight* change in orientation. It is important to keep the word *slight* in mind because it stands to reason that any approximate method will lose effectiveness for *large* deformations. The figure shows a

single structural element with surface normal \hat{n}_1 being modified so its new surface normal is \hat{n}_2 . Transpiration therefore assumes that there is no significant stretching or volumetric change within the element so that the area of each element remains constant. For a typical wing undergoing small amplitude structural deformations and control surface deflections, this is a very reasonable assumption.

Assuming that a normal has an x , y , and z component, a change in orientation is accomplished by changing the velocity boundary condition on the affected nodes. This change in boundary condition comes in the form of an additional fluid velocity outside of the existing surface elements. This additional velocity effects the way the unsteady flow solver resolves the flow tangency boundary condition, see Figure 2-7 below:

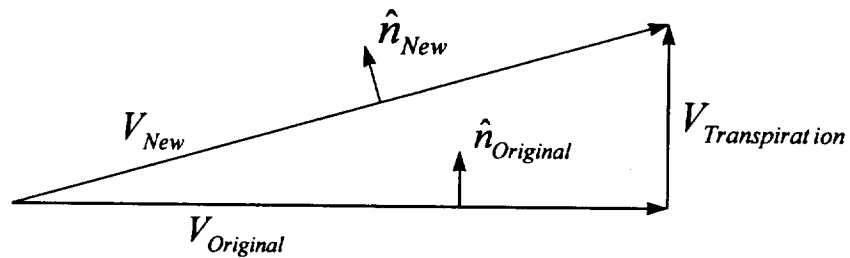


Figure 2-7: Illustration of the Transpiration Concept

In the above figure, $V_{Original}$ is the original tangential fluid velocity with normal, $\hat{n}_{Original}$. Through an aeroelastic or control surface deformation, for example, it is desired that the surface be deformed in such a way that it now has normal, \hat{n}_{New} . For the steady and unsteady cases, the flow tangency boundary condition is represented by equation (2-2) and (2-3), respectively.

$$V \cdot \hat{n} = 0 \quad (2-2)$$

$$V \cdot \hat{n} = V_b \cdot \hat{n} \quad (2-3)$$

Equation (2-2) simply states that the velocity normal to the body must be zero. Only slightly more complicated, equation (2-3) states that the fluid velocity normal to the surface must be equal to the velocity of the body normal to itself. In other words, no flow can move through a solid surface. It is necessary to point out that the V_b mentioned here is not the same as $V_{Transpiration}$ shown in Figure 2-7.

In summary, each surface element that is to undergo a change in orientation acts as a source sheet. The strength of the source is determined by the extent of the simulated deflection. Now, expand this procedure to an entire surface discretized into a large number of elements. With a known surface deformation, perhaps from a finite element solver e.g., it is desired that a surface be distorted from its original position. Within reasonable limits, this arbitrary surface deformation can be simulated with an appropriate change in the direction of the surface normal on each element making up the surface. Since the flow solver is concerned with maintaining the flow tangency boundary condition at each CFD node, the solution obtained on the simulated deformation should closely approximate that of the actual deformation.

2.4 Transpiration Concept

Of the three methods of incorporating mesh modifications into the ASE solution described in the previous section, the transpiration method shows the greatest potential for accounting for mesh deformations with the least computational overhead. Its simplicity is its greatest asset. Although the dynamics solver must still *wait* for the CFD solver to predict the new aerodynamic loads, transferring the predicted deformations to the CFD mesh is extremely fast. Since only the surfaces affected by the deflection are affected, the rest of the computational domain remains *untouched* for the duration of the

ASE simulation. Surface normals on walls, far-fields, and interior element surfaces are also not modified. Appreciable time savings are realized due to the fact that a modification to only those normals on the surface of a wing or fuselage, for example, must be modified.

2.4.1 Origins of Transpiration

Transpiration can trace its origins back to the late 1950's in a paper entitled *On Displacement Thickness* which describes the "method of equivalent sources" for modeling the influence of the boundary layer on the inviscid flow outside them [Lighthill, 1958]. Rather than thickening an actual airfoil, the boundary layer effect could be accounted for by an equivalent surface distribution of sources. This is done by specifying the necessary inflow or outflow boundary conditions on the original surface and solving for the inviscid flow. As was described in Section 2.3.4, this method requires no modification to the existing grid.

Simplicity, speed, and accuracy are the transpiration concepts greatest advantages. As has been developed, the use of the transpiration boundary condition can be implemented on an existing CFD grid with a minimal amount of computational effort. The time it takes to simulate a deformed mesh is minimized due to the fact that no actual grid deformation takes place, the computational volume is not modified, and only those surfaces that require a boundary condition modification are affected. Its accuracy has been effectively demonstrated over time through work done by Fisher, 1996, Raj & Harris, 1993, Bharadvaj, 1990.

2.4.2 Application to Current Research

Past research has demonstrated the effectiveness of the transpiration method when applied to aeroelastic problems [Fisher and Arena, 1996]. For a variety of problems covering a wide range of Mach numbers, the transpiration method proved to be a viable tool in the prediction of aeroelastic responses. Here two specific examples are covered in more detail. The first is a 2×1 plate case, the second is the AGARD wing.

The 2×1 plate consists of a flexible plate surrounded by a rigid support, see Figure 2-8 below. To evaluate the usefulness of the transpiration method on this case, the CFD mesh was deformed through a superposition of the first six natural modes, see Figure 2-9.

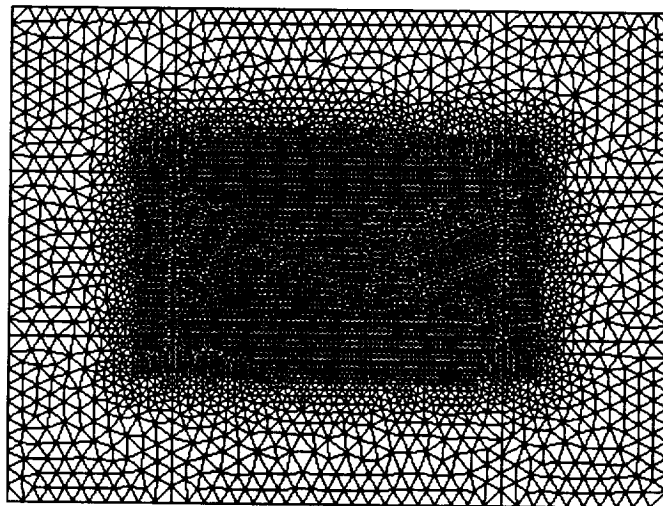


Figure 2-8: 2×1 Plate CFD Mesh

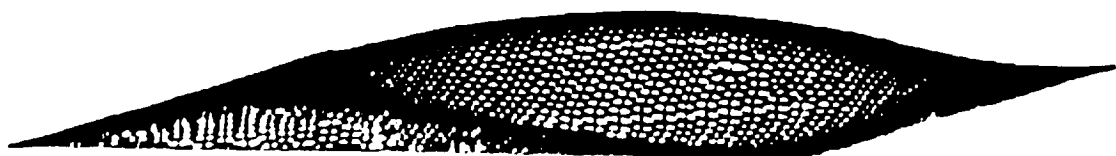


Figure 2-9: Actual 2×1 Plate Deformation

The transpiration method was used to simulate the actual deflection seen in the figure above. For this case, at Mach 0.95, relatively large surface deformations at this transonic Mach number produce strong discontinuities on the pressures along the plate.

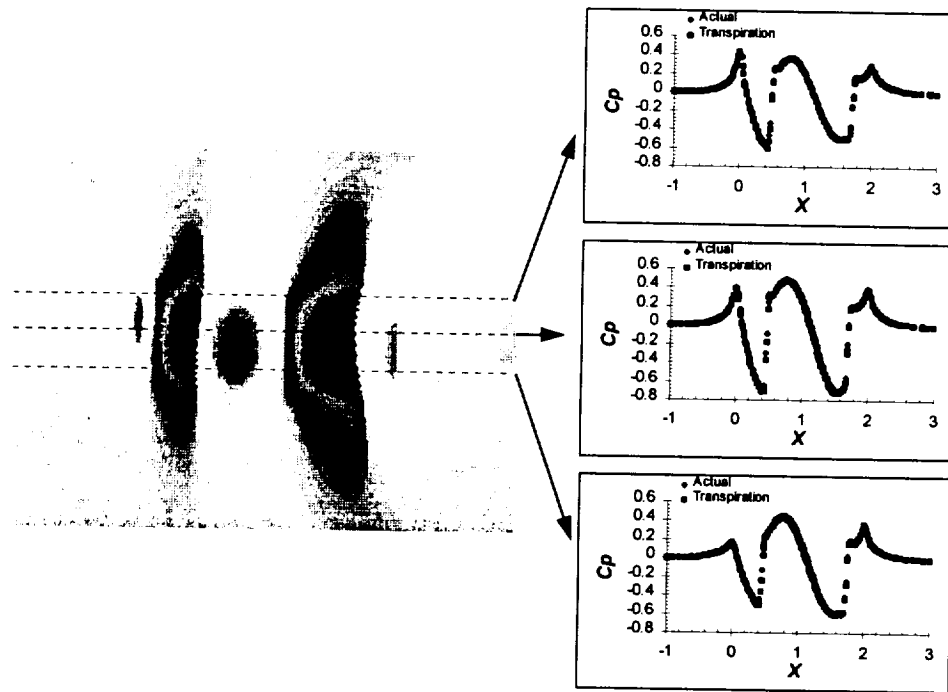


Figure 2-10: Steady Pressure Contours on the Deformed 2×1 Plate at Mach 0.95

As can be seen in Figure 2-10, the transpiration method does an excellent job of modeling the flow dynamics on the surface of the plate. In the figure above, three lengthwise pressure *cuts* show the pressure distribution along each cut. In each section, agreement between actual and simulated deflections are very good.

Another example of the application of the transpiration method is with the AGARD 445.6 wing. This standard aeroelastic test case serves as a good reference for application of the transpiration method to simulate surface deformations on a lifting surface. Figure 2-11 shows two views of the AGARD wing. The leftmost figure shows the undeformed mesh that will be used to simulate the figure on the right which is

actually deformed. This case serves to demonstrate the effectiveness of the transpiration boundary condition when applied to relatively large surface deflection. As one can tell from the figure, there are significant deformations resulting from both bending and torsional modes.

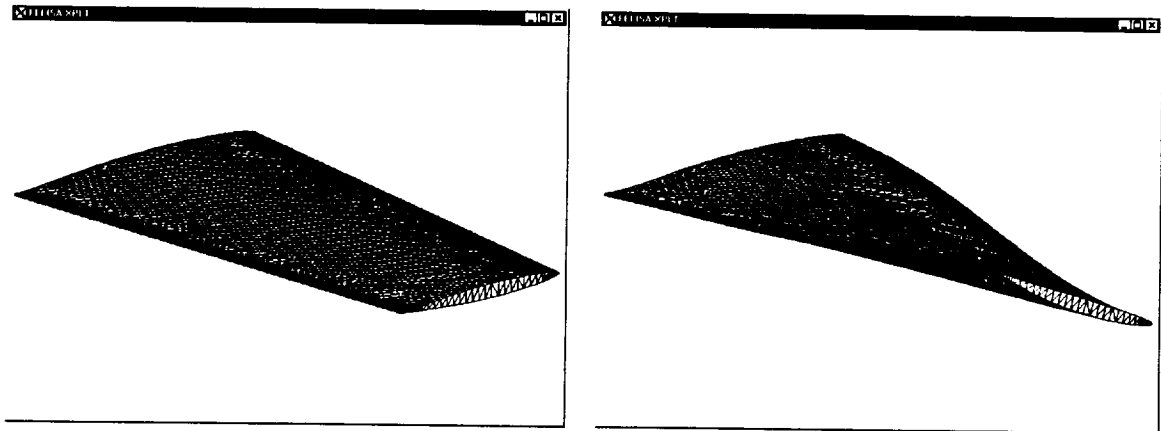


Figure 2-11: AGARD 445.6 Wing, Undeformed and Deflected CFD Meshes

As was done with the 2×1 Plate case, comparison is made between the simulated and actually deformed mesh by means of chordwise pressure cuts at several points along the span of the wing. For a Mach number of 0.678, we get Figure 2-12, below.

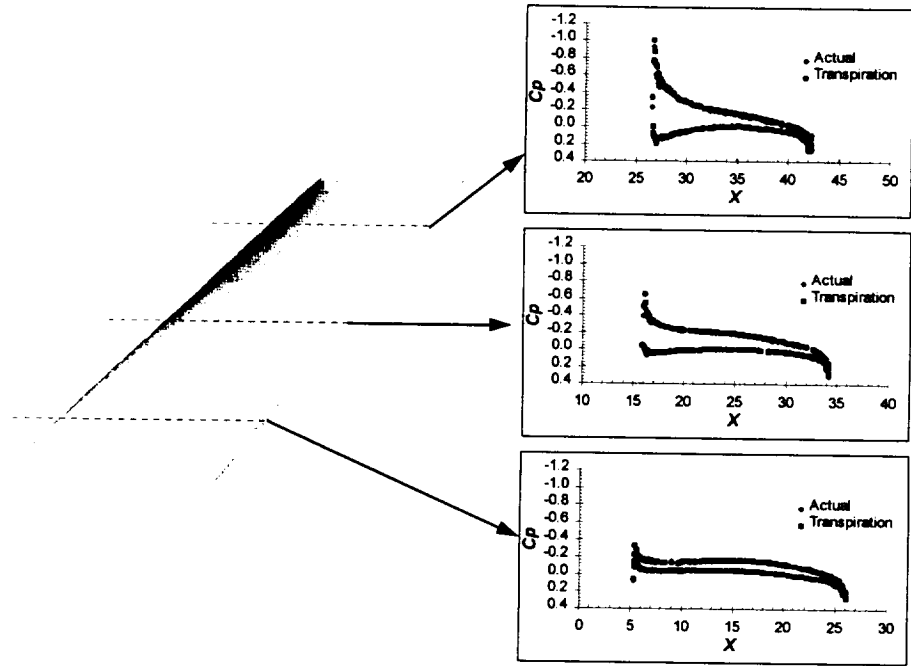


Figure 2-12: Steady Pressure Contours for the AGARD Wing at Mach 0.678

For three chordwise pressure *cuts* through different spanwise locations along the wing we once again see excellent agreement between the simulated and actual surface deformation.

What was lacking from the above two examples was a moving control surface. Relatively smooth mesh deformations, as typically occur in aeroelastic problems, are much more simple to deal with than are discontinuous surface deformations. For the scope of the current research, the appealing characteristic about the transpiration method is, oddly enough, the fact that the mesh does not move. Deflected control surfaces provide several inherent difficulties for CFD solvers. When attempting to model a control surface displacement, there are several factors that affect a CFD codes ability to handle these difficult surface transitions.

First is the very close proximity of control surface edges to adjacent parts of the airframe. Especially when using an Euler solver, these very narrow gaps present significant computational difficulties. The flow through these gaps, along surfaces which are parallel to the flow direction, will result in very high flow gradients and will effectively *wash* out other, more significant, flow physics.

The second difficulty arises from the fact that even if one assumes that there is no gap, the varying size of the face along the wing-flap intersection would be terribly difficult to account for, even in a dynamic mesh. Figure 2-13 below helps illustrate this problem.

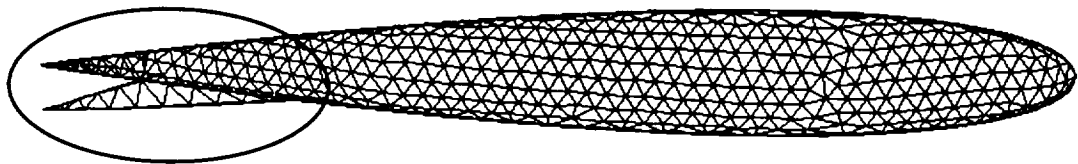


Figure 2-13: Variable Wing-Flap Intersection Example

Notice the area in the circled region in the above figure. For any change in flap angle, the intersecting surfaces and the points of intersection change. Also observe that as the flap changes position, the size and shape of the newly exposed surface changes. These surfaces, specifically the lines defining the surfaces, must be modified with each different flap angle. The addition of these surfaces is necessary to keep the solution domain closed. For the case of a wing with a finite-span flap, for example, deflection of the flap requires the definition of 4 new surfaces with each new deflection. In either a dynamic mesh or re-meshing algorithm, for example, this variation in surface definition would be difficult to account for.

Related to the second problem, is again the difficulty encountered in the immediate vicinity of the flap during a control surface deflection. With the flap in its stowed position, there is essentially a smooth, continuous surface over the entire wing. Assume that this flap, or control surface in general, is deployed several degrees. One must consider what happens to the grid in the vicinity of the flap. With a dynamic grid, the mesh must stretch to account for this displacement. The problem encountered with this mesh deformation is the amount of *mesh shearing* that must be endured for the flap to deflect.

Shown in Figure 2-15 is an example of this mesh shearing. For a simple wing with a flap lying within the span of the wing, a flap deflection similar to that of Figure 2-13 would produce surface discontinuities in the surrounding area of the flap. Figure 2-14 shows the desired 10° flap deflection. The next figure, Figure 2-15, shows how a mesh deforming algorithm might deform the existing mesh.

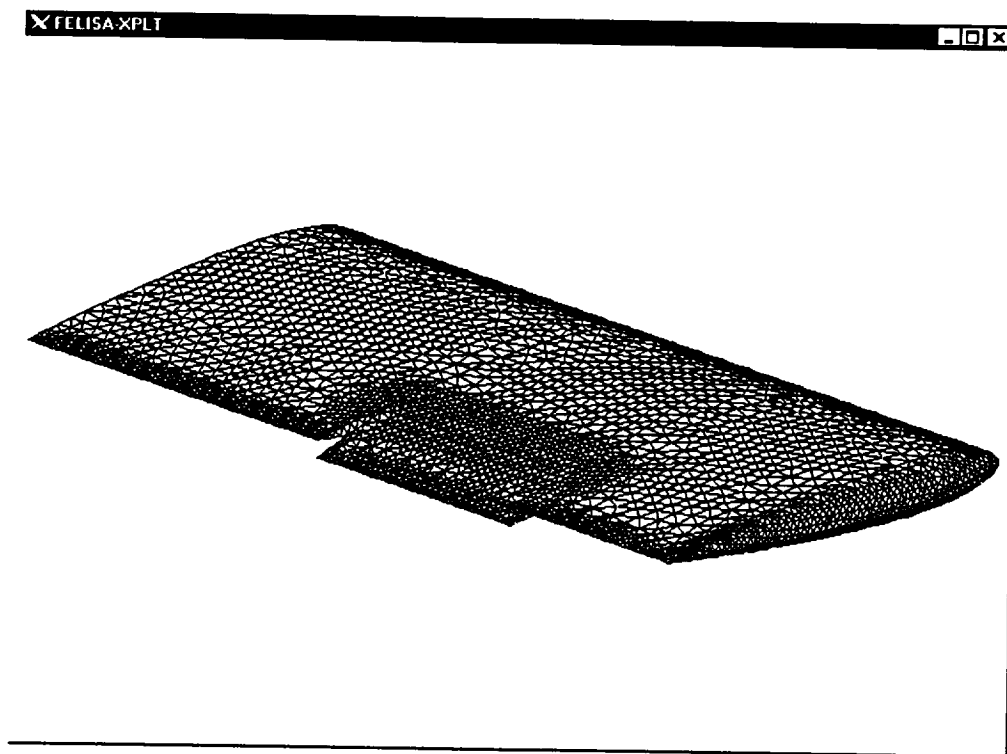


Figure 2-14: Desired Flap Deflection

Mesh shearing has the consequence of degrading the flow solution quality. Notice that in the region of the flap, mesh shearing results in the elongation of elements surrounding the wing-flap intersection. Due to this shearing effect, there now exists poor grid resolution around an area with high flow gradients, an area actually in need of grid enhancement.

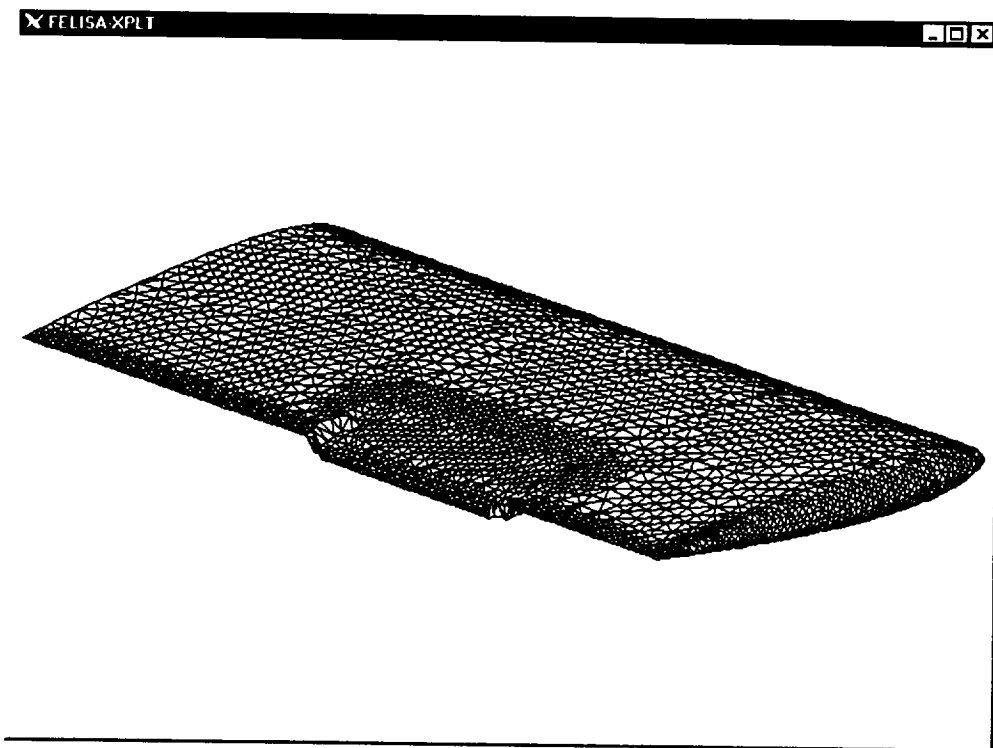


Figure 2-15: Mesh-Shearing Example

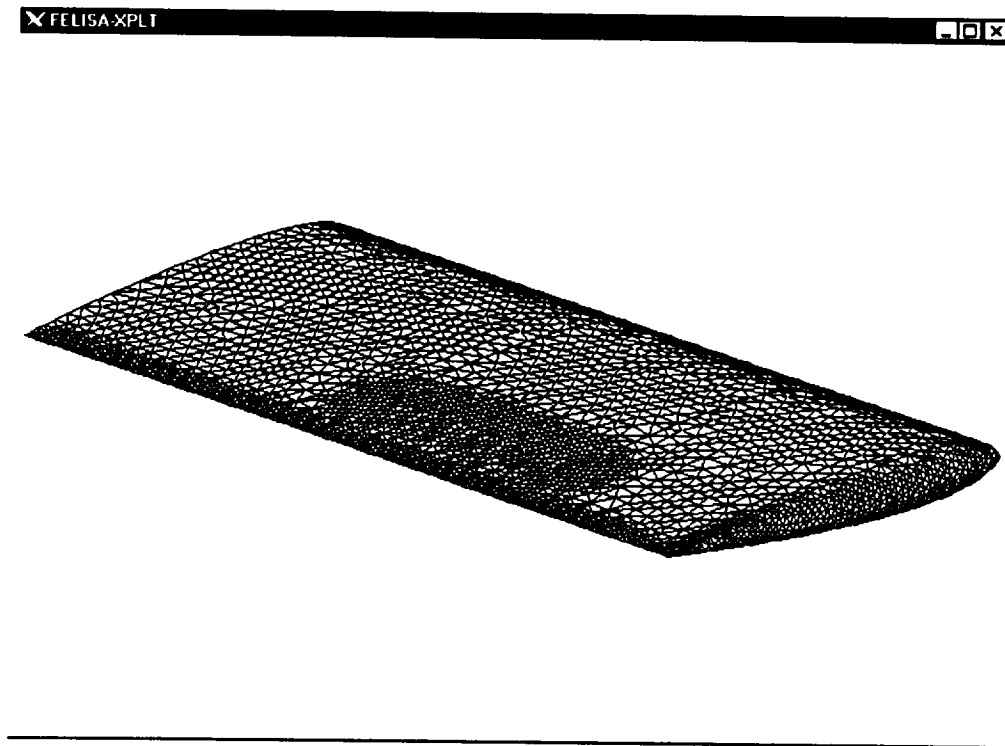


Figure 2-16: Equivalent Mesh for Transpiration

Using the concept of surface transpiration, there is no mesh deformation necessary, hence no mesh to shear. Figure 2-16 shows the only mesh needed for the application of a reasonably arbitrary flap deflection. With the above mesh, any arbitrary flap deflection can be accounted for by simply rotating the elemental normals on the flap by the desired flap deflection angle. Once again, one can see the speed at which this method may be applied.

2.5 Benchmark Models Program

The Structures Division of NASA Langley Research Center (LaRC) initiated the Benchmark Models Program (BMP) to obtain experimental data for the validation of unsteady CFD codes. A variety of models were tested in the NASA Langley Transonic Dynamics Tunnel (TDT) [Scott, Hoadley, Wieseman, & Durham, 1997]. In the BMP program, two specific models are of interest. Each model has a rectangular planform with a NACA 0012 cross-section, 16 inch chord, and 32 inch span. The first model was simply a rigid rectangular wing fitted with pressure transducers over the surface of the wing. The second model is referred to as the BACT, standing for Benchmark Active Controls Technology. Though different models, each shares identical model dimensions, and instrumentation. The only practical difference between the two models is the presence of three control surfaces. These three control surfaces, two of which can be seen in Figure 2-17, are a trailing edge control surface, and upper and lower spoilers.

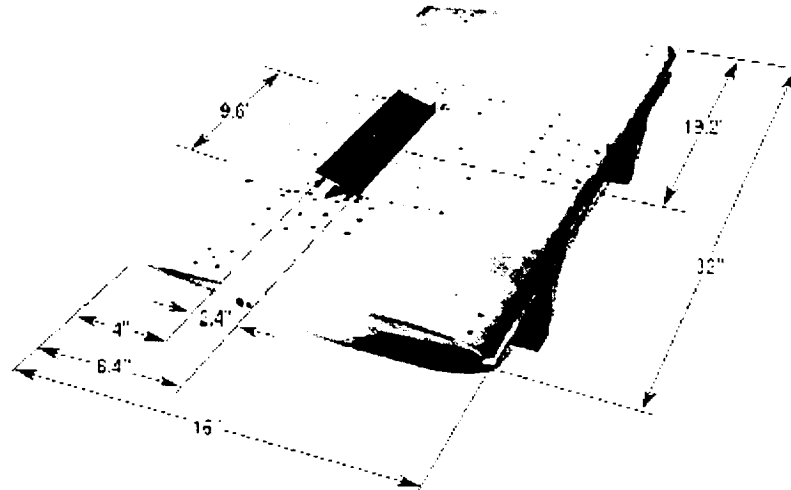


Figure 2-17: BACT Wing Model Dimensions

The control surfaces are centered along the models 60% span (19.2 in), and has a length equal to 30% (9.6 in) of the wing's span. The trailing edge control surface has a width of 25% (4 in) model chord while the spoilers have a width of 15% (2.4 in) model chord.

The first model, the NACA 0012 wing, was tested in air and provided a large experimental database. This database included steady pressure measurements, unsteady pressure measurements during flutter, and flutter boundaries over a wide Mach number range. Tested in R-12, the BACT model's primary purpose was to provide additional data for the purposes of evaluating a CFD code's effectiveness in modeling the control surfaces illustrated above.

Both models were mounted inside the TDT on a device known as the Pitch and Plunge Apparatus (PAPA) [Farmer, 1982]. Shown below in Figure 2-18, the BACT model is seen mounted to the flexible PAPA mount system.

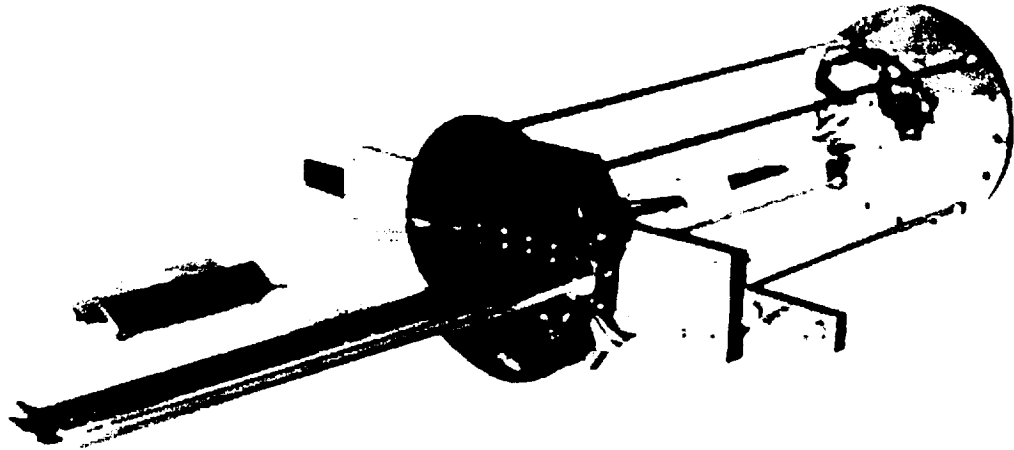


Figure 2-18: BACT Model on Flexible PAPA Mount

This mount system is simple and possesses dynamic properties that are easily obtained by analytical means. It is important to note that the PAPA mount shown above is slightly different than that described in the paper by Farmer, but these differences are primarily cosmetic.

The mount basically consists of a model mounted to a “Chevron” bracket. Seen on the Chevron mount are adjustable masses that allow adjustments to the models center of gravity location. This Chevron mount is connected to a turn table by four steel rods and a rectangular *drag strut*. The mount is designed such that it allows only two degrees of freedom: rigid body pitch and plunge. The turntable allows an arbitrary choice in angle of attack. The Chevron mount, rods, drag strut, and turntable are *hidden* behind a large splitter plate such that only the model is seen in the tunnel test section. For steady pressure tests, this mount can be *rigidified* by replacing the Chevron mount, rods, and drag strut by a large diameter (~6 in) rod.

With the quality and amount of experimental data available, these models serve as the primary experimental benchmark to which all computational results obtained from the

current research are compared. Efforts presented within this paper illustrate the implementation of the transpiration method within the STARS computer codes on: steady pressure measurements, steady control surface deflections, conventional flutter, and control inputs for purposes of flutter suppression.

CHAPTER 3

METHODOLOGY & PROCEDURE

The primary research tools for the current effort are the STARS codes developed at NASA Dryden Flight Research Center [Gupta, 1997]. The current version of STARS is the result of the evolution of the original STARS (STructural Analysis RoutineS) computer code into an highly-integrated multidisciplinary tool for the analysis of a wide variety of 2D and 3D structures. This evolution involves the addition of several *modules* to the original STARS code. Each individual module, general by design, is integrated into an effective tool for the prediction of complicated aeroelastic and aeroservoelastic problems. These modules include: structures, heat transfer, linear aerodynamics, CFD, controls engineering, and others.

3.1 STARS Modules

The scope of the current research is primarily involved with two of the modules within the STARS computer programs. For a general ASE simulation, the user is typically concerned with the structural dynamics of the system and the steady and unsteady aerodynamic characteristics. The modules used for the current effort are the structures and CFD modules, which are in turn integrated into the full ASE simulation.

3.1.1 SOLIDS Module

The SOLIDS module has a large solution bandwidth, but for problems pertinent to current research, we are concerned with the determination of the free and forced response. The free response comes from the solution of the following equation:

$$[M]\{\ddot{u}\} + [K]\{u\} = 0 \quad (3-1)$$

where [M] and [K] are the inertial and stiffness matrices, respectively. Generally, once a *solids* model is generated, STARS solves the above equation for the natural frequencies (ω) and mode shapes (ϕ). If, however, the natural frequencies and structural mode shapes are known *a priori*, one can bypass this solution and manually create the generalized mass and stiffness values.

3.1.2 CFD Module

The STARS flow solver is an Euler-based code that applies finite-element CFD on an unstructured grid. The implementation of an unstructured grid is a significant feature of the STARS computer codes. For the general three-dimensional case, the computational mesh consists of an assemblage of tetrahedra. These tetrahedra are oriented to form to the geometry being considered, thus making possible the treatment of complicated shapes.

The unstructured grid shape is assembled using the advancing front technique. This procedure consists of dividing a boundary into a finite number of points (nodes) such that the external surface is sufficiently represented. Adapted from a figure by Peiró, Peraire, and Morgan, Figure 3-1 shows how these triangles, or tetrahedra in three dimensions, are arranged beginning at these outer nodes [Peiró, Peraire, and Morgan,

1993]. Additional tetrahedra are added in such a manner that the surface *front* collapses upon itself until the entire domain is filled with tetrahedra.

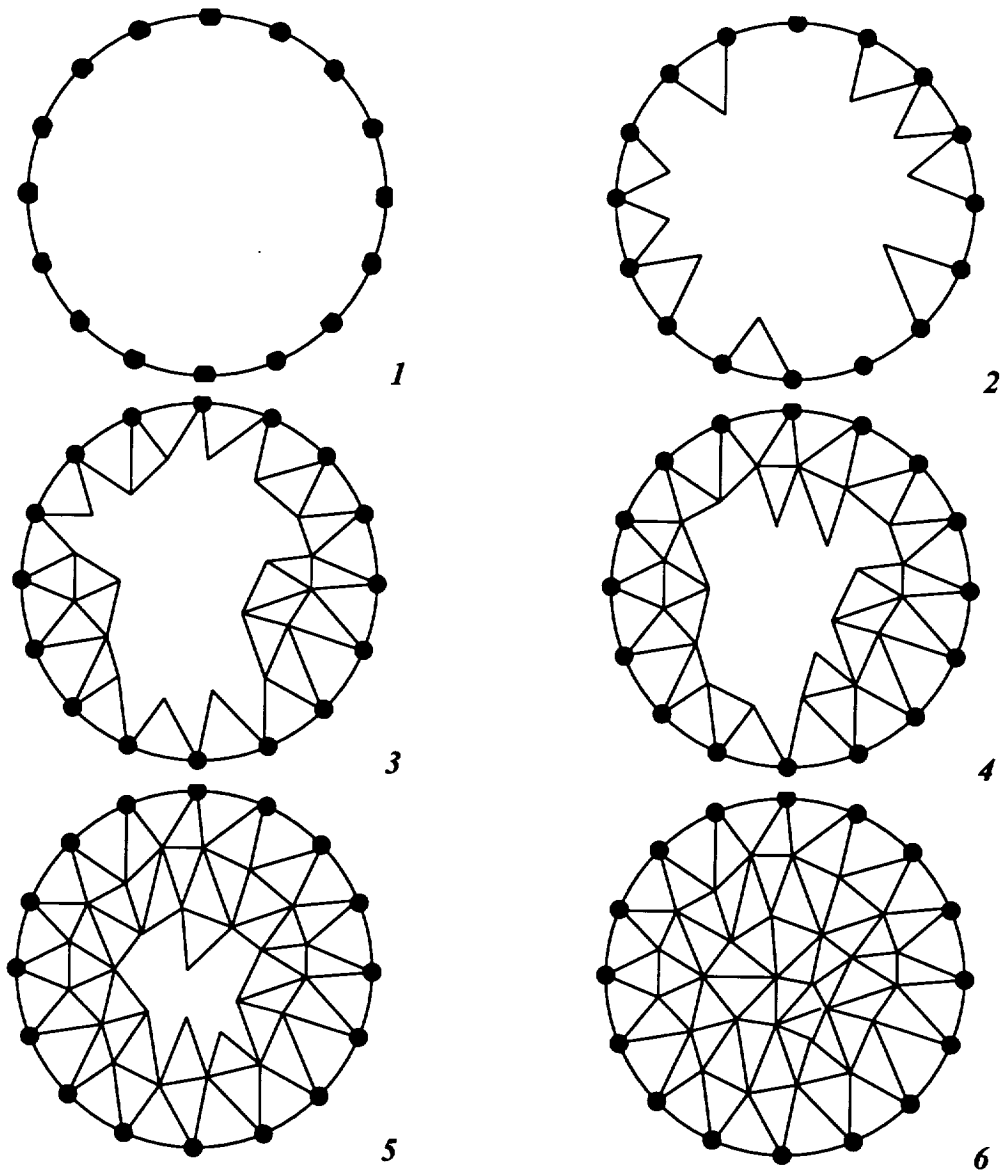


Figure 3-1: Stages of Advancing Front Technique

The CFD module, in general, consists of four major parts:

- SURFACE: Generates the two-dimensional front
- VOLUME: Generates the three-dimensional computational domain
- SETBND: Defines the boundary conditions in the domain

- EULER: Steady or unsteady Euler flow solver

Each one of the above steps, as one would surmise, need to be done in that particular order.

The user is able to specify certain parameters pertaining to the density of the CFD surface and volumetric mesh. For regions such as leading and trailing edges of wings, for example, the user may wish to define regions of higher mesh density, while maintaining low mesh density in the far-field. STARS also has the capability of adaptive re-meshing. Once a flow solution is obtained, the user has the option of letting STARS automatically adjust the existing computational grid such that regions of high gradients receive a more dense arrangement of elements.

3.1.3 Aeroelastic and Aeroservoelastic Solver

In general, the equations of motion for the coupled, time-marched ASE solution involves the solution of (3-2), which is a matrix equation of motion for an arbitrary structure in generalized coordinates.

$$[M]\{\ddot{u}\} + [C]\{\dot{u}\} + [K]\{u\} = f(t) \quad (3-2)$$

In the above equation: [M] = generalized mass matrix

[C] = generalized damping matrix

[K] = generalized stiffness matrix

{u} = generalized displacement vector

f(t) = generalized aerodynamic force vector

The general procedure, therefore, for solving aeroelastic and aeroservoelastic problems is as follows. A steady CFD solution serves as the initial conditions for the structural

dynamics solver. A perturbation about this steady CFD flow will cause a change in the structural displacement and velocity boundary conditions. These changes in displacement and velocity boundary conditions serve as boundary conditions for the next time-step in the CFD solution. Resulting forces and moments are then fed into the structural dynamics solver which in turn computes new displacement and velocity boundary conditions for the CFD flow solver. This process continues until the complete time-history is obtained. The above procedure can be visualized graphically through Figure 3-2 below.

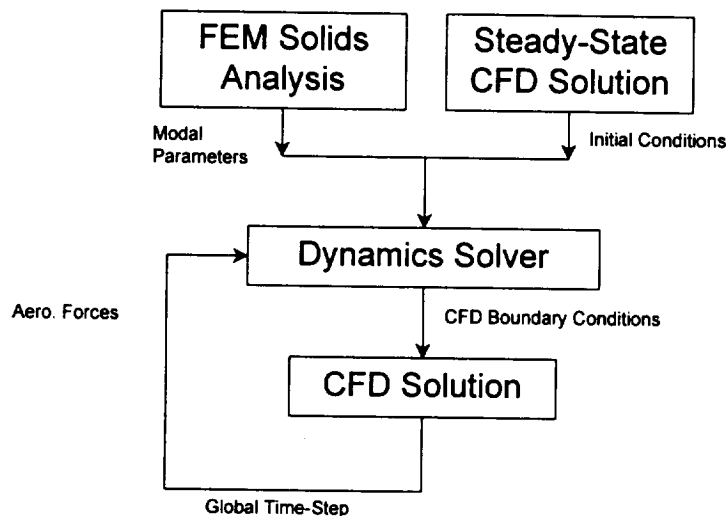


Figure 3-2: Block Diagram of Time-Marching Approach

3.2 Implementation of the BACT Model into STARS

As was mentioned in Chapter 2, the primary test cases for this effort are a NACA 0012 wing tested in air and the BACT wing tested in R-12. Both in the Benchmark Models Program and geometrically similar, models were tested under similar Mach numbers and dynamic pressures in the Langley Transonic Dynamics Tunnel at NASA

Langley Research Center. The main difference, other than the fluid medium, is the fact that the BACT wing has the capability of modeling control surface deflections, whereas the NACA 0012 wing is simply a rigid, rectangular wing with no control surfaces.

The next few sections discuss in more detail, the incorporation of both these models into STARS. Since, for all practical purposes, the two wings are exactly the same except for the trailing edge control surface, the solids and CFD models used in STARS will be the same..

3.2.1 BACT SOLIDS Model Development

Described in this section is an overview of the various steps taken to construct a finite element solids mesh to represent the BACT wing. A solids model that included the PAPA mount described in Chapter 2 was not developed due to the simple mode shapes and frequencies exhibited by the BACT-PAPA system. Since the model was constrained to only plunge and pitch, the mode shapes and natural frequencies were available from experimental data. Additionally, modeling the mount would have required a significant amount of parameter *fine-tuning* in order to assure the natural frequencies and mode shapes coincided with experimental results.

Even though the structural dynamics of the entire system were already known, a structural mesh of the wing and flap itself is still needed. Mode shapes defined with this model are in turn interpolated a CFD mesh. For too course a grid, it is possible that one may introduce errors in the interpolation from one grid to another. For this reason, care was given to provide a tighter mesh in the region of the trailing edge control surface.

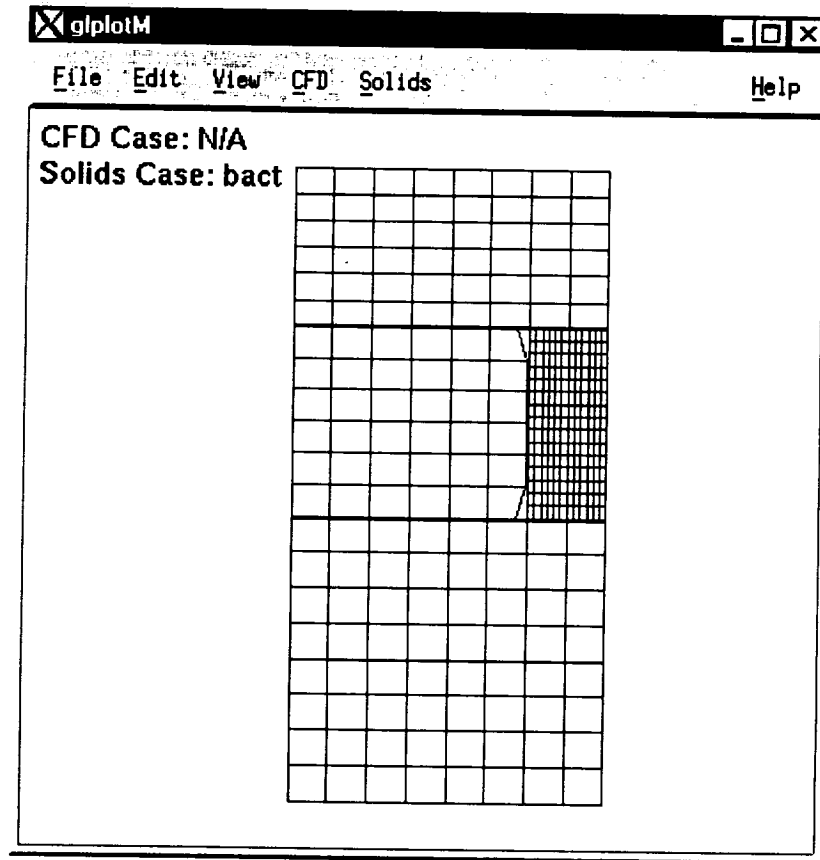


Figure 3-3: Finite Element Solids Mesh for BACT Wing

Figure 3-3 shows the resulting finite element structural mesh used in STARS. Over the majority of the wing, a relatively coarse mesh is used due to the fact that only rigid body pitch and plunge motions are encountered due to the PAPA mount. An obvious exception to the otherwise coarse mesh is the *tight* mesh in the region of the trailing edge control surface. To minimize any possible error in the interpolation from the solids mesh to the CFD mesh this region was meshed much more densely than the rest of the wing.

The majority of the solids mesh construction took place within the solids preprocessor within STARS. PREPROCS is simply a tool that guides the user through the creation of the mesh, assignment of structural properties, etc. It also formats and

writes the corresponding data file containing solution parameters, nodal properties and locations, element properties and connectivity, structural properties, materials etc. The *thick* lines running from leading to trailing edge along the edge of the trailing edge control surface and along the beginning of the flap actually correspond to small elements that had to be added manually. It was discovered that in the interpolation from the solids mesh to the CFD mesh exaggerated corresponding displacements of the flap due to the large elements adjacent to the flap. Due to the way STARS implements the interpolation, control surface deflections were seen out to locations corresponding to one half the size of the larger elements. This was the first time this problem had been encountered within STARS. Before, when modeling continuous structural deformations, this sort of problem never surfaced. To alleviate this problem, smaller elements had to be added around the entire perimeter of the flap. Deflections still get interpolated out to one half of the elements width, but the elements are sized such that these errors are negligible.

In the PREPROCS routine discussed above, elements are assigned material types and associated constants, nodes are constrained, etc. These constants, however, are not used in this particular case for reasons discussed previously. The input data file created by PREPROCS is given in Appendix A-1. Since the structural mass, damping, and stiffness characteristics are obtained experimentally, STARS allows the manual input of this data. This point is covered in more detail a little later.

3.2.1.1 Structural Mode Shape Definition

In general, once one has developed the STARS solids mesh, the solution can be set up to run the un-damped, free vibration analysis to determine a user defined number of structural natural frequencies and mode shapes. For the case of the BACT, the two

structural mode shapes are well defined, as is the control mode, and it is a relatively straightforward procedure to define ones own structural mode shapes. Discussed in the next few paragraphs is a general set of steps used in the creation of the two structural mode shapes and the control mode.

First, the necessary parameters in the solids file are set to solve for the first three natural mode shapes. Run the undamped, free vibration analysis to obtain a properly formatted *out.2* file. Although the data in the file will be replaced, STARS requires proper formatting for later modules so the file serves as a formatting tool only.

Now that an *out.2* file has been created, although filled with irrelevant data, the user defined mode shapes need to be developed and replace the data currently in the *out.2* file. To keep the problem as general as possible, a series of EXCEL workbooks are set up to contain each of the calculated mode shapes. Even though the mode shapes are known, the magnitude of the modal displacements is still arbitrary. Mode 1 is simply a rigid body plunge motion. For this mode, the spreadsheet contained a large matrix of data containing information on the nodal displacement due to a generalized displacement of 1 inch. Table 3-1 shows how the data was arranged in the spreadsheet. A similar format was used with the other two modes.

Table 3-1: Spreadsheet Layout for Manual Input of a Structural Mode

Node	Original Location			New Location			Nodal Displacement		
	X	Y	Z	X'	Y'	Z'	ΔX	ΔY	ΔZ

Each row in the above table contained data for every node in the solids file. The simplest case was rigid body plunge. In this case, one inch was added to each original *z* coordinate.

Slightly more complicated was the determination of the rigid body pitch motion. The magnitude of the rotation, so long as the rotation was a pure rotation about the models mid-chord (8 inches), was arbitrary. The modal displacement vector, however, is sensitive to this magnitude. It makes more sense to explain this point with an example. Consider the choice between a rigid body rotation (ϕ_2) of 1° or 10° . Two figures below illustrate how STARS interprets the mode shapes it creates, or the user defines.

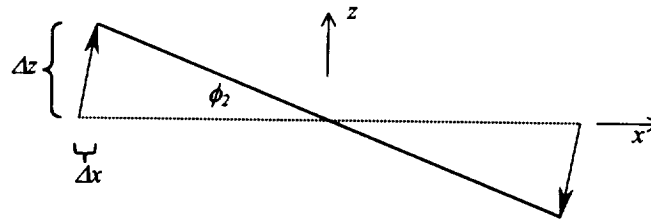


Figure 3-4: Rigid Body Pitch Mode Definition Example

Shown in Figure 3-4 is the original structural position (dashed) and the rotated position. Remembering from Table 3-1 that nodal displacements were specified such that only the original and final position are known. STARS therefore interprets the entire structural rotation as the *straight-line* displacement from the initial position to the final position. Figure 3-4 shows only the positive displacement. For an oscillatory motion, however, both positive *and* negative displacements would be encountered Figure 3-5 shows what happens for a displacement opposite that of the defined rotational mode shape.

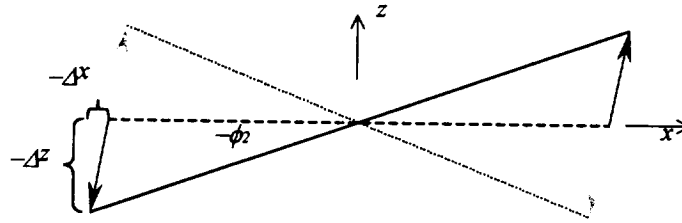


Figure 3-5: Structural Deformation Opposite Original Definition

As the structure rotates from its original position (dashed) to its specified deflection (dotted & grayed), each node follows a particular vector defined by the final displacement. As the structure rotates from this position, back through the original position, and to the position shown in Figure 3-5, it follows the path defined as shown by the vectors. One can immediately see that this structure must compress and stretch as it cycles through its motion.

We can now see the effect of the magnitude of the specified rotational mode shape. It makes sense then that if the rotation amount is *small* that any compression and stretching can be kept to a minimum. Keep in mind also that actual displacements may be larger than those originally specified, resulting in further contraction and expansion. It is apparent that a compromise is needed. Structural distortion during rotation was minimized by specifying small, 1°, rotational mode shapes, and neglecting any slight changes in the longitudinal direction, i.e. as the object rotates, only vertical motion is realized, translational motion is neglected. This effect is illustrated below in Figure 3-6.

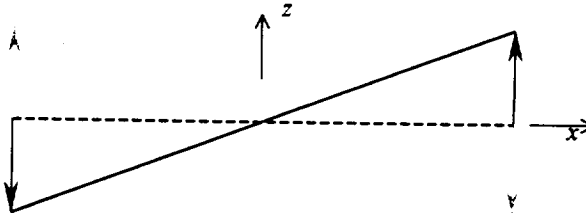


Figure 3-6: Implemented Rotational Mode Shape for STARS

The above figure is shown at an exaggerated displacement to highlight the method used. In actuality, the 1° rotation produces translational changes on the order of 0.001 inches. Additionally, neglecting this small translation allows for a more general rotation angle. For small angles, those around 8° or so, translation due to rotation can still be considered insignificant.

Finally, specification of the control mode followed much the same procedure as did the rotational rigid body mode. The difference being the fact that the control surface rotated about the $\frac{3}{4}$ chord point (12 inches) as opposed to the mid-chord. Again, modal displacement vectors were specified at each node, but only the nodes on the flap had non-zero values. The same stretching/compression problems were encountered with the flap. It was critical that the flap be modeled as accurately as possible so that any slight deflection would be correctly interpolated to the CFD grid, hence the dense mesh in Figure 3-3. The translational effects due to flap deflections were more significant than those due to the entire wing pitching because of the relative sizes of the flap and wing. As was done with the rigid body rotation, a 1° generalized displacement was used to specify the motion of the flap. The EXCEL workbooks showing the nodal displacement data are given in Appendix A-2 through A-4.

With all of the little details discussed in the previous paragraphs, it is easy to lose sight of what has actually been taking place. Up to this point a solids mesh has been generated, STARS has performed an undamped, free-vibration analysis on this mesh and has generated an *out.2* file (for formatting purposes only). The next step is to replace the data in the file with the natural frequencies and mode shapes that were developed a few paragraphs back. The data in the *out.2* file must be arranged in an exact format due to a formatted read inside STARS. Inside this file, displacement and rotation data are given for each structural node number. Displacements for each node are broken up into *x*, *y*, and *z* translations and *x*, *y*, and *z* rotations. As opposed to entering all the data manually, a quick FORTRAN program (Appendix A-5) was written that read in the data from Appendices A-2 and A-4, sorted it into the proper form and output the data into an external file. Data from this new file is in turn manually pasted into the proper location inside the *out.2* file. There is quite a bit of manual overhead when one chooses to define frequencies and mode shapes that is not involved when STARS computes them. However, time savings are realized during the latter parts of the solution when simple changes in mass, damping, stiffness, CG locations, etc. require the modification of a single parameter and not the re-definition of the basic structural mode.

Throughout this section, there has been a reference to the CFD mesh. Before discussing further structural requirements for the full ASE simulation, the development of the CFD mesh must be considered.

3.2.2 BACT CFD Model Development

The development of the CFD mesh consists of several key elements. First, the model geometry must be constructed and entered such a way that STARS can read it.

Next, the CFD mesh must be set such that the grid is sufficiently dense, or coarse, in the appropriate areas. Finally, once the CFD boundary conditions are completely specified and the solution parameters are set, the stage is set for a steady-state CFD solution.

3.2.2.1 BACT Geometry Specification in STARS

The first step in defining the CFD mesh in STARS is the specification of the lines and surfaces that will make up both the model geometry and computational domain. Described in the next few paragraphs is the development of two CFD meshes. The first mesh is the is used to investigate the application of the transpiration method for a variety of cases including steady and unsteady aeroelastic cases, steady control surface deflections, and finally control surface deformations as a means of flutter suppression. The second CFD mesh is used to compare an actual control surface deflection to one that has been modeled using the transpiration boundary condition.

Shown below in Figure 3-7 are the important labels defining the lines and surfaces of the entire computational domain.

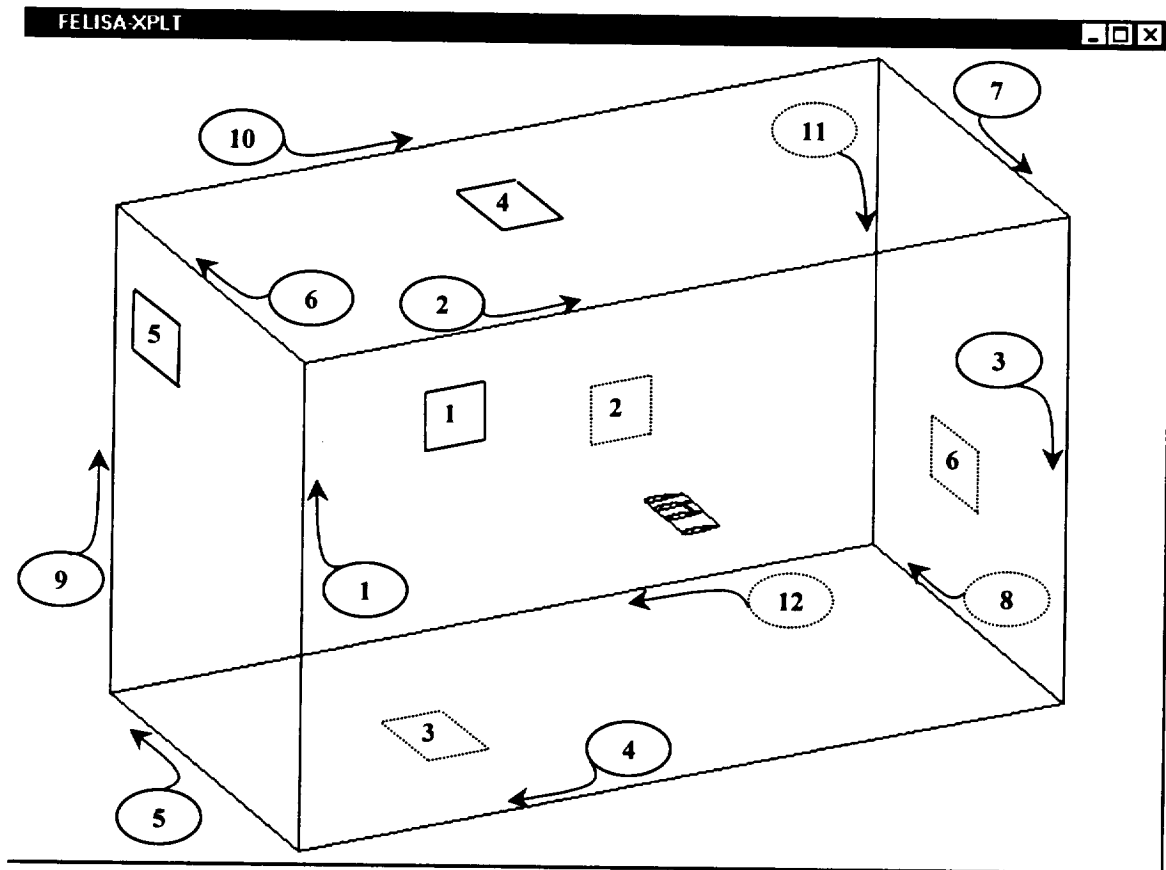


Figure 3-7: CFD Computational Volume Specification

In the above figure, the circles indicate the definition and specified direction of a line. Parallelograms indicate the existence of a surface. In both cases, dashed lines represent lines or surfaces that would be hidden in order to facilitate the visualization of the 3-D geometry. Next, a similar procedure is employed in Figure 3-8 for defining lines and surfaces on the wing itself.

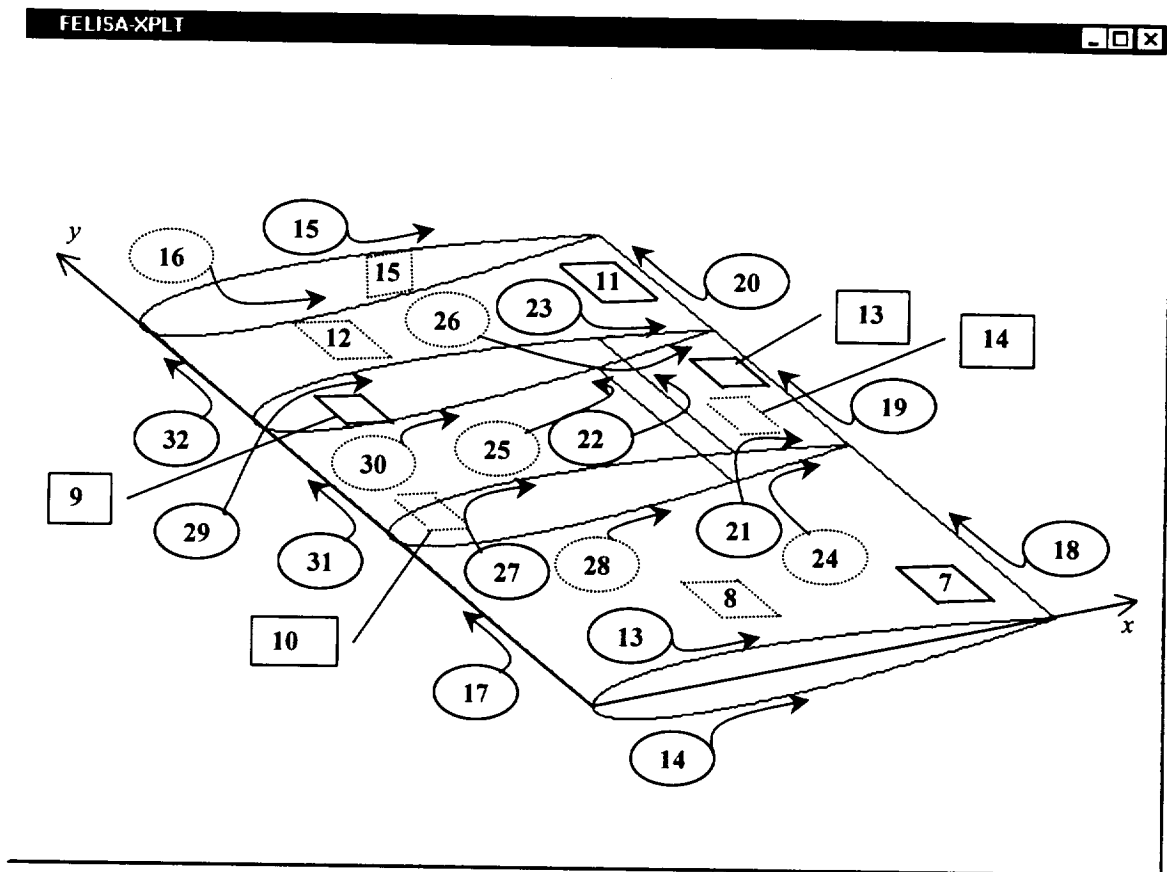


Figure 3-8: Wing Geometry Specification

To specify the chordwise points that define the NACA 0012 airfoil cross section, such as lines 13 and 14, 161 cosine spaced points outline the curve of the airfoil. Cosine spacing simply allows finer specification along the leading and trailing edges with reduced spacing over the surface of the airfoil where there is the least curvature. Admittedly, there is an excessively large number of points defining these curves, but any effort to minimize any sort of modeling error was utilized. Surface 15 corresponds to the wing tip. A rounded surface for the wing tip was included to match that of the experimental BACT model. This rounded tip is simply a surface of revolution which is defined by $\frac{1}{2}$ of the airfoil section.

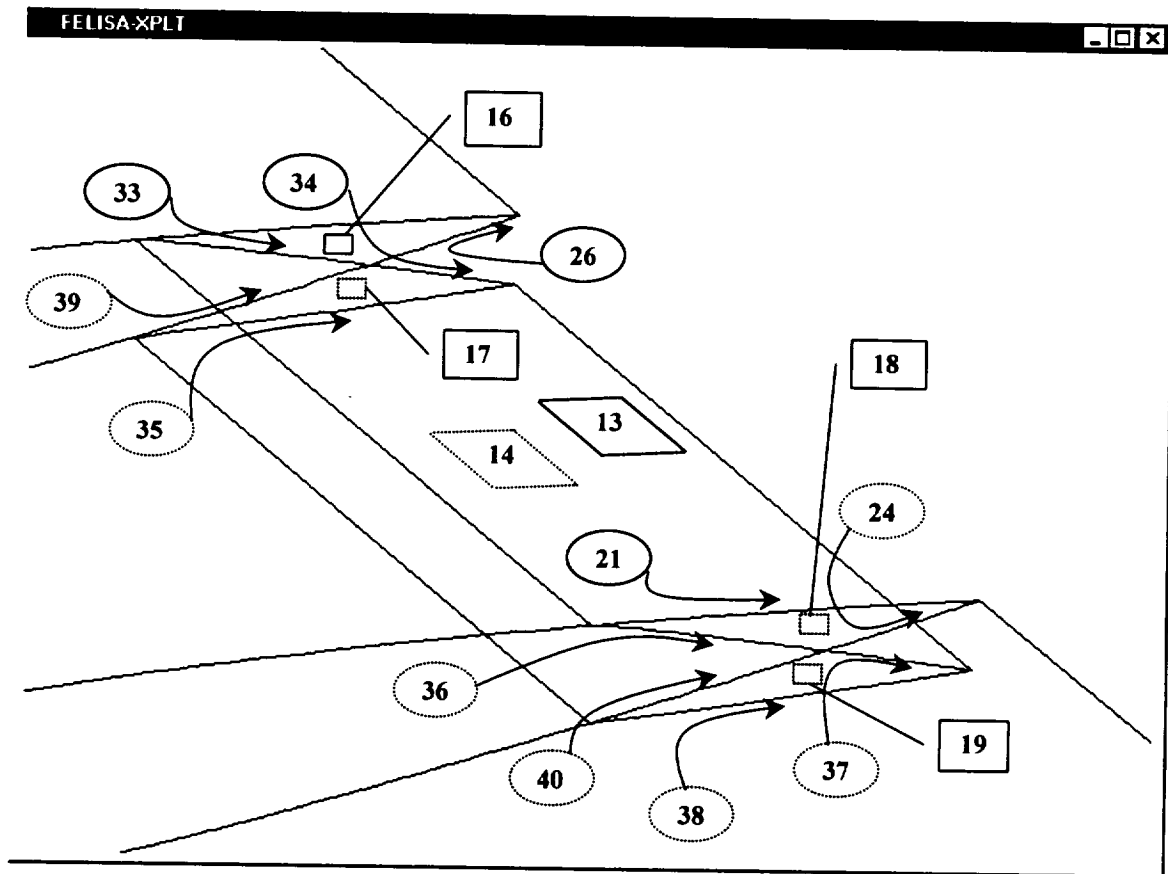


Figure 3-9: Close-Up of Deflected Flap Geometry Definition

Figure 3-9 demonstrates the additional lines and surfaces needed to define the wing geometry for a deflected control surface. For clarity, only lines and surfaces that were modified or added were included in this figure.

Addition of the control surface causes several difficulties due to the changing intersection points between the control surface and the wing. With any slight change in the deflection angle, intersection points must be recalculated and the STARS data file modified. This manual re-meshing concept is, as one would expect, time consuming. The time it takes to go from one deflection angle to another is on the order of 2 to 3 hours. That is just the time it takes to modify the wing geometry. Changes also must be made to the file that contains information about grid density and element source location

since surfaces are being displaced from their original positions. Additional time must also be spent regenerating the tetrahedral mesh throughout the entire computational domain. This process itself, can take a couple more hours. All in all, the time it takes to go from one deflection angle to another can take on the order of 5 or 6 hours to completely redefine the geometry and regenerate the computational volume. The complete data file is given in Appendix B-1.

The procedure described above serves as a very good basis for the use of the transpiration method to model these types of discontinuous deflections. In an environment where it is desired to obtain results for a number of control surface deflections, one could easily make the simple modification to the scaling factor that describes the control surface deflection angle. For example, a 0° deflection is equivalent to saying "Zero times the generalized displacement of 1° ." Similarly, for a 10° deflection, it equivalent to saying, "Ten times the generalized displacement of 1° ." It is important to note here that a positive control surface deflection angle corresponds to a downward deflection of the flap.

As in the SOLIDS definition, a series of EXCEL workbooks was set up in order to facilitate the assembly of the data file STARS uses to create the surface front. The spread sheet is set up in such a way as to automatically re-define each surface and line definition for any symmetric 4-digit NACA series airfoil cross-section. Due to the number of reference points defining the airfoil cross-section, the data file is nearly 6000 lines long. One can immediately appreciate the use of the automatic file generator for such a large number of points. For the case of the actual control surface deflection, however, the data file generation cannot be done automatically. With each deflection

angle, the intersection points discussed earlier change, so one must go through and compute the intersection points and redefine lines 24, 26, 33, 34, 36, 37, 39 and 40.

3.2.2.2 BACT Grid Specification in STARS

To this point we now have only the lines and surfaces that define the CFD geometry. Next, we need to specify the location and density of the tetrahedral elements that will define each surface and the internal volume. STARS allows one to specify point, line, or triangular sources. These sources can be thought of as sources of tetrahedral elements. Based on the specifications, tetrahedral elements will originate from the point, line, or triangle at a specified density and taper off toward larger elements based on another specification. For the BACT wing, line sources were placed along the leading and trailing edges of the wing, the upper and lower surface locations that correspond to the beginning of the control surface, and along the wing tip. An arrangement of triangular sources lie under the surfaces of the wing and control surface.

Arriving at an optimal grid density is an iterative process. One simply begins with a grid that *seems* right and iterates based on the mesh observed. With this file specified, STARS is able to assemble the mesh for each surface which can then be viewed to get a visual sense of the grid density. The resulting mesh for the BACT wing can be seen in Figure 3-10. This figure contains four different views of the surface mesh. The mesh is dense where one would expect high flow gradients, and less dense where there the flow gradients are not as sharp. Of course, it makes sense to have a more dense grid at the leading and trailing edges, at the wing tip and over the control surface region but the grid density over the upper surface of the wing seems overly dense at first glance. This is explained by the simple fact that the BACT wing was tested at transonic Mach

numbers. At a Mach number greater than Mach 0.77, transonic shocks begin to appear on the surface of the wing. As the flap rotates up and down, these shocks also translate across the surface of the wing. During flutter, as the wing pitches and plunges, the location of the shock changes once again. In a full aeroservoelastic simulation where the wing experiences each of the cases mentioned above, the location of the transonic shock can manifest itself at almost any chordwise location. Also, for this relatively low aspect ratio wing, one would expect the three-dimensional effects to be significant.

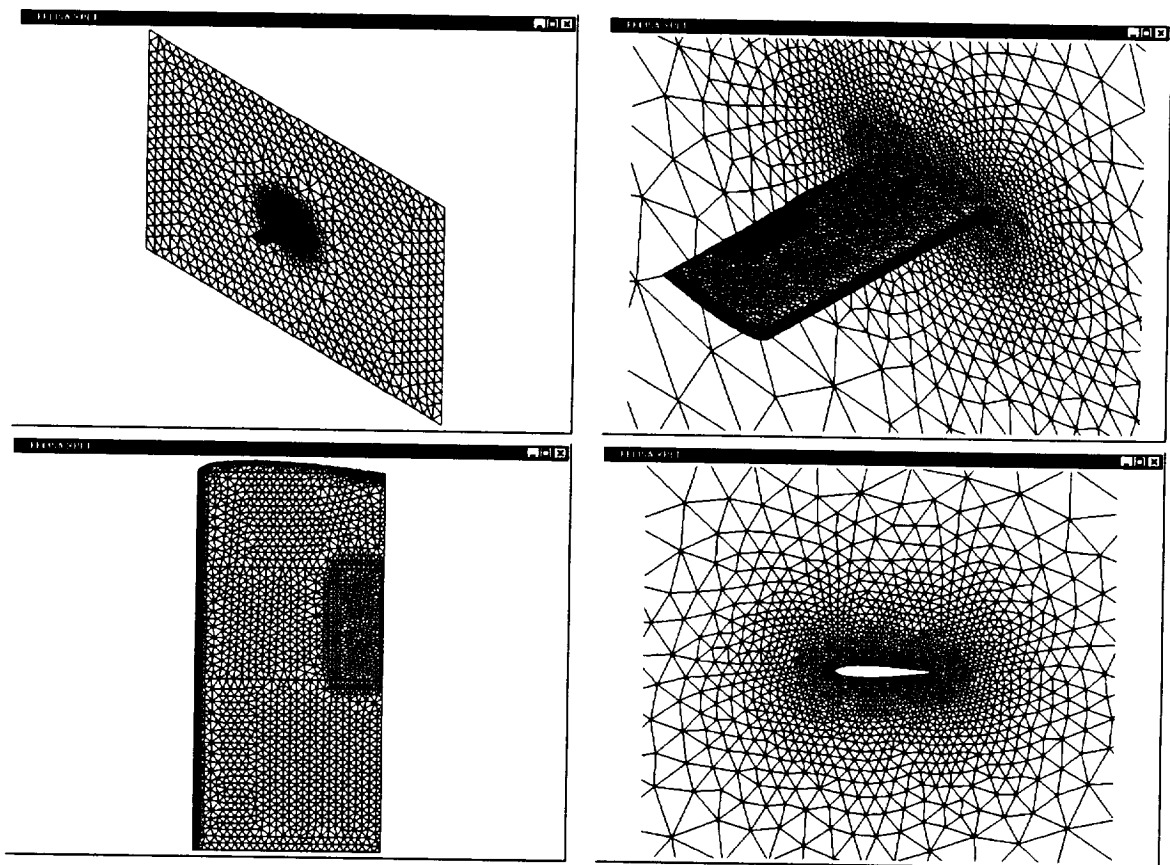


Figure 3-10: Views Showing Tetrahedral Surface Mesh on the BACT Wing

Therefore, in order to accurately capture the full three-dimensionality of the flow and the location of the transonic shocks, the grid density over the entire surface of the wing must

be kept sufficiently dense. The file containing the specifications on the location and density of the tetrahedral sources is given in Appendix B-2.

What has been constructed thus far are the wing and flow domain lines and surfaces and the surface discretization for each surface. What is lacking now are the three dimensional tetrahedra that will constitute the rest of the computational domain. What we were able to see in Figure 3-10 was the grid density on the wing and wall. Common sense dictates that the more tetrahedra one has in the flow domain, the longer the solution will take to converge. There is, therefore, a tradeoff between a sufficiently dense grid and solution time. The authors of the mesh generation code recommend Equation (3-3) as an approximation of the number of mesh points as a function of the number of surface points [Peiró, Peraire, and Morgan, 1993].

$$N'_p = C(N_p^s)^n \quad (3-3)$$

Where N'_p = Number of Mesh Nodes

C = Empirical Constant (1.62)

N_p^s = Number of Surface Nodes

n = Empirical Constant (1.15)

Table 3-2 shows a the number of surface nodes and a comparison between the number of mesh nodes resulting from running the volume generator for the BACT model, and the suggested value from (3-3). Additionally, the number of tetrahedra in the computational domain is 342,469.

Table 3-2: Actual and Suggested Number of Mesh Nodes for STARS Volume

	<i>BACT Model</i>	<i>Suggested by Eq. (3-3)</i>
Surface Nodes	8814	NA
Mesh Nodes	63902	55778

The 63,902 mesh nodes compares reasonably well with the 55,778 nodes predicted by Equation (3-3).

3.2.2.3 BACT Boundary Condition Specification in STARS

From 3.1.2 we see that the next step is to run the SETBND routine to define the boundary conditions for lines and surfaces. This routine uses the file, found in Appendix B-3, to specify walls, far-fields, symmetry planes, singularity lines, etc. STARS uses this data to assign the proper CFD boundary conditions on the nodes adjacent to the specified elements. For the BACT wing, the back wall and all of the wing surfaces are defined as *walls*. The remaining surfaces are defined with *far-field* boundary conditions. Lines along the trailing edge are defined as singularity elements. A singularity line simply defines a region in the CFD model which does not have a well defined normal, such as the trailing edge of the wing, where the upper and lower surfaces end at a sharp point, there is no way to specify a single normal. Ignoring singularities can result in abnormally high flow gradients that tend to *wash-out* the true flow physics.

The last thing that needs to be done is to specify constants that the flow solver will use throughout the solution. This is done using two files. The first is the *CONU* file. This file specifies the number of time-steps to run, the number of *inner-loops* to run at each time step and a host of other parameters. This file is given in Appendix B-4 so only those parameters that are of key interest to running a steady solution for the BACT case are discussed.

3.2.2.4 Effect of the Dissipation Parameters in STARS

Making use of the inviscid flow assumption can be problematic in the transonic flow regime. Here, transonic shocks on the surface of a wing tend to be weak. With an Euler solver, these shocks tend to be predicted later and more sharply than shown with experimental data. STARS allows the variation of a few control parameters that introduce dissipation into the numerical solution. Changing the values of $diss(1)$ and $diss(2)$ in the file *BACT.CONU*, given in Appendix B-4, had a very significant impact on the pressure distribution prediction. From their default value of 1, the constants were eventually modified to their current value of 3.5. Figure 3-11 shows the predicted pressure contours, with and without modified dissipation constants, compared to those obtained through experiment.

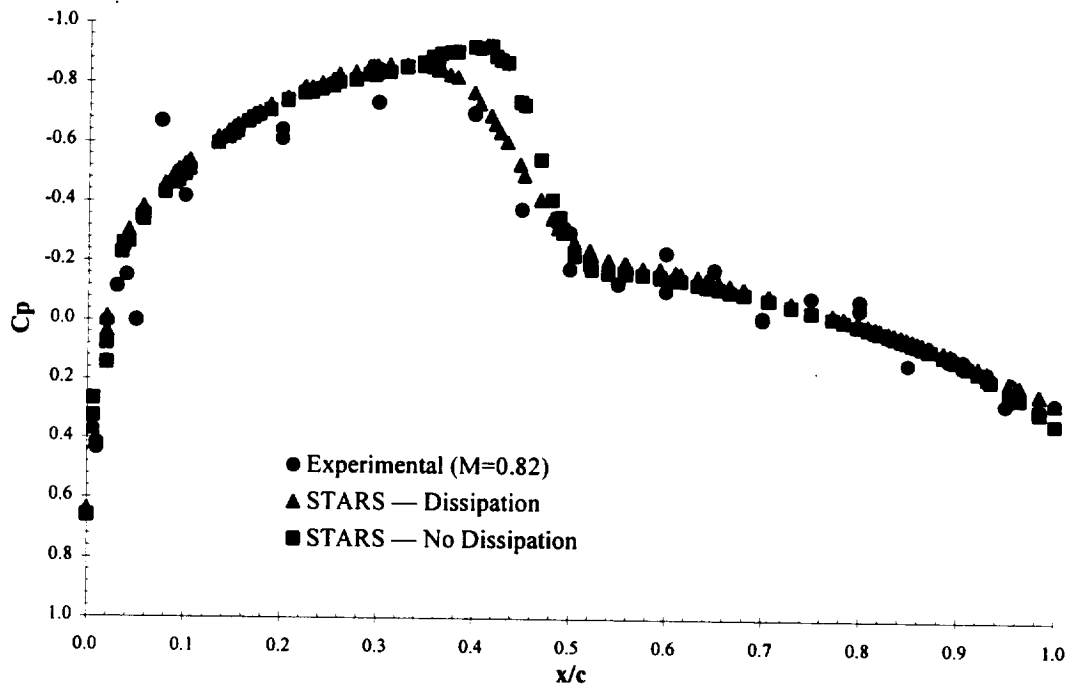


Figure 3-11: Effect of Dissipation Constants on C_p in STARS CFD Solution

As the figure illustrates, the predicted transonic shock without dissipation is predicted aft of the actual shock and is more sharp in nature. Including dissipation allows for very good agreement between experiment the STARS prediction.

Determination of the best value of the dissipation constants was an iterative process. For the range of Mach numbers at which the BACT wing was tested, the highest value of dissipation that did not cause the solution to go unstable was ~ 3.5 . Dissipation was not noted to improve the solution convergence time, which is discussed in more detail next.

3.2.2.5 Steady-State Solution Convergence Criteria

As the steady solution starts out from a given free-stream Mach number, the resulting flow-field about the geometry evolves through time. As the solution progresses STARS outputs residual values. These *residuals* are an indication of how much a flow parameter, such as density and velocity have changed since the beginning of the solution. Typically, once the residuals “become small enough”, the solution is said to have converged. What was discovered with the BACT wing, however, is that the residuals were not necessarily the best indicators of convergence. The item that ended up being the most convenient indicator of solution convergence was the maximum Mach number. The judgment of when the residuals were *low enough* was too subjective. The maximum Mach number gives a more objective view of solution convergence. To further make this point, a comparison between the two methods is given in Figure 3-12.

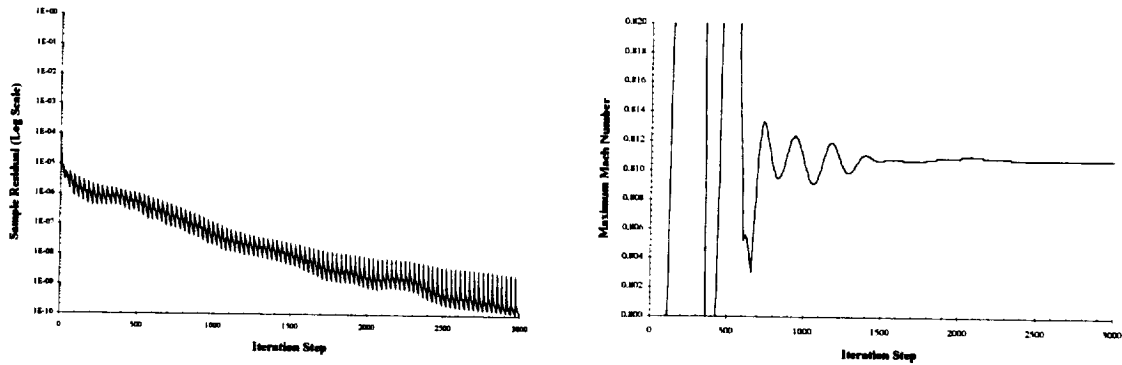


Figure 3-12: Solution Convergence Using Residuals and Maximum Mach Number

The picture on the left in the above figure shows how slowly the residual drops for a given case. Even on a log scale, there is no definite solution convergence. The picture on the right, however, clearly shows that the maximum mach number converges to one particular value.

3.2.3 BACT Uncertainty Estimation

Before the development of the aeroelastic and aeroservoelastic models are developed, one must consider the experimental uncertainty present in the BACT model. As with any experimental measurement, we expect to see a certain amount of experimental uncertainty. These experimental uncertainties, unfortunately, were not quantified for the BACT model. In an effort to determine estimates for these uncertainties, communication with Mr. Robert C. Scott and Mr. Martin R. Waszak of the NASA Langley Research Center, provided valuable insight into the uncertainty of the measurement techniques.

Since the BACT wing is considered rigid, all of the stiffness terms arrive from the use of the pitch-and-plunge-apparatus (PAPA) [Farmer, 1982]. The wing is reportedly mounted on the PAPA such that the elastic axis is coincident with the geometric center of

the PAPA mount. In the next few paragraphs, estimates in uncertainty are given for the determination of structural mass, stiffness, and damping characteristics, the location of the center of gravity relative to the elastic axis, and determination of dynamic pressure at flutter.

First, estimates in the uncertainty involved in the determination of structural stiffness and damping is covered. For a two-degree-of-freedom model, the stiffness terms of primary concern are the plunge and pitch stiffness. To measure the plunge stiffness, weights were attached at a location corresponding to the wing's mid-chord. Stiffness was then determined simply by dividing the additional weight by the resulting deflection. Similarly for the pitch stiffness, a known torque was applied about the wing's mid-chord. This known torque was divided by the resulting angular displacement in order to determine the pitch stiffness. Structural damping was determined by exciting the structure in either pitch or plunge and measuring the decay in the free-response.

Generalized mass of the pitch and plunge modes was determined from the resonant in-vacuo natural frequencies. The resonant frequencies were determined by exciting the structure in either pitch or plunge and measuring the number of cycles in a fixed time. Knowing that the natural frequency, stiffness, and mass are related by, (3-4), one can calculate the generalized mass from the measured stiffness and natural frequency. The resulting measurements from the above tests are summarized in Table 3-3. Literature only reports those values in test # 3, the author appreciates the additional data from Mr. Waszak.

$$\omega_n = \sqrt{\frac{k}{m}} \Rightarrow m = \frac{k}{\omega_n^2} \quad (3-4)$$

Table 3-3: Experimental Measurements in Structural Parameters

Test #	K_h (lb/ft)	K_α (ft·lb/rad)	g_h	g_α	ω_h (Hz)	ω_α (Hz)	M (Slug)	I_α (Slug·ft ²)
1	2659	2897	0.0015	0.0016	3.364	5.257	6.01	2.75
2	2637	2964	0.0015	0.0018	3.360	5.302	6.03	2.70
3	2686	3000	0.0014	0.0010	3.344	5.208	6.08	2.80

Recall that the Benchmark Models Program at NASA Langley involved tests on both a NACA 0012 wing as well as the BACT wing, both tested and mounted on the PAPA with the wing's mid-chord nearly coincident with the elastic axis. The two wings had the same chord, span, airfoil cross-sections, and experimental instrumentation layout. The only external differences that exist are small geometric defects, and the presence of three control surfaces. Internally, a portion of the material had to be removed for the installation of actuators etc. Despite the material removed to add the actuators and spoilers and separate the trailing edge control surface, structural characteristics are very similar between the two. Rivera and others report the values shown in Table 3-4 for the structural properties of the NACA 0012 wing and PAPA mount [Rivera, et al. 1991 & 1992].

Table 3-4: Experimental Measurements in Structural Parameters

Test	K_h (lb/ft)	K_α (ft·lb/rad)	g_h	g_α	ω_h (Hz)	ω_α (Hz)	M (Slug)	I_α (Slug·ft ²)
3/92	2659	2897	0.0024	0.0024	3.36	5.20	5.966	2.714
7/91	2697.2	2854.6	0.0034	0.0016	3.40	5.18	5.910	2.7695

Recall that values shown in Table 3-3 were obtained from the BACT wing and PAPA mount. Comparing these values, we see that the tables are very similar. This would seem to indicate that the physical differences between the model should be essentially negligible.

Next, experimental uncertainty in the determination of the center of gravity (CG) relative to the elastic axis (EA) proves to have a *very* significant effect on the prediction of the flutter boundary. In the literature, the CG's location relative to the elastic axis was reported, at best, to be nearly coincident with the mid-chord of the wing. Waszak reports the value of the inertial coupling between the pitch and plunge modes ($S_{h,\alpha}$) as being 0.0142 slug·ft. Using (3-5) below, we can estimate the relative location of the CG to the EA.

$$S_{\alpha} = m \cdot x_{cg} \quad (3-5)$$

Using the value of S_{α} reported by Waszak (1996), and the mass, we calculate that the distance from the EA to the CG is 0.028 inches. After communication with Mr. Waszak, he stated that his reported value of 0.0142, which was well within experimental uncertainty, had to be used to account for the slight difference between his computational model and experimental data.

The presumption that the CG and EA are coincident comes from qualitative observations made during testing at the NASA Langley Research Center. When measuring the plunge stiffness, weight was applied at the mid-chord of the wing. During these tests, there was no reported difference in the displacements of the leading and trailing edges indicating the absence of static coupling. Similarly, during measurement of the pitch stiffness, no static coupling was observed. In order to excite the pitch and plunge frequencies, the BACT wing and PAPA mount were excited by an initial deformation that was suddenly removed to allow the structure to vibrate freely. This was done in a manner similar to the static loading, at the mid-chord for plunge and about the mid-chord for pitch. The free vibration of the model excited in this way showed very

little pitch motion when excited in plunge in very little plunge motion when excited in pitch. This, of course, implies that the CG must be very close, if not coincident with the mid-chord. As an approximation, the relative location of the CG and the EA was estimated to be no more than 0.1 inches, or 0.625% of the chord.

From the above data, it is possible to construct a simple model from which we could quickly evaluate the importance of some of the above parameters. Using a simplified aerodynamic model and solving the equations of motion using the p -method, we can quickly solve for the divergence speed. Since the flutter speed can be solved for explicitly in the p -method, parametric studies can be done very quickly. Shown below in Figure 3-13 we see the effect of three different parameters on the flutter prediction.

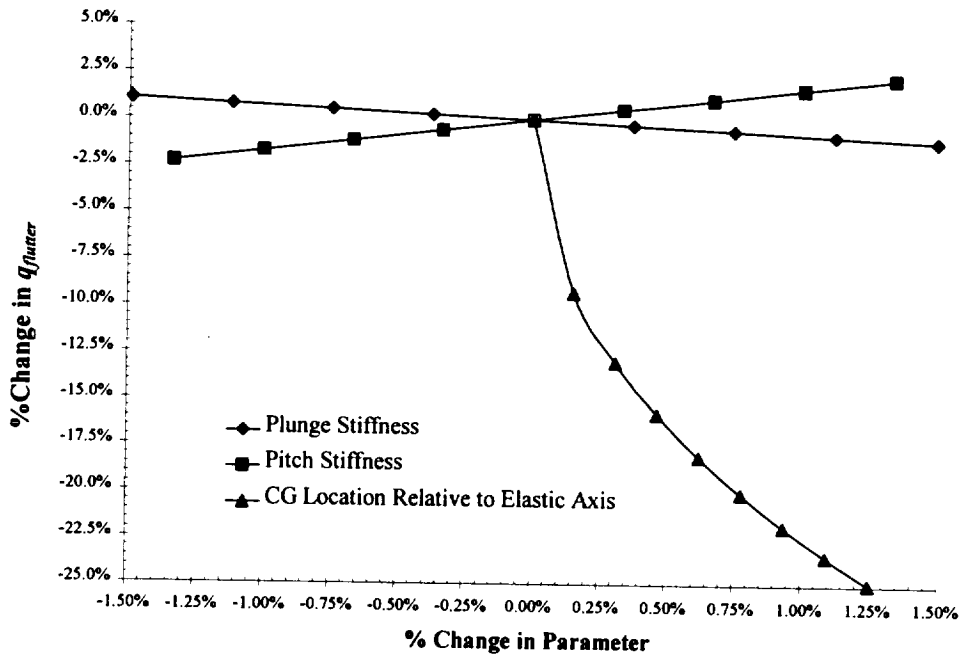


Figure 3-13: Effect of K_h , K_α , and x_{cg} Location on Flutter Prediction

In the above figure, the x axis represents small deviations from nominal values for plunge and pitch stiffness, K_h and K_α , and x_{cg} , which is a measure of the distance from the elastic

axis to the center of gravity, measured positive aft. As is shown, small changes in both plunge and pitch stiffness effect little change in the flutter prediction, $\sim\pm 2.5\%$. Small changes in x_{cg} , however, influence the flutter prediction significantly. Using the above model, changes in x_{cg} on the order of 1% can change the flutter prediction by over 20%.

Now, having the BACT's CG location specified as *nearly coincident* with the elastic axis introduces a slight difficulty in flutter prediction using STARS. For comparison with experimental data, small variations in each of these parameters can add up to large differences in flutter prediction. In addition to all of these differences, there is still the matter of determining the actual flutter point. Looking at time traces of experimental data, it is often difficult to tell exactly when the system is going unstable. Mr. Waszak estimated that the dynamic pressures that defined the flutter boundary were measured to within $\pm 2 \text{ lb/ft}^2$.

Knowledge of these and other uncertainties is fundamental to appreciating the degree to which the computational model can approximate the experimental data. When developing an aeroelastic model, we must assume that the wing is exactly rectangular, perfectly symmetric, its cross-section exactly matches that of a NACA 0012 airfoil, its mass, damping, and stiffness, and the coupling between each, is known precisely, etc. One can quickly appreciate the amount of *tolerance buildup* that is present in the experimental data. These small, relatively unknown, differences translate into a lot of *fine-tuning* of the computational model. In work presented by Waszak, flutter prediction within 7% of experimental data was considered "...pretty good..." [Waszak, 1998].

3.2.4 BACT Aeroelastic/Aeroservoelastic Development

From 3.2.1, 3.2.2, and 3.2.3, we now have a solids model with three specified mode shapes, a CFD model, and an appreciation of the experimental uncertainty involved in the aeroelastic data. As developed previously, aeroelasticity is the coupled response of the two aforementioned models. From section 3.2.2 we have the capability of producing a steady CFD solution from which to begin an unsteady simulation. Next, the mode shapes specified in the SOLIDS module for the finite element structural mesh must be interpolated to the CFD mesh. Using the orthogonal property of the natural mode shapes, a superposition of these natural mode shapes can be used to represent an arbitrary structural deformation.

As mentioned previously, if the natural frequencies, mode shapes and other structural properties are known beforehand, they may be entered manually into STARS. Before the interpolation begins, STARS must know which surfaces represent moving boundaries. This is done with information contained inside the file BACT.SCALARS, given in Appendix B-5. This file contains a variety of other parameters of interest to the unsteady solution, but those are not of particular interest and will not be covered. When the interpolation from the SOLIDS mesh to the CFD mesh occurs it creates an *ARRAYS* file. This file contains information regarding the natural frequencies for each mode shape, the generalized mass, stiffness, and damping matrices and nodal displacements for each CFD node which represent nodal displacements on surfaces in the CFD mesh for each mode shape. The BACT case has 3 modes: plunge, pitch, and a control mode that represents the moving control surface. The mass, stiffness, and damping matrices are therefore 3x3 matrices. There are three sets of nodal displacement, or AERO vectors,

one for each mode that specify the generalized displacement of each CFD node for each mode shape. Only the top portion of the BACT.ARRAYS file is given in Appendix B-6 because the file is over 26,000 lines long.

In STARS, the mass, damping and stiffness matrices were manually entered into the BACT.ARRAYS file such that they matched those reported in test #3 for the BACT wing. Since geometric data was entered into stars in units of inches, units of mass are in slinches as opposed to slugs. Where a slug has dimensions of $\text{lbf}\cdot\text{s}^2/\text{ft}$, a slinch has dimensions of $\text{lbf}\cdot\text{s}^2/\text{in}$. The conversion is, therefore, $1 \text{ slinch} = 12 \text{ slug}$. Observing the plunge equation we encounter no dimensional conflict within STARS. Noting the moment equation, (3-6)-(3-13), we see the possibility for a slight discrepancy. Beginning with the general equation for the moment in (3-6) we see the following.

$$I\ddot{\alpha} + \beta\dot{\alpha} + K\alpha = M \quad (3-6)$$

The moment is simply the integral of The moment is simply the integral of the pressure times the mode shape, so substituting this into (3-6) we arrive at (3-7).

$$I\ddot{\alpha} + \beta\dot{\alpha} + K\alpha = \int p\phi dx \quad (3.7)$$

In STARS, however, we have the following definition, shown in (3-8).

$$\int p\phi dx = M\alpha_0 = \alpha_0 \int p\phi dx \quad (3.8)$$

Where α_0 , is the generalized pitch displacement of 1° . Rearranging the equations, we get STARS definition of the pitch moment in (3-9).

$$\alpha_0 I\ddot{\alpha} + \alpha_0 \beta\dot{\alpha} + \alpha_0 K\alpha = \int p\phi dx \quad (3.9)$$

Solution of (3-9) assumes α in units of radians, so using (3-10) we must convert the angular displacements and velocities displacements into dimensional form consistent with the generalized displacement.

$$\alpha = \frac{\pi}{180} q = \alpha_0 q \quad (3.10)$$

We can now substitute this relation back into (3-9) and obtain (3-11).

$$\alpha_0 I \left(\frac{\pi}{180} \ddot{\alpha} \right) + \alpha_0 \beta \left(\frac{\pi}{180} \dot{\alpha} \right) + \alpha_0 K \left(\frac{\pi}{180} \alpha \right) = \int p \phi dx \quad (3-11)$$

Now, units are consistent on both the left and right-hand sides and can be arranged into a more convenient form, shown in (3-12).

$$\left(\alpha_0 \frac{\pi}{180} I \right) \ddot{\alpha} + \left(\alpha_0 \frac{\pi}{180} \beta \right) \dot{\alpha} + \left(\alpha_0 \frac{\pi}{180} K \right) \alpha = \int p \phi dx \quad (3-12)$$

Remembering that the generalized pitch displacement was 1° or $\pi/180$ radians we can go ahead and multiply the generalized displacement by the $\pi/180$ factor and obtain (3-13).

$$\left(\frac{\pi^2}{180^2} I \right) \ddot{\alpha} + \left(\frac{\pi^2}{180^2} \beta \right) \dot{\alpha} + \left(\frac{\pi^2}{180^2} K \right) \alpha = \int p \phi dx \quad (3-13)$$

Since generalized displacements for the wing and flap are specified as 1° , parameter entry into the system matrices within STARS requires a pre-multiplication by $\pi^2/180^2$. Note that this problem was not encountered for the plunge degree of freedom since both the generalized displacement and mode-shape are in inches.

Shown below in (3-14) is the mass matrix that is entered into the *BACT.ARRAYS* file. Notice that rows 2 and 3 are pre-multiplied by the $\pi^2/180^2$ scaling factor.

$$\begin{bmatrix} m & S_{h,\alpha} & S_{h,\delta} \\ \frac{\pi^2}{180^2} S_a & \frac{\pi^2}{180^2} I_a & \frac{\pi^2}{180^2} S_{\alpha,\delta} \\ \frac{\pi^2}{180^2} S_{h,\delta} & \frac{\pi^2}{180^2} S_{\alpha,\delta} & \frac{\pi^2}{180^2} I_\delta \end{bmatrix} \quad (3-14)$$

- Where:
- m — Generalized Mass (Plunge)
 - I_α — Generalized Mass (Pitch)
 - I_δ — Generalized Mass (Control Surface)
 - $S_{h,\alpha}$ — Plunge-Pitch Inertial Coupling Term
 - $S_{h,\delta}$ — Plunge-Control Surface Inertial Coupling Term
 - $S_{\alpha,\delta}$ — Pitch-Control Surface Inertial Coupling Term

Similarly, the damping matrix is shown in (3-15):

$$\begin{bmatrix} g_h & 0 & 0 \\ 0 & \frac{\pi^2}{180^2} g_\alpha & 0 \\ 0 & 0 & \frac{\pi^2}{180^2} g_\delta \end{bmatrix} \quad (3-15)$$

- Where
- g_h — Generalized Plunge Damping
 - g_α — Generalized Pitch Damping
 - g_δ — Generalized Control Surface Damping

In the above relationships, g is defined to be $M \cdot 2 \cdot \zeta \cdot \omega_n$, where M , ζ , and ω_n are the appropriate generalized mass, damping, and natural frequency.

$$\begin{bmatrix} k_h & 0 & 0 \\ 0 & \frac{\pi^2}{180^2} k_\alpha & 0 \\ 0 & 0 & \frac{\pi^2}{180^2} k_\delta \end{bmatrix} \quad (3-16)$$

As mentioned earlier, the uncertainty present in the BACT affects the values that are entered into (3-14) to (3-16). From the sensitivity study, we saw that the most sensitive uncertainty exists in the specification of the pitch-plunge coupling term S_α since this related directly to x_{cg} as discussed in the previous section. Final system matrices were obtained after *fine-tuning* the parameters and are given in Table 3-5.

Table 3-5: BACT Model Parameters in STARS

Generalized Mass Matrix		
0.50667	0.0506667	0.00288
0.154339×10^{-4}	0.0102350	0.57390×10^{-5}
0.877298×10^{-6}	0.57390×10^{-5}	0.40134×10^{-1}

Generalized Damping Matrix		
0.029819	0.0	0.0
0.0	0.66985×10^{-3}	0.0
0.0	0.0	0.0

Generalized Stiffness Matrix		
0.223833×10^5	0.0	0.0
0.0	0.109500×10^2	0.0
0.0	0.0	0.1096623×10^4

3.2.4.1 Time-Step Definition in STARS

The time-step used in STARS is computed using (3-17) where the parameters *freq* and *nstpe* are defined in the *CONU* file, *M* is the free-stream Mach number and *a* is the sonic velocity.

$$dt = \frac{2\pi}{freq \cdot nstpe \cdot (M \cdot a)} \quad (3-17)$$

Until recently, there has been no prescribed method of determining the time-step. A generally accepted rule-of-thumb was to make certain that at a single period of oscillation at the highest frequency was made up of at least 30-40 time-steps. For supersonic cases,

this seems to work just fine. In subsonic flow, however, wake effects are propagated throughout the entire computational domain. More recently, *freq*, is defined to be similar to the highest natural frequency in the SOLIDS model. The parameter *nstpe* can then be thought of as the number of time steps per period of oscillation. One can also look at this another way. In STARS, the default value of *nstpe* is 1. Instead of letting *freq* represent the highest frequency, it may be arbitrarily set such that one obtains an equivalent time-step within STARS. Either method works equally well, but letting *freq* represent a true frequency and increasing the number of steps per period (*nstpe*), makes more intuitive sense.

For proper flow dynamics, the user is concerned with the number of *inner* CFD iterations per time step (*ncycl*), and the length of the time-step. A recent investigation in STARS with a simple NACA 0012 airfoil provided valuable insight into the relative importance of *ncycl* and *dt*. The study was done using the problem of a suddenly accelerated wing in subsonic flow (Wagner Problem) where the lift and drag are time-evolving parameters. While changing the parameters *ncycl* and *dt*, plots of the changing lift were obtained and plotted vs. a non-dimensional time parameter. Each of the following plots were obtained for an impulsively started NACA 0012 airfoil at Mach 0.3 at $\alpha=5^\circ$.

As Figure 3-14 demonstrates, for a given value of *ncycl* the time varying lift is highly dependent on the size of the time-step. The disadvantage of going with a small time step is, of course, the fact that it will require additional computational time to run an equivalent job which incorporates the larger time step.

Another option is to keep the time-step the same, but let the CFD solver perform more iterations at each time-step. This case is demonstrated in Figure 3-15 where we see the effect of time step on differing values of *ncycl*. Shown here is, again, a high degree of sensitivity to the size of the time-step for a given value of *ncycl*. For the time-step of 0.1 in the upper plot, changing the value of *ncycl* shows a definite effect. The lower plot shows that for a much smaller time step, 0.025, the plots of *Cl* vs. *t** are virtually identical despite the fact that values of *ncycl* differ by a factor of 4. The conclusion, therefore, is that the importance of a *small* time-step outweighs the importance of increasing the number of CFD iterations per time-step.

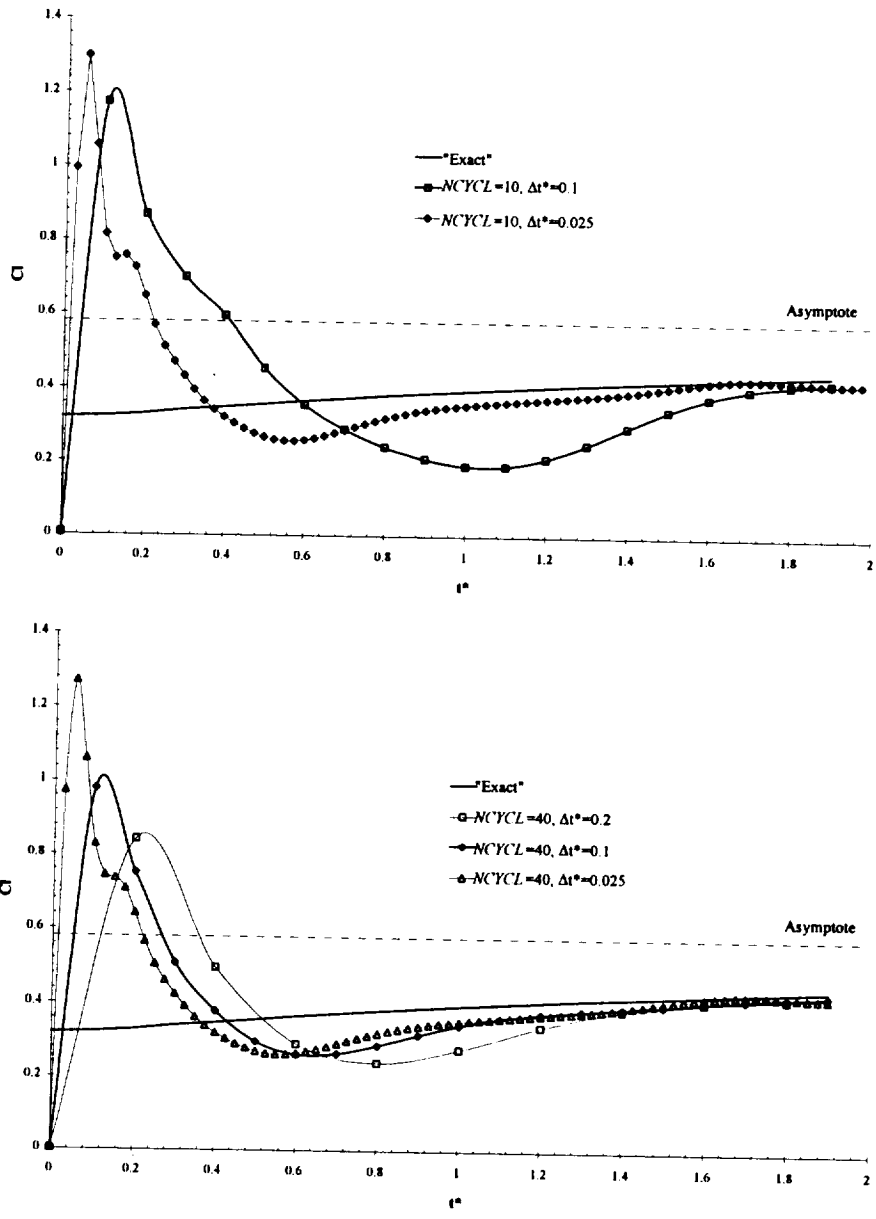


Figure 3-14: Effect of Time-Step at Two Different Values of n_{CYCL} on the Lift Evolution for an Impulsively Started NACA 0012 Airfoil at Mach 0.3, $\alpha=5^\circ$

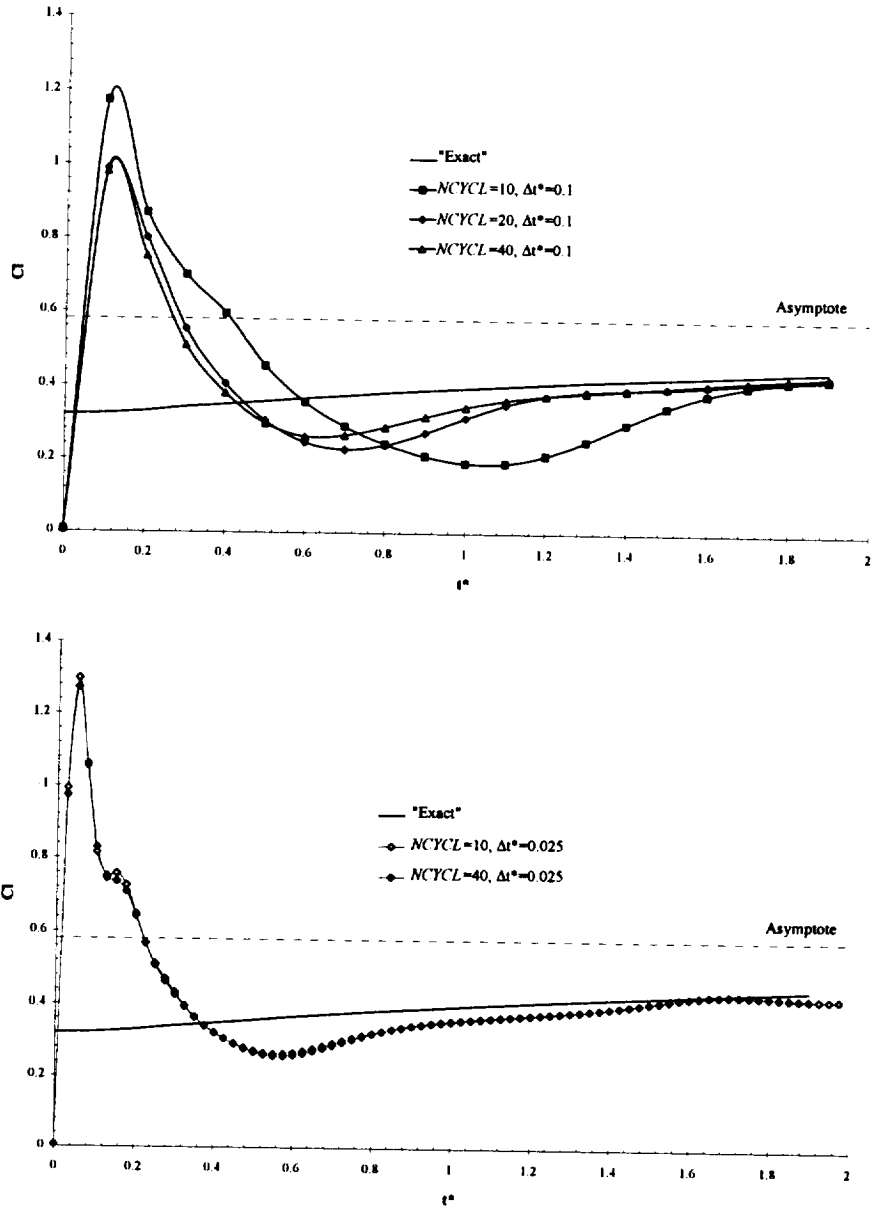


Figure 3-15: Effect of *ncycl* with at Two Different Time-Steps on the Lift Evolution for an Impulsively Started NACA 0012 Airfoil at Mach 0.3, $\alpha=5^\circ$

To begin the ASE simulation, we must have first generated the *ARRAYS* file and completed a steady state CFD solution at the reference Mach number. Once the parameters are set in the *SCALARS* file, and the *CONU* file is configured properly, an ASE solution may be started. The length of the solution is determined primarily by parameters in the *CONU* file. There are a lot of parameters set in this file, but for the

ASE simulation, we are primarily concerned with the values of *nstep* and *ncycl*. The total number of time-steps is specified with *nstep*. The number of inner CFD iterations per time step is specified with *ncycl*. For instance, with *nstep* = 500, and *ncycl* = 40, the ASE simulation would last for a total of 500 *outer* time steps. At each *inner* time-step, 40 CFD iterations are allowed for the computation of the new aerodynamic forces. All together, these parameters specify that 500×40 CFD iterations.

3.2.4.2 Modal Identification Technique

With each CFD iteration taking on the order of 30 seconds, we quickly see how time-consuming these ASE simulations are. For the BACT, the *nstep* and *ncycl* were generally 5000 and 40. Assuming 30 seconds per CFD step and doing the math, we estimate that an EULER solution for a single transient may take on the order of 69 days on an IBM RS6000 3BT. The general procedure required that the solution be monitored and when the time-histories *looked* to be going unstable, assume that is the flutter point and kill the solution. The nature of the BACT system makes this method impractical. Observe the following figure which is a portion of an actual time-history obtained from STARS.

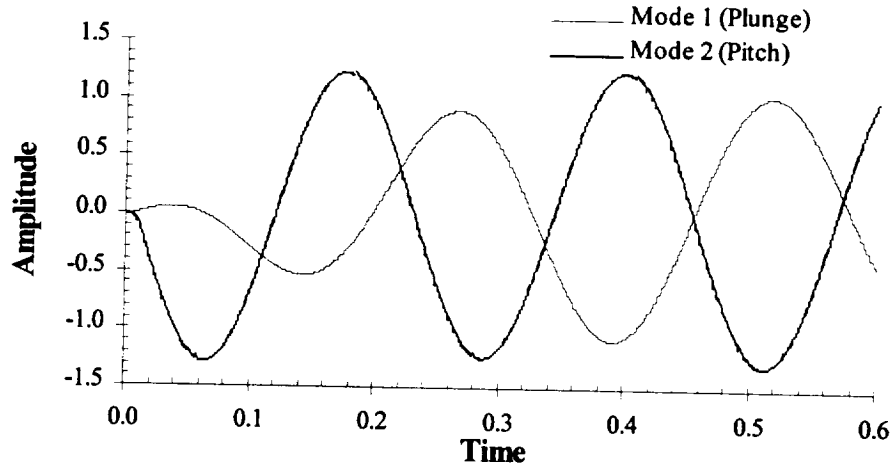


Figure 3-16: Abbreviated Time-History of BACT Wing in STARS

From Figure 3-16, it appears that the solution is going unstable. Typically, that would have been considered *good enough* but allow the solution to continue for the full 5000 time-steps and we obtain the following time-history.

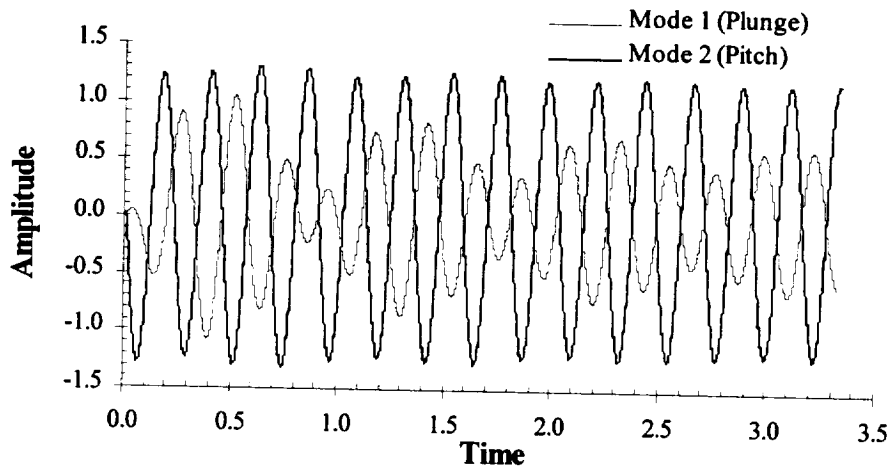


Figure 3-17: Complete 5000-Step Time-History of BACT Wing in STARS

Allowing the solution to continue for the full 5000 steps, Figure 3-17 shows that mode 1 exhibits a slight amount of damped-beating while mode 2 is lightly damped, therefore not

yet at the flutter point. Beyond visual interpretation, a modal identification technique provides damping characteristics for each structural mode [Eckhart, 1998]. Given a time-history from STARS, this tool provides the user with both a damping frequency and damping factor.

3.2.4.3 System Identification Technique

For each flutter point, one must generally take a trial-and-error approach in the determination of the flutter point. Trials are made until dynamic pressures on each side of the flutter point are obtained. This is, of course, very time consuming. The determination of a complete flutter boundary for a problem of this type could easily take several months. Recent work by Cowan, allows the use of a system identification procedure to model the coupled structural/CFD system. [Cowan, 1998]. This has the significant benefit of accelerating the time required for a full ASE simulation. Essentially eliminating the CFD solver, which makes up the vast majority of time during a coupled simulation, and replacing it with an algebraic transfer function reduces ASE run-times from days and months to minutes. For the same 5000 step solution described previously, an ASE simulation is obtained in about 5 minutes, as opposed to 69 days.

This system identification procedure is currently implemented into the STARS and provides a very accurate prediction of the full Euler solution. To model the system, each mode is displaced from an initially steady-state CFD solution through a known input referred to as a multi-step. Forcing the CFD model with these known modal inputs during an Euler solution allows STARS to compute the aerodynamic forces due to these known inputs. The system identification procedure then constructs an ARMA model based on the known inputs and resulting outputs. Once the system is modeled, the Euler

aerodynamic solver is essentially “replaced” with a much faster system of algebraic equations.

The multi-step sequence used on the BACT wing is given in Figure 3-18 and specified with parameters in the *SCALARS* file. The duration of the multi-step is determined by the following equation: $5 + isize(4nr + 3)$, where *isize* is the magnitude of the multi-step and *nr* are the number of modes to be excited. For the BACT, *isize* and *nr* were generally set as 10 and 3, respectively resulting in a duration of 155 time-steps. The actual CFD solution extended to 240 time-steps to insure that all of the aerodynamics have enough time to come to steady-state values.

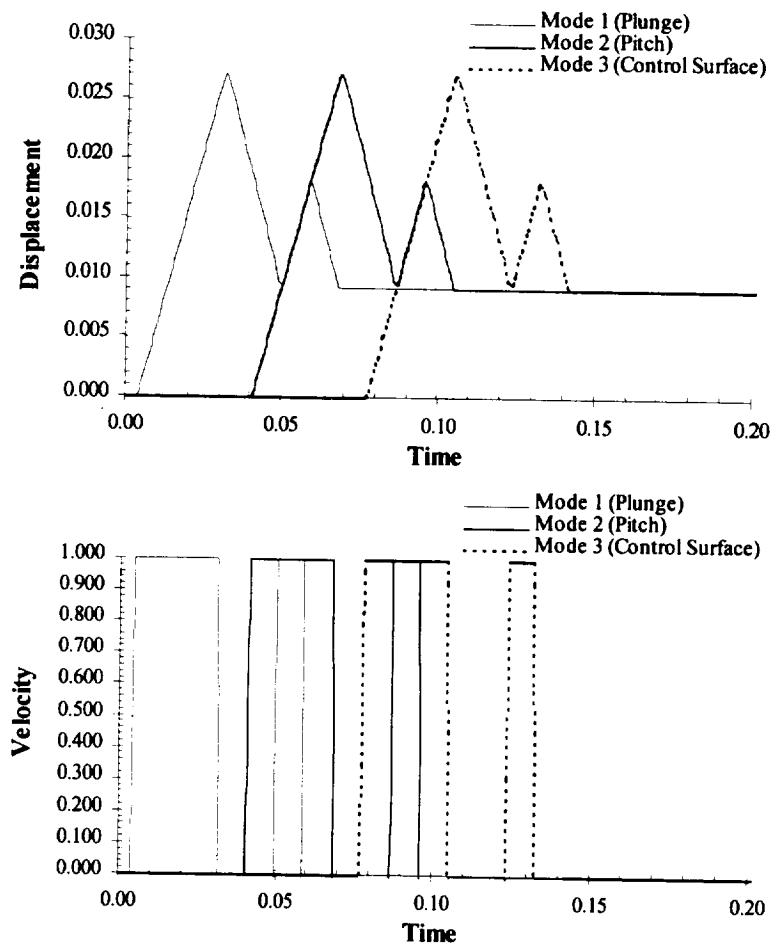


Figure 3-18: Multi-Step Sequence for the BACT Wing (3-Modes)

Notice that each mode is forced to undergo a displacement resulting from a specified velocity. These displacements and velocities, through the transpiration method, are implemented as unsteady boundary conditions in the CFD flow solver. The resulting aerodynamic forces and moments resulting from this sequence of events are then modeled. The extent to which these models actually fit the data is described in more detail in Chapter 4, but Figure 3-19 shows a comparison of the actual and modeled response to the multi-step shown previously.

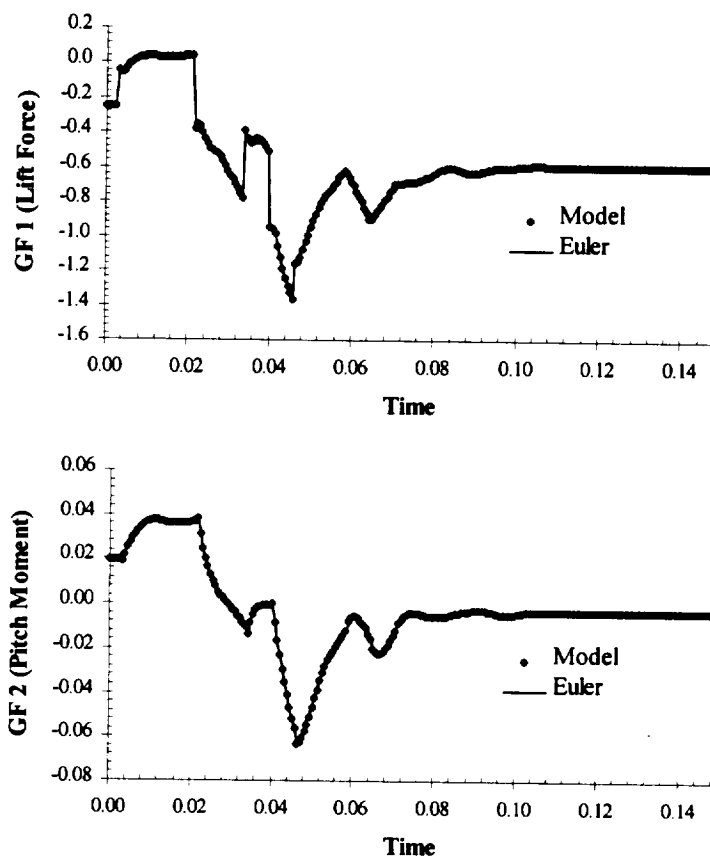


Figure 3-19: Modeled and Actual Response to Multi-Step Input

Similar results are obtained for all other Mach numbers under consideration and are given in Chapter 4. Further validation and references are found in the original work by Cowan.

3.2.4.4 Control Law Development

The final objective of the current work is to use the trailing edge control surface on the BACT wing as a means of flutter suppression. In a paper by Waszak, the BACT wing is modeled at Mach 0.77 in a MATLAB program [Waszak, 1996-97]. The program developed essentially provides the user with a state-space representation of the BACT/PAPA system at a user-defined q at Mach 0.77. Using only a portion of the program, models of the BACT/PAPA system were obtained at three different dynamic pressures: a little below, close to, and beyond the flutter point. The resulting state-space system was then condensed down into a single *group* in SIMULINK. Shown in Figure 3-20 is the complete model developed with its core element being the q -dependant state-space model obtained from the MATLAB program.

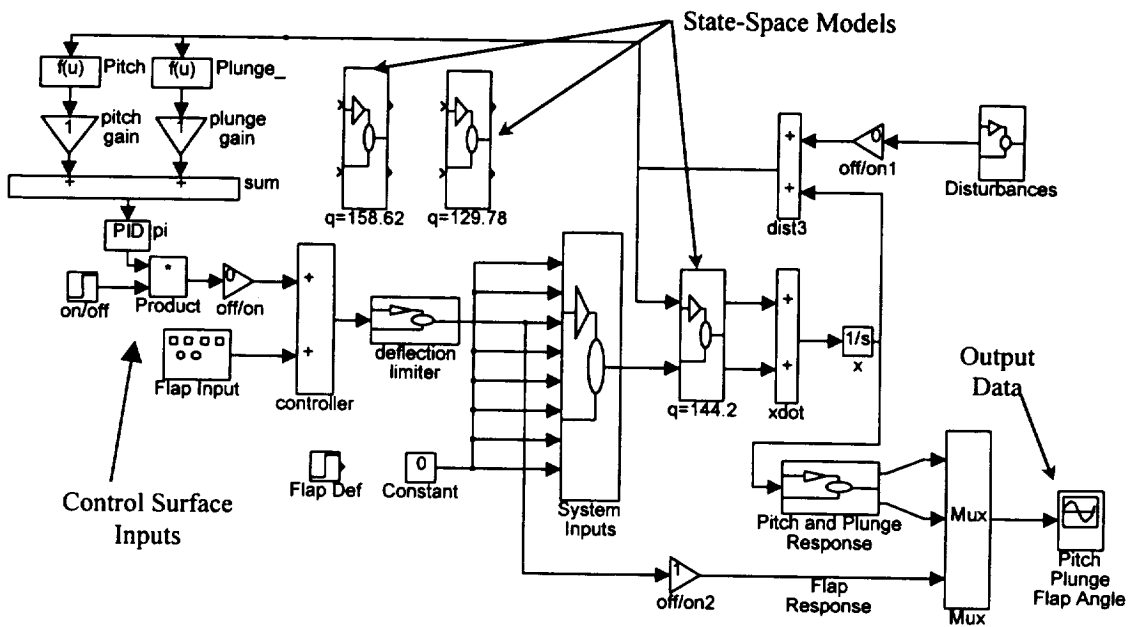


Figure 3-20: MATLAB/SIMULINK® Model of BACT with Control

While looking complicated, this is a relatively simple block diagram of the entire system. The entire diagram basically consists of four parts: state inputs and outputs, disturbance inputs, controllable and control surface inputs, and a means of viewing the output. In the center of the diagram is the BACT/PAPA system with its associated inputs and outputs. In the upper right are the disturbance inputs from which one may *disturb* pitch, plunge, and a host of other parameters. The upper left of the figure is essentially the control portion of the diagram, where the deflection of the control surface is controlled through simple P, PI, PD, or PID control based on pitch and/or plunge rates or displacements. Left of center are separate control surface inputs. If control is turned off, arbitrary control surface displacements, sine waves etc., can be input into the system. The lower right-hand-side of the figure contains blocks that display pitch, plunge, and control surface deflection as a function of time. This tool was used to gain an understanding of the effectiveness of different control laws before their implementation into STARS.

Shown below in (3-18) and (3-19) are the equations for lift and moment of the BACT/PAPA system employed in the model shown above.

$$L = qSC_L = qS \left[C_{L_0} + C_{L_\alpha} \alpha + C_{L_\delta} \delta + \frac{\bar{c}}{2U_0} (C_{L_\alpha} \dot{\alpha} + C_{L_q} \dot{\theta} + C_{L_\delta} \dot{\delta}) \right] \quad (3-18)$$

$$M = qS\bar{c}C_M = qS\bar{c} \left[C_{M_0} + C_{M_\alpha} \alpha + C_{M_\delta} \delta + \frac{\bar{c}}{2U_0} (C_{M_\alpha} \dot{\alpha} + C_{M_q} \dot{\theta} + C_{M_\delta} \dot{\delta}) \right] \quad (3-19)$$

Static aerodynamic parameters were obtained from experimental data and previous wind-tunnel experiments, force and moment data at various angles of attack and control surface positions were used to compute most of the stability and control derivatives, while dynamic derivatives were obtained from computational analysis. Parameters unknown or unavailable were assumed to be zero.

Though simplified through modeling assumptions, the model proved to be a very useful tool in obtaining quick qualitative data regarding flutter suppression using the trailing edge control surface. Despite the quality of this data, the majority of ASE simulation was conducted in STARS since the modeling simplifications are not a limiting factor. Of particular interest are the additional aerodynamic mass and damping terms that result from the plunging motion of the wing and the effect on lift and moment due to the rate at which the control surface deflects.

In general, any control law will have as its output a desired flap position. Waszak reports the control surface actuator's transfer function as (3-20) where k (1.02 deg/deg) is the actuator gain, ζ (.56) is the damping ratio, ω (rad/sec) is the natural frequency, δ_s is the desired control surface deflection, and δ is the actual resulting deflection.

$$\frac{\delta}{\delta_s} = \frac{k\omega}{s^2 + 2\zeta\omega s + \omega^2} \quad (3-20)$$

For our purpose, however, it is more convenient to move from the frequency domain back to the time domain. The corresponding differential equation is shown in (3-21).

$$\ddot{\delta} + 2\zeta\omega\dot{\delta} + \omega^2\delta = k\omega^2\delta_s \quad (3-21)$$

To begin putting the above equation into state-space format, we'll make the following substitutions: $x_1 = \delta$ and $x_2 = \dot{\delta} = \dot{x}_1$. Taking derivatives of these equations results in the following: $\dot{x}_1 = \dot{\delta} = x_2$ and $\dot{x}_2 = \ddot{\delta} = \ddot{x}_1$. Using these relationships, we re-write (3-21) in the following form: $\dot{x}_2 + 2\zeta\omega x_2 + \omega^2 x_1 = k\omega^2 \delta_s$. We now have two first-order differential equations which we can write in state-space format, see (3-22).

$$\begin{bmatrix} \dot{x}_1 \\ \dot{x}_2 \end{bmatrix} = \begin{bmatrix} 0 & 1 \\ -\omega^2 & -2\zeta\omega \end{bmatrix} \begin{bmatrix} x_1 \\ x_2 \end{bmatrix} + \begin{bmatrix} 0 \\ k\omega^2 \delta_s \end{bmatrix} \quad (3-22)$$

To actually implement these equations into STARS, the time-derivatives are replaced by the following relationships shown in (3-23) and (3-24) where n is the current value, and $n-1$ represents past values.

$$\frac{x_1^n - x_1^{n-1}}{\Delta t} = x_2^{n-1} \quad (3-23)$$

$$\frac{x_2^n - x_2^{n-1}}{\Delta t} = k\omega^2 \delta_s - 2\zeta\omega x_2^{n-1} - \omega^2 x_1^{n-1} \quad (3-24)$$

Solving each for the current values of x_1 and x_2 yields (3-25) and (3-26).

$$x_1^n = x_1^{n-1} + x_2^{n-1} \Delta t \quad (3-25)$$

$$x_2^n = (k\omega^2 \delta_s - 2\zeta\omega x_2^{n-1} - \omega^2 x_1^{n-1}) \Delta t + x_2^{n-1} \quad (3-26)$$

Up till this point, the desired control surface position has been arbitrary. For our purpose, the desired flap angle will be a function of plunge displacement and velocity, and angular displacement and velocity. The resulting control law is shown in (3-27), where the gains K_i are not necessarily absolute. Given the range of Mach numbers, it is assumed that some sort of gain-scheduling, based on both Mach number and dynamic pressure, is needed.

$$\delta_s = K_1 h + K_2 \dot{h} + K_3 \theta + K_4 \dot{\theta} \quad (3-27)$$

The resulting gains and time-histories for a variety of Mach numbers are described further in Chapter 4.

CHAPTER 4

RESULTS

It is the intent of the current effort to demonstrate the effectiveness of the transpiration method in its application to steady and unsteady flow conditions. Based on these results, the implementation of a discrete-time control law within STARS is discussed in regard to active flutter-suppression for the BACT wing. In a logical series of steps, this chapter will present results starting with steady-flow simulations, which include the effects of a deflected control surface, eventually leading up to both the open and closed-loop aeroservoelastic response. Where available, comparisons are made to experimental data.

4.1 Steady Results Without Control Surface Deflections

The starting point of all unsteady cases in STARS, the steady state solution, must be fully converged before starting an unsteady job. For the final CFD mesh on the BACT wing, the steady solution was run for 3000 steps to assure that the solution had, in fact, converged to a steady state value. Convergence was assured using the maximum Mach number criterion discussed in section 3.2.2.5. Experimental data are available for the majority of test cases discussed in this section.

Remembering that the BACT CFD model is actually the CFD model for both the NACA 0012 wing as well as the BACT wing, the differences between the two should be

noted here. With an undeflected control surface, there should be no difference between the two models since they are geometrically similar. Aside from slight manufacturing differences, however, the two models were tested in a different fluid medium. The NACA 0012 wing was tested in air ($\gamma=1.4$) and the BACT wing was tested in R-12 ($\gamma=1.148$). As far as the calculation of the pressure coefficient is concerned, the value of the ratio of specific heats, γ , acts only as a scaling factor in steady simulations. Experimental steady data presented here comes from pressure transducers located at the NACA 0012 wing's 60% span [Rivera, et al, 1992]. More significant later, this 60% span location corresponds to a distance of 19.2 inches from the wings root which, for the BACT wing, corresponds to the mid-span of the control surface.

The next six figures, Figure 4-1 to Figure 4-6, show steady pressure data obtained at Mach numbers of 0.51, 0.67, 0.71, 0.77, 0.80, and 0.82, respectively. Each figure shows pressure data at an angle of attack of 0° , with a control surface deflection of 0° . As each of the figures shows, agreement between predicted and experimental data is very good, even at the higher transonic Mach numbers. Typically, as was briefly mentioned in Chapter 2, Euler flow solvers over-predict both the location and strength of transonic shocks. One common factor in each of the figures seems to be the fact that STARS tends to predict a slightly higher suction peak, though still within the upper range of the experimental scatter.

The BACT wing's critical Mach number appears to be ~ 0.77 which coincides with that of a NACA 0012 airfoil. At this point, flow accelerates from the free-stream Mach number of 0.77 to just sonic on the surface of the wing. Cases run at Mach numbers greater than 0.77 clearly show the existence of these transonic shocks.

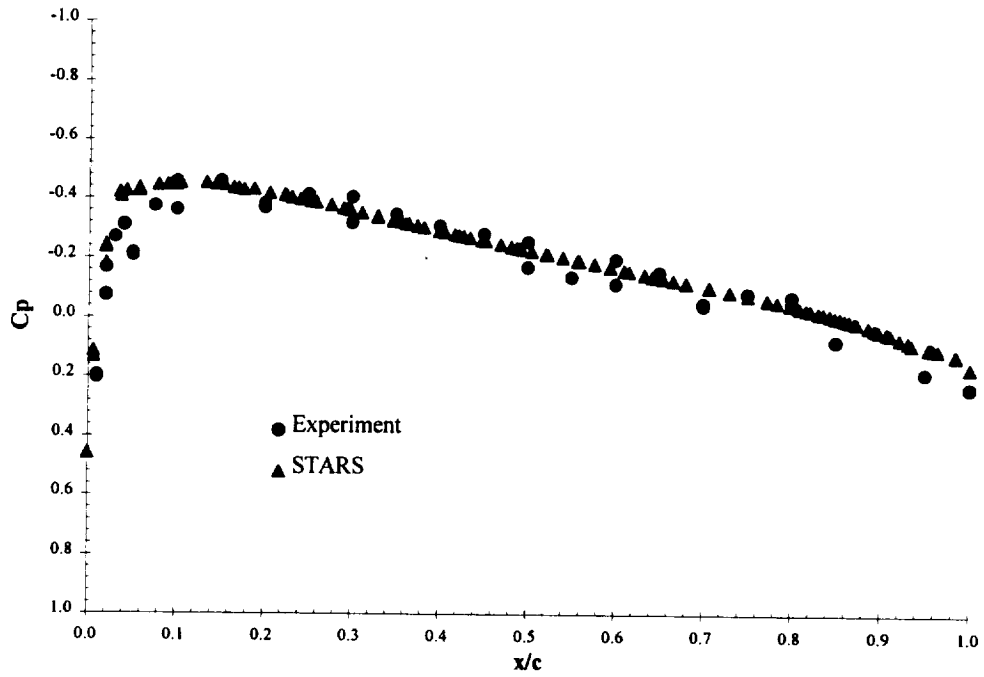


Figure 4-1: Steady Chordwise Pressure at Mach 0.51, $\alpha=0^\circ$, $\delta=0^\circ$, 60% Span

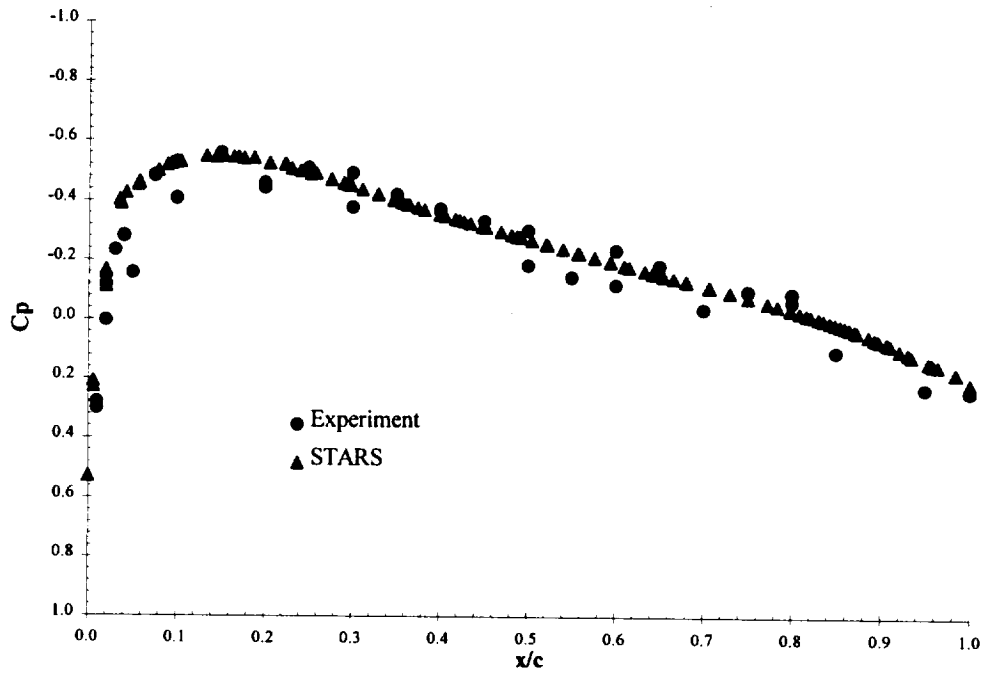


Figure 4-2: Steady Chordwise Pressure at Mach 0.67, $\alpha=0^\circ$, $\delta=0^\circ$, 60% Span

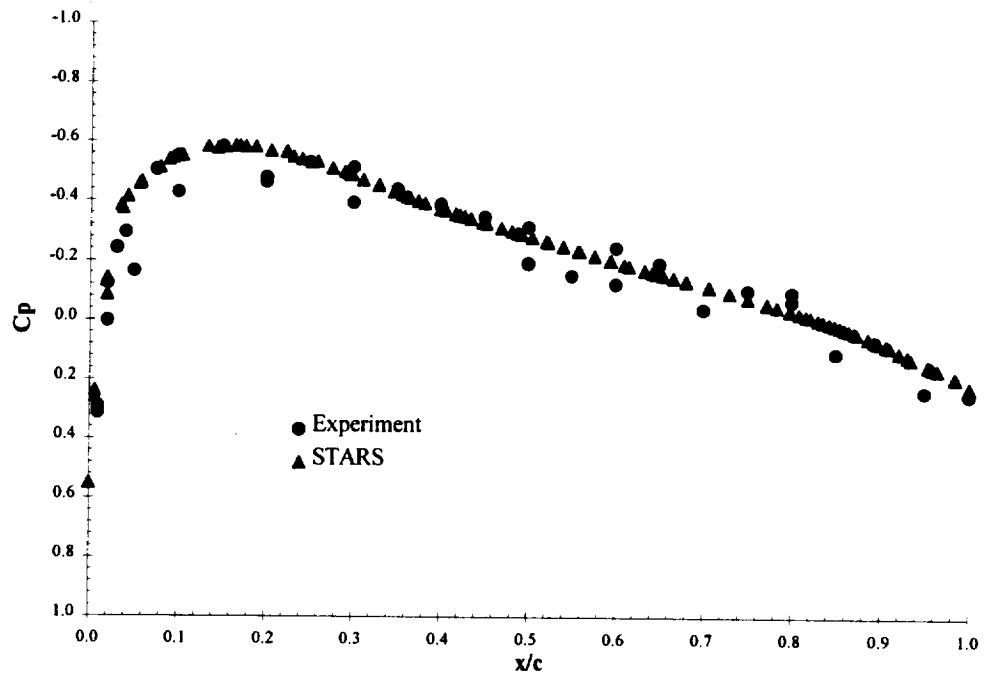


Figure 4-3: Steady Chordwise Pressure at Mach 0.71, $\alpha=0^\circ$, $\delta=0^\circ$, 60% Span

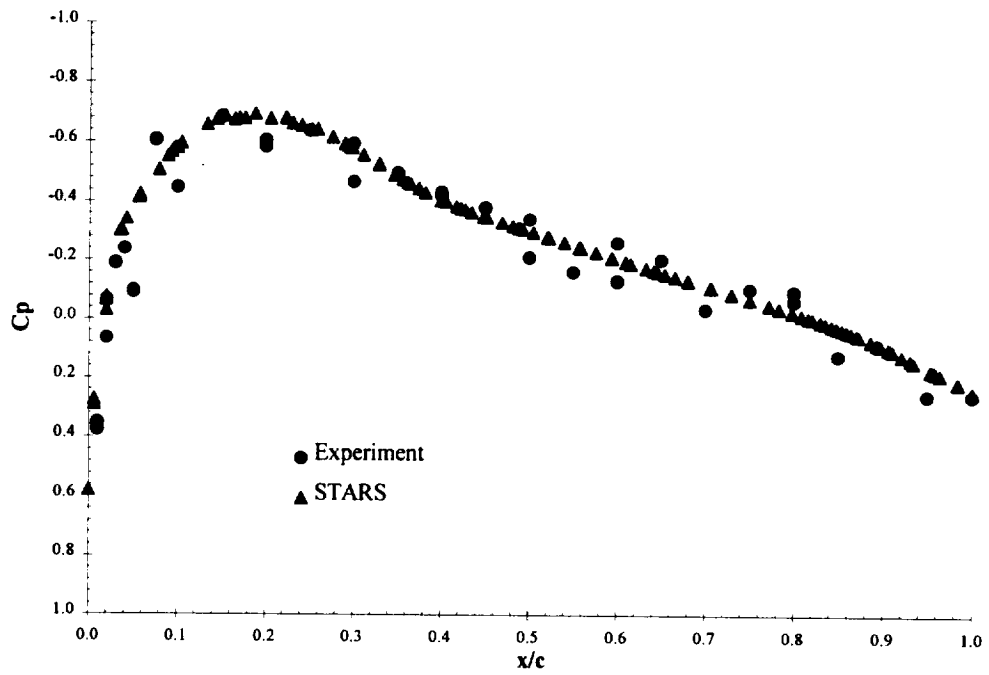


Figure 4-4: Steady Chordwise Pressure at Mach 0.77, $\alpha=0^\circ$, $\delta=0^\circ$, 60% Span

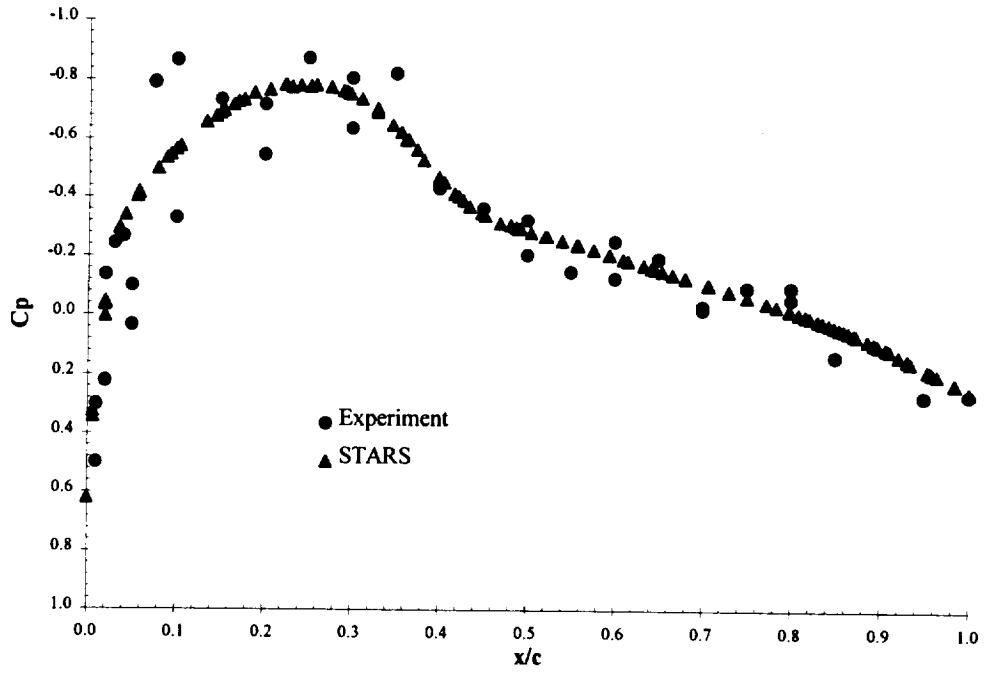


Figure 4-5: Steady Chordwise Pressure at Mach 0.80, $\alpha=0^\circ$, $\delta=0^\circ$, 60% Span

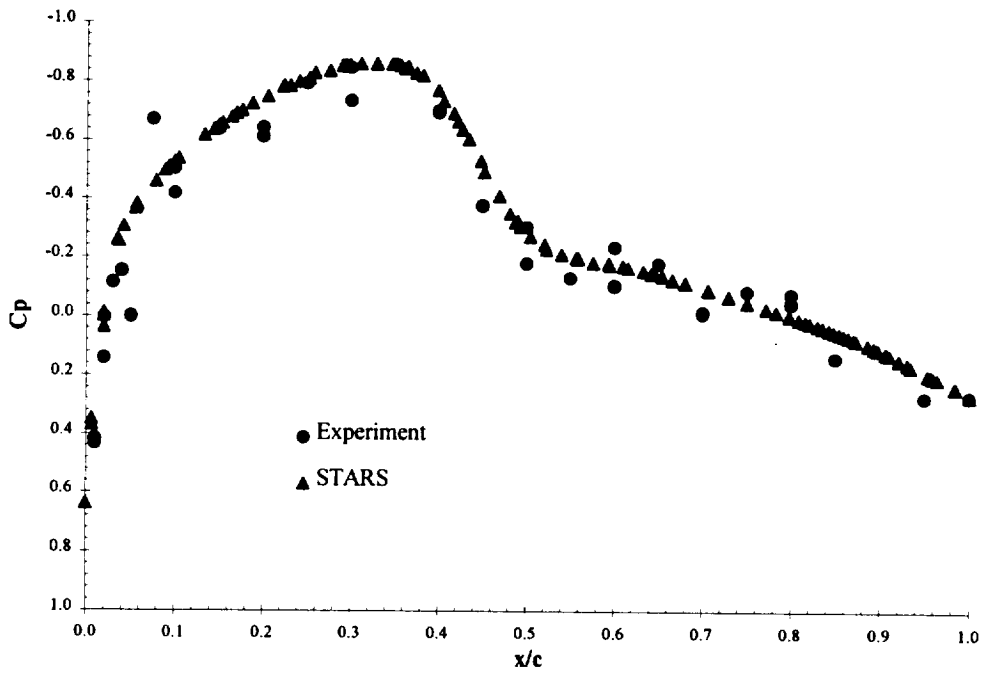


Figure 4-6: Steady Chordwise Pressure at Mach 0.82, $\alpha=0^\circ$, $\delta=0^\circ$, 60% Span

Also accounting for the slight difference between predicted and experimental data is a transition strip running approximately one inch from the leading edge of the wing. There were no quantified uncertainties presented for these data, but judging from the scatter in the pressure data, STARS predicts pressures that lie well within the experimental scatter over the entire range of Mach numbers. Scatter is particularly evident in Figure 4-5.

Solutions in the vicinity of Mach 0.77 took the most time to converge. At, and slightly beyond, Mach 0.77 when shocks first begin to appear, solution convergence is hampered as STARS resolves the location of the transonic shock. For lack of a better term, the location of the shock seems to *dance* around a narrow portion of the wing's surface. Though not a problem for the steady case, per-se, a lack of resolution in the shock locations could pose a problem with the unsteady flow solution. Addressed later, the solution to this obstacle is to make sure that plenty of iterations are allowed for the solution to completely converge at each solution time-step.

4.2 Steady Results With Control Surface Deflections

The steady results presented above did not have to make use of the transpiration boundary condition. For the case of a steady control surface deflection, there will be the first actual application of the transpiration method thus far in this study. To show the effectiveness of the transpiration method, a couple of different comparisons must be made independent of one another. First, pressure distributions and contours are compared for the case of a physical and transpired control surface deflection. Second, resulting pressure data for a simulated control surface deflection is compared to experimental data from the BACT wing.

4.2.1 Steady Solutions for Transpired and Actual Control Surface Deflections

Recall that a CFD model for an actual control surface deflection was constructed in addition to the standard CFD mesh for the wing. For purposes of comparison, a 10° control surface deflection is compared to that of a simulated 10° deflection angle. The 10° deflection angle was used to illustrate the effectiveness of the transpiration method for relatively large surface deflections. Shown below in Figure 4-7 is a comparison between the deflected and un-deflected CFD grids.

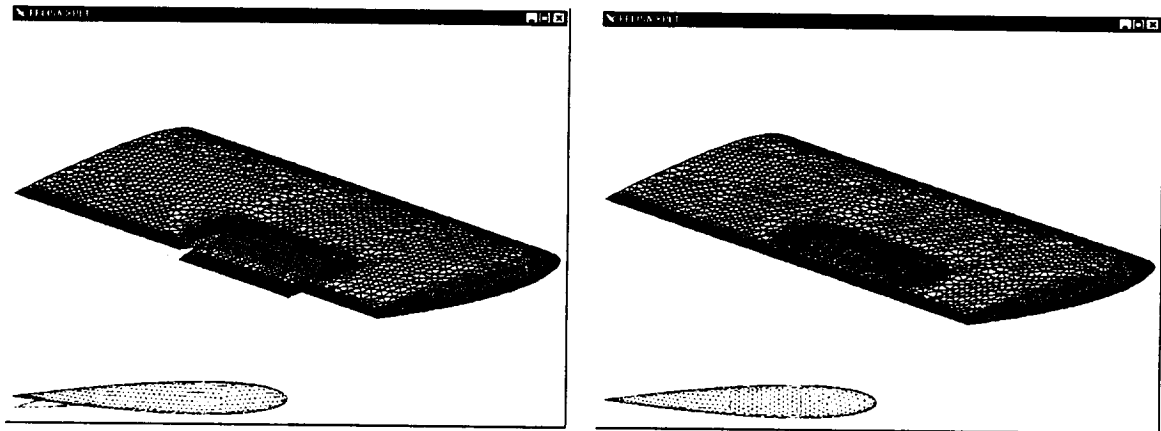


Figure 4-7: Comparison of Actual and Simulated 10° Control Surface Deflections

In the above figure, one can clearly see the extent of the flap deflection. An Euler solver would not be expected to detect or account for the likely separation and boundary layer-shock interaction for such a large control surface deflection. The comparison with this large control surface deflection is, therefore, used to demonstrate that the transpiration method is as accurate as the limitations imposed by the inviscid flow assumption.

The first comparison of an actual and simulated control surface deflection is at Mach 0.77, 0° angle of attack, and 10° (downward) flap deflection. A qualitative comparison of the pictures in Figure 4-8 shows very good agreement between an actual and simulated control surface deflection. A more quantitative comparison can be made

with a comparison of the steady pressure distributions at the 60% span location, which corresponds to the $\frac{1}{2}$ span of the control surface.

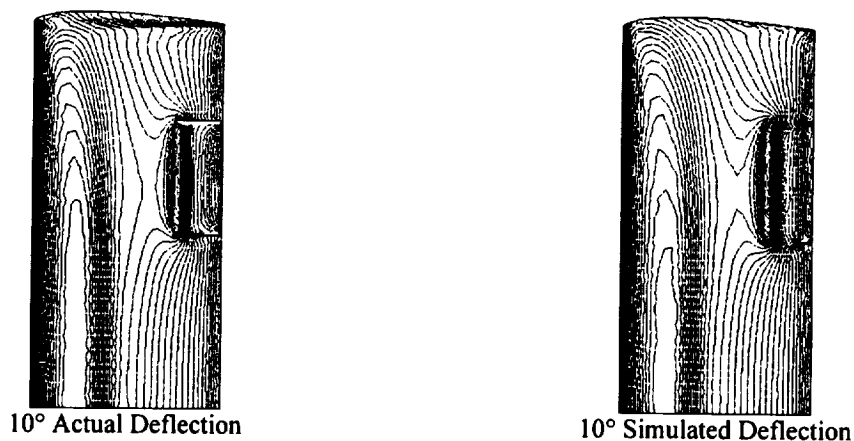


Figure 4-8: Surface Pressure Contours at Mach 0.77, 10° Control Surface Deflection

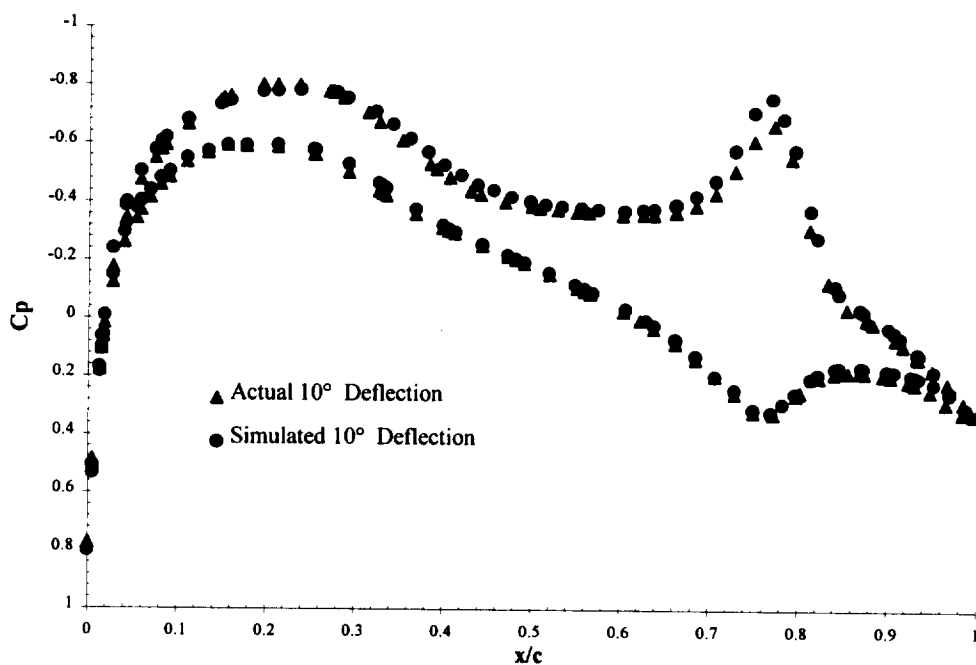


Figure 4-9: Comparison of Predicted Pressure Distributions for an Actual and Simulated 10° Control Surface Deflection at Mach 0.77, $0^\circ \alpha$

Figure 4-9 shows the excellent quantitative agreement between the predicted pressure distribution for the actual and simulated control surface deflection. With only

the slight discrepancy located at the x/c location which corresponds to the wing/control surface interface. The rest of the data points essentially lie directly on top of one-another. The resulting differences in lift and moment predictions will also be small enough to be considered insignificant.

At a slightly higher Mach number, Mach 0.82, similar results are presented. From Figure 4-10 we again good qualitative agreement is seen between the pressure contours not only on the wing, but out to the wall as well. Except for the fact that one can actually see a physical deflection in the picture on the left, there is essentially no visual difference. Quantitative agreement is again evaluated with the comparison of pressure distributions at the 60% span location, see Figure 4-11. As was seen at Mach 0.77, the only noticeable discrepancy between the pressure distributions is again at the same location, the wing/control surface interface. One also notes the significant three dimensional effects that are captured as well.

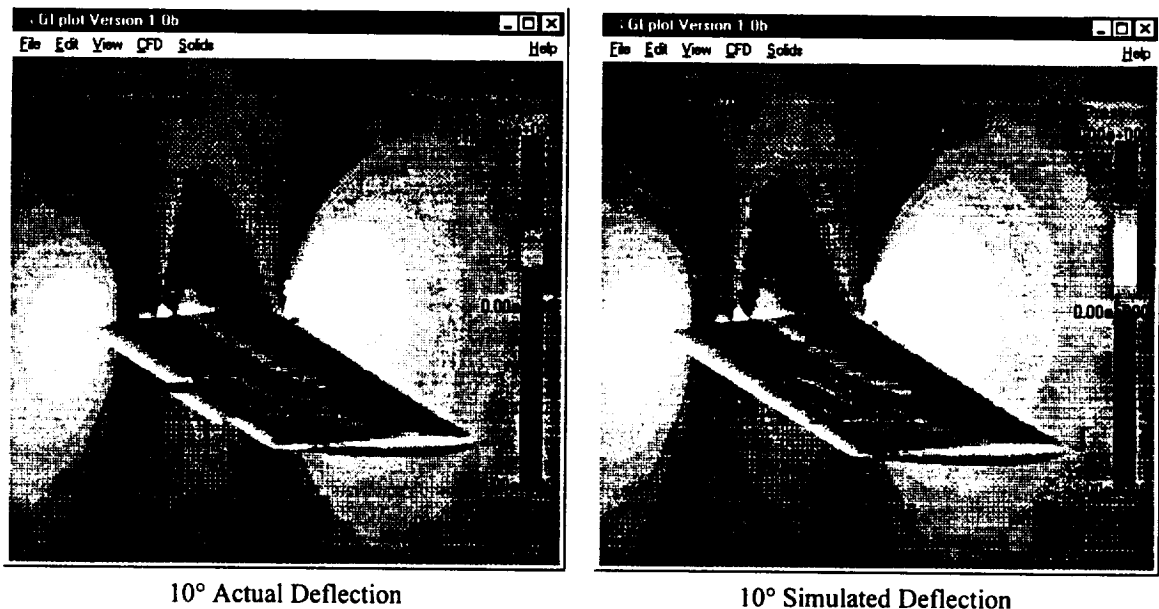


Figure 4-10: Pressure Contours at Mach 0.82, 10° Control Surface Deflection

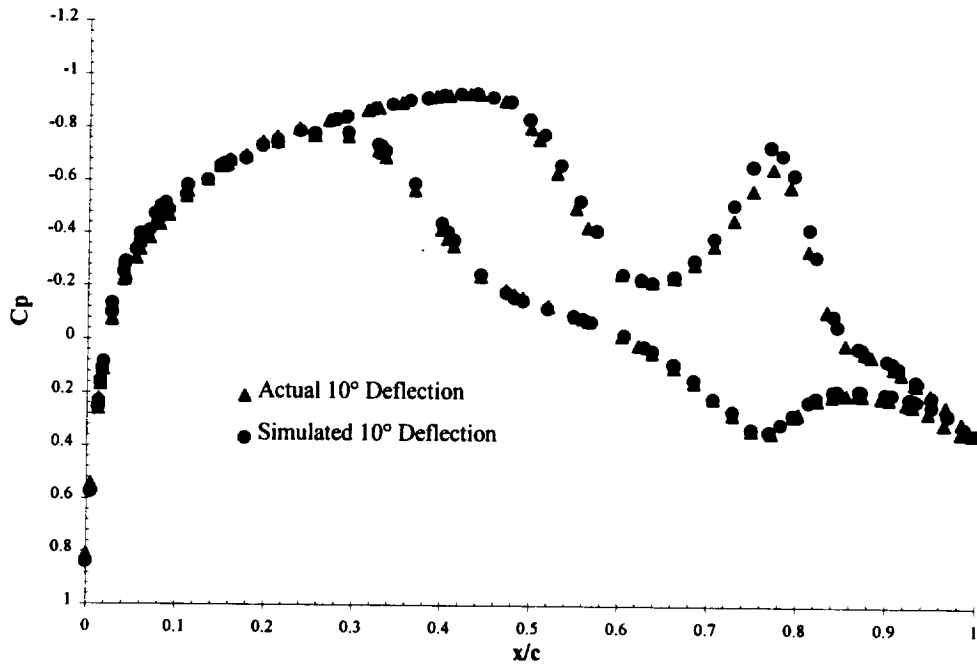


Figure 4-11: Comparison of Predicted Pressure Distributions for an Actual and Simulated 10° Control Surface Deflection at Mach 0.82, 0° α

The point as been made that the pressure distributions match well across the chord, but what about the significant three-dimensionality of the flow at the trailing edge. With a control surface deflection, one would expect to see counter-rotating vortices generated at the control surface edges, such as the vortices at the wing tip. Similar to the way pressure data is obtained, STARS can also look at velocity vectors through a *slice* in the computational domain. Shown in Figure 4-12 are velocity contours as seen looking at the trailing edge towards the leading edge. The difference between the two pictures comes after close inspection of the trailing edge in the region of the control surface. In the top picture, one can see a physical discontinuity where the trailing edge of the control surface has actually separated from the rest of the wing. These figures clearly show that the transpiration method does an excellent job of capturing all of the flow physics.

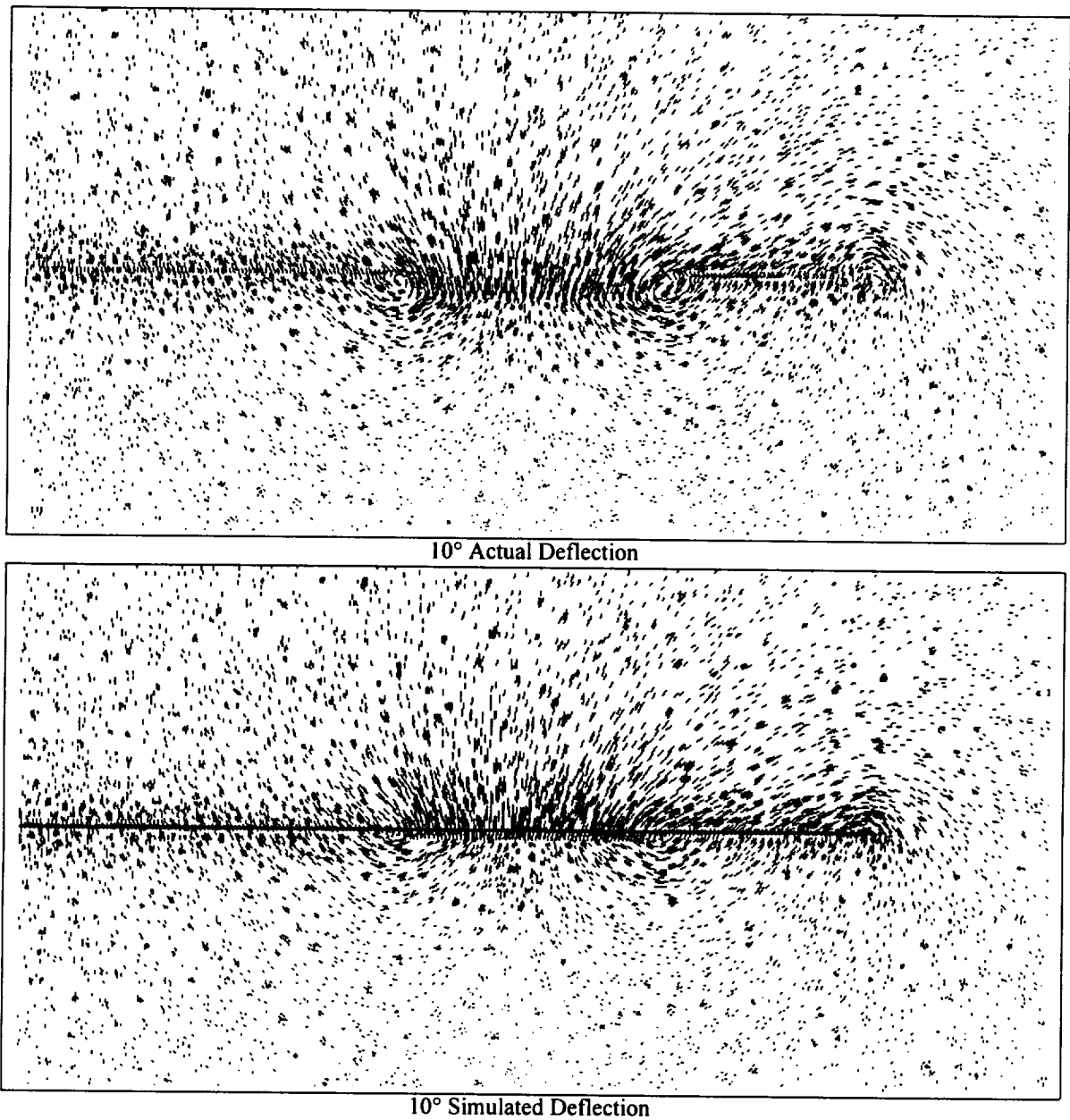


Figure 4-12: Cross-Flow Velocity Vectors at the Trailing Edge of the BACT Wing With an Actual and Simulated 10° Control Surface Deflection

What has been shown thus far are results confirming that STARS provides an accurate prediction of steady pressures on an undeformed wing. This is verified with a comparison to experimental results. Next, the pressures obtained from a simulated control surface were shown to be at least as accurate, within engineering accuracy, as those obtained from an actual control surface deflection. Next, we'll see the extent to

which the simulated flap deflection matches experimental data. The fact that all of the following experimental data is compared to a simulated flap deflection using the transpiration method in STARS must be reiterated. Once the solution converged, the scalar multiple of the generalized control surface deflection was changed and another simulation started almost immediately.

4.2.2 Steady Solutions for Transpired Control Surface Deflections Compared With Experimental Data

Beginning at Mach 0.77 comparison with experimental data is shown for control surface deflections of 2°, 5°, and 10°. Figure 4-13-Figure 4-15 again show chordwise pressure distributions at the 60% span location. One again observes very good agreement for both the 2° and 5° control surface deflections. Minor differences in peak suction are observed, but again not far from the experimental scatter. Slight differences can also be accounted for due to small deviations from nominal values of Mach number, angle of attack, and control surface deflection angle. Table 4-1-Table 4-3 show comparisons of nominal values used in STARS with actual experimental values.

Table 4-1: Nominal and Actual Parameters for Mach 0.77, $\alpha=0^\circ$, $\delta=2^\circ$

	<i>STARS</i>	<i>Experiment</i>
Mach #	0.77	0.771
Angle of Attack (°)	0.0	0.0304
Control Surface Angle (°)	2.0	1.9594

Table 4-2: Nominal and Actual Parameters for Mach 0.77, $\alpha=0^\circ$, $\delta=5^\circ$

	<i>STARS</i>	<i>Experiment</i>
Mach #	0.77	0.768
Angle of Attack (°)	0.0	0.0306
Control Surface Angle (°)	5.0	4.9647

Table 4-3: Nominal and Actual Parameters for Mach 0.77, $\alpha=0^\circ$, $\delta=10^\circ$

	<i>STARS</i>	<i>Experiment</i>
Mach #	0.77	0.767
Angle of Attack ($^\circ$)	0.0	0.0311
Control Surface Angle ($^\circ$)	10.0	9.9534

For the 10° deflection we see, for the first time, pressure data that agrees poorly in the region of the control surface. As was expected with the utilization of an Euler code, the obvious viscous effects due to boundary layer and shock interactions cannot be accounted for. The 10° case has been used primarily to show comparison between actual and simulated control surface deflections within STARS. A realistic prediction can be expected for control surface deflections of $\sim 7^\circ$ or 8° , which would still be considered large for control applications. As mentioned previously, this is a limitation of the inviscid flow solver, *not* the transpiration method.

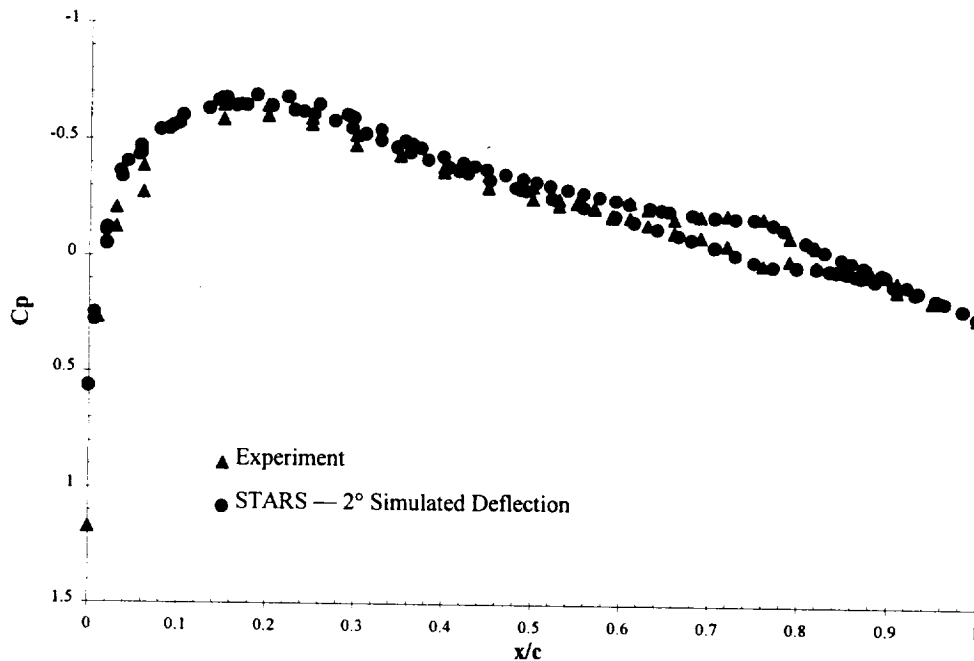


Figure 4-13: Comparison of Predicted and Experimental Chordwise Pressure Distributions at Mach 0.77, $\alpha=0^\circ$, $\delta=2^\circ$

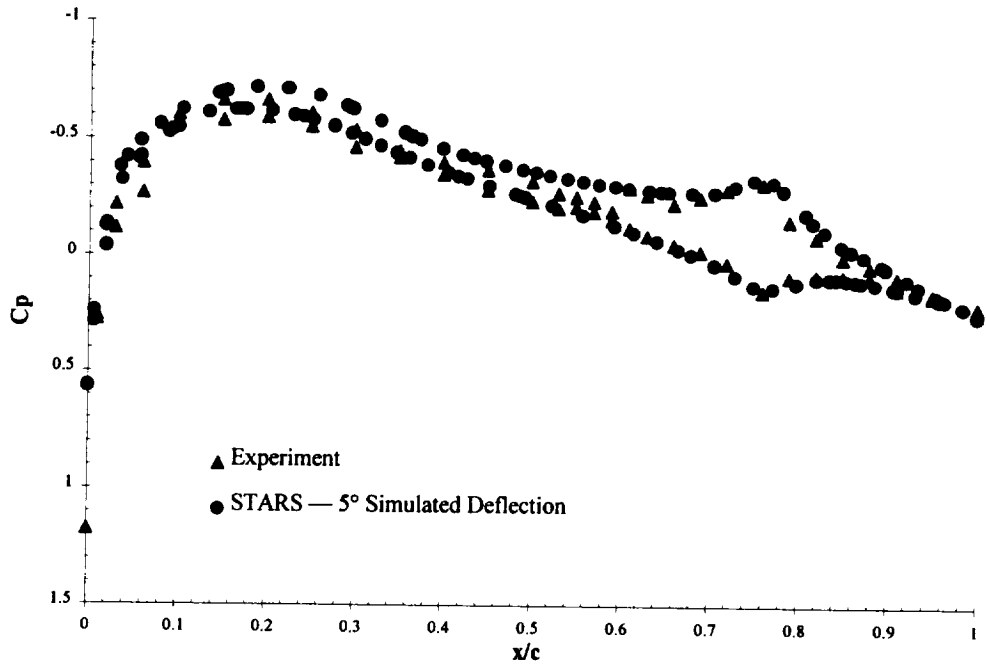


Figure 4-14: Comparison of Predicted and Experimental Chordwise Pressure Distributions at Mach 0.77, $\alpha=0^\circ$, $\delta=5^\circ$

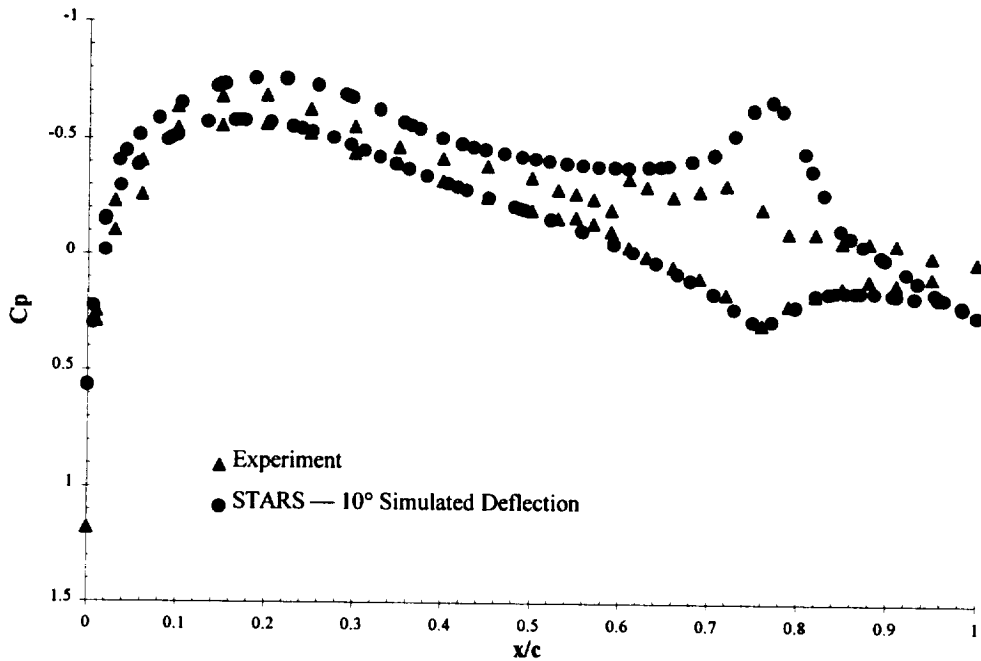


Figure 4-15: Comparison of Predicted and Experimental Chordwise Pressure Distributions at Mach 0.77, $\alpha=0^\circ$, $\delta=10^\circ$

Similar to the results presented above for Mach 0.77, chordwise pressure distributions at Mach 0.82 for control surface deflections of 2°, 5°, and 10° are presented in Figure 4-16-Figure 4-18. As before, differences exist between nominal values of Mach number, angle of attack and control surface deflection. Table 4-4-Table 4-6 again show a comparison between the nominal values used in STARS and those actually seen in experiment. The tables also serve to show that differences between nominal and desired parameters as well as small geometric anomalies account for a portion of the variations seen between computational predictions and experimental data.

Table 4-4: Nominal and Actual Parameters for Mach 0.82, $\alpha=0^\circ$, $\delta=2^\circ$

	<i>STARS</i>	<i>Experiment</i>
Mach #	0.82	0.81753
Angle of Attack (°)	0.0	0.0288
Control Surface Angle (°)	2.0	1.7017

Table 4-5: Nominal and Actual Parameters for Mach 0.82, $\alpha=0^\circ$, $\delta=5^\circ$

	<i>STARS</i>	<i>Experiment</i>
Mach #	0.82	0.81993
Angle of Attack (°)	0.0	0.0291
Control Surface Angle (°)	5.0	4.7044

Table 4-6: Nominal and Actual Parameters for Mach 0.82, $\alpha=0^\circ$, $\delta=10^\circ$

	<i>STARS</i>	<i>Experiment</i>
Mach #	0.82	0.81824
Angle of Attack (°)	0.0	0.03
Control Surface Angle (°)	10.0	9.6813

As is characteristic for Euler solvers in this particular range of Mach numbers, the transonic shock is predicted slightly aft of the position shown experimentally. As with Mach 0.77, the 2° and 5° control surface deflection angles are in reasonable agreement

with experiment. Again, the 10° deflection angle induces boundary layer-shock interactions that cannot be resolved within the inviscid flow assumption.

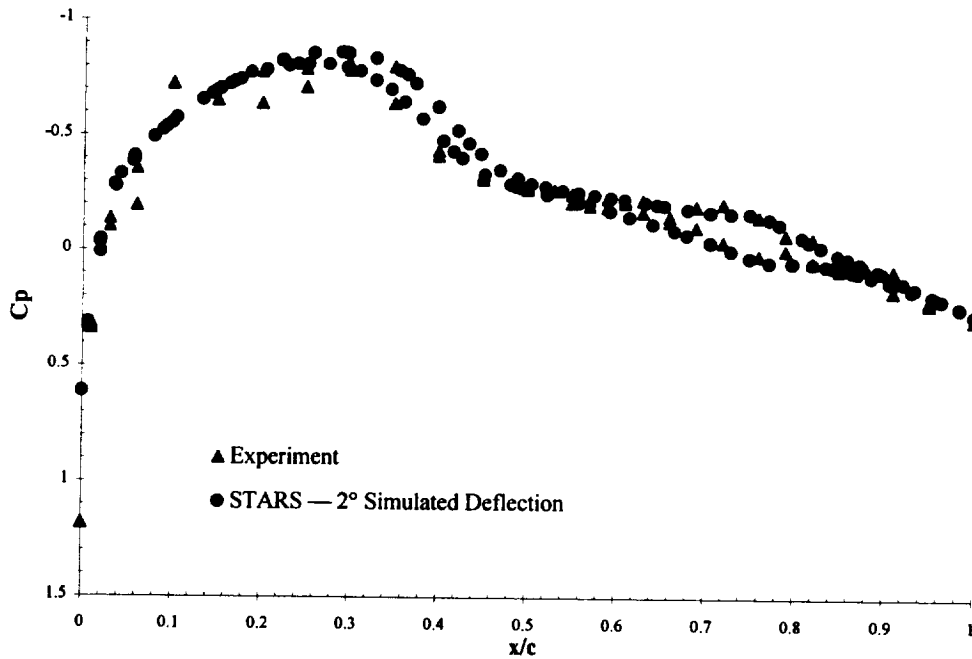


Figure 4-16: Comparison of Predicted and Experimental Chordwise Pressure Distributions at Mach 0.82, $\alpha=0^\circ$, $\delta=2^\circ$

One would expect similar results for other Mach numbers. Mach 0.77 and Mach 0.82 were chosen due to the unique complexities present with each. Mach 0.77 was shown to be the approximate critical Mach number, and Mach 0.82 highlights the significant three-dimensional effects introduced with a control surface deflection. Results would be expected to be as good, if not better, than those shown above for Mach numbers lower than 0.77 due to the limited existence of transonic shocks.

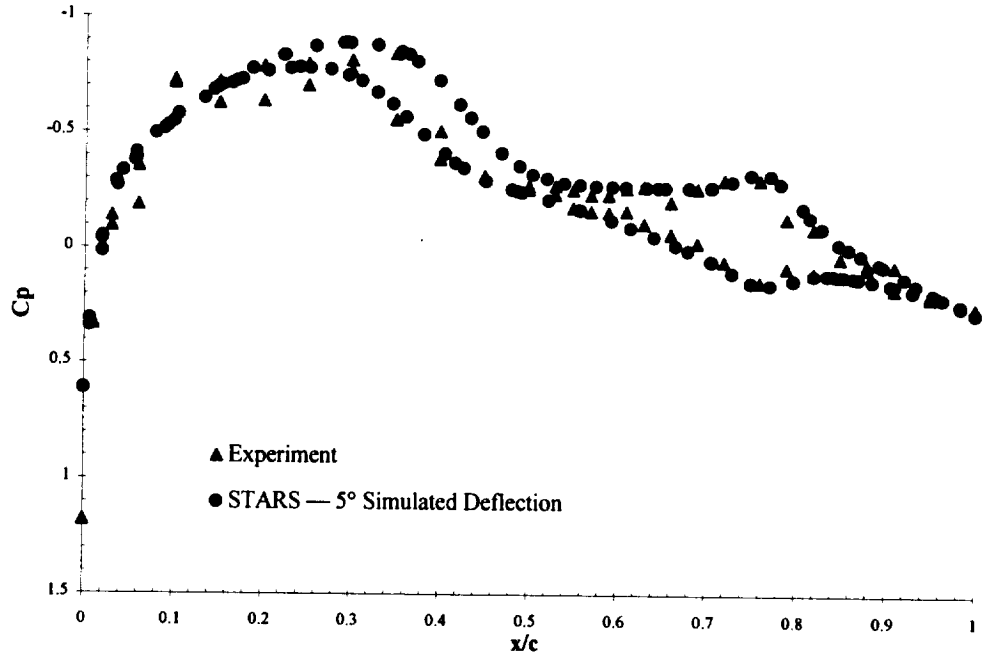


Figure 4-17: Comparison of Predicted and Experimental Chordwise Pressure Distributions at Mach 0.82, $\alpha=0^\circ$, $\delta=5^\circ$

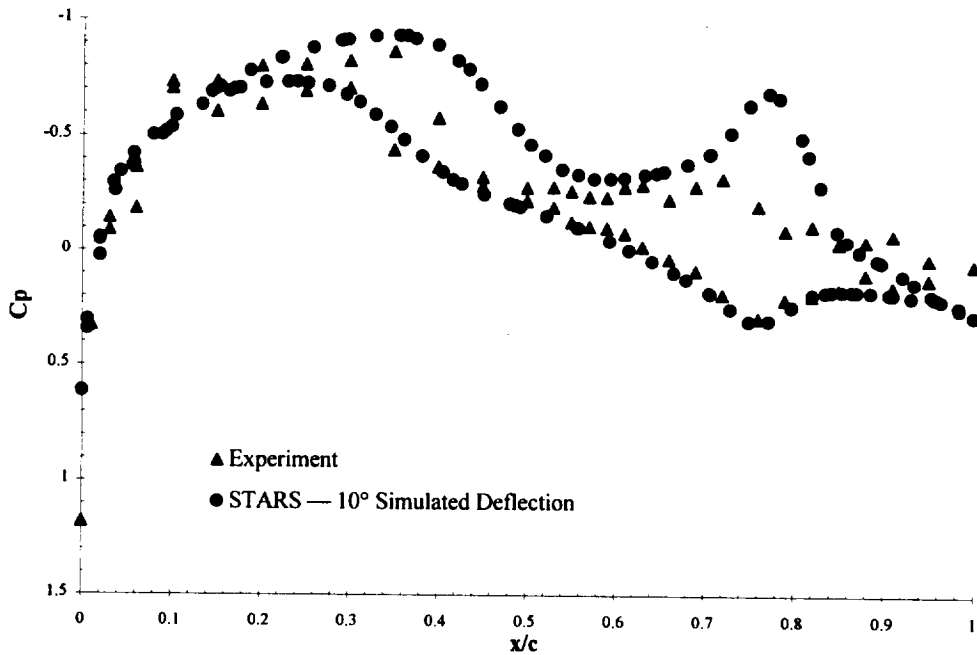


Figure 4-18: Comparison of Predicted and Experimental Chordwise Pressure Distributions at Mach 0.82, $\alpha=0^\circ$, $\delta=10^\circ$

4.3 Aeroelastic Results

Up to this point, results have focused on the comparison of steady data obtained in STARS compared with experimental data. Steady cases, with no control surface deflections showed good agreement at all Mach numbers, and simulated control surface deflections of 2° and 5° at both Mach 0.77 and 0.82 agreed reasonably well with experimental data. The next logical step is to investigate the flutter prediction as obtained using STARS compared to that predicted experimentally.

4.3.1 Unsteady Data for the BACT and NACA 0012 Wings Tested at Langley

Shown in Figure 4-19 is a comparison of the experimental flutter boundaries obtained for both the NACA 0012 wing tested in air, and the BACT wing tested in R-12.

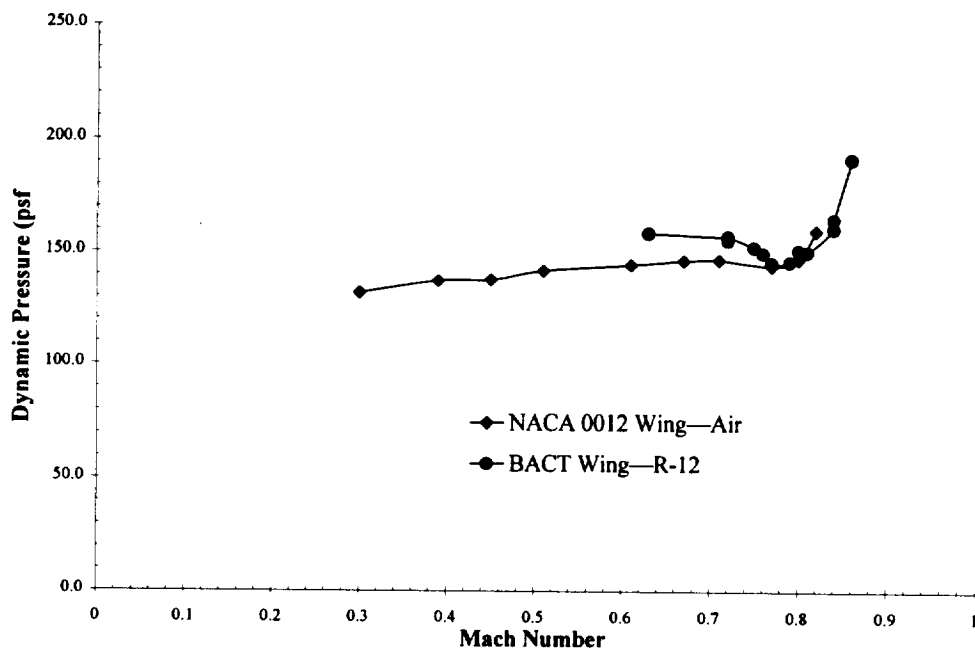


Figure 4-19: Flutter Boundary Comparison Between 2 Geometrically Similar Wings: NACA 0012 Wing (Air) & BACT Wing (R-12)

Except for Mach numbers in the narrow range of 0.77-0.80, there exists small differences in the flutter boundary predictions.

Differences could exist for several reasons. First, the models were tested in a different fluids, air and R-12. R-12 is often used in transonic and supersonic tunnels as a means of obtaining higher Reynolds and Mach numbers. For similar power input, the Mach number can be increased by a factor of 2.5 while the Reynolds number can be increased by a factor of 3.6 [Pope, 1954]. As was described in 3.2.3, the relative location of the center of gravity and elastic axis plays a significant role in the flutter characteristics. Any slight difference in the way these models were mounted would most likely be amplified here.

4.3.2 System Identification Parameters and Effectiveness

As was discussed in Chapter 3, STARS flutter prediction was accelerated using a system identification procedure. Good agreement, as one would imagine, is directly a function of how well the model matched the Euler prediction given the same multi-step input. The parameters, Na and Nb are specified at the end of the *SCALARS* file. Once the Euler multi-step is complete, the Na and Nb parameters specify the order of the ARMA model used in the system identification procedure. As suggested by Cowan, a general rule of thumb is that Nb should always be greater than Na to ensure a stable model. Summarized in Table 4-7 are the model parameters, Na and Nb , and the scaled RMS errors that indicate the degree to which the model successfully duplicated the full Euler solution.

Table 4-7: Model Orders and Associated RMS Errors at Various Mach Numbers

<i>Mach</i>	<i>Na</i>	<i>Nb</i>	<i>Scaled RMS Error</i>		
			(1)	(2)	(3)
0.51	4	11	0.457E-2	0.678E-2	0.114E-1
0.67	4	10	0.686E-3	0.122E-2	0.605E-3
0.71	4	13	0.727E-3	0.170E-2	0.119E-2
0.77	3	11	0.551E-4	0.433E-4	0.217E-4
0.80	4	12	0.637E-3	0.318E-2	0.189E-2
0.82	4	12	0.709E-3	0.152E-2	0.240E-2

To more fully appreciate the ability to model the actual system, Figure 4-20 to Figure 4-25 show a superposition of the model and Euler solution obtained using the multi-step sequence. This multi-step sequence is used to *train* the system model based on the generalized forces resulting from a known input. Plotted are generalized forces vs. dimensional time where *GF1*, *GF2*, and *GF3* are measures of the lift, pitch moment, and control surface hinge moment, respectively. For a fixed control surface position ($\delta=0^\circ$), generalized force 3 does not actually get used in the model for determining the conventional flutter boundary since the control surface is held stationary during the aeroelastic case. The following section, however, makes use of the control surface as a means of flutter suppression.

What the aforementioned figures demonstrate is the ability of a system model to correctly predict generalized forces during a controlled input. The complete effectiveness must ultimately be measured by the extent to which the model predicts generalized forces, displacements, and velocities during the general flutter case where modal displacements and velocities are those resulting from the unsteady response. As mentioned previously, the amount of time it would take to validate every system model would take over one year to complete on current hardware. Presented in Figure 4-26 to Figure 4-29 is a portion of a single validation at Mach 0.82. Notice that for both

generalized displacement and velocity, the system model is virtually indistinguishable from the Euler prediction. The Euler validation extends over a small portion of the model due to the amount of time it takes to generate solutions. The small number of cycles shown took on the order of 10 days to complete. As demonstrated by Cowan, once the model correctly predicts a couple of Euler CFD cycles, the rest of the time-history will continue in a similar manner. Cowan provides numerous test-cases with Euler validations for a variety of cases including the AGARD 445.6 wing, a supersonic panel case, a generic hypersonic vehicle, and others [Cowan, 1998]. Based on the effectiveness of the system identification procedure, further validation is deemed unnecessary at this point.

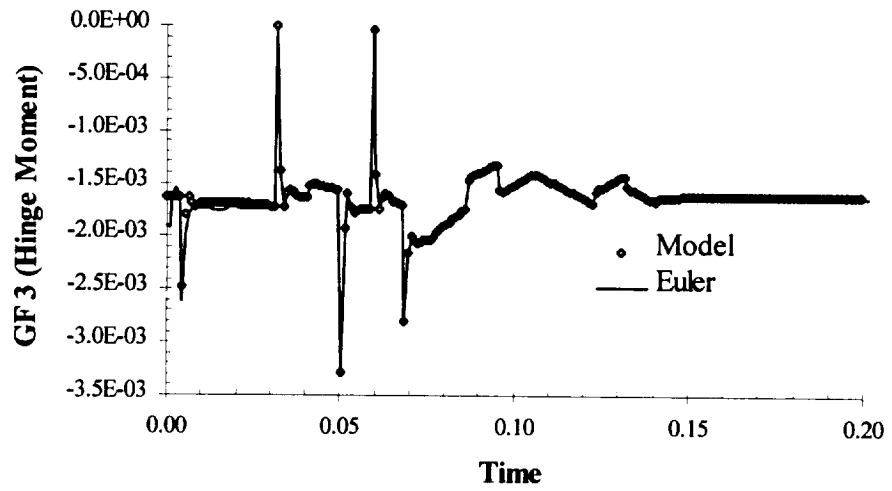
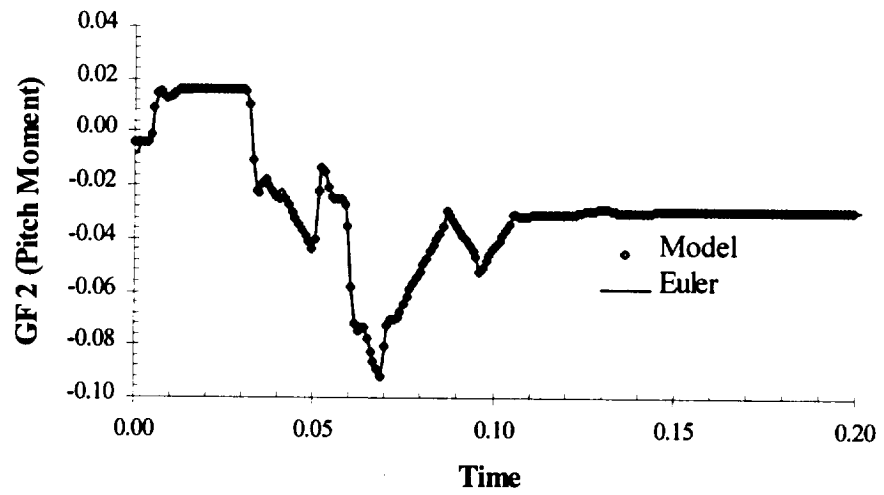
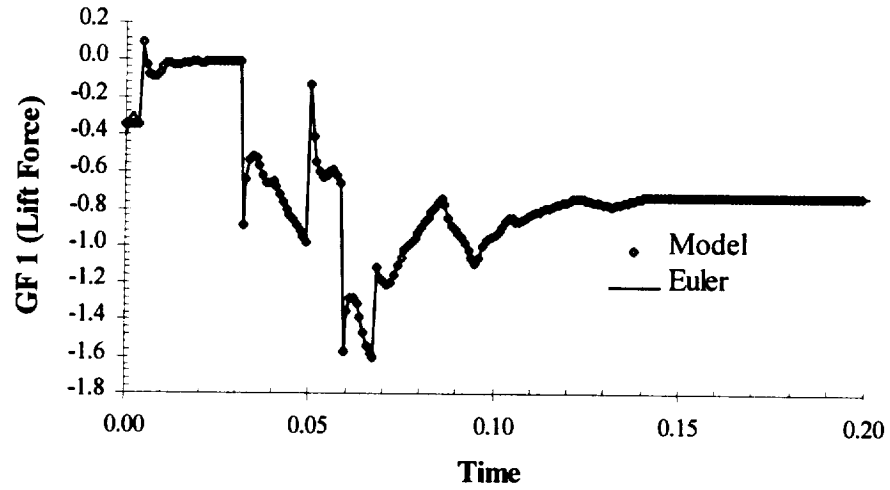


Figure 4-20: Training Data at Mach 0.51, $q=141.8$ psf

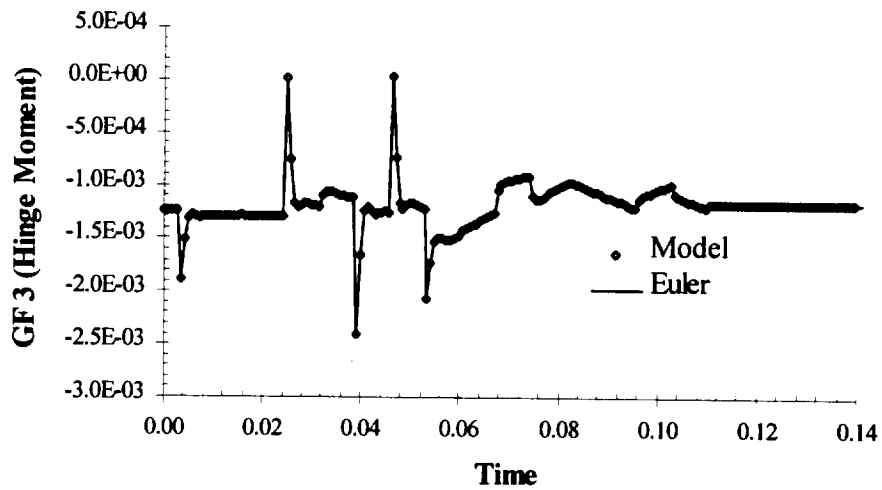
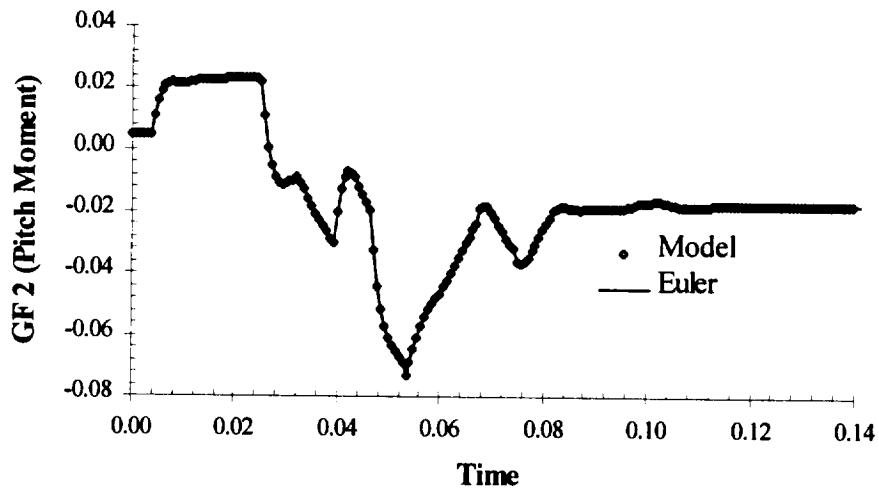
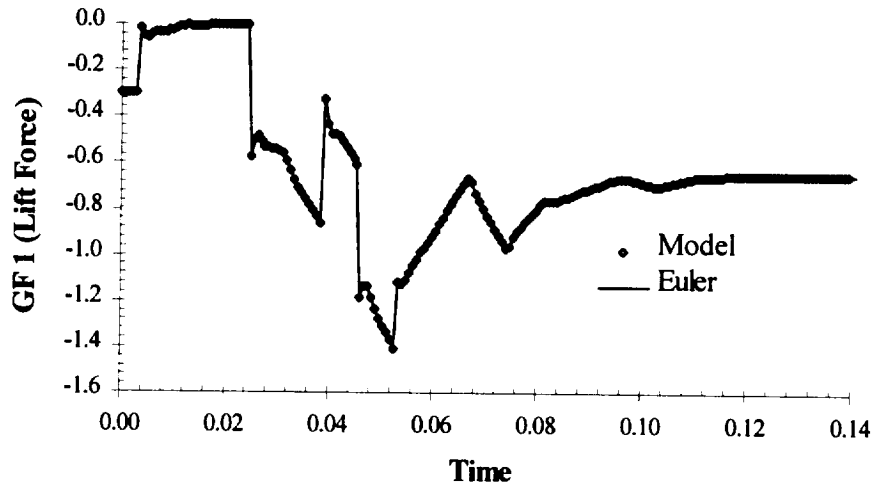


Figure 4-21: Training Data at Mach 0.67, $q=146.5$ psf

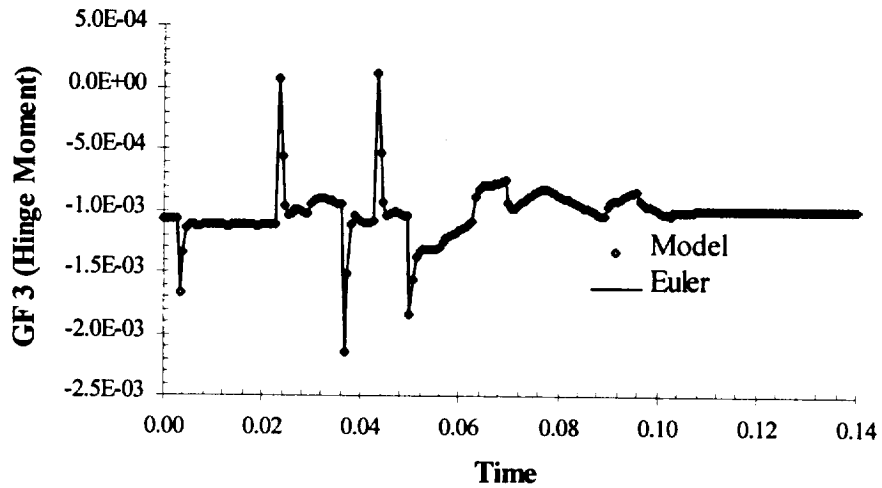
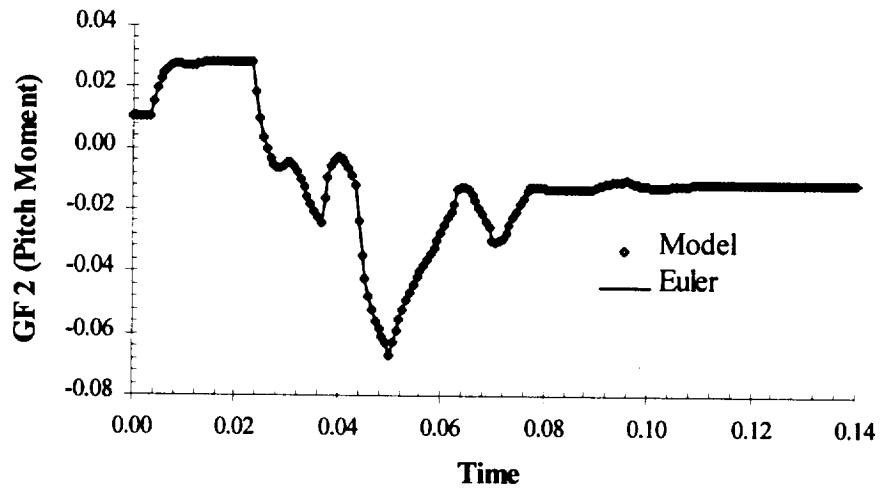
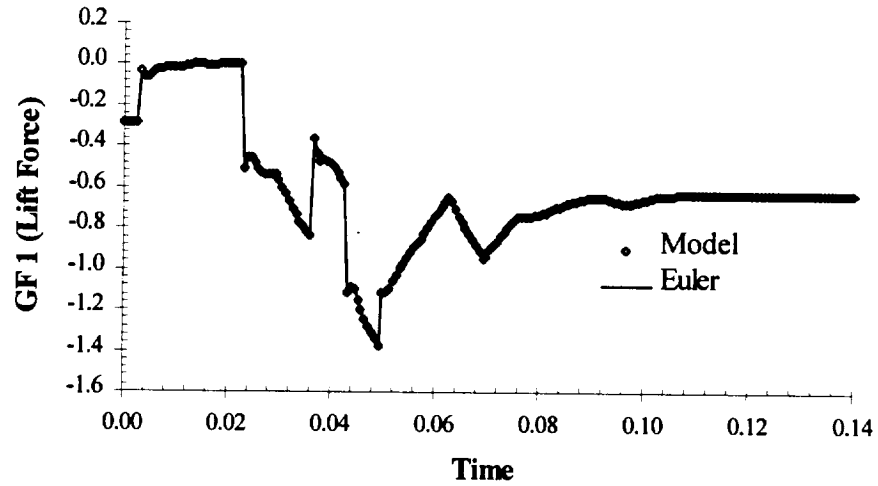


Figure 4-22: Training Data at Mach 0.71, $q=146.9$ psf

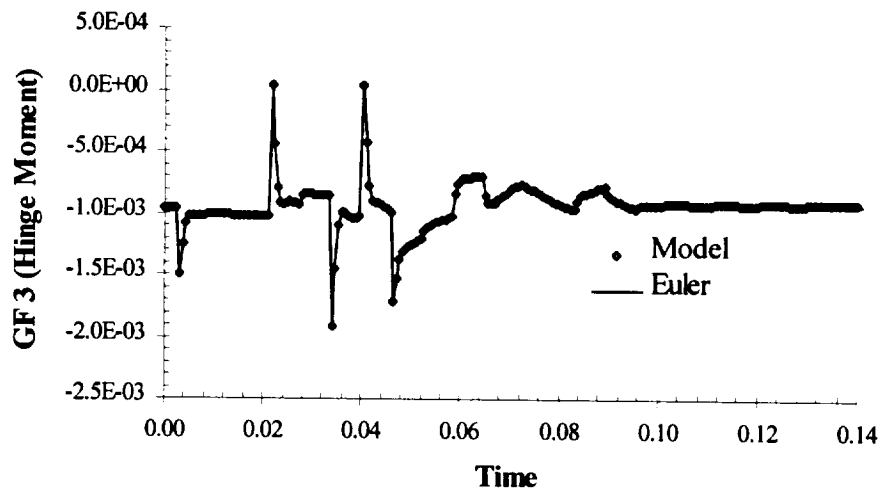
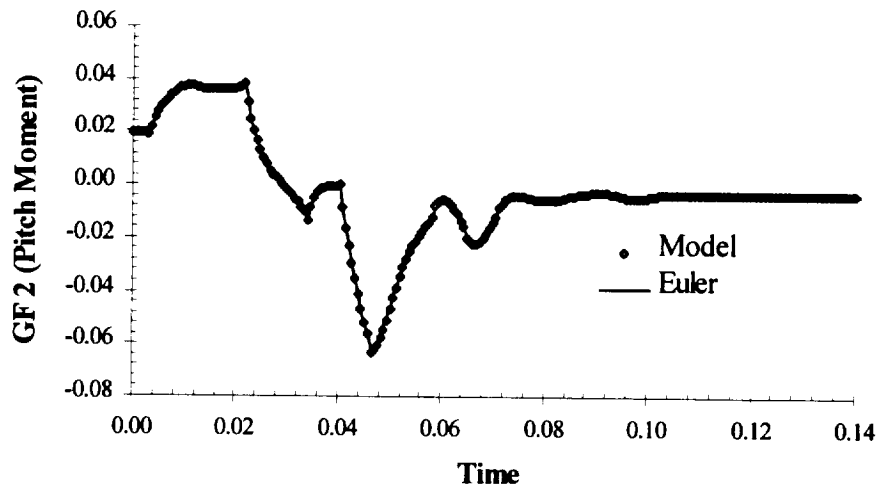
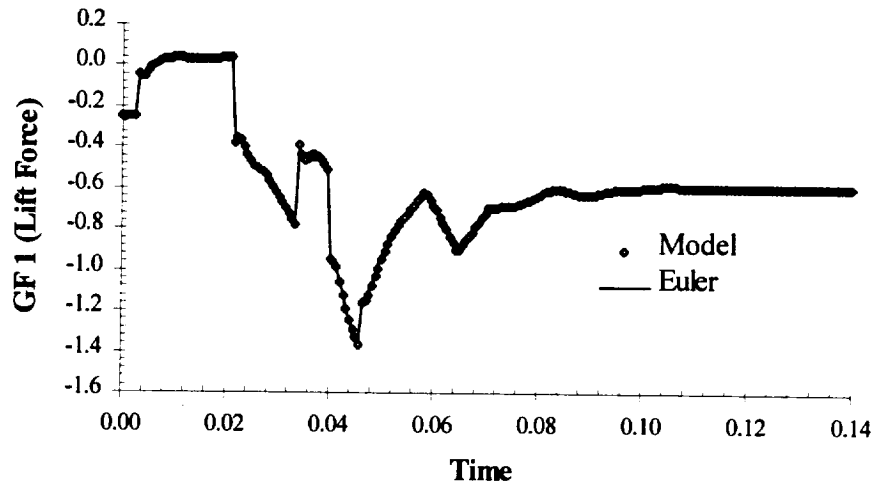


Figure 4-23: Training Data at Mach 0.77, $q=144.2$ psf

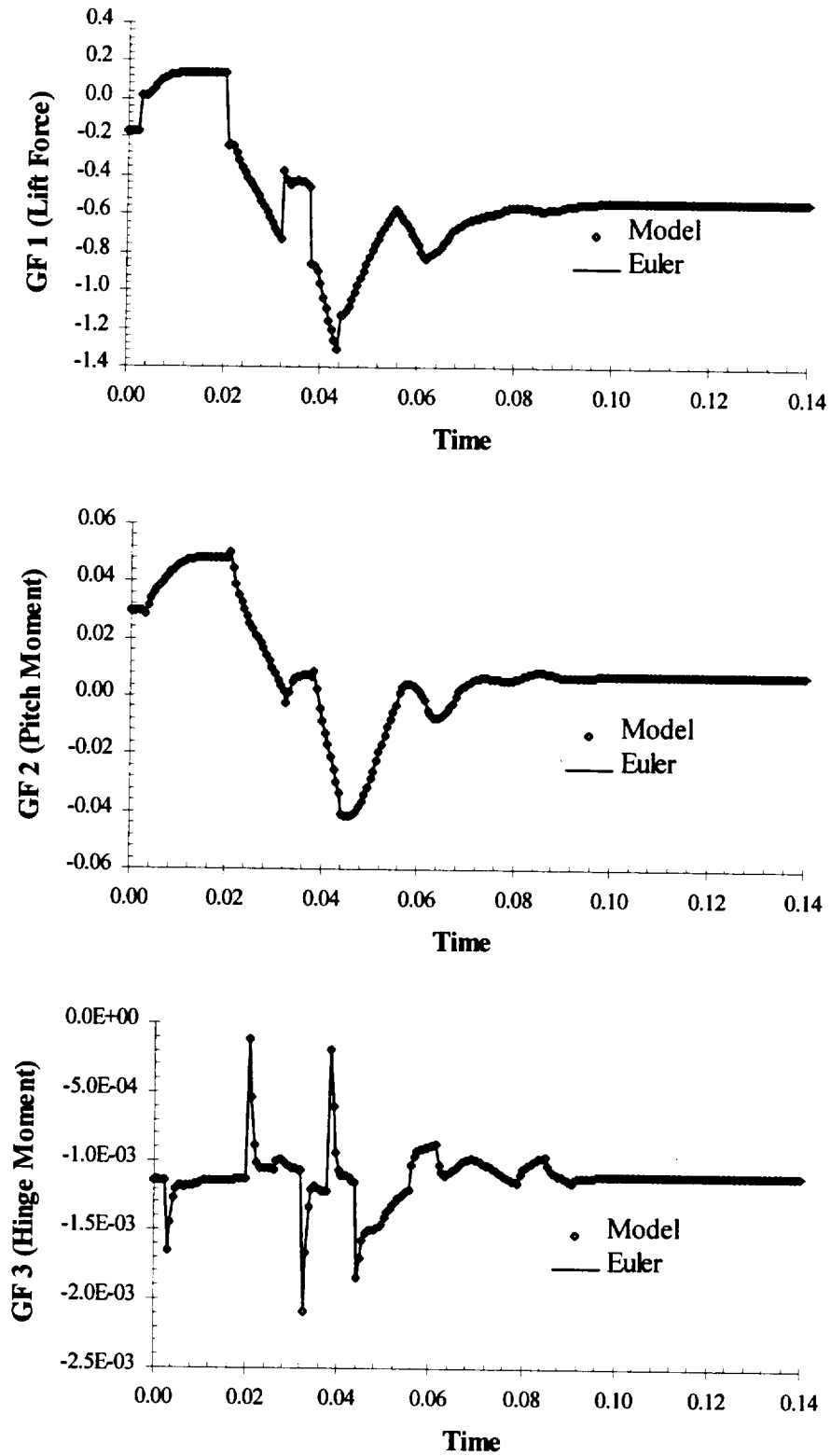


Figure 4-24: Training Data at Mach 0.80, $q=147.2$ psf

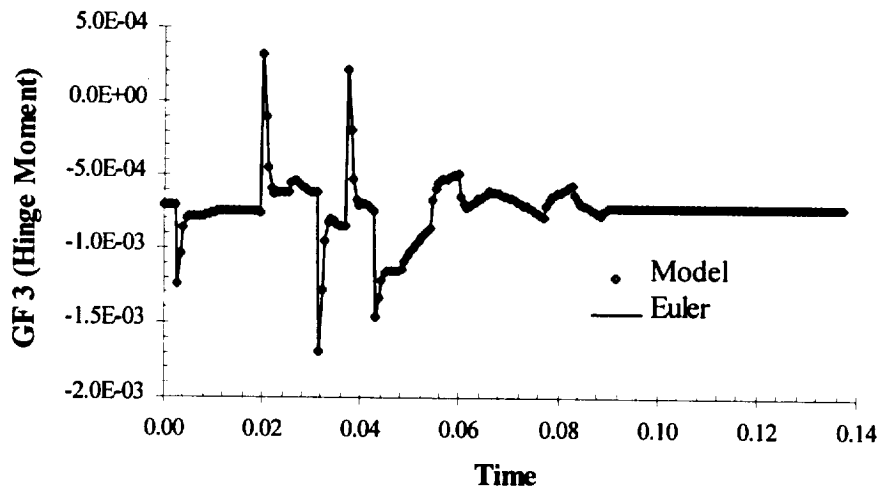
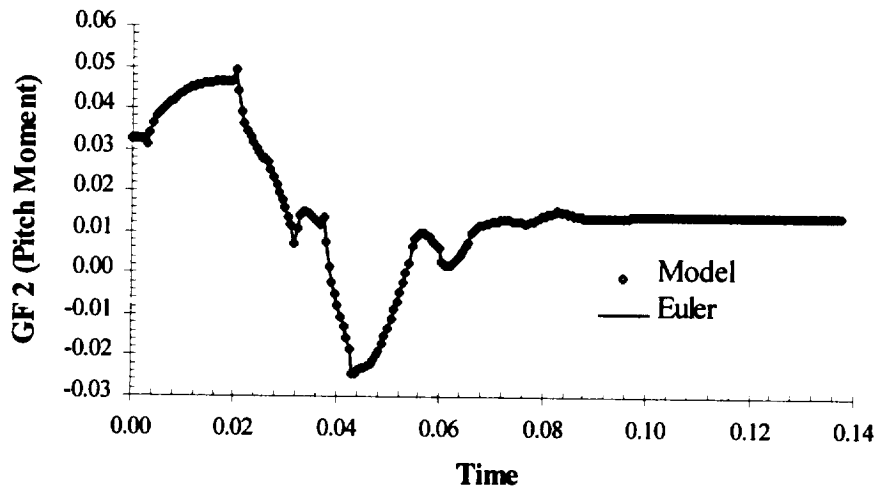
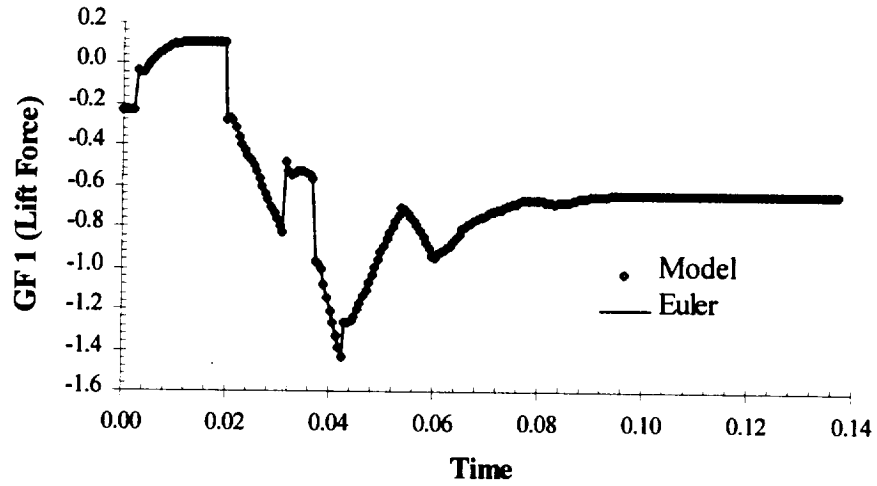


Figure 4-25: Training Data at Mach 0.82, $q=159.9$ psf

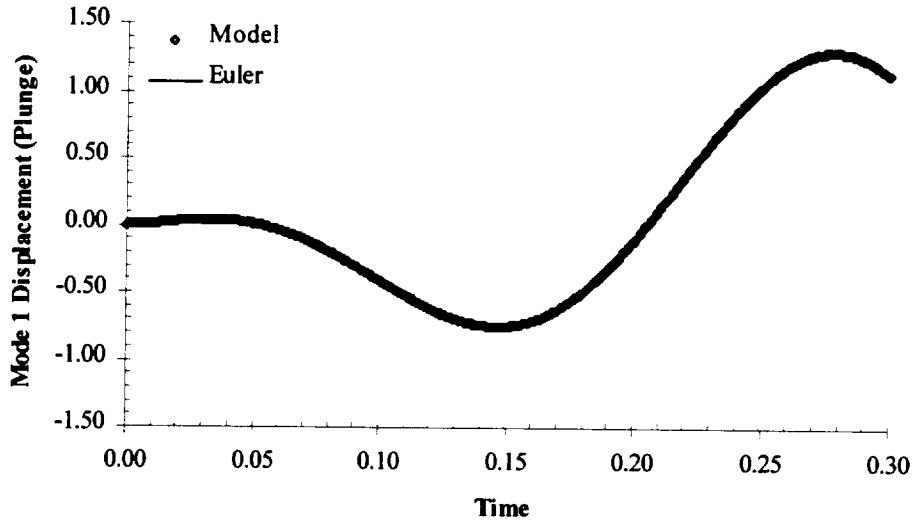


Figure 4-26: Model Validation for STARS CFD/ASE: Model at Mach 0.82 for Plunge Displacement (in)

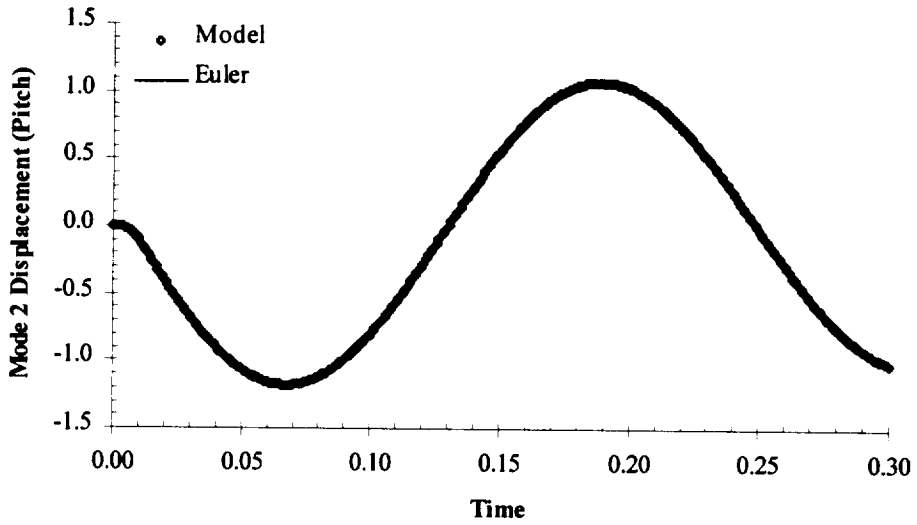


Figure 4-27: Model Validation for STARS CFD/ASE: Model at Mach 0.82 for Pitch Displacement (deg)

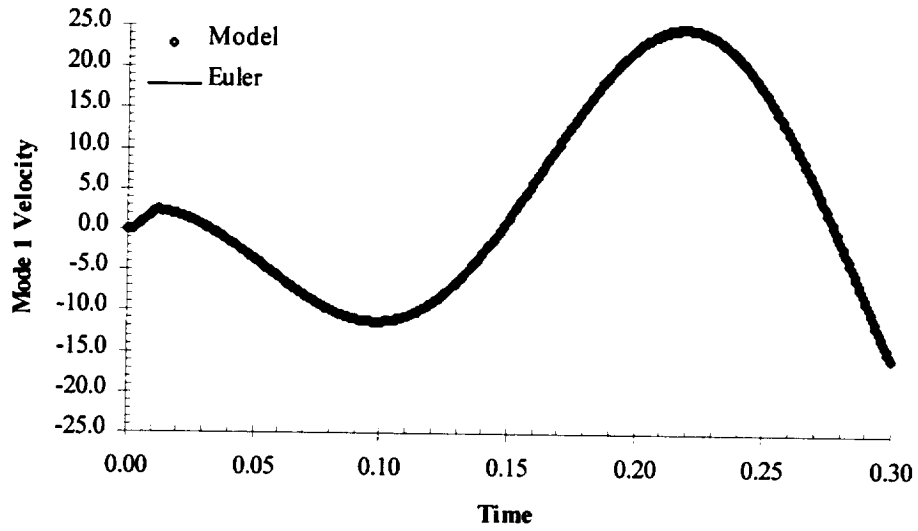


Figure 4-28: Model Validation for STARS CFD/ASE: Model at Mach 0.82 for Plunge Velocity (in/sec)

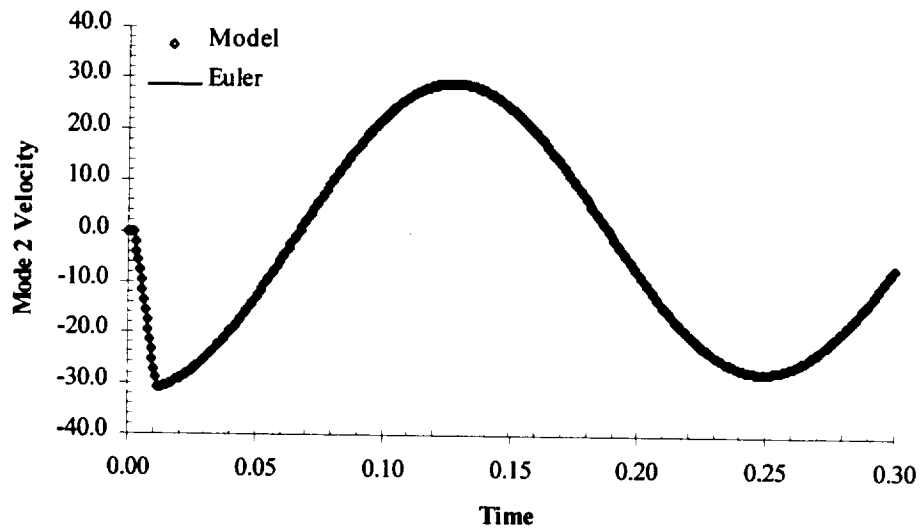


Figure 4-29: Model Validation for STARS CFD/ASE: Model at Mach 0.82 for Pitch Velocity (deg/sec)

4.3.3 Flutter Prediction Using STARS

As a culmination of all of the above efforts, let's turn to the predicted flutter boundary using STARS. As was demonstrated in Chapter 3, there is a significant sensitivity to the location of the center of gravity relative to the elastic axis ($S_{h,\alpha}$). For simplicity, the p -method was used for quick parametric studies of plunge and pitch stiffness as well as $S_{h,\alpha}$. The fully 3-D, nonlinear STARS model also showed this same sort of sensitivity as is seen in Figure 4-30.

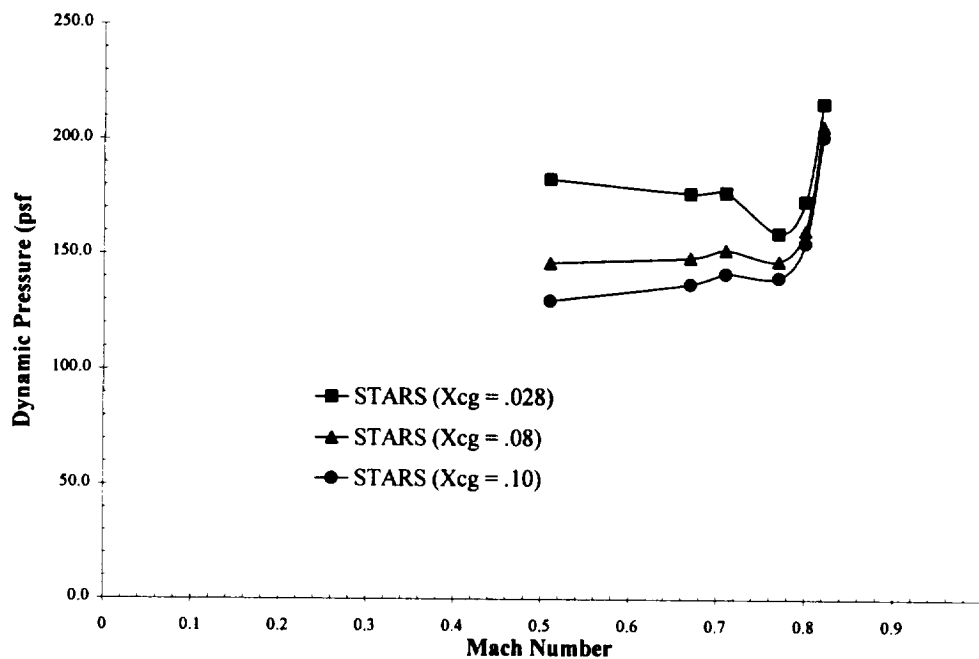


Figure 4-30: Flutter Boundary Prediction for Different x_{cg} Locations

In the above figure, we see three different flutter boundary predictions for slight changes in CG location relative to the elastic axis. As one would expect, as x_{cg} moves aft of mid chord, the predicted flutter point drops. This is perhaps the most effective demonstration

thus-far of the sensitivity that exists with this particular choice of CG location. Table 4-8 quantifies the data given in the previous figure.

Table 4-8: Sensitivity to x_{cg} for the NACA 0012 & BACT Wings in STARS

<i>Mach</i>	<i>Dynamic Pressure @ Flutter (psf) for:</i>		
	$x_{cg}=0.028''$	$x_{cg}=0.08''$	$x_{cg}=0.10''$
0.51	182.5	146.0	129.7
0.67	176.5	148.3	136.9
0.71	176.9	151.8	141.6
0.77	159.2	147.0	139.9
0.80	173.2	160.5	154.9
0.82	215.9	206.2	201.3

Shown in Table 4-9 are the resulting changes in flutter prediction across the entire Mach number range for less than a 1% change in x_{cg} . As was quickly demonstrated using the p -method with simplified linear aerodynamics, a 1% change can very significantly alter the flutter prediction. It is interesting that the apparent sensitivity to x_{cg} seems to diminish with increasing Mach number.

Table 4-9: Percent Change in $q_{flutter}$ for a 0.9% Shift in x_{cg} (8.028'' \Rightarrow 8.10'')

<i>Mach</i>	<i>% Change in $q_{flutter}$</i>
0.51	-28.9%
0.67	-22.4%
0.71	-20.0%
0.77	-12.2%
0.80	-10.6%
0.82	-6.8%

This x_{cg} shift results from moving the cg's location, relative to the elastic axis, aft from 8.028'' to 8.10'', where the wing's mid-chord is at 8.0''. Through personal contact with Mr. Waszak, experimental results show that a shift in x_{cg} from 8.0 to 8.1 at Mach 0.77 resulted in a change in $q_{flutter}$ from 169 psf to 148 psf [Waszak, 1998]. For this similar

shift in x_{cg} , the resulting 12% drop in $q_{flutter}$ compares well to the change noticed in STARS.

As seen in Figure 4-31, STARS flutter prediction, in general, compared well with experimental data. Error in the estimates in the flutter boundary were minimized through the use of the modal identification technique described previously. At each Mach number, the model was ran in small increments of dynamic pressure, at which mode 1 and 2 damping values were recorded. Once the mode 2 (Pitch) damping went from a positive to a negative number, a linear interpolation between the two points provided an estimate for the flutter point.

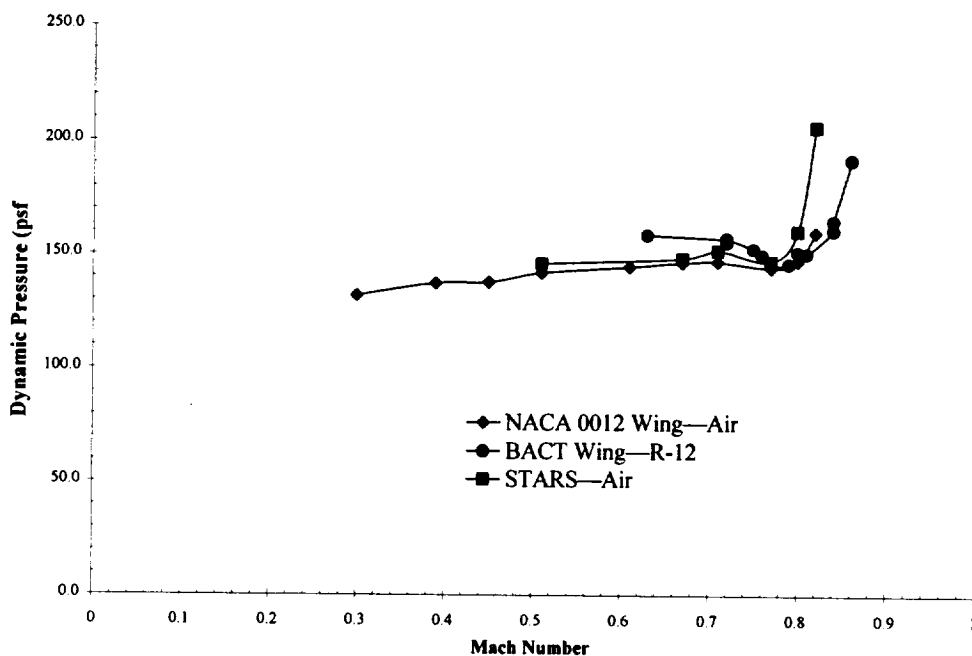


Figure 4-31: STARS Flutter Prediction Compared with Experimental Results from the NACA 0012 Wing and the BACT Wing

From Mach 0.51 to 0.77, predicted values of $q_{flutter}$ were less than 4% different than experiment. As was noticed in the experimental data, the predicted flutter boundary increased sharply past the transonic dip. Though slightly higher than observed through

experiment, predicted results compared reasonably well considering the fact that differences in flutter prediction past the transonic dip appear exaggerated due to the very good agreement prior to the dip.

4.4 Aeroservoelastic Results

The natural extension of work done to this point is to use the control surface on the BACT wing to suppress flutter. The actual design of the control law, as was mentioned in Chapter 3, was assisted through the use of a computational MATLAB[®] model developed by Waszak. The MATLAB[®] model allowed very quick studies on the effectiveness of different control laws for the BACT wind-tunnel model at Mach 0.77. Shown in the following figure is an example plot obtained from the investigation using the MATLAB[®] model. Initially control is off and the system oscillates towards flutter. At $t=0.8$ sec, control is activated and the entire response plotted. The plot on the left shows plunge and pitch positions in inches and degrees, respectively. The plot on the right shows control surface position. The plots were kept separate to allow better visualization of the system dynamics.

Figure 4-32 shows a representative flutter suppression example using the MATLAB model. Control laws for the such models were kept relatively simple to facilitate their implementation into STARS.

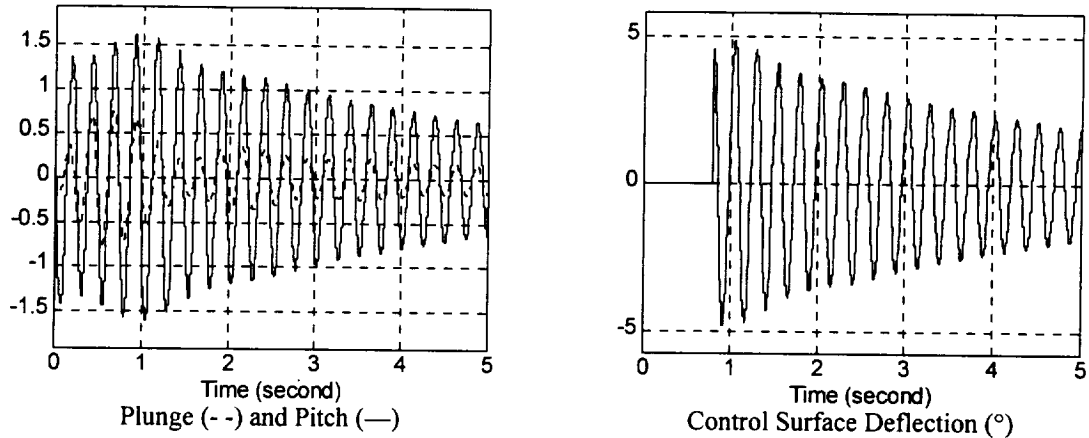


Figure 4-32: MATLAB® Flutter Suppression Example

4.4.1 Control Law Development

In deciding on a control law, it was noted that the lift was much more affected through a change in pitch angle than in control surface deflection. With $C_{L_\alpha} = 4.584$ and $C_{L_\delta} = 0.63$, we see that the effect of α on lift is more than 7 times greater than the effect of δ . Additionally, with $C_{M_\alpha} = 1.490$ and $C_{M_\delta} = -0.0246$, we see that the effect of α on moment is more than 60 times that of δ . Since the data was unavailable, the trailing edge rate effects were ignored in the MATLAB model. These effects, after analyzing a step-input to the control surface in STARS, showed to be of significant value. Since this research effort focuses on the feasibility of simulating control surface deflections during flutter using the transpiration boundary condition, effort given to the development of a control algorithm was for the purpose of demonstrating the feasibility of ASE control of the BACT wing within STARS.

4.4.2 Control Implementation into STARS

With the simulation acceleration provided through the system identification technique, changes in control laws and control gains could be seen relatively quickly. A study of this type using the Euler solver would be very impractical if one had to wait for several weeks to see if a control algorithm worked. For example, using the estimated solution duration developed in section 3.2.4.2, a single 5000 step time history requires approximately 70 days to complete. Now, consider trying numerous control algorithms, or even simple gain changes where each parameter change requires another 60 or 70 days to complete. Again, these numbers illustrate this impracticality since a single control law, at a single Mach number and dynamic pressure could easily take several years to complete. In this effort, control is demonstrated at Mach 0.51, 0.77, and 0.82. As with the case of the flutter boundaries, validation is given at a single Mach number, 0.77, due to time restrictions.

For the actual implementation into STARS, the following block diagram illustrates the control algorithm desired. Since the position and velocity are already updated and calculated at each time step within STARS, the feed back control law is based upon proportional feedback of plunge and pitch magnitude, as well as plunge and pitch rates.

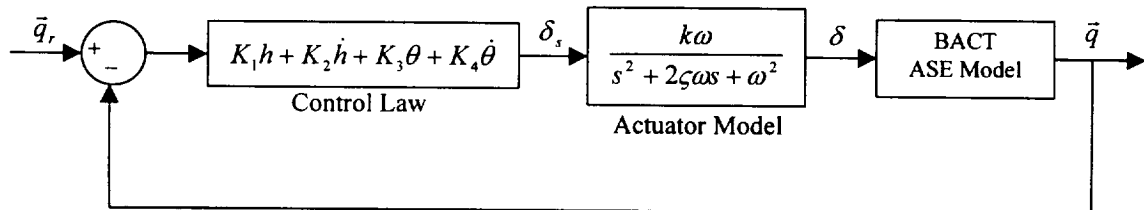


Figure 4-33: Block Diagram of Control Implemented into STARS

Typically, q_r , the vector of desired modal displacements and velocities, will be zero. The control law simply calculates a desired control surface position, δ_s , based on the specified gains. The actual control surface deflection, δ , is subject to the actuator model introduced in section 3.2.4.4. From the actuator model, a new displacement and velocity is calculated and enforced at each discrete time step.

Shown below is a portion of the code modified in *CFDASE* to input control surface deflections and velocities into STARS. These control surface deflections follow the adapted actuator model originally developed by Waszak.

```

:
elseif ( ibcx .eq. 2 ) then                                ibcx=2 Specifies ASE Control to be Used

CHS   Define Controls Parameters                            Actuator Model Parameters
      k = 1.02
      zeta = .56
      omega = 165.3

CHS   Delay Control For a While...                          Delays control for 50 steps
      if (istep .gt. 50 ) then

CHS   Define New C.S. Position                               Compute New Desired C.S. Angle
      xn1(3) = DELT*xn16old+xn13old

CHS   Limit C.S. Deflection Amount                           Limits C.S. Deflection to ± 15°
      if (xn1(3) .GT. 15.0) then
        xn1(3) = 15.0
      elseif (xn1(3) .LT. -15.0) then
        xn1(3) = -15.0
      end if

CHS   Define New C.S. Velocity                               Compute New Desired C.S. Ang. Vel.
      xn1(6) = DELT*( -10.0*rbcx*xn1(1)-0.5*rbcx*xn(4) -
&                2.0*rbcx*xn1(5) ) *k*omega*omega-
&                DELT*2*zeta*omega*xn16old-
&                DELT*omega*omega*xn13old+
&                xn16old
      else                                                    C.S. Held Steady While Control is Off
      xn1(3) = 0.0
      xn1(6) = 0.0
      end if

:

```

In the section of the code above, the parameters *ibcx* and *rbcx* are defined in the *SCALARS* file. For purposes of control, *ibcx* tells the code that control is desired after the 50th time step. The 50 step delay simply allows the BACT system to work past any flow transients due to the impulsive force before control is activated. The proportional gain is set with the *rbcx* parameter. The variables *xnl(1)*, *xnl(2)*, *xnl(3)*, *xnl(4)*, *xnl(5)*, and *xnl(6)* are the mode 1,2, and 3 generalized displacements and velocities, respectively.

4.4.3 Flutter Suppression for the BACT Wing Using STARS

Implementing these modifications in an aeroservoelastic application lacks only a control algorithm. Since the research is more focused upon the feasibility of control, control laws are not optimized for performance, but rather demonstrate the ability for STARS to be applied to this sort of problem.

During the implementation process, it was discovered that the typical multi-step sequence did not convey enough information to completely model the control surface. The effects of plunging and pitching the wing had much greater effects on the generalized forces than did the *small* control surface deflections. This can be seen from the multi-step training data shown in Figure 4-20 through Figure 4-25. The solution was to simply allow the multi-step corresponding to the control surface deflection to have a higher magnitude than that of the plunge and pitch degrees of freedom. Figure 4-34 shows the new multi-step sequence adapted for the ASE portion of the study. The figure clearly shows the additional magnitude present in both the displacement and velocity inputs for mode 3. In this case, increasing the magnitude by a factor of three worked sufficiently well.

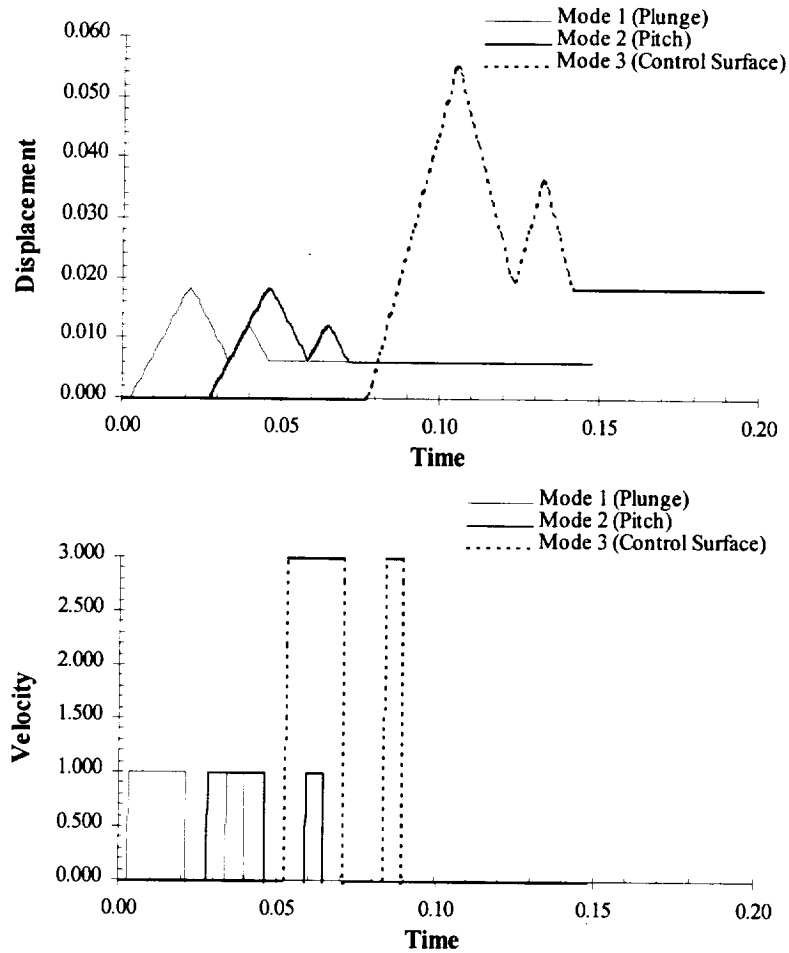


Figure 4-34: Modified Multi-Step Sequence Used for ASE

As was with the previous cases, the extent to which the system model predicted the Euler solution is first judged by a solution comparison using the multi-step. Figure 4-35 shows the resulting generalized forces resulting from the new multi step. For this case, at Mach 0.77, one can see a much more defined response, as compared to Figure 4-23, in modes 1 and 2 due to the deflection of the control surface. This additional data significantly improved the system models ability to predict the Euler solution.

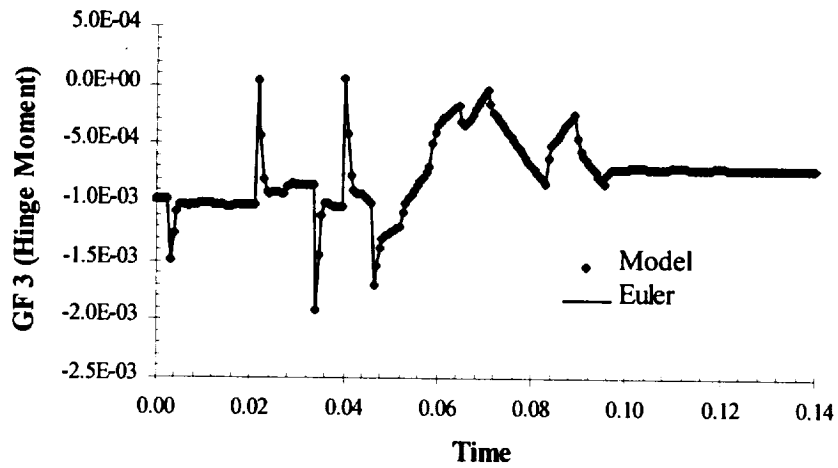
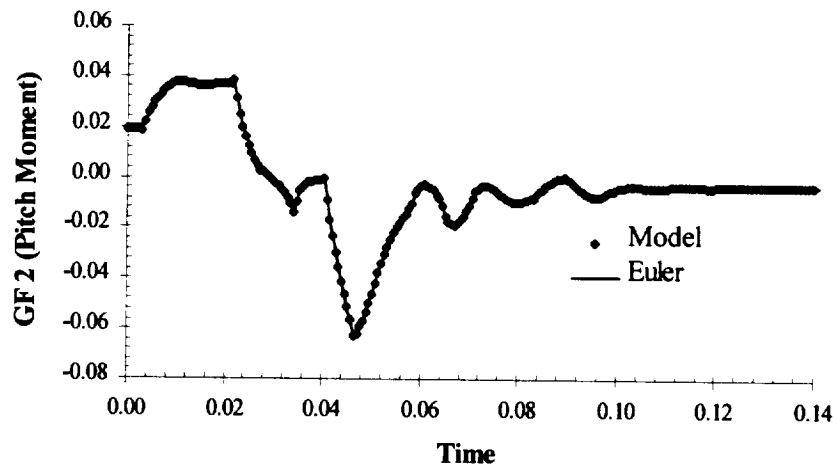
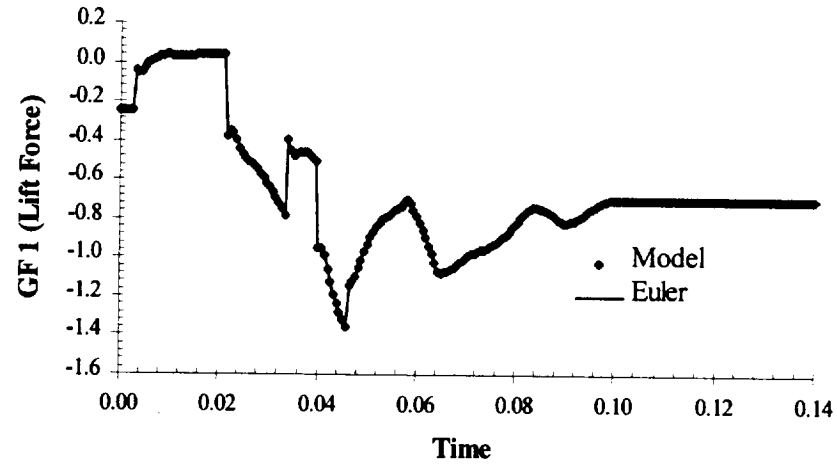
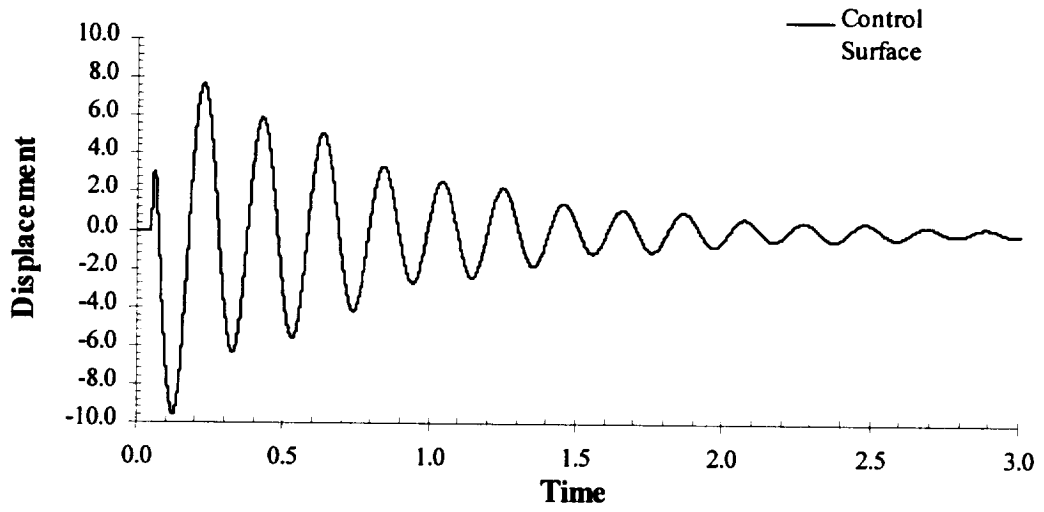
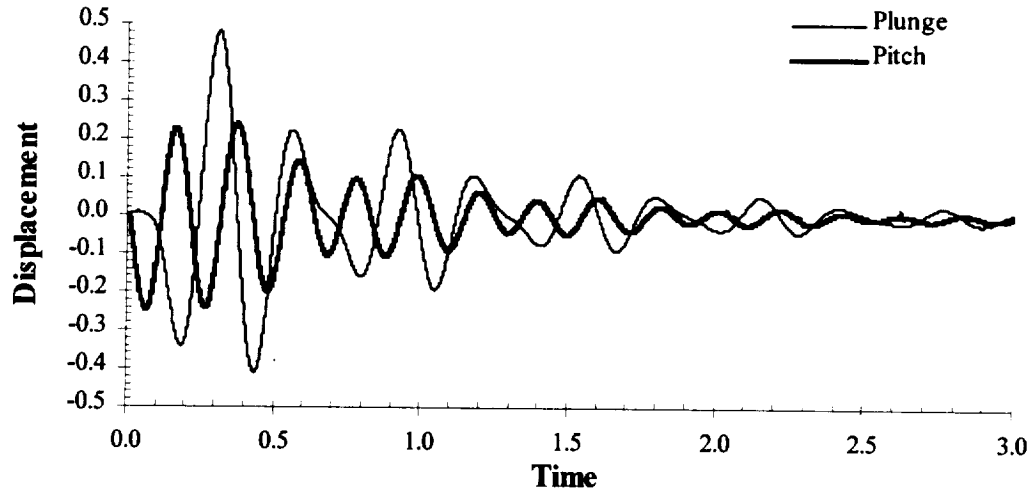


Figure 4-35: Multi-Step Response for Model and Euler Solutions

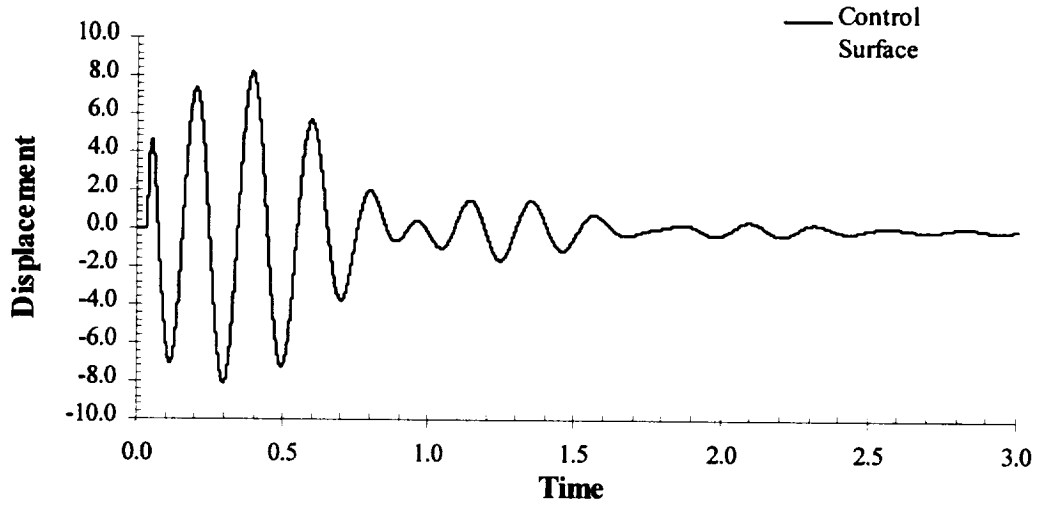
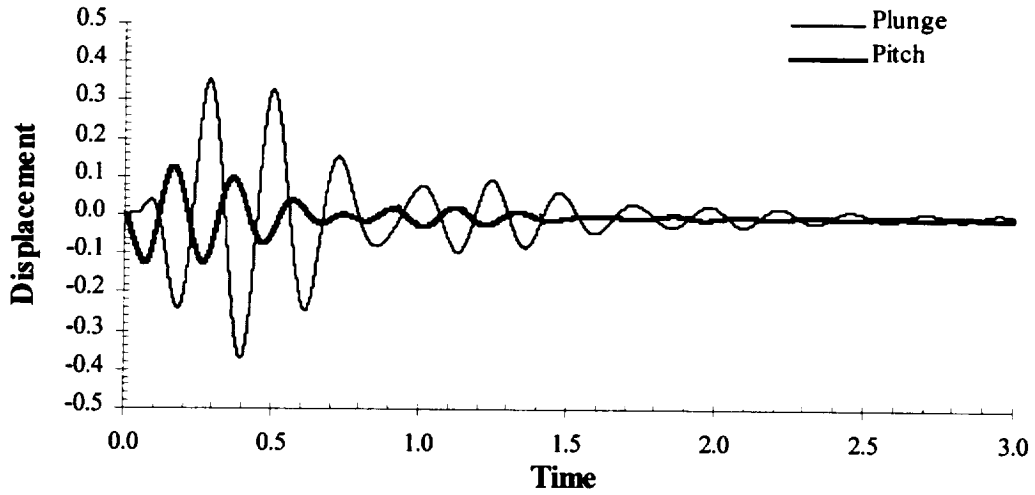
Figure 4-36, Figure 4-37, and Figure 4-39 show the resulting time histories with the trailing edge control surface effectively damping out a response that would otherwise tend towards flutter. Control of this single-input, multi-output system actually proved to be slightly illusive. Choosing a control law based on a trial and error approach for a system as highly coupled as this was not a simple task.

Many combinations of control algorithms and gains were tested and the final control law used results more from empirical observations of many time-histories. The control method that seemed to work the best was one that quickly damped out the pitch motion. This makes sense since it is typically the pitch degree-of-freedom driving the system towards instability. Control on pitch alone did not work quite as desired so a contribution due to the plunge position was eventually added. Each of the following figures shows that the control law worked as it was supposed to. In each case, pitch motion is initially more highly damped than plunge motion, with both pitch and plunge eventually tending towards zero displacement.



Control Law: $\delta_s = 5h - 1.2\dot{\alpha}$

Figure 4-36: Aeroservoelastic Response at Mach 0.51



$$\text{Control Law: } \delta_s = -(10h + 0.5\dot{h} + 2\dot{\alpha})$$

Figure 4-37: Aeroservoelastic Response at Mach 0.77

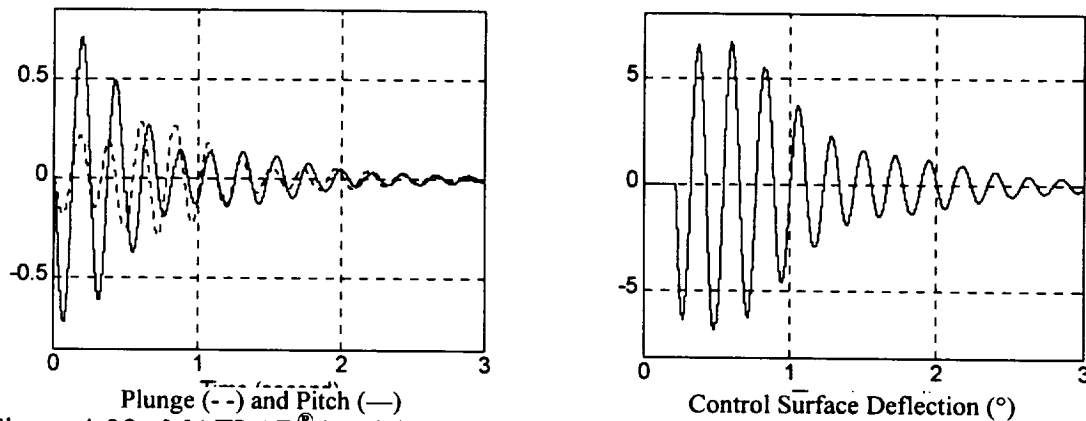
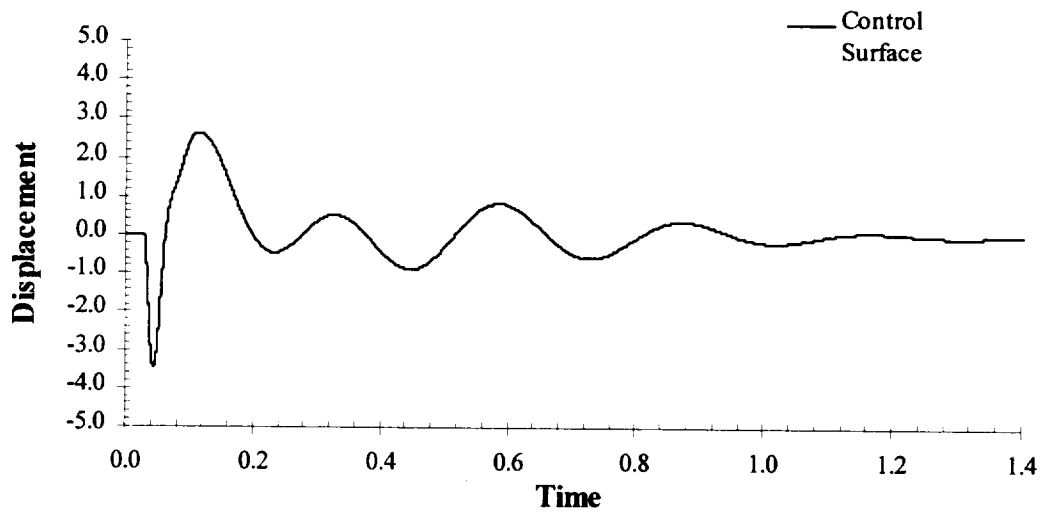
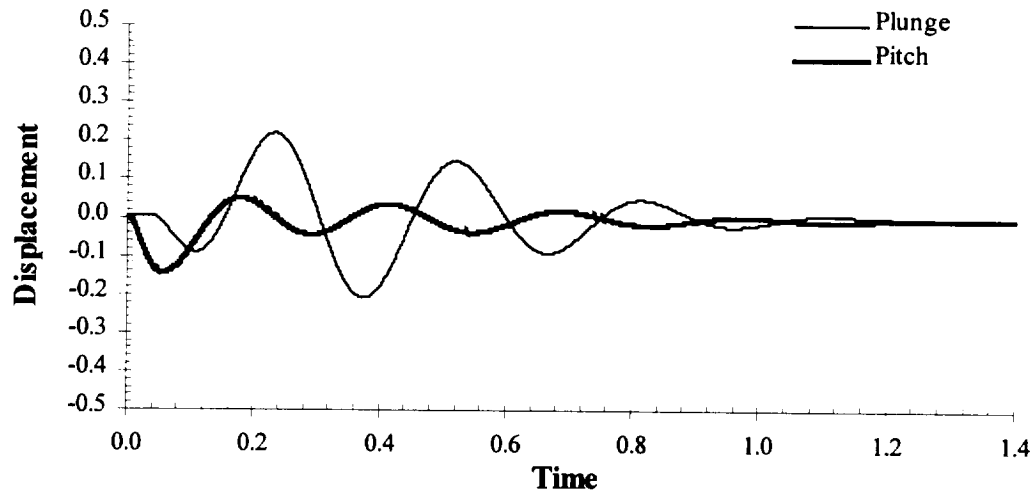


Figure 4-38: MATLAB® Model Comparison Using a Similar Control Law at Mach 0.77



Control Law: $\delta_s = 5h + 1.2\dot{\alpha}$

Figure 4-39: Aeroservoelastic Response at Mach 0.82

Figure 4-38 shows a similar control law implemented at Mach 0.77 in the MATLAB model. Comparing with Figure 4-37, we see that both models agree reasonably well and show pitch motion is eliminated first, with plunge motion following.

The Mach 0.82 case had an interesting occurrence. In order to control the plunge and pitch motions, the sign of the plunge gain had to be changed. With the critical Mach number for the BACT wing being approximately 0.77, a very definite transonic shock exists at Mach 0.82. With the center of pressure moved further back on the wing due to

the presence of the shock, the control law used in the two previous cases was no longer valid.

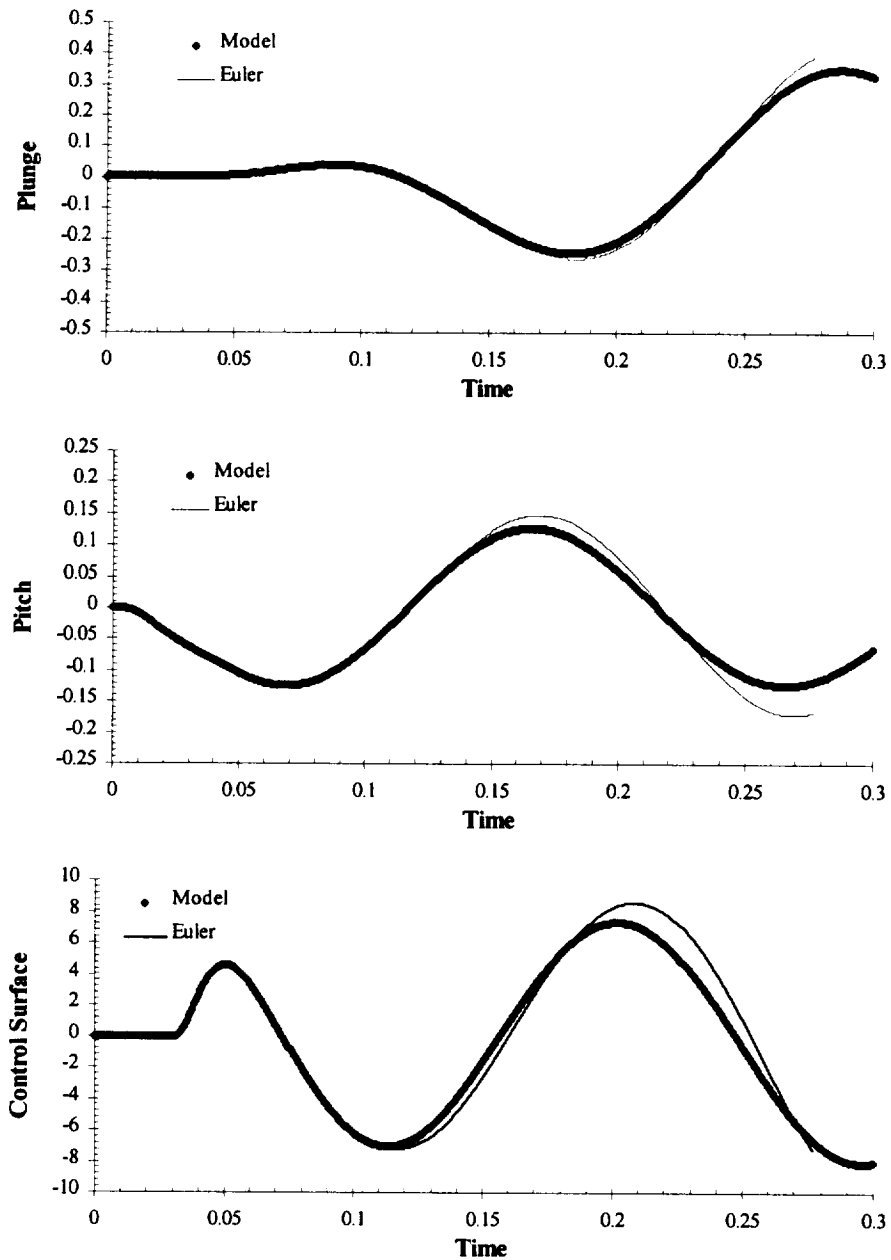


Figure 4-40: Euler Validation of the Modeled Aeroservoelastic Response at Mach 0.77

Shown in Figure 4-40 is the Euler validation of the system model for Mach 0.77. More so than was seen with the previous validation case, we see more significant differences between the system model and the Euler solution. These differences exhibit

one of the limitations within the system model. The system model assumes that in a small region of the steady state solution, perturbations are essentially linear. Typically this is true, but remember that Mach 0.77 is the apparent critical Mach number for the BACT wing. With no deflected control surface, there are no shocks on the surface of the wing but as one can see, control surface deflections approach 10° during the control sequence. With a significant control surface deflection, however, shocks begin to form in the region of the deflection. The presence of these shocks introduce nonlinearities into the solution that were not present during the multi-step solution which is used to train the model. From the above figure, we observe is a loss of predicted control surface effectiveness, but the general trend is in agreement with that predicted by the model.

There is no comparison with experimental data presented for this case, but, as was seen for the case of a steady flap deflection, reasonable results could be expected as long as the control surface deflection during control is not greater than 7° or 8° , or in cases where significant viscous effects are present.

CHAPTER 5

CONCLUSIONS AND RECOMMENDATIONS

5.1 Conclusions

The objective of the research conducted was to demonstrate the effectiveness of the transpiration method when applied to: steady control surface deflections, unsteady aeroelastic applications, and unsteady aeroservoelastic control. Previously, the transpiration method was demonstrated to be effective on continuous geometric deflections in cases such as the AGARD 445.6 and the 2×1 Plate. The current effort successfully applied the transpiration method, through STARS, on a problem involving the additional complexities associated with discontinuous deformations. Additionally, research focused on the implementation of a discrete-time control algorithm into STARS and was demonstrated to be effective for flutter suppression at a variety of Mach numbers.

The primary test cases for this effort were the NACA 0012 wing and the BACT wind-tunnel model, both developed and tested at the NASA Langley Research Center under the Benchmark Models Program. At all Mach numbers investigated, steady pressure distributions without a control surface deflection matched very well, even for the cases involving transonic shocks.

When compared to a mesh with a physical 10° control surface deflection, simulated 10° deflections at both Mach 0.77 and 0.82 matched the Euler prediction from

1

STARS very well. These results indicated that the transpiration method was at least as accurate as the Euler prediction. When compared to experimental data at Mach 0.77 and Mach 0.82 with control surface deflections of 2°, 5° and 10°, pressure distributions using simulated control surface deflections of 2° and 5° matched well. With a 10° deflection, however, it appeared that the significant viscous effects present with such a large deflection made the flow physics intractable for the use of an Euler flow solver.

Experimental results were often subject to slight differences from nominal experimental parameters. Flutter prediction was demonstrated to be highly sensitive to the location of the center of gravity relative to the elastic axis (x_{cg}). Changes in x_{cg} of less than 1% were also shown to affect flutter prediction differently across the range of Mach numbers tested. Also mentioned was the difficulty in the determination of the exact dynamic pressure at the onset of flutter. The determination of the actual flutter point is often a subjective judgement. STARS used a modal identification procedure to alleviate the subjectivity in this judgement.

Prediction of the flutter boundary also compared well with experimental data from both the NACA 0012 wing tested in air and the BACT wing tested in R-12. For Mach numbers ranging from 0.51 to 0.77, differences from experimental data were less than 4%. Past the transonic dip at Mach 0.77, computational results, compared to experimental data, show a more aggressive increase in dynamic pressure at flutter (q_f) at both Mach 0.80 and 0.82.

For the first time, aeroservoelastic control of a body using the transpiration method was implemented into STARS. For control based on plunge position and pitch-rate, time-histories at Mach 0.51, 0.77, and 0.82 show that the transpiration boundary

condition can successfully be employed during a full ASE simulation. An Euler validation for control at Mach 0.77 showed good agreement between the actual Euler solution and that predicted by the system model.

5.2 Recommendations

Validation of the system-identification technique showed that the system model adequately modeled the actual coupled structural/aerodynamic problem. Due to significant time constraints, however, validation of each flutter point could take a great deal of computational time to complete. However accurate the model, an Euler validation is the only way to truly validate all of the computational data presented in this paper. As was demonstrated in the ASE simulation, significant nonlinear effects can be introduced during control which introduce slight discrepancies between the Euler and model solutions, and therefore must be accounted for.

Finally, it is still possible that a more efficient/effective control algorithm exists. The robustness of the current control law was not fully investigated, specifically the effect of dynamic pressure. For the purpose of demonstrating the aeroservoelastic capability in STARS, however, the control law adopted is adequate.

For future work, a method of extracting stability and control derivatives from the system model could prove very useful. One could then combine the structural and aerodynamic state space equations with an arbitrary control law in a program such as MATLAB. With a complete model in MATLAB, a much more sophisticated control analysis would be possible allowing the controller to be designed in MATLAB and validated through its implementation into STARS.

Additionally, an ASE simulation could be expanded beyond that of a simple wing/flap geometry. As a feasibility study, the BACT wing provided valuable insight into ASE implementation into STARS. For the general ASE simulation, one could expand the current problem to include rigid body modes and model an entire aircraft. Modeling the entire aircraft would allow a more general prediction of the complete flight dynamics during an ASE simulation.

BIBLIOGRAPHY

- Arena, A.S. Jr. (1996-1998). Assistant Professor, Oklahoma State University. Personal Communications.
- Batina, J.T. (1989). Unsteady Euler Airfoil Solutions Using Unstructured Dynamic Meshes. AIAA 89-0115, American Institute of Aeronautics and Astronautics.
- Cowan, T.J. (1998). Efficient Aeroelastic CFD Predictions Using System Identification, Masters Thesis, Oklahoma State University.
- Dowell, E.H., Crawley, E.F., Curtiss, Jr., H.C., Peters, D.A., Scanlan, R.H., and Sisto, F. (1995). A Modern Course in Aeroelasticity (3rd edition), Kluwer Academic Publishers.
- Eckhart, C.L. (1998). Using ARMA Models to Identify Modal Parameters for Flutter Boundary Prediction, Masters Thesis, Oklahoma State University.
- Farmer, M.G. (1982). A Two-Degree-of-Freedom Flutter Mount System with Low Damping for Testing Rigid Wings at Different Angles of Attack. NASA TM-83302.
- Fisher, C.F., and Arena, Jr., A.S. (1996). On the Transpiration Method for Efficient Aeroelastic Analysis Using an Euler Solver. AIAA 96-3436, American Institute of Aeronautics and Astronautics.
- Gupta, K.K. (1997). STARS – An Integrated General-Purpose Finite Element Structural, Aeroelastic, and Aeroservoelastic Analysis Computer Program. NASA TM-4795.
- Lighthill, M.J. (1958). *On Displacement Thickness*. Journal of Fluid Mechanics, 4(4), 383-392.
- Malone, J.B., Sankar, L.N., and Sotomayer, W.A. (1984). Unsteady Aerodynamic Modeling of a Fighter Wing in Transonic Flow. AIAA 84-1566, American Institute of Aeronautics and Astronautics.
- Malone, J.B., and Sankar, L.N. (1985). Unsteady Full Potential Calculations for Complex Wing-Body Configurations. AIAA 85-4062, American Institute of Aeronautics and Astronautics.
- Peiró, J., Peraire, J., and Morgan, K. (1993) FELISA SYSTEM Reference Material Part 1—Basic Theory.

- Pope, Alan (1954). Wind-Tunnel Testing (2nd edition), John Wiley & Sons, New York.
- Raj, P. and Harris, B. (1993). Using Surface Transpiration with an Euler Method for Cost-effective Aerodynamic Analysis. AIAA 93-3506, American Institute of Aeronautics and Astronautics.
- Rausch, R.D., Batina, J.T., and yang, H.T.Y. (1989). Euler Flutter Analysis of Airfoils Using Unstructured Dynamic Meshes. *Journal of Aircraft*, Vol. 27, No. 5, May 1990, pp. 436-443.
- Rivera, A.J., Jr., Dansberry, B.E., Farmer, M.G., Eckstrom, C.V., Seidel, D. A., and Bennett, R.M. (1991). Experimental Flutter Boundaries With Unsteady Pressure Distributions for the NACA 0012 Benchmark Model. NASA-TM-104072.
- Rivera, A.J., Jr., Dansberry, B.E., Bennett, R.M., Durham, M.H., and Silva, W.A. (1992). NACA 0012 Benchmark Model Experimental Flutter Results With Unsteady Pressure Distributions. NASA-TM-107581.
- Rivera, A.J., Jr., Dansberry, B.E., Durham, M.H., Bennett, R.M., and Silva, W.A. (1992). Pressure Measurements on a Rectangular Wing With a NACA 0012 Airfoil During Conventional Flutter. NASA-TM-104211.
- Robinson, B.A., Batina, J.T., and Yang, H.T.Y. (1989). Aeroelastic Analysis of Wings Using the Euler Equations with a Deforming Mesh. *Journal of Aircraft*, Vol. 28, No. 11, May 1991, pp. 781-788.
- Ruo, S.Y., and Sankar, N.L. (1988). Euler Calculations for Wing-Alone Configurations. *Journal of Aircraft*, Vol. 25, No. 5, May 1988, pp. 436-441.
- Sankar, N.L., Malone, J.B., and Tassa, Y. (1981). An Implicit Conservative Algorithm for Steady and Unsteady Three-Dimensional Transonic Potential Flows. AIAA 81-1016, American Institute of Aeronautics and Astronautics.
- Sankar, N.L., Ruo, S.Y., and Malone, J.B. (1986). Application of Surface Transpiration in Computational Aerodynamics. AIAA 86-0511, American Institute of Aeronautics and Astronautics.
- Sankar, N.L., Malone, J.B., and Schuster, D. (1987). Euler Solutions for Transonic Flow Past a Fighter Wing. *Journal of Aircraft*, Vol. 24, No. 1, Jan. 1987, pp. 10-16.
- Scott, R.C., Hoadley, S.T. Wiesman, C.D. and Durham, M.H. (1997). The Benchmark Active Controls Technology Model Aerodynamic Data. AIAA 97-0829, American Institute of Aeronautics and Astronautics.
- Scott, R.C. (1998). Aerospace Engineer, NASA Langley Research Center. Personal Communications.

- Waszak, M.R. and Fung, J. (1996). Parameter Identification and Analysis of Actuators for the BACT Wind-Tunnel Model. AIAA 96-3362, American Institute of Aeronautics and Astronautics.
- Waszak, M.R. (1996). Modeling of the Benchmark Active Controls Technology Wind-Tunnel Model for Application to Flutter Suppression. AIAA 96-3437, American Institute of Aeronautics and Astronautics.
- Waszak, M.R. (1997). BACT Simulation User Guide (v. 7.0). NASA-TM-97-206252.
- Waszak, M.R. (1998). Aerospace Research Engineer, NASA Langley Research Center. Personal Communications.

APPENDICES

APPENDIX A-1

STARS-SOLIDS Data File (NOPAPA.DAT)

BACT Wing With Flap, No PAPA Mount

404, 354, 5, 6, 3, 3, 0, 0, 0, 0

0, 0, 0, 0, 0, 0, 0, 0, 0

1, 1, 0, 0, 0, 0, 0, 0

2, 0, 0, 0, 0, 0, 0, 1, 0, 0

1, 3, 0, .1000E+04, .0000E+00, .0000E+00

\$NODAL DATA

13 .0000 .0000 .0000 0 0 0 0 0 0 0 0 0
 14 2.0000 .0000 .0000 0 0 0 0 0 0 0 0 0
 52 4.0000 .0000 .0000 0 0 0 0 0 0 0 0 0
 53 6.0000 .0000 .0000 0 0 0 0 0 0 0 0 0
 54 8.0000 .0000 .0000 0 0 0 0 0 0 0 0 0
 55 10.0000 .0000 .0000 0 0 0 0 0 0 0 0 0
 56 12.0000 .0000 .0000 0 0 0 0 0 0 0 0 0
 90 14.0000 .0000 .0000 0 0 0 0 0 0 0 0 0
 91 16.0000 .0000 .0000 0 0 0 0 0 0 0 0 0
 300 16.0000 14.4000 .0000 0 0 0 0 0 0 0 0 0
 301 16.0000 15.0400 .0000 0 0 0 0 0 0 0 0 0
 302 16.0000 15.6800 .0000 0 0 0 0 0 0 0 0 0
 303 16.0000 16.3200 .0000 0 0 0 0 0 0 0 0 0
 304 16.0000 16.9600 .0000 0 0 0 0 0 0 0 0 0
 305 16.0000 17.6000 .0000 0 0 0 0 0 0 0 0 0
 306 16.0000 18.2400 .0000 0 0 0 0 0 0 0 0 0
 307 16.0000 18.8800 .0000 0 0 0 0 0 0 0 0 0
 308 16.0000 19.5200 .0000 0 0 0 0 0 0 0 0 0
 309 16.0000 20.1600 .0000 0 0 0 0 0 0 0 0 0
 310 16.0000 20.8000 .0000 0 0 0 0 0 0 0 0 0
 311 16.0000 21.4400 .0000 0 0 0 0 0 0 0 0 0
 312 16.0000 22.0800 .0000 0 0 0 0 0 0 0 0 0
 313 16.0000 22.7200 .0000 0 0 0 0 0 0 0 0 0
 314 16.0000 23.3600 .0000 0 0 0 0 0 0 0 0 0
 315 16.0000 24.0000 .0000 0 0 0 0 0 0 0 0 0
 316 15.6667 14.4000 .0000 0 0 0 0 0 0 0 0 0
 317 15.6667 15.0400 .0000 0 0 0 0 0 0 0 0 0
 318 15.6667 15.6800 .0000 0 0 0 0 0 0 0 0 0
 319 15.6667 16.3200 .0000 0 0 0 0 0 0 0 0 0
 320 15.6667 16.9600 .0000 0 0 0 0 0 0 0 0 0
 321 15.6667 17.6000 .0000 0 0 0 0 0 0 0 0 0
 322 15.6667 18.2400 .0000 0 0 0 0 0 0 0 0 0
 323 15.6667 18.8800 .0000 0 0 0 0 0 0 0 0 0
 324 15.6667 19.5200 .0000 0 0 0 0 0 0 0 0 0
 325 15.6667 20.1600 .0000 0 0 0 0 0 0 0 0 0
 326 15.6667 20.8000 .0000 0 0 0 0 0 0 0 0 0
 327 15.6667 21.4400 .0000 0 0 0 0 0 0 0 0 0
 328 15.6667 22.0800 .0000 0 0 0 0 0 0 0 0 0
 329 15.6667 22.7200 .0000 0 0 0 0 0 0 0 0 0
 330 15.6667 23.3600 .0000 0 0 0 0 0 0 0 0 0
 331 15.6667 24.0000 .0000 0 0 0 0 0 0 0 0 0
 332 15.3333 14.4000 .0000 0 0 0 0 0 0 0 0 0
 333 15.3333 15.0400 .0000 0 0 0 0 0 0 0 0 0
 334 15.3333 15.6800 .0000 0 0 0 0 0 0 0 0 0
 335 15.3333 16.3200 .0000 0 0 0 0 0 0 0 0 0
 336 15.3333 16.9600 .0000 0 0 0 0 0 0 0 0 0

337 15.3333 17.6000 .0000 0 0 0 0 0 0 0 0 0
 338 15.3333 18.2400 .0000 0 0 0 0 0 0 0 0 0
 339 15.3333 18.8800 .0000 0 0 0 0 0 0 0 0 0
 340 15.3333 19.5200 .0000 0 0 0 0 0 0 0 0 0
 341 15.3333 20.1600 .0000 0 0 0 0 0 0 0 0 0
 342 15.3333 20.8000 .0000 0 0 0 0 0 0 0 0 0
 343 15.3333 21.4400 .0000 0 0 0 0 0 0 0 0 0
 344 15.3333 22.0800 .0000 0 0 0 0 0 0 0 0 0
 345 15.3333 22.7200 .0000 0 0 0 0 0 0 0 0 0
 346 15.3333 23.3600 .0000 0 0 0 0 0 0 0 0 0
 347 15.3333 24.0000 .0000 0 0 0 0 0 0 0 0 0
 348 15.0000 14.4000 .0000 0 0 0 0 0 0 0 0 0
 349 15.0000 15.0400 .0000 0 0 0 0 0 0 0 0 0
 350 15.0000 15.6800 .0000 0 0 0 0 0 0 0 0 0
 351 15.0000 16.3200 .0000 0 0 0 0 0 0 0 0 0
 352 15.0000 16.9600 .0000 0 0 0 0 0 0 0 0 0
 353 15.0000 17.6000 .0000 0 0 0 0 0 0 0 0 0
 354 15.0000 18.2400 .0000 0 0 0 0 0 0 0 0 0
 355 15.0000 18.8800 .0000 0 0 0 0 0 0 0 0 0
 356 15.0000 19.5200 .0000 0 0 0 0 0 0 0 0 0
 357 15.0000 20.1600 .0000 0 0 0 0 0 0 0 0 0
 358 15.0000 20.8000 .0000 0 0 0 0 0 0 0 0 0
 359 15.0000 21.4400 .0000 0 0 0 0 0 0 0 0 0
 360 15.0000 22.0800 .0000 0 0 0 0 0 0 0 0 0
 361 15.0000 22.7200 .0000 0 0 0 0 0 0 0 0 0
 362 15.0000 23.3600 .0000 0 0 0 0 0 0 0 0 0
 363 15.0000 24.0000 .0000 0 0 0 0 0 0 0 0 0
 364 14.6667 14.4000 .0000 0 0 0 0 0 0 0 0 0
 365 14.6667 15.0400 .0000 0 0 0 0 0 0 0 0 0
 366 14.6667 15.6800 .0000 0 0 0 0 0 0 0 0 0
 367 14.6667 16.3200 .0000 0 0 0 0 0 0 0 0 0
 368 14.6667 16.9600 .0000 0 0 0 0 0 0 0 0 0
 369 14.6667 17.6000 .0000 0 0 0 0 0 0 0 0 0
 370 14.6667 18.2400 .0000 0 0 0 0 0 0 0 0 0
 371 14.6667 18.8800 .0000 0 0 0 0 0 0 0 0 0
 372 14.6667 19.5200 .0000 0 0 0 0 0 0 0 0 0
 373 14.6667 20.1600 .0000 0 0 0 0 0 0 0 0 0
 374 14.6667 20.8000 .0000 0 0 0 0 0 0 0 0 0
 375 14.6667 21.4400 .0000 0 0 0 0 0 0 0 0 0
 376 14.6667 22.0800 .0000 0 0 0 0 0 0 0 0 0
 377 14.6667 22.7200 .0000 0 0 0 0 0 0 0 0 0
 378 14.6667 23.3600 .0000 0 0 0 0 0 0 0 0 0
 379 14.6667 24.0000 .0000 0 0 0 0 0 0 0 0 0
 380 14.3333 14.4000 .0000 0 0 0 0 0 0 0 0 0
 381 14.3333 15.0400 .0000 0 0 0 0 0 0 0 0 0
 382 14.3333 15.6800 .0000 0 0 0 0 0 0 0 0 0
 383 14.3333 16.3200 .0000 0 0 0 0 0 0 0 0 0
 384 14.3333 16.9600 .0000 0 0 0 0 0 0 0 0 0
 385 14.3333 17.6000 .0000 0 0 0 0 0 0 0 0 0
 386 14.3333 18.2400 .0000 0 0 0 0 0 0 0 0 0
 387 14.3333 18.8800 .0000 0 0 0 0 0 0 0 0 0
 388 14.3333 19.5200 .0000 0 0 0 0 0 0 0 0 0
 389 14.3333 20.1600 .0000 0 0 0 0 0 0 0 0 0

685 .0000 14.3000 .0000 0 0 0 0 0 0 0 0 0
686 2.0000 14.3000 .0000 0 0 0 0 0 0 0 0 0
687 4.0000 14.3000 .0000 0 0 0 0 0 0 0 0 0
688 6.0000 14.3000 .0000 0 0 0 0 0 0 0 0 0
689 8.0000 14.3000 .0000 0 0 0 0 0 0 0 0 0
690 10.0000 14.3000 .0000 0 0 0 0 0 0 0 0 0
691 12.0000 14.3000 .0000 0 0 0 0 0 0 0 0 0
692 14.0000 14.3000 .0000 0 0 0 0 0 0 0 0 0
693 16.0000 14.3000 .0000 0 0 0 0 0 0 0 0 0
694 .0000 24.1000 .0000 0 0 0 0 0 0 0 0 0
695 2.0000 24.1000 .0000 0 0 0 0 0 0 0 0 0
696 4.0000 24.1000 .0000 0 0 0 0 0 0 0 0 0
697 6.0000 24.1000 .0000 0 0 0 0 0 0 0 0 0
698 8.0000 24.1000 .0000 0 0 0 0 0 0 0 0 0
699 10.0000 24.1000 .0000 0 0 0 0 0 0 0 0 0
700 12.0000 24.1000 .0000 0 0 0 0 0 0 0 0 0
701 14.0000 24.1000 .0000 0 0 0 0 0 0 0 0 0
702 16.0000 24.1000 .0000 0 0 0 0 0 0 0 0 0
703 11.4000 14.4000 .0000 0 0 0 0 0 0 0 0 0
704 11.9000 16.0000 .0000 0 0 0 0 0 0 0 0 0
705 11.9000 17.6000 .0000 0 0 0 0 0 0 0 0 0
706 11.9000 19.2000 .0000 0 0 0 0 0 0 0 0 0
707 11.9000 20.8000 .0000 0 0 0 0 0 0 0 0 0
708 11.9000 22.4000 .0000 0 0 0 0 0 0 0 0 0
709 11.4000 24.0000 .0000 0 0 0 0 0 0 0 0 0

\$ ELEMENT CONNECTIVITY CONDITIONS

2 300 300 301 317 316 0 0 0 0 5 3 0 0 0 0
2 301 301 302 318 317 0 0 0 0 5 3 0 0 0 0
2 302 302 303 319 318 0 0 0 0 5 3 0 0 0 0
2 303 303 304 320 319 0 0 0 0 5 3 0 0 0 0
2 304 304 305 321 320 0 0 0 0 5 3 0 0 0 0
2 305 305 306 322 321 0 0 0 0 5 3 0 0 0 0
2 306 306 307 323 322 0 0 0 0 5 3 0 0 0 0
2 307 307 308 324 323 0 0 0 0 5 3 0 0 0 0
2 308 308 309 325 324 0 0 0 0 5 3 0 0 0 0
2 309 309 310 326 325 0 0 0 0 5 3 0 0 0 0
2 310 310 311 327 326 0 0 0 0 5 3 0 0 0 0
2 311 311 312 328 327 0 0 0 0 5 3 0 0 0 0
2 312 312 313 329 328 0 0 0 0 5 3 0 0 0 0
2 313 313 314 330 329 0 0 0 0 5 3 0 0 0 0
2 314 314 315 331 330 0 0 0 0 5 3 0 0 0 0
2 315 316 317 333 332 0 0 0 0 5 3 0 0 0 0
2 316 317 318 334 333 0 0 0 0 5 3 0 0 0 0
2 317 318 319 335 334 0 0 0 0 5 3 0 0 0 0
2 318 319 320 336 335 0 0 0 0 5 3 0 0 0 0
2 319 320 321 337 336 0 0 0 0 5 3 0 0 0 0
2 320 321 322 338 337 0 0 0 0 5 3 0 0 0 0
2 321 322 323 339 338 0 0 0 0 5 3 0 0 0 0
2 322 323 324 340 339 0 0 0 0 5 3 0 0 0 0
2 323 324 325 341 340 0 0 0 0 5 3 0 0 0 0
2 324 325 326 342 341 0 0 0 0 5 3 0 0 0 0
2 325 326 327 343 342 0 0 0 0 5 3 0 0 0 0
2 326 327 328 344 343 0 0 0 0 5 3 0 0 0 0
2 327 328 329 345 344 0 0 0 0 5 3 0 0 0 0
2 328 329 330 346 345 0 0 0 0 5 3 0 0 0 0
2 329 330 331 347 346 0 0 0 0 5 3 0 0 0 0
2 330 332 333 349 348 0 0 0 0 5 3 0 0 0 0
2 331 333 334 350 349 0 0 0 0 5 3 0 0 0 0
2 332 334 335 351 350 0 0 0 0 5 3 0 0 0 0
2 333 335 336 352 351 0 0 0 0 5 3 0 0 0 0
2 334 336 337 353 352 0 0 0 0 5 3 0 0 0 0
2 335 337 338 354 353 0 0 0 0 5 3 0 0 0 0
2 336 338 339 355 354 0 0 0 0 5 3 0 0 0 0
2 337 339 340 356 355 0 0 0 0 5 3 0 0 0 0
2 338 340 341 357 356 0 0 0 0 5 3 0 0 0 0
2 339 341 342 358 357 0 0 0 0 5 3 0 0 0 0
2 340 342 343 359 358 0 0 0 0 5 3 0 0 0 0
2 341 343 344 360 359 0 0 0 0 5 3 0 0 0 0
2 342 344 345 361 360 0 0 0 0 5 3 0 0 0 0
2 343 345 346 362 361 0 0 0 0 5 3 0 0 0 0

2 344 346 347 363 362 0 0 0 0 5 3 0 0 0 0
2 345 348 349 365 364 0 0 0 0 5 3 0 0 0 0
2 346 349 350 366 365 0 0 0 0 5 3 0 0 0 0
2 347 350 351 367 366 0 0 0 0 5 3 0 0 0 0
2 348 351 352 368 367 0 0 0 0 5 3 0 0 0 0
2 349 352 353 369 368 0 0 0 0 5 3 0 0 0 0
2 350 353 354 370 369 0 0 0 0 5 3 0 0 0 0
2 351 354 355 371 370 0 0 0 0 5 3 0 0 0 0
2 352 355 356 372 371 0 0 0 0 5 3 0 0 0 0
2 353 356 357 373 372 0 0 0 0 5 3 0 0 0 0
2 354 357 358 374 373 0 0 0 0 5 3 0 0 0 0
2 355 358 359 375 374 0 0 0 0 5 3 0 0 0 0
2 356 359 360 376 375 0 0 0 0 5 3 0 0 0 0
2 357 360 361 377 376 0 0 0 0 5 3 0 0 0 0
2 358 361 362 378 377 0 0 0 0 5 3 0 0 0 0
2 359 362 363 379 378 0 0 0 0 5 3 0 0 0 0
2 360 364 365 381 380 0 0 0 0 5 3 0 0 0 0
2 361 365 366 382 381 0 0 0 0 5 3 0 0 0 0
2 362 366 367 383 382 0 0 0 0 5 3 0 0 0 0
2 363 367 368 384 383 0 0 0 0 5 3 0 0 0 0
2 364 368 369 385 384 0 0 0 0 5 3 0 0 0 0
2 365 369 370 386 385 0 0 0 0 5 3 0 0 0 0
2 366 370 371 387 386 0 0 0 0 5 3 0 0 0 0
2 367 371 372 388 387 0 0 0 0 5 3 0 0 0 0
2 368 372 373 389 388 0 0 0 0 5 3 0 0 0 0
2 369 373 374 390 389 0 0 0 0 5 3 0 0 0 0
2 370 374 375 391 390 0 0 0 0 5 3 0 0 0 0
2 371 375 376 392 391 0 0 0 0 5 3 0 0 0 0
2 372 376 377 393 392 0 0 0 0 5 3 0 0 0 0
2 373 377 378 394 393 0 0 0 0 5 3 0 0 0 0
2 374 378 379 395 394 0 0 0 0 5 3 0 0 0 0
2 375 380 381 397 396 0 0 0 0 5 3 0 0 0 0
2 376 381 382 398 397 0 0 0 0 5 3 0 0 0 0
2 377 382 383 399 398 0 0 0 0 5 3 0 0 0 0
2 378 383 384 400 399 0 0 0 0 5 3 0 0 0 0
2 379 384 385 401 400 0 0 0 0 5 3 0 0 0 0
2 380 385 386 402 401 0 0 0 0 5 3 0 0 0 0
2 381 386 387 403 402 0 0 0 0 5 3 0 0 0 0
2 382 387 388 404 403 0 0 0 0 5 3 0 0 0 0
2 383 388 389 405 404 0 0 0 0 5 3 0 0 0 0
2 384 389 390 406 405 0 0 0 0 5 3 0 0 0 0
2 385 390 391 407 406 0 0 0 0 5 3 0 0 0 0
2 386 391 392 408 407 0 0 0 0 5 3 0 0 0 0
2 387 392 393 409 408 0 0 0 0 5 3 0 0 0 0
2 388 393 394 410 409 0 0 0 0 5 3 0 0 0 0
2 389 394 395 411 410 0 0 0 0 5 3 0 0 0 0
2 390 396 397 413 412 0 0 0 0 5 3 0 0 0 0
2 391 397 398 414 413 0 0 0 0 5 3 0 0 0 0
2 392 398 399 415 414 0 0 0 0 5 3 0 0 0 0
2 393 399 400 416 415 0 0 0 0 5 3 0 0 0 0
2 394 400 401 417 416 0 0 0 0 5 3 0 0 0 0
2 395 401 402 418 417 0 0 0 0 5 3 0 0 0 0
2 396 402 403 419 418 0 0 0 0 5 3 0 0 0 0
2 397 403 404 420 419 0 0 0 0 5 3 0 0 0 0
2 398 404 405 421 420 0 0 0 0 5 3 0 0 0 0
2 399 405 406 422 421 0 0 0 0 5 3 0 0 0 0
2 400 406 407 423 422 0 0 0 0 5 3 0 0 0 0
2 401 407 408 424 423 0 0 0 0 5 3 0 0 0 0
2 402 408 409 425 424 0 0 0 0 5 3 0 0 0 0
2 403 409 410 426 425 0 0 0 0 5 3 0 0 0 0
2 404 410 411 427 426 0 0 0 0 5 3 0 0 0 0
2 405 412 413 429 428 0 0 0 0 5 3 0 0 0 0
2 406 413 414 430 429 0 0 0 0 5 3 0 0 0 0
2 407 414 415 431 430 0 0 0 0 5 3 0 0 0 0
2 408 415 416 432 431 0 0 0 0 5 3 0 0 0 0
2 409 416 417 433 432 0 0 0 0 5 3 0 0 0 0
2 410 417 418 434 433 0 0 0 0 5 3 0 0 0 0
2 411 418 419 435 434 0 0 0 0 5 3 0 0 0 0
2 412 419 420 436 435 0 0 0 0 5 3 0 0 0 0
2 413 420 421 437 436 0 0 0 0 5 3 0 0 0 0

2 414 421 422 438 437 0 0 0 0 5 3 0 0 0 0
2 415 422 423 439 438 0 0 0 0 5 3 0 0 0 0
2 416 423 424 440 439 0 0 0 0 5 3 0 0 0 0
2 417 424 425 441 440 0 0 0 0 5 3 0 0 0 0
2 418 425 426 442 441 0 0 0 0 5 3 0 0 0 0
2 419 426 427 443 442 0 0 0 0 5 3 0 0 0 0
2 420 428 429 445 444 0 0 0 0 5 3 0 0 0 0
2 421 429 430 446 445 0 0 0 0 5 3 0 0 0 0
2 422 430 431 447 446 0 0 0 0 5 3 0 0 0 0
2 423 431 432 448 447 0 0 0 0 5 3 0 0 0 0
2 424 432 433 449 448 0 0 0 0 5 3 0 0 0 0
2 425 433 434 450 449 0 0 0 0 5 3 0 0 0 0
2 426 434 435 451 450 0 0 0 0 5 3 0 0 0 0
2 427 435 436 452 451 0 0 0 0 5 3 0 0 0 0
2 428 436 437 453 452 0 0 0 0 5 3 0 0 0 0
2 429 437 438 454 453 0 0 0 0 5 3 0 0 0 0
2 430 438 439 455 454 0 0 0 0 5 3 0 0 0 0
2 431 439 440 456 455 0 0 0 0 5 3 0 0 0 0
2 432 440 441 457 456 0 0 0 0 5 3 0 0 0 0
2 433 441 442 458 457 0 0 0 0 5 3 0 0 0 0
2 434 442 443 459 458 0 0 0 0 5 3 0 0 0 0
2 435 444 445 461 460 0 0 0 0 5 3 0 0 0 0
2 436 445 446 462 461 0 0 0 0 5 3 0 0 0 0
2 437 446 447 463 462 0 0 0 0 5 3 0 0 0 0
2 438 447 448 464 463 0 0 0 0 5 3 0 0 0 0
2 439 448 449 465 464 0 0 0 0 5 3 0 0 0 0
2 440 449 450 466 465 0 0 0 0 5 3 0 0 0 0
2 441 450 451 467 466 0 0 0 0 5 3 0 0 0 0
2 442 451 452 468 467 0 0 0 0 5 3 0 0 0 0
2 443 452 453 469 468 0 0 0 0 5 3 0 0 0 0
2 444 453 454 470 469 0 0 0 0 5 3 0 0 0 0
2 445 454 455 471 470 0 0 0 0 5 3 0 0 0 0
2 446 455 456 472 471 0 0 0 0 5 3 0 0 0 0
2 447 456 457 473 472 0 0 0 0 5 3 0 0 0 0
2 448 457 458 474 473 0 0 0 0 5 3 0 0 0 0
2 449 458 459 475 474 0 0 0 0 5 3 0 0 0 0
2 450 460 461 477 476 0 0 0 0 5 3 0 0 0 0
2 451 461 462 478 477 0 0 0 0 5 3 0 0 0 0
2 452 462 463 479 478 0 0 0 0 5 3 0 0 0 0
2 453 463 464 480 479 0 0 0 0 5 3 0 0 0 0
2 454 464 465 481 480 0 0 0 0 5 3 0 0 0 0
2 455 465 466 482 481 0 0 0 0 5 3 0 0 0 0
2 456 466 467 483 482 0 0 0 0 5 3 0 0 0 0
2 457 467 468 484 483 0 0 0 0 5 3 0 0 0 0
2 458 468 469 485 484 0 0 0 0 5 3 0 0 0 0
2 459 469 470 486 485 0 0 0 0 5 3 0 0 0 0
2 460 470 471 487 486 0 0 0 0 5 3 0 0 0 0
2 461 471 472 488 487 0 0 0 0 5 3 0 0 0 0
2 462 472 473 489 488 0 0 0 0 5 3 0 0 0 0
2 463 473 474 490 489 0 0 0 0 5 3 0 0 0 0
2 464 474 475 491 490 0 0 0 0 5 3 0 0 0 0
2 465 476 477 493 492 0 0 0 0 5 3 0 0 0 0
2 466 477 478 494 493 0 0 0 0 5 3 0 0 0 0
2 467 478 479 495 494 0 0 0 0 5 3 0 0 0 0
2 468 479 480 496 495 0 0 0 0 5 3 0 0 0 0
2 469 480 481 497 496 0 0 0 0 5 3 0 0 0 0
2 470 481 482 498 497 0 0 0 0 5 3 0 0 0 0
2 471 482 483 499 498 0 0 0 0 5 3 0 0 0 0
2 472 483 484 500 499 0 0 0 0 5 3 0 0 0 0
2 473 484 485 501 500 0 0 0 0 5 3 0 0 0 0
2 474 485 486 502 501 0 0 0 0 5 3 0 0 0 0
2 475 486 487 503 502 0 0 0 0 5 3 0 0 0 0
2 476 487 488 504 503 0 0 0 0 5 3 0 0 0 0
2 477 488 489 505 504 0 0 0 0 5 3 0 0 0 0
2 478 489 490 506 505 0 0 0 0 5 3 0 0 0 0
2 479 490 491 507 506 0 0 0 0 5 3 0 0 0 0
2 480 91 509 517 90 0 0 0 0 5 3 0 0 0 0
2 481 509 510 518 517 0 0 0 0 5 3 0 0 0 0
2 482 510 511 519 518 0 0 0 0 5 3 0 0 0 0
2 483 511 512 520 519 0 0 0 0 5 3 0 0 0 0

2 484 512 513 521 520 0 0 0 0 5 3 0 0 0 0
2 485 513 514 522 521 0 0 0 0 5 3 0 0 0 0
2 486 514 515 523 522 0 0 0 0 5 3 0 0 0 0
2 487 515 693 692 523 0 0 0 0 5 3 0 0 0 0
2 488 90 517 526 56 0 0 0 0 5 3 0 0 0 0
2 489 517 518 527 526 0 0 0 0 5 3 0 0 0 0
2 490 518 519 528 527 0 0 0 0 5 3 0 0 0 0
2 491 519 520 529 528 0 0 0 0 5 3 0 0 0 0
2 492 520 521 530 529 0 0 0 0 5 3 0 0 0 0
2 493 521 522 531 530 0 0 0 0 5 3 0 0 0 0
2 494 522 523 532 531 0 0 0 0 5 3 0 0 0 0
2 495 523 692 691 532 0 0 0 0 5 3 0 0 0 0
2 496 56 526 534 55 0 0 0 0 5 3 0 0 0 0
2 497 526 527 535 534 0 0 0 0 5 3 0 0 0 0
2 498 527 528 536 535 0 0 0 0 5 3 0 0 0 0
2 499 528 529 537 536 0 0 0 0 5 3 0 0 0 0
2 500 529 530 538 537 0 0 0 0 5 3 0 0 0 0
2 501 530 531 539 538 0 0 0 0 5 3 0 0 0 0
2 502 531 532 540 539 0 0 0 0 5 3 0 0 0 0
2 503 532 691 690 540 0 0 0 0 5 3 0 0 0 0
2 504 55 534 543 54 0 0 0 0 5 3 0 0 0 0
2 505 534 535 544 543 0 0 0 0 5 3 0 0 0 0
2 506 535 536 545 544 0 0 0 0 5 3 0 0 0 0
2 507 536 537 546 545 0 0 0 0 5 3 0 0 0 0
2 508 537 538 547 546 0 0 0 0 5 3 0 0 0 0
2 509 538 539 548 547 0 0 0 0 5 3 0 0 0 0
2 510 539 540 549 548 0 0 0 0 5 3 0 0 0 0
2 511 540 690 689 549 0 0 0 0 5 3 0 0 0 0
2 512 54 543 552 53 0 0 0 0 5 3 0 0 0 0
2 513 543 544 553 552 0 0 0 0 5 3 0 0 0 0
2 514 544 545 554 553 0 0 0 0 5 3 0 0 0 0
2 515 545 546 555 554 0 0 0 0 5 3 0 0 0 0
2 516 546 547 556 555 0 0 0 0 5 3 0 0 0 0
2 517 547 548 557 556 0 0 0 0 5 3 0 0 0 0
2 518 548 549 558 557 0 0 0 0 5 3 0 0 0 0
2 519 549 689 688 558 0 0 0 0 5 3 0 0 0 0
2 520 53 552 561 52 0 0 0 0 5 3 0 0 0 0
2 521 552 553 562 561 0 0 0 0 5 3 0 0 0 0
2 522 553 554 563 562 0 0 0 0 5 3 0 0 0 0
2 523 554 555 564 563 0 0 0 0 5 3 0 0 0 0
2 524 555 556 565 564 0 0 0 0 5 3 0 0 0 0
2 525 556 557 566 565 0 0 0 0 5 3 0 0 0 0
2 526 557 558 567 566 0 0 0 0 5 3 0 0 0 0
2 527 558 688 687 567 0 0 0 0 5 3 0 0 0 0
2 528 52 561 570 14 0 0 0 0 5 3 0 0 0 0
2 529 561 562 571 570 0 0 0 0 5 3 0 0 0 0
2 530 562 563 572 571 0 0 0 0 5 3 0 0 0 0
2 531 563 564 573 572 0 0 0 0 5 3 0 0 0 0
2 532 564 565 574 573 0 0 0 0 5 3 0 0 0 0
2 533 565 566 575 574 0 0 0 0 5 3 0 0 0 0
2 534 566 567 576 575 0 0 0 0 5 3 0 0 0 0
2 535 567 687 686 576 0 0 0 0 5 3 0 0 0 0
2 536 14 570 579 13 0 0 0 0 5 3 0 0 0 0
2 537 570 571 580 579 0 0 0 0 5 3 0 0 0 0
2 538 571 572 581 580 0 0 0 0 5 3 0 0 0 0
2 539 572 573 582 581 0 0 0 0 5 3 0 0 0 0
2 540 573 574 583 582 0 0 0 0 5 3 0 0 0 0
2 541 574 575 584 583 0 0 0 0 5 3 0 0 0 0
2 542 575 576 585 584 0 0 0 0 5 3 0 0 0 0
2 543 576 686 685 585 0 0 0 0 5 3 0 0 0 0
2 544 492 587 704 703 0 0 0 0 5 3 0 0 0 0
2 545 587 497 705 704 0 0 0 0 5 3 0 0 0 0
2 546 497 589 706 705 0 0 0 0 5 3 0 0 0 0
2 547 589 502 707 706 0 0 0 0 5 3 0 0 0 0
2 548 502 591 708 707 0 0 0 0 5 3 0 0 0 0
2 549 591 507 709 708 0 0 0 0 5 3 0 0 0 0
2 550 541 592 598 550 0 0 0 0 5 3 0 0 0 0
2 551 592 593 599 598 0 0 0 0 5 3 0 0 0 0
2 552 593 594 600 599 0 0 0 0 5 3 0 0 0 0
2 553 594 595 601 600 0 0 0 0 5 3 0 0 0 0

2 554 595 596 602 601 0 0 0 0 5 3 0 0 0 0
 2 555 596 597 603 602 0 0 0 0 5 3 0 0 0 0
 2 556 550 598 604 559 0 0 0 0 5 3 0 0 0 0
 2 557 598 599 605 604 0 0 0 0 5 3 0 0 0 0
 2 558 599 600 606 605 0 0 0 0 5 3 0 0 0 0
 2 559 600 601 607 606 0 0 0 0 5 3 0 0 0 0
 2 560 601 602 608 607 0 0 0 0 5 3 0 0 0 0
 2 561 602 603 609 608 0 0 0 0 5 3 0 0 0 0
 2 562 559 604 610 568 0 0 0 0 5 3 0 0 0 0
 2 563 604 605 611 610 0 0 0 0 5 3 0 0 0 0
 2 564 605 606 612 611 0 0 0 0 5 3 0 0 0 0
 2 565 606 607 613 612 0 0 0 0 5 3 0 0 0 0
 2 566 607 608 614 613 0 0 0 0 5 3 0 0 0 0
 2 567 608 609 615 614 0 0 0 0 5 3 0 0 0 0
 2 568 568 610 616 577 0 0 0 0 5 3 0 0 0 0
 2 569 610 611 617 616 0 0 0 0 5 3 0 0 0 0
 2 570 611 612 618 617 0 0 0 0 5 3 0 0 0 0
 2 571 612 613 619 618 0 0 0 0 5 3 0 0 0 0
 2 572 613 614 620 619 0 0 0 0 5 3 0 0 0 0
 2 573 614 615 621 620 0 0 0 0 5 3 0 0 0 0
 2 574 577 616 622 586 0 0 0 0 5 3 0 0 0 0
 2 575 616 617 623 622 0 0 0 0 5 3 0 0 0 0
 2 576 617 618 624 623 0 0 0 0 5 3 0 0 0 0
 2 577 618 619 625 624 0 0 0 0 5 3 0 0 0 0
 2 578 619 620 626 625 0 0 0 0 5 3 0 0 0 0
 2 579 620 621 627 626 0 0 0 0 5 3 0 0 0 0
 2 580 702 628 635 701 0 0 0 0 5 3 0 0 0 0
 2 581 628 629 636 635 0 0 0 0 5 3 0 0 0 0
 2 582 629 630 637 636 0 0 0 0 5 3 0 0 0 0
 2 583 630 631 638 637 0 0 0 0 5 3 0 0 0 0
 2 584 631 632 639 638 0 0 0 0 5 3 0 0 0 0
 2 585 632 633 640 639 0 0 0 0 5 3 0 0 0 0
 2 586 701 635 641 700 0 0 0 0 5 3 0 0 0 0
 2 587 635 636 642 641 0 0 0 0 5 3 0 0 0 0
 2 588 636 637 643 642 0 0 0 0 5 3 0 0 0 0
 2 589 637 638 644 643 0 0 0 0 5 3 0 0 0 0
 2 590 638 639 645 644 0 0 0 0 5 3 0 0 0 0
 2 591 639 640 646 645 0 0 0 0 5 3 0 0 0 0
 2 592 700 641 647 699 0 0 0 0 5 3 0 0 0 0
 2 593 641 642 648 647 0 0 0 0 5 3 0 0 0 0
 2 594 642 643 649 648 0 0 0 0 5 3 0 0 0 0
 2 595 643 644 650 649 0 0 0 0 5 3 0 0 0 0
 2 596 644 645 651 650 0 0 0 0 5 3 0 0 0 0
 2 597 645 646 652 651 0 0 0 0 5 3 0 0 0 0
 2 598 699 647 653 698 0 0 0 0 5 3 0 0 0 0
 2 599 647 648 654 653 0 0 0 0 5 3 0 0 0 0
 2 600 648 649 655 654 0 0 0 0 5 3 0 0 0 0
 2 601 649 650 656 655 0 0 0 0 5 3 0 0 0 0
 2 602 650 651 657 656 0 0 0 0 5 3 0 0 0 0
 2 603 651 652 658 657 0 0 0 0 5 3 0 0 0 0
 2 604 698 653 659 697 0 0 0 0 5 3 0 0 0 0
 2 605 653 654 660 659 0 0 0 0 5 3 0 0 0 0
 2 606 654 655 661 660 0 0 0 0 5 3 0 0 0 0
 2 607 655 656 662 661 0 0 0 0 5 3 0 0 0 0
 2 608 656 657 663 662 0 0 0 0 5 3 0 0 0 0
 2 609 657 658 664 663 0 0 0 0 5 3 0 0 0 0
 2 610 697 659 665 696 0 0 0 0 5 3 0 0 0 0
 2 611 659 660 666 665 0 0 0 0 5 3 0 0 0 0
 2 612 660 661 667 666 0 0 0 0 5 3 0 0 0 0
 2 613 661 662 668 667 0 0 0 0 5 3 0 0 0 0
 2 614 662 663 669 668 0 0 0 0 5 3 0 0 0 0
 2 615 663 664 670 669 0 0 0 0 5 3 0 0 0 0
 2 616 696 665 671 695 0 0 0 0 5 3 0 0 0 0
 2 617 665 666 672 671 0 0 0 0 5 3 0 0 0 0
 2 618 666 667 673 672 0 0 0 0 5 3 0 0 0 0
 2 619 667 668 674 673 0 0 0 0 5 3 0 0 0 0
 2 620 668 669 675 674 0 0 0 0 5 3 0 0 0 0
 2 621 669 670 676 675 0 0 0 0 5 3 0 0 0 0
 2 622 695 671 677 694 0 0 0 0 5 3 0 0 0 0
 2 623 671 672 678 677 0 0 0 0 5 3 0 0 0 0

2 624 672 673 679 678 0 0 0 0 5 3 0 0 0 0
 2 625 673 674 680 679 0 0 0 0 5 3 0 0 0 0
 2 626 674 675 681 680 0 0 0 0 5 3 0 0 0 0
 2 627 675 676 682 681 0 0 0 0 5 3 0 0 0 0
 2 628 627 621 695 694 0 0 0 0 5 3 0 0 0 0
 2 629 621 615 696 695 0 0 0 0 5 3 0 0 0 0
 2 630 615 609 697 696 0 0 0 0 5 3 0 0 0 0
 2 631 609 603 698 697 0 0 0 0 5 3 0 0 0 0
 2 632 603 597 699 698 0 0 0 0 5 3 0 0 0 0
 3 633 709 700 699 0 0 0 0 0 5 3 0 0 0 0
 2 634 507 411 701 700 0 0 0 0 5 3 0 0 0 0
 2 635 411 315 702 701 0 0 0 0 5 3 0 0 0 0
 2 636 685 686 577 586 0 0 0 0 5 3 0 0 0 0
 2 637 686 687 568 577 0 0 0 0 5 3 0 0 0 0
 2 638 687 688 559 568 0 0 0 0 5 3 0 0 0 0
 2 639 688 689 550 559 0 0 0 0 5 3 0 0 0 0
 2 640 689 690 541 550 0 0 0 0 5 3 0 0 0 0
 3 641 690 691 703 0 0 0 0 0 5 3 0 0 0 0
 2 642 691 692 396 492 0 0 0 0 5 3 0 0 0 0
 2 643 692 693 300 396 0 0 0 0 5 3 0 0 0 0
 3 644 703 541 690 0 0 0 0 0 5 3 0 0 0 0
 3 645 492 703 691 0 0 0 0 0 5 3 0 0 0 0
 3 646 709 699 597 0 0 0 0 0 5 3 0 0 0 0
 3 647 709 507 700 0 0 0 0 0 5 3 0 0 0 0
 2 648 703 704 592 541 0 0 0 0 5 3 0 0 0 0
 2 649 704 705 593 592 0 0 0 0 5 3 0 0 0 0
 2 650 705 706 594 593 0 0 0 0 5 3 0 0 0 0
 2 651 706 707 595 594 0 0 0 0 5 3 0 0 0 0
 2 652 707 708 596 595 0 0 0 0 5 3 0 0 0 0
 2 653 708 709 597 596 0 0 0 0 5 3 0 0 0 0

\$LINE ELEMENT BASIC PROPERTIES

1 .3058E-01 .1488E-02 .7442E-02 .7442E+00 .1100E+01 .1100E+01
 2 .7500E+00 .5664E-01 .3906E-02 .5625E+00 .1000E+01 .1000E+01
 3 .3058E+00 .1488E-01 .7442E-02 .7442E-02 .1100E+01 .1100E+01

\$SHELL ELEMENT THICKNESSES

1 .1500E+01 .0000E+00 .0000E+00
 2 .1500E+01 .0000E+00 .0000E+00
 3 .2500E+00 .0000E+00 .0000E+00

\$MATERIAL PROPERTIES

1 1
 .1000E+08 .3000E+00 .0000E+00 .2539E-03 .0000E+00 .0000E+00
 2 1
 .1000E+08 .3000E+00 .0000E+00 .2593E-03 .0000E+00 .0000E+00
 3 1
 .3000E+08 .3000E+00 .0000E+00 .7306E-03 .0000E+00 .0000E+00
 4 1
 .3000E+08 .3000E+00 .0000E+00 .7306E-03 .0000E+00 .0000E+00
 5 1
 .1030E+12 .3000E+00 .0000E+00 .2539E-08 .0000E+00 .0000E+00

APPENDIX A-2

STARS-SOLIDS Generalized Mode 1 Displacement Definition (Plunge)

Node	Original XYZ Location			New XYZ Location			Nodal Displacement		
	X	Y	Z	X'	Y'	Z'	ΔX	Δy	ΔZ
13	0	0	0	0	1	0	0	1	0
14	2	0	0	2	1	0	0	1	0
52	4	0	0	4	1	0	0	1	0
53	6	0	0	6	1	0	0	1	0
54	8	0	0	8	1	0	0	1	0
55	10	0	0	10	1	0	0	1	0
56	12	0	0	12	1	0	0	1	0
90	14	0	0	14	1	0	0	1	0
91	16	0	0	16	1	0	0	1	0
300	16	14.4	0	16	15.4	0	0	1	0
301	16	15.04	0	16	16.04	0	0	1	0
302	16	15.68	0	16	16.68	0	0	1	0
303	16	16.32	0	16	17.32	0	0	1	0
304	16	16.96	0	16	17.96	0	0	1	0
305	16	17.6	0	16	18.6	0	0	1	0
306	16	18.24	0	16	19.24	0	0	1	0
307	16	18.88	0	16	19.88	0	0	1	0
308	16	19.52	0	16	20.52	0	0	1	0
309	16	20.16	0	16	21.16	0	0	1	0
310	16	20.8	0	16	21.8	0	0	1	0
311	16	21.44	0	16	22.44	0	0	1	0
312	16	22.08	0	16	23.08	0	0	1	0
313	16	22.72	0	16	23.72	0	0	1	0
314	16	23.36	0	16	24.36	0	0	1	0
315	16	24	0	16	25	0	0	1	0
316	15.6667	14.4	0	15.6667	15.4	0	0	1	0
317	15.6667	15.04	0	15.6667	16.04	0	0	1	0
318	15.6667	15.68	0	15.6667	16.68	0	0	1	0
319	15.6667	16.32	0	15.6667	17.32	0	0	1	0
320	15.6667	16.96	0	15.6667	17.96	0	0	1	0
321	15.6667	17.6	0	15.6667	18.6	0	0	1	0
322	15.6667	18.24	0	15.6667	19.24	0	0	1	0
323	15.6667	18.88	0	15.6667	19.88	0	0	1	0
324	15.6667	19.52	0	15.6667	20.52	0	0	1	0
325	15.6667	20.16	0	15.6667	21.16	0	0	1	0
326	15.6667	20.8	0	15.6667	21.8	0	0	1	0
327	15.6667	21.44	0	15.6667	22.44	0	0	1	0
328	15.6667	22.08	0	15.6667	23.08	0	0	1	0
329	15.6667	22.72	0	15.6667	23.72	0	0	1	0
330	15.6667	23.36	0	15.6667	24.36	0	0	1	0
331	15.6667	24	0	15.6667	25	0	0	1	0
332	15.3333	14.4	0	15.3333	15.4	0	0	1	0
333	15.3333	15.04	0	15.3333	16.04	0	0	1	0
334	15.3333	15.68	0	15.3333	16.68	0	0	1	0
335	15.3333	16.32	0	15.3333	17.32	0	0	1	0
336	15.3333	16.96	0	15.3333	17.96	0	0	1	0
337	15.3333	17.6	0	15.3333	18.6	0	0	1	0
338	15.3333	18.24	0	15.3333	19.24	0	0	1	0
339	15.3333	18.88	0	15.3333	19.88	0	0	1	0
340	15.3333	19.52	0	15.3333	20.52	0	0	1	0
341	15.3333	20.16	0	15.3333	21.16	0	0	1	0
342	15.3333	20.8	0	15.3333	21.8	0	0	1	0

343	15.3333	21.44	0	15.3333	22.44	0	0	1	0
344	15.3333	22.08	0	15.3333	23.08	0	0	1	0
345	15.3333	22.72	0	15.3333	23.72	0	0	1	0
346	15.3333	23.36	0	15.3333	24.36	0	0	1	0
347	15.3333	24	0	15.3333	25	0	0	1	0
348	15	14.4	0	15	15.4	0	0	1	0
349	15	15.04	0	15	16.04	0	0	1	0
350	15	15.68	0	15	16.68	0	0	1	0
351	15	16.32	0	15	17.32	0	0	1	0
352	15	16.96	0	15	17.96	0	0	1	0
353	15	17.6	0	15	18.6	0	0	1	0
354	15	18.24	0	15	19.24	0	0	1	0
355	15	18.88	0	15	19.88	0	0	1	0
356	15	19.52	0	15	20.52	0	0	1	0
357	15	20.16	0	15	21.16	0	0	1	0
358	15	20.8	0	15	21.8	0	0	1	0
359	15	21.44	0	15	22.44	0	0	1	0
360	15	22.08	0	15	23.08	0	0	1	0
361	15	22.72	0	15	23.72	0	0	1	0
362	15	23.36	0	15	24.36	0	0	1	0
363	15	24	0	15	25	0	0	1	0
364	14.6667	14.4	0	14.6667	15.4	0	0	1	0
365	14.6667	15.04	0	14.6667	16.04	0	0	1	0
366	14.6667	15.68	0	14.6667	16.68	0	0	1	0
367	14.6667	16.32	0	14.6667	17.32	0	0	1	0
368	14.6667	16.96	0	14.6667	17.96	0	0	1	0
369	14.6667	17.6	0	14.6667	18.6	0	0	1	0
370	14.6667	18.24	0	14.6667	19.24	0	0	1	0
371	14.6667	18.88	0	14.6667	19.88	0	0	1	0
372	14.6667	19.52	0	14.6667	20.52	0	0	1	0
373	14.6667	20.16	0	14.6667	21.16	0	0	1	0
374	14.6667	20.8	0	14.6667	21.8	0	0	1	0
375	14.6667	21.44	0	14.6667	22.44	0	0	1	0
376	14.6667	22.08	0	14.6667	23.08	0	0	1	0
377	14.6667	22.72	0	14.6667	23.72	0	0	1	0
378	14.6667	23.36	0	14.6667	24.36	0	0	1	0
379	14.6667	24	0	14.6667	25	0	0	1	0
380	14.3333	14.4	0	14.3333	15.4	0	0	1	0
381	14.3333	15.04	0	14.3333	16.04	0	0	1	0
382	14.3333	15.68	0	14.3333	16.68	0	0	1	0
383	14.3333	16.32	0	14.3333	17.32	0	0	1	0
384	14.3333	16.96	0	14.3333	17.96	0	0	1	0
385	14.3333	17.6	0	14.3333	18.6	0	0	1	0
386	14.3333	18.24	0	14.3333	19.24	0	0	1	0
387	14.3333	18.88	0	14.3333	19.88	0	0	1	0
388	14.3333	19.52	0	14.3333	20.52	0	0	1	0
389	14.3333	20.16	0	14.3333	21.16	0	0	1	0
390	14.3333	20.8	0	14.3333	21.8	0	0	1	0
391	14.3333	21.44	0	14.3333	22.44	0	0	1	0
392	14.3333	22.08	0	14.3333	23.08	0	0	1	0
393	14.3333	22.72	0	14.3333	23.72	0	0	1	0
394	14.3333	23.36	0	14.3333	24.36	0	0	1	0
395	14.3333	24	0	14.3333	25	0	0	1	0
396	14	14.4	0	14	15.4	0	0	1	0
397	14	15.04	0	14	16.04	0	0	1	0
398	14	15.68	0	14	16.68	0	0	1	0
399	14	16.32	0	14	17.32	0	0	1	0
400	14	16.96	0	14	17.96	0	0	1	0
401	14	17.6	0	14	18.6	0	0	1	0
402	14	18.24	0	14	19.24	0	0	1	0
403	14	18.88	0	14	19.88	0	0	1	0
404	14	19.52	0	14	20.52	0	0	1	0
405	14	20.16	0	14	21.16	0	0	1	0
406	14	20.8	0	14	21.8	0	0	1	0
407	14	21.44	0	14	22.44	0	0	1	0
408	14	22.08	0	14	23.08	0	0	1	0
409	14	22.72	0	14	23.72	0	0	1	0
410	14	23.36	0	14	24.36	0	0	1	0
411	14	24	0	14	25	0	0	1	0
412	13.6667	14.4	0	13.6667	15.4	0	0	1	0
413	13.6667	15.04	0	13.6667	16.04	0	0	1	0
414	13.6667	15.68	0	13.6667	16.68	0	0	1	0

415	13.6667	16.32	0	13.6667	17.32	0	0	1	0
416	13.6667	16.96	0	13.6667	17.96	0	0	1	0
417	13.6667	17.6	0	13.6667	18.6	0	0	1	0
418	13.6667	18.24	0	13.6667	19.24	0	0	1	0
419	13.6667	18.88	0	13.6667	19.88	0	0	1	0
420	13.6667	19.52	0	13.6667	20.52	0	0	1	0
421	13.6667	20.16	0	13.6667	21.16	0	0	1	0
422	13.6667	20.8	0	13.6667	21.8	0	0	1	0
423	13.6667	21.44	0	13.6667	22.44	0	0	1	0
424	13.6667	22.08	0	13.6667	23.08	0	0	1	0
425	13.6667	22.72	0	13.6667	23.72	0	0	1	0
426	13.6667	23.36	0	13.6667	24.36	0	0	1	0
427	13.6667	24	0	13.6667	25	0	0	1	0
428	13.3333	14.4	0	13.3333	15.4	0	0	1	0
429	13.3333	15.04	0	13.3333	16.04	0	0	1	0
430	13.3333	15.68	0	13.3333	16.68	0	0	1	0
431	13.3333	16.32	0	13.3333	17.32	0	0	1	0
432	13.3333	16.96	0	13.3333	17.96	0	0	1	0
433	13.3333	17.6	0	13.3333	18.6	0	0	1	0
434	13.3333	18.24	0	13.3333	19.24	0	0	1	0
435	13.3333	18.88	0	13.3333	19.88	0	0	1	0
436	13.3333	19.52	0	13.3333	20.52	0	0	1	0
437	13.3333	20.16	0	13.3333	21.16	0	0	1	0
438	13.3333	20.8	0	13.3333	21.8	0	0	1	0
439	13.3333	21.44	0	13.3333	22.44	0	0	1	0
440	13.3333	22.08	0	13.3333	23.08	0	0	1	0
441	13.3333	22.72	0	13.3333	23.72	0	0	1	0
442	13.3333	23.36	0	13.3333	24.36	0	0	1	0
443	13.3333	24	0	13.3333	25	0	0	1	0
444	13	14.4	0	13	15.4	0	0	1	0
445	13	15.04	0	13	16.04	0	0	1	0
446	13	15.68	0	13	16.68	0	0	1	0
447	13	16.32	0	13	17.32	0	0	1	0
448	13	16.96	0	13	17.96	0	0	1	0
449	13	17.6	0	13	18.6	0	0	1	0
450	13	18.24	0	13	19.24	0	0	1	0
451	13	18.88	0	13	19.88	0	0	1	0
452	13	19.52	0	13	20.52	0	0	1	0
453	13	20.16	0	13	21.16	0	0	1	0
454	13	20.8	0	13	21.8	0	0	1	0
455	13	21.44	0	13	22.44	0	0	1	0
456	13	22.08	0	13	23.08	0	0	1	0
457	13	22.72	0	13	23.72	0	0	1	0
458	13	23.36	0	13	24.36	0	0	1	0
459	13	24	0	13	25	0	0	1	0
460	12.6667	14.4	0	12.6667	15.4	0	0	1	0
461	12.6667	15.04	0	12.6667	16.04	0	0	1	0
462	12.6667	15.68	0	12.6667	16.68	0	0	1	0
463	12.6667	16.32	0	12.6667	17.32	0	0	1	0
464	12.6667	16.96	0	12.6667	17.96	0	0	1	0
465	12.6667	17.6	0	12.6667	18.6	0	0	1	0
466	12.6667	18.24	0	12.6667	19.24	0	0	1	0
467	12.6667	18.88	0	12.6667	19.88	0	0	1	0
468	12.6667	19.52	0	12.6667	20.52	0	0	1	0
469	12.6667	20.16	0	12.6667	21.16	0	0	1	0
470	12.6667	20.8	0	12.6667	21.8	0	0	1	0
471	12.6667	21.44	0	12.6667	22.44	0	0	1	0
472	12.6667	22.08	0	12.6667	23.08	0	0	1	0
473	12.6667	22.72	0	12.6667	23.72	0	0	1	0
474	12.6667	23.36	0	12.6667	24.36	0	0	1	0
475	12.6667	24	0	12.6667	25	0	0	1	0
476	12.3333	14.4	0	12.3333	15.4	0	0	1	0
477	12.3333	15.04	0	12.3333	16.04	0	0	1	0
478	12.3333	15.68	0	12.3333	16.68	0	0	1	0
479	12.3333	16.32	0	12.3333	17.32	0	0	1	0
480	12.3333	16.96	0	12.3333	17.96	0	0	1	0
481	12.3333	17.6	0	12.3333	18.6	0	0	1	0
482	12.3333	18.24	0	12.3333	19.24	0	0	1	0
483	12.3333	18.88	0	12.3333	19.88	0	0	1	0
484	12.3333	19.52	0	12.3333	20.52	0	0	1	0
485	12.3333	20.16	0	12.3333	21.16	0	0	1	0
486	12.3333	20.8	0	12.3333	21.8	0	0	1	0

487	12.3333	21.44	0	12.3333	22.44	0	0	1	0
488	12.3333	22.08	0	12.3333	23.08	0	0	1	0
489	12.3333	22.72	0	12.3333	23.72	0	0	1	0
490	12.3333	23.36	0	12.3333	24.36	0	0	1	0
491	12.3333	24	0	12.3333	25	0	0	1	0
492	12	14.4	0	12	15.4	0	0	1	0
493	12	15.04	0	12	16.04	0	0	1	0
494	12	15.68	0	12	16.68	0	0	1	0
495	12	16.32	0	12	17.32	0	0	1	0
496	12	16.96	0	12	17.96	0	0	1	0
497	12	17.6	0	12	18.6	0	0	1	0
498	12	18.24	0	12	19.24	0	0	1	0
499	12	18.88	0	12	19.88	0	0	1	0
500	12	19.52	0	12	20.52	0	0	1	0
501	12	20.16	0	12	21.16	0	0	1	0
502	12	20.8	0	12	21.8	0	0	1	0
503	12	21.44	0	12	22.44	0	0	1	0
504	12	22.08	0	12	23.08	0	0	1	0
505	12	22.72	0	12	23.72	0	0	1	0
506	12	23.36	0	12	24.36	0	0	1	0
507	12	24	0	12	25	0	0	1	0
509	16	1.8	0	16	2.8	0	0	1	0
510	16	3.6	0	16	4.6	0	0	1	0
511	16	5.4	0	16	6.4	0	0	1	0
512	16	7.2	0	16	8.2	0	0	1	0
513	16	9	0	16	10	0	0	1	0
514	16	10.8	0	16	11.8	0	0	1	0
515	16	12.6	0	16	13.6	0	0	1	0
517	14	1.8	0	14	2.8	0	0	1	0
518	14	3.6	0	14	4.6	0	0	1	0
519	14	5.4	0	14	6.4	0	0	1	0
520	14	7.2	0	14	8.2	0	0	1	0
521	14	9	0	14	10	0	0	1	0
522	14	10.8	0	14	11.8	0	0	1	0
523	14	12.6	0	14	13.6	0	0	1	0
526	12	1.8	0	12	2.8	0	0	1	0
527	12	3.6	0	12	4.6	0	0	1	0
528	12	5.4	0	12	6.4	0	0	1	0
529	12	7.2	0	12	8.2	0	0	1	0
530	12	9	0	12	10	0	0	1	0
531	12	10.8	0	12	11.8	0	0	1	0
532	12	12.6	0	12	13.6	0	0	1	0
534	10	1.8	0	10	2.8	0	0	1	0
535	10	3.6	0	10	4.6	0	0	1	0
536	10	5.4	0	10	6.4	0	0	1	0
537	10	7.2	0	10	8.2	0	0	1	0
538	10	9	0	10	10	0	0	1	0
539	10	10.8	0	10	11.8	0	0	1	0
540	10	12.6	0	10	13.6	0	0	1	0
541	10	14.4	0	10	15.4	0	0	1	0
543	8	1.8	0	8	2.8	0	0	1	0
544	8	3.6	0	8	4.6	0	0	1	0
545	8	5.4	0	8	6.4	0	0	1	0
546	8	7.2	0	8	8.2	0	0	1	0
547	8	9	0	8	10	0	0	1	0
548	8	10.8	0	8	11.8	0	0	1	0
549	8	12.6	0	8	13.6	0	0	1	0
550	8	14.4	0	8	15.4	0	0	1	0
552	6	1.8	0	6	2.8	0	0	1	0
553	6	3.6	0	6	4.6	0	0	1	0
554	6	5.4	0	6	6.4	0	0	1	0
555	6	7.2	0	6	8.2	0	0	1	0
556	6	9	0	6	10	0	0	1	0
557	6	10.8	0	6	11.8	0	0	1	0
558	6	12.6	0	6	13.6	0	0	1	0
559	6	14.4	0	6	15.4	0	0	1	0
561	4	1.8	0	4	2.8	0	0	1	0
562	4	3.6	0	4	4.6	0	0	1	0
563	4	5.4	0	4	6.4	0	0	1	0
564	4	7.2	0	4	8.2	0	0	1	0
565	4	9	0	4	10	0	0	1	0
566	4	10.8	0	4	11.8	0	0	1	0

567	4	12.6	0	4	13.6	0	0	1	0
568	4	14.4	0	4	15.4	0	0	1	0
570	2	1.8	0	2	2.8	0	0	1	0
571	2	3.6	0	2	4.6	0	0	1	0
572	2	5.4	0	2	6.4	0	0	1	0
573	2	7.2	0	2	8.2	0	0	1	0
574	2	9	0	2	10	0	0	1	0
575	2	10.8	0	2	11.8	0	0	1	0
576	2	12.6	0	2	13.6	0	0	1	0
577	2	14.4	0	2	15.4	0	0	1	0
579	0	1.8	0	0	2.8	0	0	1	0
580	0	3.6	0	0	4.6	0	0	1	0
581	0	5.4	0	0	6.4	0	0	1	0
582	0	7.2	0	0	8.2	0	0	1	0
583	0	9	0	0	10	0	0	1	0
584	0	10.8	0	0	11.8	0	0	1	0
585	0	12.6	0	0	13.6	0	0	1	0
586	0	14.4	0	0	15.4	0	0	1	0
587	12	16	0	12	17	0	0	1	0
589	12	19.2	0	12	20.2	0	0	1	0
591	12	22.4	0	12	23.4	0	0	1	0
592	10	16	0	10	17	0	0	1	0
593	10	17.6	0	10	18.6	0	0	1	0
594	10	19.2	0	10	20.2	0	0	1	0
595	10	20.8	0	10	21.8	0	0	1	0
596	10	22.4	0	10	23.4	0	0	1	0
597	10	24	0	10	25	0	0	1	0
598	8	16	0	8	17	0	0	1	0
599	8	17.6	0	8	18.6	0	0	1	0
600	8	19.2	0	8	20.2	0	0	1	0
601	8	20.8	0	8	21.8	0	0	1	0
602	8	22.4	0	8	23.4	0	0	1	0
603	8	24	0	8	25	0	0	1	0
604	6	16	0	6	17	0	0	1	0
605	6	17.6	0	6	18.6	0	0	1	0
606	6	19.2	0	6	20.2	0	0	1	0
607	6	20.8	0	6	21.8	0	0	1	0
608	6	22.4	0	6	23.4	0	0	1	0
609	6	24	0	6	25	0	0	1	0
610	4	16	0	4	17	0	0	1	0
611	4	17.6	0	4	18.6	0	0	1	0
612	4	19.2	0	4	20.2	0	0	1	0
613	4	20.8	0	4	21.8	0	0	1	0
614	4	22.4	0	4	23.4	0	0	1	0
615	4	24	0	4	25	0	0	1	0
616	2	16	0	2	17	0	0	1	0
617	2	17.6	0	2	18.6	0	0	1	0
618	2	19.2	0	2	20.2	0	0	1	0
619	2	20.8	0	2	21.8	0	0	1	0
620	2	22.4	0	2	23.4	0	0	1	0
621	2	24	0	2	25	0	0	1	0
622	0	16	0	0	17	0	0	1	0
623	0	17.6	0	0	18.6	0	0	1	0
624	0	19.2	0	0	20.2	0	0	1	0
625	0	20.8	0	0	21.8	0	0	1	0
626	0	22.4	0	0	23.4	0	0	1	0
627	0	24	0	0	25	0	0	1	0
628	16	25.3333	0	16	26.3333	0	0	1	0
629	16	26.6667	0	16	27.6667	0	0	1	0
630	16	28	0	16	29	0	0	1	0
631	16	29.3333	0	16	30.3333	0	0	1	0
632	16	30.6667	0	16	31.6667	0	0	1	0
633	16	32	0	16	33	0	0	1	0
635	14	25.3333	0	14	26.3333	0	0	1	0
636	14	26.6667	0	14	27.6667	0	0	1	0
637	14	28	0	14	29	0	0	1	0
638	14	29.3333	0	14	30.3333	0	0	1	0
639	14	30.6667	0	14	31.6667	0	0	1	0
640	14	32	0	14	33	0	0	1	0
641	12	25.3333	0	12	26.3333	0	0	1	0
642	12	26.6667	0	12	27.6667	0	0	1	0
643	12	28	0	12	29	0	0	1	0

644	12	29.3333	0	12	30.3333	0	0	1	0
645	12	30.6667	0	12	31.6667	0	0	1	0
646	12	32	0	12	33	0	0	1	0
647	10	25.3333	0	10	26.3333	0	0	1	0
648	10	26.6667	0	10	27.6667	0	0	1	0
649	10	28	0	10	29	0	0	1	0
650	10	29.3333	0	10	30.3333	0	0	1	0
651	10	30.6667	0	10	31.6667	0	0	1	0
652	10	32	0	10	33	0	0	1	0
653	8	25.3333	0	8	26.3333	0	0	1	0
654	8	26.6667	0	8	27.6667	0	0	1	0
655	8	28	0	8	29	0	0	1	0
656	8	29.3333	0	8	30.3333	0	0	1	0
657	8	30.6667	0	8	31.6667	0	0	1	0
658	8	32	0	8	33	0	0	1	0
659	6	25.3333	0	6	26.3333	0	0	1	0
660	6	26.6667	0	6	27.6667	0	0	1	0
661	6	28	0	6	29	0	0	1	0
662	6	29.3333	0	6	30.3333	0	0	1	0
663	6	30.6667	0	6	31.6667	0	0	1	0
664	6	32	0	6	33	0	0	1	0
665	4	25.3333	0	4	26.3333	0	0	1	0
666	4	26.6667	0	4	27.6667	0	0	1	0
667	4	28	0	4	29	0	0	1	0
668	4	29.3333	0	4	30.3333	0	0	1	0
669	4	30.6667	0	4	31.6667	0	0	1	0
670	4	32	0	4	33	0	0	1	0
671	2	25.3333	0	2	26.3333	0	0	1	0
672	2	26.6667	0	2	27.6667	0	0	1	0
673	2	28	0	2	29	0	0	1	0
674	2	29.3333	0	2	30.3333	0	0	1	0
675	2	30.6667	0	2	31.6667	0	0	1	0
676	2	32	0	2	33	0	0	1	0
677	0	25.3333	0	0	26.3333	0	0	1	0
678	0	26.6667	0	0	27.6667	0	0	1	0
679	0	28	0	0	29	0	0	1	0
680	0	29.3333	0	0	30.3333	0	0	1	0
681	0	30.6667	0	0	31.6667	0	0	1	0
682	0	32	0	0	33	0	0	1	0
685	0	14.3	0	0	15.3	0	0	1	0
686	2	14.3	0	2	15.3	0	0	1	0
687	4	14.3	0	4	15.3	0	0	1	0
688	6	14.3	0	6	15.3	0	0	1	0
689	8	14.3	0	8	15.3	0	0	1	0
690	10	14.3	0	10	15.3	0	0	1	0
691	12	14.3	0	12	15.3	0	0	1	0
692	14	14.3	0	14	15.3	0	0	1	0
693	16	14.3	0	16	15.3	0	0	1	0
694	0	24.1	0	0	25.1	0	0	1	0
695	2	24.1	0	2	25.1	0	0	1	0
696	4	24.1	0	4	25.1	0	0	1	0
697	6	24.1	0	6	25.1	0	0	1	0
698	8	24.1	0	8	25.1	0	0	1	0
699	10	24.1	0	10	25.1	0	0	1	0
700	12	24.1	0	12	25.1	0	0	1	0
701	14	24.1	0	14	25.1	0	0	1	0
702	16	24.1	0	16	25.1	0	0	1	0
703	11.4	14.4	0	11.4	15.4	0	0	1	0
704	11.9	16	0	11.9	17	0	0	1	0
705	11.9	17.6	0	11.9	18.6	0	0	1	0
706	11.9	19.2	0	11.9	20.2	0	0	1	0
707	11.9	20.8	0	11.9	21.8	0	0	1	0
708	11.9	22.4	0	11.9	23.4	0	0	1	0
709	11.4	24	0	11.4	25	0	0	1	0

APPENDIX A-3

STARS-SOLIDS Generalized Mode 2 Displacement Definition (Pitch)

Node	Original XYZ Location			New XYZ Location			Nodal Displacement		
	X	Y	Z	X'	Y'	Z'	ΔX	ΔY	ΔZ
13	0	0	0	0.001218	0	0.139619	0.001218	0	0.139619
14	2	0	0	2.000914	0	0.104714	0.000914	0	0.104714
52	4	0	0	4.000609	0	0.06981	0.000609	0	0.06981
53	6	0	0	6.000305	0	0.034905	0.000305	0	0.034905
54	8	0	0	8	0	0	0	0	0
55	10	0	0	9.999695	0	-0.0349	-0.0003	0	-0.0349
56	12	0	0	11.99939	0	-0.06981	-0.00061	0	-0.06981
90	14	0	0	13.99909	0	-0.10471	-0.00091	0	-0.10471
91	16	0	0	15.99878	0	-0.13962	-0.00122	0	-0.13962
300	16	14.4	0	15.99878	14.4	-0.13962	-0.00122	0	-0.13962
301	16	15.04	0	15.99878	15.04	-0.13962	-0.00122	0	-0.13962
302	16	15.68	0	15.99878	15.68	-0.13962	-0.00122	0	-0.13962
303	16	16.32	0	15.99878	16.32	-0.13962	-0.00122	0	-0.13962
304	16	16.96	0	15.99878	16.96	-0.13962	-0.00122	0	-0.13962
305	16	17.6	0	15.99878	17.6	-0.13962	-0.00122	0	-0.13962
306	16	18.24	0	15.99878	18.24	-0.13962	-0.00122	0	-0.13962
307	16	18.88	0	15.99878	18.88	-0.13962	-0.00122	0	-0.13962
308	16	19.52	0	15.99878	19.52	-0.13962	-0.00122	0	-0.13962
309	16	20.16	0	15.99878	20.16	-0.13962	-0.00122	0	-0.13962
310	16	20.8	0	15.99878	20.8	-0.13962	-0.00122	0	-0.13962
311	16	21.44	0	15.99878	21.44	-0.13962	-0.00122	0	-0.13962
312	16	22.08	0	15.99878	22.08	-0.13962	-0.00122	0	-0.13962
313	16	22.72	0	15.99878	22.72	-0.13962	-0.00122	0	-0.13962
314	16	23.36	0	15.99878	23.36	-0.13962	-0.00122	0	-0.13962
315	16	24	0	15.99878	24	-0.13962	-0.00122	0	-0.13962
316	15.6667	14.4	0	15.66553	14.4	-0.1338	-0.00117	0	-0.1338
317	15.6667	15.04	0	15.66553	15.04	-0.1338	-0.00117	0	-0.1338
318	15.6667	15.68	0	15.66553	15.68	-0.1338	-0.00117	0	-0.1338
319	15.6667	16.32	0	15.66553	16.32	-0.1338	-0.00117	0	-0.1338
320	15.6667	16.96	0	15.66553	16.96	-0.1338	-0.00117	0	-0.1338
321	15.6667	17.6	0	15.66553	17.6	-0.1338	-0.00117	0	-0.1338
322	15.6667	18.24	0	15.66553	18.24	-0.1338	-0.00117	0	-0.1338
323	15.6667	18.88	0	15.66553	18.88	-0.1338	-0.00117	0	-0.1338
324	15.6667	19.52	0	15.66553	19.52	-0.1338	-0.00117	0	-0.1338
325	15.6667	20.16	0	15.66553	20.16	-0.1338	-0.00117	0	-0.1338
326	15.6667	20.8	0	15.66553	20.8	-0.1338	-0.00117	0	-0.1338
327	15.6667	21.44	0	15.66553	21.44	-0.1338	-0.00117	0	-0.1338
328	15.6667	22.08	0	15.66553	22.08	-0.1338	-0.00117	0	-0.1338
329	15.6667	22.72	0	15.66553	22.72	-0.1338	-0.00117	0	-0.1338
330	15.6667	23.36	0	15.66553	23.36	-0.1338	-0.00117	0	-0.1338
331	15.6667	24	0	15.66553	24	-0.1338	-0.00117	0	-0.1338
332	15.3333	14.4	0	15.33218	14.4	-0.12798	-0.00112	0	-0.12798
333	15.3333	15.04	0	15.33218	15.04	-0.12798	-0.00112	0	-0.12798
334	15.3333	15.68	0	15.33218	15.68	-0.12798	-0.00112	0	-0.12798
335	15.3333	16.32	0	15.33218	16.32	-0.12798	-0.00112	0	-0.12798
336	15.3333	16.96	0	15.33218	16.96	-0.12798	-0.00112	0	-0.12798
337	15.3333	17.6	0	15.33218	17.6	-0.12798	-0.00112	0	-0.12798
338	15.3333	18.24	0	15.33218	18.24	-0.12798	-0.00112	0	-0.12798
339	15.3333	18.88	0	15.33218	18.88	-0.12798	-0.00112	0	-0.12798
340	15.3333	19.52	0	15.33218	19.52	-0.12798	-0.00112	0	-0.12798
341	15.3333	20.16	0	15.33218	20.16	-0.12798	-0.00112	0	-0.12798
342	15.3333	20.8	0	15.33218	20.8	-0.12798	-0.00112	0	-0.12798

343	15.3333	21.44	0	15.33218	21.44	-0.12798	-0.00112	0	-0.12798
344	15.3333	22.08	0	15.33218	22.08	-0.12798	-0.00112	0	-0.12798
345	15.3333	22.72	0	15.33218	22.72	-0.12798	-0.00112	0	-0.12798
346	15.3333	23.36	0	15.33218	23.36	-0.12798	-0.00112	0	-0.12798
347	15.3333	24	0	15.33218	24	-0.12798	-0.00112	0	-0.12798
348	15	14.4	0	14.99893	14.4	-0.12217	-0.00107	0	-0.12217
349	15	15.04	0	14.99893	15.04	-0.12217	-0.00107	0	-0.12217
350	15	15.68	0	14.99893	15.68	-0.12217	-0.00107	0	-0.12217
351	15	16.32	0	14.99893	16.32	-0.12217	-0.00107	0	-0.12217
352	15	16.96	0	14.99893	16.96	-0.12217	-0.00107	0	-0.12217
353	15	17.6	0	14.99893	17.6	-0.12217	-0.00107	0	-0.12217
354	15	18.24	0	14.99893	18.24	-0.12217	-0.00107	0	-0.12217
355	15	18.88	0	14.99893	18.88	-0.12217	-0.00107	0	-0.12217
356	15	19.52	0	14.99893	19.52	-0.12217	-0.00107	0	-0.12217
357	15	20.16	0	14.99893	20.16	-0.12217	-0.00107	0	-0.12217
358	15	20.8	0	14.99893	20.8	-0.12217	-0.00107	0	-0.12217
359	15	21.44	0	14.99893	21.44	-0.12217	-0.00107	0	-0.12217
360	15	22.08	0	14.99893	22.08	-0.12217	-0.00107	0	-0.12217
361	15	22.72	0	14.99893	22.72	-0.12217	-0.00107	0	-0.12217
362	15	23.36	0	14.99893	23.36	-0.12217	-0.00107	0	-0.12217
363	15	24	0	14.99893	24	-0.12217	-0.00107	0	-0.12217
364	14.6667	14.4	0	14.66568	14.4	-0.11635	-0.00102	0	-0.11635
365	14.6667	15.04	0	14.66568	15.04	-0.11635	-0.00102	0	-0.11635
366	14.6667	15.68	0	14.66568	15.68	-0.11635	-0.00102	0	-0.11635
367	14.6667	16.32	0	14.66568	16.32	-0.11635	-0.00102	0	-0.11635
368	14.6667	16.96	0	14.66568	16.96	-0.11635	-0.00102	0	-0.11635
369	14.6667	17.6	0	14.66568	17.6	-0.11635	-0.00102	0	-0.11635
370	14.6667	18.24	0	14.66568	18.24	-0.11635	-0.00102	0	-0.11635
371	14.6667	18.88	0	14.66568	18.88	-0.11635	-0.00102	0	-0.11635
372	14.6667	19.52	0	14.66568	19.52	-0.11635	-0.00102	0	-0.11635
373	14.6667	20.16	0	14.66568	20.16	-0.11635	-0.00102	0	-0.11635
374	14.6667	20.8	0	14.66568	20.8	-0.11635	-0.00102	0	-0.11635
375	14.6667	21.44	0	14.66568	21.44	-0.11635	-0.00102	0	-0.11635
376	14.6667	22.08	0	14.66568	22.08	-0.11635	-0.00102	0	-0.11635
377	14.6667	22.72	0	14.66568	22.72	-0.11635	-0.00102	0	-0.11635
378	14.6667	23.36	0	14.66568	23.36	-0.11635	-0.00102	0	-0.11635
379	14.6667	24	0	14.66568	24	-0.11635	-0.00102	0	-0.11635
380	14.3333	14.4	0	14.33234	14.4	-0.11053	-0.00096	0	-0.11053
381	14.3333	15.04	0	14.33234	15.04	-0.11053	-0.00096	0	-0.11053
382	14.3333	15.68	0	14.33234	15.68	-0.11053	-0.00096	0	-0.11053
383	14.3333	16.32	0	14.33234	16.32	-0.11053	-0.00096	0	-0.11053
384	14.3333	16.96	0	14.33234	16.96	-0.11053	-0.00096	0	-0.11053
385	14.3333	17.6	0	14.33234	17.6	-0.11053	-0.00096	0	-0.11053
386	14.3333	18.24	0	14.33234	18.24	-0.11053	-0.00096	0	-0.11053
387	14.3333	18.88	0	14.33234	18.88	-0.11053	-0.00096	0	-0.11053
388	14.3333	19.52	0	14.33234	19.52	-0.11053	-0.00096	0	-0.11053
389	14.3333	20.16	0	14.33234	20.16	-0.11053	-0.00096	0	-0.11053
390	14.3333	20.8	0	14.33234	20.8	-0.11053	-0.00096	0	-0.11053
391	14.3333	21.44	0	14.33234	21.44	-0.11053	-0.00096	0	-0.11053
392	14.3333	22.08	0	14.33234	22.08	-0.11053	-0.00096	0	-0.11053
393	14.3333	22.72	0	14.33234	22.72	-0.11053	-0.00096	0	-0.11053
394	14.3333	23.36	0	14.33234	23.36	-0.11053	-0.00096	0	-0.11053
395	14.3333	24	0	14.33234	24	-0.11053	-0.00096	0	-0.11053
396	14	14.4	0	13.99909	14.4	-0.10471	-0.00091	0	-0.10471
397	14	15.04	0	13.99909	15.04	-0.10471	-0.00091	0	-0.10471
398	14	15.68	0	13.99909	15.68	-0.10471	-0.00091	0	-0.10471
399	14	16.32	0	13.99909	16.32	-0.10471	-0.00091	0	-0.10471
400	14	16.96	0	13.99909	16.96	-0.10471	-0.00091	0	-0.10471
401	14	17.6	0	13.99909	17.6	-0.10471	-0.00091	0	-0.10471
402	14	18.24	0	13.99909	18.24	-0.10471	-0.00091	0	-0.10471
403	14	18.88	0	13.99909	18.88	-0.10471	-0.00091	0	-0.10471
404	14	19.52	0	13.99909	19.52	-0.10471	-0.00091	0	-0.10471
405	14	20.16	0	13.99909	20.16	-0.10471	-0.00091	0	-0.10471
406	14	20.8	0	13.99909	20.8	-0.10471	-0.00091	0	-0.10471
407	14	21.44	0	13.99909	21.44	-0.10471	-0.00091	0	-0.10471
408	14	22.08	0	13.99909	22.08	-0.10471	-0.00091	0	-0.10471
409	14	22.72	0	13.99909	22.72	-0.10471	-0.00091	0	-0.10471
410	14	23.36	0	13.99909	23.36	-0.10471	-0.00091	0	-0.10471
411	14	24	0	13.99909	24	-0.10471	-0.00091	0	-0.10471
412	13.6667	14.4	0	13.66584	14.4	-0.0989	-0.00086	0	-0.0989
413	13.6667	15.04	0	13.66584	15.04	-0.0989	-0.00086	0	-0.0989
414	13.6667	15.68	0	13.66584	15.68	-0.0989	-0.00086	0	-0.0989

415	13.6667	16.32	0	13.66584	16.32	-0.0989	-0.00086	0	-0.0989
416	13.6667	16.96	0	13.66584	16.96	-0.0989	-0.00086	0	-0.0989
417	13.6667	17.6	0	13.66584	17.6	-0.0989	-0.00086	0	-0.0989
418	13.6667	18.24	0	13.66584	18.24	-0.0989	-0.00086	0	-0.0989
419	13.6667	18.88	0	13.66584	18.88	-0.0989	-0.00086	0	-0.0989
420	13.6667	19.52	0	13.66584	19.52	-0.0989	-0.00086	0	-0.0989
421	13.6667	20.16	0	13.66584	20.16	-0.0989	-0.00086	0	-0.0989
422	13.6667	20.8	0	13.66584	20.8	-0.0989	-0.00086	0	-0.0989
423	13.6667	21.44	0	13.66584	21.44	-0.0989	-0.00086	0	-0.0989
424	13.6667	22.08	0	13.66584	22.08	-0.0989	-0.00086	0	-0.0989
425	13.6667	22.72	0	13.66584	22.72	-0.0989	-0.00086	0	-0.0989
426	13.6667	23.36	0	13.66584	23.36	-0.0989	-0.00086	0	-0.0989
427	13.6667	24	0	13.66584	24	-0.0989	-0.00086	0	-0.0989
428	13.3333	14.4	0	13.33249	14.4	-0.09308	-0.00081	0	-0.09308
429	13.3333	15.04	0	13.33249	15.04	-0.09308	-0.00081	0	-0.09308
430	13.3333	15.68	0	13.33249	15.68	-0.09308	-0.00081	0	-0.09308
431	13.3333	16.32	0	13.33249	16.32	-0.09308	-0.00081	0	-0.09308
432	13.3333	16.96	0	13.33249	16.96	-0.09308	-0.00081	0	-0.09308
433	13.3333	17.6	0	13.33249	17.6	-0.09308	-0.00081	0	-0.09308
434	13.3333	18.24	0	13.33249	18.24	-0.09308	-0.00081	0	-0.09308
435	13.3333	18.88	0	13.33249	18.88	-0.09308	-0.00081	0	-0.09308
436	13.3333	19.52	0	13.33249	19.52	-0.09308	-0.00081	0	-0.09308
437	13.3333	20.16	0	13.33249	20.16	-0.09308	-0.00081	0	-0.09308
438	13.3333	20.8	0	13.33249	20.8	-0.09308	-0.00081	0	-0.09308
439	13.3333	21.44	0	13.33249	21.44	-0.09308	-0.00081	0	-0.09308
440	13.3333	22.08	0	13.33249	22.08	-0.09308	-0.00081	0	-0.09308
441	13.3333	22.72	0	13.33249	22.72	-0.09308	-0.00081	0	-0.09308
442	13.3333	23.36	0	13.33249	23.36	-0.09308	-0.00081	0	-0.09308
443	13.3333	24	0	13.33249	24	-0.09308	-0.00081	0	-0.09308
444	13	14.4	0	12.99924	14.4	-0.08726	-0.00076	0	-0.08726
445	13	15.04	0	12.99924	15.04	-0.08726	-0.00076	0	-0.08726
446	13	15.68	0	12.99924	15.68	-0.08726	-0.00076	0	-0.08726
447	13	16.32	0	12.99924	16.32	-0.08726	-0.00076	0	-0.08726
448	13	16.96	0	12.99924	16.96	-0.08726	-0.00076	0	-0.08726
449	13	17.6	0	12.99924	17.6	-0.08726	-0.00076	0	-0.08726
450	13	18.24	0	12.99924	18.24	-0.08726	-0.00076	0	-0.08726
451	13	18.88	0	12.99924	18.88	-0.08726	-0.00076	0	-0.08726
452	13	19.52	0	12.99924	19.52	-0.08726	-0.00076	0	-0.08726
453	13	20.16	0	12.99924	20.16	-0.08726	-0.00076	0	-0.08726
454	13	20.8	0	12.99924	20.8	-0.08726	-0.00076	0	-0.08726
455	13	21.44	0	12.99924	21.44	-0.08726	-0.00076	0	-0.08726
456	13	22.08	0	12.99924	22.08	-0.08726	-0.00076	0	-0.08726
457	13	22.72	0	12.99924	22.72	-0.08726	-0.00076	0	-0.08726
458	13	23.36	0	12.99924	23.36	-0.08726	-0.00076	0	-0.08726
459	13	24	0	12.99924	24	-0.08726	-0.00076	0	-0.08726
460	12.6667	14.4	0	12.66599	14.4	-0.08145	-0.00071	0	-0.08145
461	12.6667	15.04	0	12.66599	15.04	-0.08145	-0.00071	0	-0.08145
462	12.6667	15.68	0	12.66599	15.68	-0.08145	-0.00071	0	-0.08145
463	12.6667	16.32	0	12.66599	16.32	-0.08145	-0.00071	0	-0.08145
464	12.6667	16.96	0	12.66599	16.96	-0.08145	-0.00071	0	-0.08145
465	12.6667	17.6	0	12.66599	17.6	-0.08145	-0.00071	0	-0.08145
466	12.6667	18.24	0	12.66599	18.24	-0.08145	-0.00071	0	-0.08145
467	12.6667	18.88	0	12.66599	18.88	-0.08145	-0.00071	0	-0.08145
468	12.6667	19.52	0	12.66599	19.52	-0.08145	-0.00071	0	-0.08145
469	12.6667	20.16	0	12.66599	20.16	-0.08145	-0.00071	0	-0.08145
470	12.6667	20.8	0	12.66599	20.8	-0.08145	-0.00071	0	-0.08145
471	12.6667	21.44	0	12.66599	21.44	-0.08145	-0.00071	0	-0.08145
472	12.6667	22.08	0	12.66599	22.08	-0.08145	-0.00071	0	-0.08145
473	12.6667	22.72	0	12.66599	22.72	-0.08145	-0.00071	0	-0.08145
474	12.6667	23.36	0	12.66599	23.36	-0.08145	-0.00071	0	-0.08145
475	12.6667	24	0	12.66599	24	-0.08145	-0.00071	0	-0.08145
476	12.3333	14.4	0	12.33264	14.4	-0.07563	-0.00066	0	-0.07563
477	12.3333	15.04	0	12.33264	15.04	-0.07563	-0.00066	0	-0.07563
478	12.3333	15.68	0	12.33264	15.68	-0.07563	-0.00066	0	-0.07563
479	12.3333	16.32	0	12.33264	16.32	-0.07563	-0.00066	0	-0.07563
480	12.3333	16.96	0	12.33264	16.96	-0.07563	-0.00066	0	-0.07563
481	12.3333	17.6	0	12.33264	17.6	-0.07563	-0.00066	0	-0.07563
482	12.3333	18.24	0	12.33264	18.24	-0.07563	-0.00066	0	-0.07563
483	12.3333	18.88	0	12.33264	18.88	-0.07563	-0.00066	0	-0.07563
484	12.3333	19.52	0	12.33264	19.52	-0.07563	-0.00066	0	-0.07563
485	12.3333	20.16	0	12.33264	20.16	-0.07563	-0.00066	0	-0.07563
486	12.3333	20.8	0	12.33264	20.8	-0.07563	-0.00066	0	-0.07563

487	12.3333	21.44	0	12.33264	21.44	-0.07563	-0.00066	0	-0.07563
488	12.3333	22.08	0	12.33264	22.08	-0.07563	-0.00066	0	-0.07563
489	12.3333	22.72	0	12.33264	22.72	-0.07563	-0.00066	0	-0.07563
490	12.3333	23.36	0	12.33264	23.36	-0.07563	-0.00066	0	-0.07563
491	12.3333	24	0	12.33264	24	-0.07563	-0.00066	0	-0.07563
492	12	14.4	0	11.99939	14.4	-0.06981	-0.00061	0	-0.06981
493	12	15.04	0	11.99939	15.04	-0.06981	-0.00061	0	-0.06981
494	12	15.68	0	11.99939	15.68	-0.06981	-0.00061	0	-0.06981
495	12	16.32	0	11.99939	16.32	-0.06981	-0.00061	0	-0.06981
496	12	16.96	0	11.99939	16.96	-0.06981	-0.00061	0	-0.06981
497	12	17.6	0	11.99939	17.6	-0.06981	-0.00061	0	-0.06981
498	12	18.24	0	11.99939	18.24	-0.06981	-0.00061	0	-0.06981
499	12	18.88	0	11.99939	18.88	-0.06981	-0.00061	0	-0.06981
500	12	19.52	0	11.99939	19.52	-0.06981	-0.00061	0	-0.06981
501	12	20.16	0	11.99939	20.16	-0.06981	-0.00061	0	-0.06981
502	12	20.8	0	11.99939	20.8	-0.06981	-0.00061	0	-0.06981
503	12	21.44	0	11.99939	21.44	-0.06981	-0.00061	0	-0.06981
504	12	22.08	0	11.99939	22.08	-0.06981	-0.00061	0	-0.06981
505	12	22.72	0	11.99939	22.72	-0.06981	-0.00061	0	-0.06981
506	12	23.36	0	11.99939	23.36	-0.06981	-0.00061	0	-0.06981
507	12	24	0	11.99939	24	-0.06981	-0.00061	0	-0.06981
509	16	1.8	0	15.99878	1.8	-0.13962	-0.00122	0	-0.13962
510	16	3.6	0	15.99878	3.6	-0.13962	-0.00122	0	-0.13962
511	16	5.4	0	15.99878	5.4	-0.13962	-0.00122	0	-0.13962
512	16	7.2	0	15.99878	7.2	-0.13962	-0.00122	0	-0.13962
513	16	9	0	15.99878	9	-0.13962	-0.00122	0	-0.13962
514	16	10.8	0	15.99878	10.8	-0.13962	-0.00122	0	-0.13962
515	16	12.6	0	15.99878	12.6	-0.13962	-0.00122	0	-0.13962
517	14	1.8	0	13.99909	1.8	-0.10471	-0.00091	0	-0.10471
518	14	3.6	0	13.99909	3.6	-0.10471	-0.00091	0	-0.10471
519	14	5.4	0	13.99909	5.4	-0.10471	-0.00091	0	-0.10471
520	14	7.2	0	13.99909	7.2	-0.10471	-0.00091	0	-0.10471
521	14	9	0	13.99909	9	-0.10471	-0.00091	0	-0.10471
522	14	10.8	0	13.99909	10.8	-0.10471	-0.00091	0	-0.10471
523	14	12.6	0	13.99909	12.6	-0.10471	-0.00091	0	-0.10471
526	12	1.8	0	11.99939	1.8	-0.06981	-0.00061	0	-0.06981
527	12	3.6	0	11.99939	3.6	-0.06981	-0.00061	0	-0.06981
528	12	5.4	0	11.99939	5.4	-0.06981	-0.00061	0	-0.06981
529	12	7.2	0	11.99939	7.2	-0.06981	-0.00061	0	-0.06981
530	12	9	0	11.99939	9	-0.06981	-0.00061	0	-0.06981
531	12	10.8	0	11.99939	10.8	-0.06981	-0.00061	0	-0.06981
532	12	12.6	0	11.99939	12.6	-0.06981	-0.00061	0	-0.06981
534	10	1.8	0	9.999695	1.8	-0.0349	-0.0003	0	-0.0349
535	10	3.6	0	9.999695	3.6	-0.0349	-0.0003	0	-0.0349
536	10	5.4	0	9.999695	5.4	-0.0349	-0.0003	0	-0.0349
537	10	7.2	0	9.999695	7.2	-0.0349	-0.0003	0	-0.0349
538	10	9	0	9.999695	9	-0.0349	-0.0003	0	-0.0349
539	10	10.8	0	9.999695	10.8	-0.0349	-0.0003	0	-0.0349
540	10	12.6	0	9.999695	12.6	-0.0349	-0.0003	0	-0.0349
541	10	14.4	0	9.999695	14.4	-0.0349	-0.0003	0	-0.0349
543	8	1.8	0	8	1.8	0	0	0	0
544	8	3.6	0	8	3.6	0	0	0	0
545	8	5.4	0	8	5.4	0	0	0	0
546	8	7.2	0	8	7.2	0	0	0	0
547	8	9	0	8	9	0	0	0	0
548	8	10.8	0	8	10.8	0	0	0	0
549	8	12.6	0	8	12.6	0	0	0	0
550	8	14.4	0	8	14.4	0	0	0	0
552	6	1.8	0	6.000305	1.8	0.034905	0.000305	0	0.034905
553	6	3.6	0	6.000305	3.6	0.034905	0.000305	0	0.034905
554	6	5.4	0	6.000305	5.4	0.034905	0.000305	0	0.034905
555	6	7.2	0	6.000305	7.2	0.034905	0.000305	0	0.034905
556	6	9	0	6.000305	9	0.034905	0.000305	0	0.034905
557	6	10.8	0	6.000305	10.8	0.034905	0.000305	0	0.034905
558	6	12.6	0	6.000305	12.6	0.034905	0.000305	0	0.034905
559	6	14.4	0	6.000305	14.4	0.034905	0.000305	0	0.034905
561	4	1.8	0	4.000609	1.8	0.06981	0.000609	0	0.06981
562	4	3.6	0	4.000609	3.6	0.06981	0.000609	0	0.06981
563	4	5.4	0	4.000609	5.4	0.06981	0.000609	0	0.06981
564	4	7.2	0	4.000609	7.2	0.06981	0.000609	0	0.06981
565	4	9	0	4.000609	9	0.06981	0.000609	0	0.06981
566	4	10.8	0	4.000609	10.8	0.06981	0.000609	0	0.06981

567	4	12.6	0	4.000609	12.6	0.06981	0.000609	0	0.06981
568	4	14.4	0	4.000609	14.4	0.06981	0.000609	0	0.06981
570	2	1.8	0	2.000914	1.8	0.104714	0.000914	0	0.104714
571	2	3.6	0	2.000914	3.6	0.104714	0.000914	0	0.104714
572	2	5.4	0	2.000914	5.4	0.104714	0.000914	0	0.104714
573	2	7.2	0	2.000914	7.2	0.104714	0.000914	0	0.104714
574	2	9	0	2.000914	9	0.104714	0.000914	0	0.104714
575	2	10.8	0	2.000914	10.8	0.104714	0.000914	0	0.104714
576	2	12.6	0	2.000914	12.6	0.104714	0.000914	0	0.104714
577	2	14.4	0	2.000914	14.4	0.104714	0.000914	0	0.104714
579	0	1.8	0	0.001218	1.8	0.139619	0.001218	0	0.139619
580	0	3.6	0	0.001218	3.6	0.139619	0.001218	0	0.139619
581	0	5.4	0	0.001218	5.4	0.139619	0.001218	0	0.139619
582	0	7.2	0	0.001218	7.2	0.139619	0.001218	0	0.139619
583	0	9	0	0.001218	9	0.139619	0.001218	0	0.139619
584	0	10.8	0	0.001218	10.8	0.139619	0.001218	0	0.139619
585	0	12.6	0	0.001218	12.6	0.139619	0.001218	0	0.139619
586	0	14.4	0	0.001218	14.4	0.139619	0.001218	0	0.139619
587	12	16	0	11.99939	16	-0.06981	-0.00061	0	-0.06981
589	12	19.2	0	11.99939	19.2	-0.06981	-0.00061	0	-0.06981
591	12	22.4	0	11.99939	22.4	-0.06981	-0.00061	0	-0.06981
592	10	16	0	9.999695	16	-0.0349	-0.0003	0	-0.0349
593	10	17.6	0	9.999695	17.6	-0.0349	-0.0003	0	-0.0349
594	10	19.2	0	9.999695	19.2	-0.0349	-0.0003	0	-0.0349
595	10	20.8	0	9.999695	20.8	-0.0349	-0.0003	0	-0.0349
596	10	22.4	0	9.999695	22.4	-0.0349	-0.0003	0	-0.0349
597	10	24	0	9.999695	24	-0.0349	-0.0003	0	-0.0349
598	8	16	0	8	16	0	0	0	0
599	8	17.6	0	8	17.6	0	0	0	0
600	8	19.2	0	8	19.2	0	0	0	0
601	8	20.8	0	8	20.8	0	0	0	0
602	8	22.4	0	8	22.4	0	0	0	0
603	8	24	0	8	24	0	0	0	0
604	6	16	0	6.000305	16	0.034905	0.000305	0	0.034905
605	6	17.6	0	6.000305	17.6	0.034905	0.000305	0	0.034905
606	6	19.2	0	6.000305	19.2	0.034905	0.000305	0	0.034905
607	6	20.8	0	6.000305	20.8	0.034905	0.000305	0	0.034905
608	6	22.4	0	6.000305	22.4	0.034905	0.000305	0	0.034905
609	6	24	0	6.000305	24	0.034905	0.000305	0	0.034905
610	4	16	0	4.000609	16	0.06981	0.000609	0	0.06981
611	4	17.6	0	4.000609	17.6	0.06981	0.000609	0	0.06981
612	4	19.2	0	4.000609	19.2	0.06981	0.000609	0	0.06981
613	4	20.8	0	4.000609	20.8	0.06981	0.000609	0	0.06981
614	4	22.4	0	4.000609	22.4	0.06981	0.000609	0	0.06981
615	4	24	0	4.000609	24	0.06981	0.000609	0	0.06981
616	2	16	0	2.000914	16	0.104714	0.000914	0	0.104714
617	2	17.6	0	2.000914	17.6	0.104714	0.000914	0	0.104714
618	2	19.2	0	2.000914	19.2	0.104714	0.000914	0	0.104714
619	2	20.8	0	2.000914	20.8	0.104714	0.000914	0	0.104714
620	2	22.4	0	2.000914	22.4	0.104714	0.000914	0	0.104714
621	2	24	0	2.000914	24	0.104714	0.000914	0	0.104714
622	0	16	0	0.001218	16	0.139619	0.001218	0	0.139619
623	0	17.6	0	0.001218	17.6	0.139619	0.001218	0	0.139619
624	0	19.2	0	0.001218	19.2	0.139619	0.001218	0	0.139619
625	0	20.8	0	0.001218	20.8	0.139619	0.001218	0	0.139619
626	0	22.4	0	0.001218	22.4	0.139619	0.001218	0	0.139619
627	0	24	0	0.001218	24	0.139619	0.001218	0	0.139619
628	16	25.3333	0	15.99878	25.3333	-0.13962	-0.00122	0	-0.13962
629	16	26.6667	0	15.99878	26.6667	-0.13962	-0.00122	0	-0.13962
630	16	28	0	15.99878	28	-0.13962	-0.00122	0	-0.13962
631	16	29.3333	0	15.99878	29.3333	-0.13962	-0.00122	0	-0.13962
632	16	30.6667	0	15.99878	30.6667	-0.13962	-0.00122	0	-0.13962
633	16	32	0	15.99878	32	-0.13962	-0.00122	0	-0.13962
635	14	25.3333	0	13.99909	25.3333	-0.10471	-0.00091	0	-0.10471
636	14	26.6667	0	13.99909	26.6667	-0.10471	-0.00091	0	-0.10471
637	14	28	0	13.99909	28	-0.10471	-0.00091	0	-0.10471
638	14	29.3333	0	13.99909	29.3333	-0.10471	-0.00091	0	-0.10471
639	14	30.6667	0	13.99909	30.6667	-0.10471	-0.00091	0	-0.10471
640	14	32	0	13.99909	32	-0.10471	-0.00091	0	-0.10471
641	12	25.3333	0	11.99939	25.3333	-0.06981	-0.00061	0	-0.06981
642	12	26.6667	0	11.99939	26.6667	-0.06981	-0.00061	0	-0.06981
643	12	28	0	11.99939	28	-0.06981	-0.00061	0	-0.06981

644	12	29.3333	0	11.99939	29.3333	-0.06981	-0.00061	0	-0.06981
645	12	30.6667	0	11.99939	30.6667	-0.06981	-0.00061	0	-0.06981
646	12	32	0	11.99939	32	-0.06981	-0.00061	0	-0.06981
647	10	25.3333	0	9.999695	25.3333	-0.0349	-0.0003	0	-0.0349
648	10	26.6667	0	9.999695	26.6667	-0.0349	-0.0003	0	-0.0349
649	10	28	0	9.999695	28	-0.0349	-0.0003	0	-0.0349
650	10	29.3333	0	9.999695	29.3333	-0.0349	-0.0003	0	-0.0349
651	10	30.6667	0	9.999695	30.6667	-0.0349	-0.0003	0	-0.0349
652	10	32	0	9.999695	32	-0.0349	-0.0003	0	-0.0349
653	8	25.3333	0	8	25.3333	0	0	0	0
654	8	26.6667	0	8	26.6667	0	0	0	0
655	8	28	0	8	28	0	0	0	0
656	8	29.3333	0	8	29.3333	0	0	0	0
657	8	30.6667	0	8	30.6667	0	0	0	0
658	8	32	0	8	32	0	0	0	0
659	6	25.3333	0	6.000305	25.3333	0.034905	0.000305	0	0.034905
660	6	26.6667	0	6.000305	26.6667	0.034905	0.000305	0	0.034905
661	6	28	0	6.000305	28	0.034905	0.000305	0	0.034905
662	6	29.3333	0	6.000305	29.3333	0.034905	0.000305	0	0.034905
663	6	30.6667	0	6.000305	30.6667	0.034905	0.000305	0	0.034905
664	6	32	0	6.000305	32	0.034905	0.000305	0	0.034905
665	4	25.3333	0	4.000609	25.3333	0.06981	0.000609	0	0.06981
666	4	26.6667	0	4.000609	26.6667	0.06981	0.000609	0	0.06981
667	4	28	0	4.000609	28	0.06981	0.000609	0	0.06981
668	4	29.3333	0	4.000609	29.3333	0.06981	0.000609	0	0.06981
669	4	30.6667	0	4.000609	30.6667	0.06981	0.000609	0	0.06981
670	4	32	0	4.000609	32	0.06981	0.000609	0	0.06981
671	2	25.3333	0	2.000914	25.3333	0.104714	0.000914	0	0.104714
672	2	26.6667	0	2.000914	26.6667	0.104714	0.000914	0	0.104714
673	2	28	0	2.000914	28	0.104714	0.000914	0	0.104714
674	2	29.3333	0	2.000914	29.3333	0.104714	0.000914	0	0.104714
675	2	30.6667	0	2.000914	30.6667	0.104714	0.000914	0	0.104714
676	2	32	0	2.000914	32	0.104714	0.000914	0	0.104714
677	0	25.3333	0	0.001218	25.3333	0.139619	0.001218	0	0.139619
678	0	26.6667	0	0.001218	26.6667	0.139619	0.001218	0	0.139619
679	0	28	0	0.001218	28	0.139619	0.001218	0	0.139619
680	0	29.3333	0	0.001218	29.3333	0.139619	0.001218	0	0.139619
681	0	30.6667	0	0.001218	30.6667	0.139619	0.001218	0	0.139619
682	0	32	0	0.001218	32	0.139619	0.001218	0	0.139619
685	0	14.3	0	0.001218	14.3	0.139619	0.001218	0	0.139619
686	2	14.3	0	2.000914	14.3	0.104714	0.000914	0	0.104714
687	4	14.3	0	4.000609	14.3	0.06981	0.000609	0	0.06981
688	6	14.3	0	6.000305	14.3	0.034905	0.000305	0	0.034905
689	8	14.3	0	8	14.3	0	0	0	0
690	10	14.3	0	9.999695	14.3	-0.0349	-0.0003	0	-0.0349
691	12	14.3	0	11.99939	14.3	-0.06981	-0.00061	0	-0.06981
692	14	14.3	0	13.99909	14.3	-0.10471	-0.00091	0	-0.10471
693	16	14.3	0	15.99878	14.3	-0.13962	-0.00122	0	-0.13962
694	0	24.1	0	0.001218	24.1	0.139619	0.001218	0	0.139619
695	2	24.1	0	2.000914	24.1	0.104714	0.000914	0	0.104714
696	4	24.1	0	4.000609	24.1	0.06981	0.000609	0	0.06981
697	6	24.1	0	6.000305	24.1	0.034905	0.000305	0	0.034905
698	8	24.1	0	8	24.1	0	0	0	0
699	10	24.1	0	9.999695	24.1	-0.0349	-0.0003	0	-0.0349
700	12	24.1	0	11.99939	24.1	-0.06981	-0.00061	0	-0.06981
701	14	24.1	0	13.99909	24.1	-0.10471	-0.00091	0	-0.10471
702	16	24.1	0	15.99878	24.1	-0.13962	-0.00122	0	-0.13962
703	11.4	14.4	0	11.39948	14.4	-0.05934	-0.00052	0	-0.05934
704	11.9	16	0	11.89941	16	-0.06806	-0.00059	0	-0.06806
705	11.9	17.6	0	11.89941	17.6	-0.06806	-0.00059	0	-0.06806
706	11.9	19.2	0	11.89941	19.2	-0.06806	-0.00059	0	-0.06806
707	11.9	20.8	0	11.89941	20.8	-0.06806	-0.00059	0	-0.06806
708	11.9	22.4	0	11.89941	22.4	-0.06806	-0.00059	0	-0.06806
709	11.4	24	0	11.39948	24	-0.05934	-0.00052	0	-0.05934

APPENDIX A-4

STARS-SOLIDS Generalized Mode 3 Displacement Definition (Control Mode)

Node	Original XYZ Location			New XYZ Location			Nodal Displacement		
	X	Y	Z	X'	Y'	Z'	ΔX	ΔY	ΔZ
13	0	0	0	0	0	0	0	0	0
14	2	0	0	2	0	0	0	0	0
52	4	0	0	4	0	0	0	0	0
53	6	0	0	6	0	0	0	0	0
54	8	0	0	8	0	0	0	0	0
55	10	0	0	10	0	0	0	0	0
56	12	0	0	12	0	0	0	0	0
90	14	0	0	14	0	0	0	0	0
91	16	0	0	16	0	0	0	0	0
300	16	14.4	0	16.0692	14.4	0.06981	0.0692	0	0.06981
301	16	15.04	0	16.0692	15.04	0.06981	0.0692	0	0.06981
302	16	15.68	0	16.0692	15.68	0.06981	0.0692	0	0.06981
303	16	16.32	0	16.0692	16.32	0.06981	0.0692	0	0.06981
304	16	16.96	0	16.0692	16.96	0.06981	0.0692	0	0.06981
305	16	17.6	0	16.0692	17.6	0.06981	0.0692	0	0.06981
306	16	18.24	0	16.0692	18.24	0.06981	0.0692	0	0.06981
307	16	18.88	0	16.0692	18.88	0.06981	0.0692	0	0.06981
308	16	19.52	0	16.0692	19.52	0.06981	0.0692	0	0.06981
309	16	20.16	0	16.0692	20.16	0.06981	0.0692	0	0.06981
310	16	20.8	0	16.0692	20.8	0.06981	0.0692	0	0.06981
311	16	21.44	0	16.0692	21.44	0.06981	0.0692	0	0.06981
312	16	22.08	0	16.0692	22.08	0.06981	0.0692	0	0.06981
313	16	22.72	0	16.0692	22.72	0.06981	0.0692	0	0.06981
314	16	23.36	0	16.0692	23.36	0.06981	0.0692	0	0.06981
315	16	24	0	16.0692	24	0.06981	0.0692	0	0.06981
316	15.6667	14.4	0	15.73013	14.4	0.063993	0.063434	0	0.063993
317	15.6667	15.04	0	15.73013	15.04	0.063993	0.063434	0	0.063993
318	15.6667	15.68	0	15.73013	15.68	0.063993	0.063434	0	0.063993
319	15.6667	16.32	0	15.73013	16.32	0.063993	0.063434	0	0.063993
320	15.6667	16.96	0	15.73013	16.96	0.063993	0.063434	0	0.063993
321	15.6667	17.6	0	15.73013	17.6	0.063993	0.063434	0	0.063993
322	15.6667	18.24	0	15.73013	18.24	0.063993	0.063434	0	0.063993
323	15.6667	18.88	0	15.73013	18.88	0.063993	0.063434	0	0.063993
324	15.6667	19.52	0	15.73013	19.52	0.063993	0.063434	0	0.063993
325	15.6667	20.16	0	15.73013	20.16	0.063993	0.063434	0	0.063993
326	15.6667	20.8	0	15.73013	20.8	0.063993	0.063434	0	0.063993
327	15.6667	21.44	0	15.73013	21.44	0.063993	0.063434	0	0.063993
328	15.6667	22.08	0	15.73013	22.08	0.063993	0.063434	0	0.063993
329	15.6667	22.72	0	15.73013	22.72	0.063993	0.063434	0	0.063993
330	15.6667	23.36	0	15.73013	23.36	0.063993	0.063434	0	0.063993
331	15.6667	24	0	15.73013	24	0.063993	0.063434	0	0.063993
332	15.3333	14.4	0	15.39097	14.4	0.058174	0.057666	0	0.058174
333	15.3333	15.04	0	15.39097	15.04	0.058174	0.057666	0	0.058174
334	15.3333	15.68	0	15.39097	15.68	0.058174	0.057666	0	0.058174
335	15.3333	16.32	0	15.39097	16.32	0.058174	0.057666	0	0.058174
336	15.3333	16.96	0	15.39097	16.96	0.058174	0.057666	0	0.058174
337	15.3333	17.6	0	15.39097	17.6	0.058174	0.057666	0	0.058174
338	15.3333	18.24	0	15.39097	18.24	0.058174	0.057666	0	0.058174
339	15.3333	18.88	0	15.39097	18.88	0.058174	0.057666	0	0.058174
340	15.3333	19.52	0	15.39097	19.52	0.058174	0.057666	0	0.058174
341	15.3333	20.16	0	15.39097	20.16	0.058174	0.057666	0	0.058174
342	15.3333	20.8	0	15.39097	20.8	0.058174	0.057666	0	0.058174

487	12.3333	21.44	0	12.33907	21.44	0.005817	0.005766	0	0.005817
488	12.3333	22.08	0	12.33907	22.08	0.005817	0.005766	0	0.005817
489	12.3333	22.72	0	12.33907	22.72	0.005817	0.005766	0	0.005817
490	12.3333	23.36	0	12.33907	23.36	0.005817	0.005766	0	0.005817
491	12.3333	24	0	12.33907	24	0.005817	0.005766	0	0.005817
492	12	14.4	0	12	14.4	0	0	0	0
493	12	15.04	0	12	15.04	0	0	0	0
494	12	15.68	0	12	15.68	0	0	0	0
495	12	16.32	0	12	16.32	0	0	0	0
496	12	16.96	0	12	16.96	0	0	0	0
497	12	17.6	0	12	17.6	0	0	0	0
498	12	18.24	0	12	18.24	0	0	0	0
499	12	18.88	0	12	18.88	0	0	0	0
500	12	19.52	0	12	19.52	0	0	0	0
501	12	20.16	0	12	20.16	0	0	0	0
502	12	20.8	0	12	20.8	0	0	0	0
503	12	21.44	0	12	21.44	0	0	0	0
504	12	22.08	0	12	22.08	0	0	0	0
505	12	22.72	0	12	22.72	0	0	0	0
506	12	23.36	0	12	23.36	0	0	0	0
507	12	24	0	12	24	0	0	0	0
509	16	1.8	0	16	1.8	0	0	0	0
510	16	3.6	0	16	3.6	0	0	0	0
511	16	5.4	0	16	5.4	0	0	0	0
512	16	7.2	0	16	7.2	0	0	0	0
513	16	9	0	16	9	0	0	0	0
514	16	10.8	0	16	10.8	0	0	0	0
515	16	12.6	0	16	12.6	0	0	0	0
517	14	1.8	0	14	1.8	0	0	0	0
518	14	3.6	0	14	3.6	0	0	0	0
519	14	5.4	0	14	5.4	0	0	0	0
520	14	7.2	0	14	7.2	0	0	0	0
521	14	9	0	14	9	0	0	0	0
522	14	10.8	0	14	10.8	0	0	0	0
523	14	12.6	0	14	12.6	0	0	0	0
526	12	1.8	0	12	1.8	0	0	0	0
527	12	3.6	0	12	3.6	0	0	0	0
528	12	5.4	0	12	5.4	0	0	0	0
529	12	7.2	0	12	7.2	0	0	0	0
530	12	9	0	12	9	0	0	0	0
531	12	10.8	0	12	10.8	0	0	0	0
532	12	12.6	0	12	12.6	0	0	0	0
534	10	1.8	0	10	1.8	0	0	0	0
535	10	3.6	0	10	3.6	0	0	0	0
536	10	5.4	0	10	5.4	0	0	0	0
537	10	7.2	0	10	7.2	0	0	0	0
538	10	9	0	10	9	0	0	0	0
539	10	10.8	0	10	10.8	0	0	0	0
540	10	12.6	0	10	12.6	0	0	0	0
541	10	14.4	0	10	14.4	0	0	0	0
543	8	1.8	0	8	1.8	0	0	0	0
544	8	3.6	0	8	3.6	0	0	0	0
545	8	5.4	0	8	5.4	0	0	0	0
546	8	7.2	0	8	7.2	0	0	0	0
547	8	9	0	8	9	0	0	0	0
548	8	10.8	0	8	10.8	0	0	0	0
549	8	12.6	0	8	12.6	0	0	0	0
550	8	14.4	0	8	14.4	0	0	0	0
552	6	1.8	0	6	1.8	0	0	0	0
553	6	3.6	0	6	3.6	0	0	0	0
554	6	5.4	0	6	5.4	0	0	0	0
555	6	7.2	0	6	7.2	0	0	0	0
556	6	9	0	6	9	0	0	0	0
557	6	10.8	0	6	10.8	0	0	0	0
558	6	12.6	0	6	12.6	0	0	0	0
559	6	14.4	0	6	14.4	0	0	0	0
561	4	1.8	0	4	1.8	0	0	0	0
562	4	3.6	0	4	3.6	0	0	0	0
563	4	5.4	0	4	5.4	0	0	0	0
564	4	7.2	0	4	7.2	0	0	0	0
565	4	9	0	4	9	0	0	0	0
566	4	10.8	0	4	10.8	0	0	0	0

567	4	12.6	0	4	12.6	0	0	0	0
568	4	14.4	0	4	14.4	0	0	0	0
570	2	1.8	0	2	1.8	0	0	0	0
571	2	3.6	0	2	3.6	0	0	0	0
572	2	5.4	0	2	5.4	0	0	0	0
573	2	7.2	0	2	7.2	0	0	0	0
574	2	9	0	2	9	0	0	0	0
575	2	10.8	0	2	10.8	0	0	0	0
576	2	12.6	0	2	12.6	0	0	0	0
577	2	14.4	0	2	14.4	0	0	0	0
579	0	1.8	0	0	1.8	0	0	0	0
580	0	3.6	0	0	3.6	0	0	0	0
581	0	5.4	0	0	5.4	0	0	0	0
582	0	7.2	0	0	7.2	0	0	0	0
583	0	9	0	0	9	0	0	0	0
584	0	10.8	0	0	10.8	0	0	0	0
585	0	12.6	0	0	12.6	0	0	0	0
586	0	14.4	0	0	14.4	0	0	0	0
587	12	16	0	12	16	0	0	0	0
589	12	19.2	0	12	19.2	0	0	0	0
591	12	22.4	0	12	22.4	0	0	0	0
592	10	16	0	10	16	0	0	0	0
593	10	17.6	0	10	17.6	0	0	0	0
594	10	19.2	0	10	19.2	0	0	0	0
595	10	20.8	0	10	20.8	0	0	0	0
596	10	22.4	0	10	22.4	0	0	0	0
597	10	24	0	10	24	0	0	0	0
598	8	16	0	8	16	0	0	0	0
599	8	17.6	0	8	17.6	0	0	0	0
600	8	19.2	0	8	19.2	0	0	0	0
601	8	20.8	0	8	20.8	0	0	0	0
602	8	22.4	0	8	22.4	0	0	0	0
603	8	24	0	8	24	0	0	0	0
604	6	16	0	6	16	0	0	0	0
605	6	17.6	0	6	17.6	0	0	0	0
606	6	19.2	0	6	19.2	0	0	0	0
607	6	20.8	0	6	20.8	0	0	0	0
608	6	22.4	0	6	22.4	0	0	0	0
609	6	24	0	6	24	0	0	0	0
610	4	16	0	4	16	0	0	0	0
611	4	17.6	0	4	17.6	0	0	0	0
612	4	19.2	0	4	19.2	0	0	0	0
613	4	20.8	0	4	20.8	0	0	0	0
614	4	22.4	0	4	22.4	0	0	0	0
615	4	24	0	4	24	0	0	0	0
616	2	16	0	2	16	0	0	0	0
617	2	17.6	0	2	17.6	0	0	0	0
618	2	19.2	0	2	19.2	0	0	0	0
619	2	20.8	0	2	20.8	0	0	0	0
620	2	22.4	0	2	22.4	0	0	0	0
621	2	24	0	2	24	0	0	0	0
622	0	16	0	0	16	0	0	0	0
623	0	17.6	0	0	17.6	0	0	0	0
624	0	19.2	0	0	19.2	0	0	0	0
625	0	20.8	0	0	20.8	0	0	0	0
626	0	22.4	0	0	22.4	0	0	0	0
627	0	24	0	0	24	0	0	0	0
628	16	25.3333	0	16	25.3333	0	0	0	0
629	16	26.6667	0	16	26.6667	0	0	0	0
630	16	28	0	16	28	0	0	0	0
631	16	29.3333	0	16	29.3333	0	0	0	0
632	16	30.6667	0	16	30.6667	0	0	0	0
633	16	32	0	16	32	0	0	0	0
635	14	25.3333	0	14	25.3333	0	0	0	0
636	14	26.6667	0	14	26.6667	0	0	0	0
637	14	28	0	14	28	0	0	0	0
638	14	29.3333	0	14	29.3333	0	0	0	0
639	14	30.6667	0	14	30.6667	0	0	0	0
640	14	32	0	14	32	0	0	0	0
641	12	25.3333	0	12	25.3333	0	0	0	0
642	12	26.6667	0	12	26.6667	0	0	0	0
643	12	28	0	12	28	0	0	0	0

644	12	29.3333	0	12	29.3333	0	0	0	0
645	12	30.6667	0	12	30.6667	0	0	0	0
646	12	32	0	12	32	0	0	0	0
647	10	25.3333	0	10	25.3333	0	0	0	0
648	10	26.6667	0	10	26.6667	0	0	0	0
649	10	28	0	10	28	0	0	0	0
650	10	29.3333	0	10	29.3333	0	0	0	0
651	10	30.6667	0	10	30.6667	0	0	0	0
652	10	32	0	10	32	0	0	0	0
653	8	25.3333	0	8	25.3333	0	0	0	0
654	8	26.6667	0	8	26.6667	0	0	0	0
655	8	28	0	8	28	0	0	0	0
656	8	29.3333	0	8	29.3333	0	0	0	0
657	8	30.6667	0	8	30.6667	0	0	0	0
658	8	32	0	8	32	0	0	0	0
659	6	25.3333	0	6	25.3333	0	0	0	0
660	6	26.6667	0	6	26.6667	0	0	0	0
661	6	28	0	6	28	0	0	0	0
662	6	29.3333	0	6	29.3333	0	0	0	0
663	6	30.6667	0	6	30.6667	0	0	0	0
664	6	32	0	6	32	0	0	0	0
665	4	25.3333	0	4	25.3333	0	0	0	0
666	4	26.6667	0	4	26.6667	0	0	0	0
667	4	28	0	4	28	0	0	0	0
668	4	29.3333	0	4	29.3333	0	0	0	0
669	4	30.6667	0	4	30.6667	0	0	0	0
670	4	32	0	4	32	0	0	0	0
671	2	25.3333	0	2	25.3333	0	0	0	0
672	2	26.6667	0	2	26.6667	0	0	0	0
673	2	28	0	2	28	0	0	0	0
674	2	29.3333	0	2	29.3333	0	0	0	0
675	2	30.6667	0	2	30.6667	0	0	0	0
676	2	32	0	2	32	0	0	0	0
677	0	25.3333	0	0	25.3333	0	0	0	0
678	0	26.6667	0	0	26.6667	0	0	0	0
679	0	28	0	0	28	0	0	0	0
680	0	29.3333	0	0	29.3333	0	0	0	0
681	0	30.6667	0	0	30.6667	0	0	0	0
682	0	32	0	0	32	0	0	0	0
685	0	14.3	0	0	14.3	0	0	0	0
686	2	14.3	0	2	14.3	0	0	0	0
687	4	14.3	0	4	14.3	0	0	0	0
688	6	14.3	0	6	14.3	0	0	0	0
689	8	14.3	0	8	14.3	0	0	0	0
690	10	14.3	0	10	14.3	0	0	0	0
691	12	14.3	0	12	14.3	0	0	0	0
692	14	14.3	0	14	14.3	0	0	0	0
693	16	14.3	0	16	14.3	0	0	0	0
694	0	24.1	0	0	24.1	0	0	0	0
695	2	24.1	0	2	24.1	0	0	0	0
696	4	24.1	0	4	24.1	0	0	0	0
697	6	24.1	0	6	24.1	0	0	0	0
698	8	24.1	0	8	24.1	0	0	0	0
699	10	24.1	0	10	24.1	0	0	0	0
700	12	24.1	0	12	24.1	0	0	0	0
701	14	24.1	0	14	24.1	0	0	0	0
702	16	24.1	0	16	24.1	0	0	0	0
703	11.4	14.4	0	11.4	14.4	0	0	0	0
704	11.9	16	0	11.9	16	0	0	0	0
705	11.9	17.6	0	11.9	17.6	0	0	0	0
706	11.9	19.2	0	11.9	19.2	0	0	0	0
707	11.9	20.8	0	11.9	20.8	0	0	0	0
708	11.9	22.4	0	11.9	22.4	0	0	0	0
709	11.4	24	0	11.4	24	0	0	0	0

APPENDIX A-5

Program to Write Nodal Displacement Data into STARS-SOLIDS Format

```
program new_out2.f
C Reads in a file named: 3modes.txt and writes to 3 files
C formatted as *.out.2 should be.
  implicit none
  integer i,j,k,dof,node,zero,nmodes,nm1,nm2,nm3,nd1,nd2,nd3
  real node_data(10000,7,3),disp
  open(unit=10,file='3modes.txt')
  zero=0
C Read in header data
  read(10,*) nmodes
  read(10,*) nm1,nd1
  read(10,*) nm2,nd2
  read(10,*) nm3,nd3
C Read in nodal dof and disp data
  do i=1,(nm1*nd1)
    read(10,*) node,dof,disp
    if(dof .eq. 1) then
      node_data(node,1,1)=disp
    else if (dof .eq. 2) then
      node_data(node,2,1)=disp
    else if (dof .eq. 3) then
      node_data(node,3,1)=disp
    else if (dof .eq. 4) then
      node_data(node,4,1)=disp
    else if (dof .eq. 5) then
      node_data(node,5,1)=disp
    else
      node_data(node,6,1)=disp
    end if
    node_data(node,7,1)=node
  end do
  do i=1,(nm2*nd2)
    read(10,*) node,dof,disp
    if(dof .eq. 1) then
      node_data(node,1,2)=disp
    else if (dof .eq. 2) then
      node_data(node,2,2)=disp
    else if (dof .eq. 3) then
      node_data(node,3,2)=disp
    else if (dof .eq. 4) then
      node_data(node,4,2)=disp
    else if (dof .eq. 5) then
      node_data(node,5,2)=disp
```



```

        else
            node_data(node,6,2)=disp
        end if
        node_data(node,7,2)=node
    end do
do i=1,(nm3*nd3)
    read(10,*) node,dof,disp
    if(dof .eq. 1) then
        node_data(node,1,3)=disp
    else if (dof .eq. 2) then
        node_data(node,2,3)=disp
    else if (dof .eq. 3) then
        node_data(node,3,3)=disp
    else if (dof .eq. 4) then
        node_data(node,4,3)=disp
    else if (dof .eq. 5) then
        node_data(node,5,3)=disp
    else
        node_data(node,6,3)=disp
    end if
    node_data(node,7,3)=node
end do
close(10)
C Write to 3 files
do k=1,3
    j=1
    if (k .eq. 1) open(unit=15,file='out1.dat')
    if (k .eq. 2) then
        close(15)
        open(unit=15,file='out2.dat')
    end if
    if (k .eq. 3) then
        close(15)
        open(unit=15,file='out3.dat')
    end if
    write(15,1000)
    write(15,1001)
    do i = 1,10000
        if (node_data(i,7,k) .eq. i) then
            write(15,1002) i,j,
&            node_data(i,1,k),node_data(i,2,k),
&            node_data(i,3,k),node_data(i,4,k),
&            node_data(i,5,k),node_data(i,6,k)
            j=j+1
        end if
    end do
end do
1000 format(7x,'NODE')
1001 format(5x,'EXT',3x,'INT',6x,'X-DISPL.',6x,'Y-DISPL.',
&        6x,'Z-DISPL.',6x,'X-ROTN.',7x,'Y-ROTN.',7x,
&        'Z-ROTN.'/)
1002 format(5x,i3,3x,i3,4x,E12.6,2x,E12.6,2x,E12.6,2x,E12.6,
&        2x,E12.6,2x,E12.6)

stop
end

```

APPENDIX B-1

STARS-CFD Geometry Data File (*BACT.DAT*)

BACTNACA 0012 Wing & Flap	0.000000	0	0.000000	3.954741	0	0.948188
32 15	0.001542	0	0.027865	4.091030	0	0.951432
Curve Components	0.006168	0	0.055494	4.228826	0	0.954057
1 1	0.013875	0	0.082883	4.368076	0	0.956067
2	0.024661	0	0.110027	4.508726	0	0.957468
-160 0 -100	0.038522	0	0.136923	4.650722	0	0.958266
-160 0 100	0.055452	0	0.163563	4.794009	0	0.958466
2 1	0.075445	0	0.189942	4.938533	0	0.958077
2	0.098493	0	0.216053	5.084236	0	0.957106
-160 0 100	0.124587	0	0.241889	5.231064	0	0.955562
160 0 100	0.153718	0	0.267440	5.378959	0	0.953453
3 1	0.185873	0	0.292700	5.527864	0	0.950789
2	0.221041	0	0.317658	5.677723	0	0.947580
160 0 100	0.259207	0	0.342306	5.828476	0	0.943836
160 0 -100	0.300358	0	0.366632	5.980067	0	0.939569
4 1	0.344477	0	0.390628	6.132437	0	0.934789
2	0.391548	0	0.414281	6.285527	0	0.929508
160 0 -100	0.441552	0	0.437581	6.439277	0	0.923739
-160 0 -100	0.494469	0	0.460516	6.593630	0	0.917493
5 1	0.550281	0	0.483075	6.748524	0	0.910783
2	0.608964	0	0.505246	6.903901	0	0.903623
-160 0 -100	0.670496	0	0.527017	7.059701	0	0.896025
-160 160 -100	0.734855	0	0.548375	7.215863	0	0.888002
6 1	0.802014	0	0.569308	7.372327	0	0.879569
2	0.871948	0	0.589805	7.529034	0	0.870739
-160 0 100	0.944630	0	0.609852	7.685921	0	0.861525
-160 160 100	1.020032	0	0.629438	7.842930	0	0.851942
7 1	1.098125	0	0.648550	8.000000	0	0.842004
2	1.178879	0	0.667177	8.157070	0	0.831724
160 0 100	1.262262	0	0.685306	8.314079	0	0.821117
160 160 100	1.348243	0	0.702927	8.470966	0	0.810197
8 1	1.436788	0	0.720029	8.627673	0	0.798978
2	1.527864	0	0.736599	8.784137	0	0.787473
160 0 -100	1.621435	0	0.752628	8.940299	0	0.775697
160 160 -100	1.717465	0	0.768107	9.096099	0	0.763664
9 1	1.815916	0	0.783024	9.251476	0	0.751388
2	1.916752	0	0.797372	9.406370	0	0.738882
-160 160 -100	2.019933	0	0.811141	9.560723	0	0.726159
-160 160 100	2.125420	0	0.824323	9.714473	0	0.713235
10 1	2.233171	0	0.836912	9.867563	0	0.700121
2	2.343146	0	0.848899	10.019933	0	0.686832
-160 160 100	2.455301	0	0.860280	10.171524	0	0.673381
160 160 100	2.569594	0	0.871048	10.322277	0	0.659780
11 1	2.685980	0	0.881199	10.472136	0	0.646042
2	2.804416	0	0.890728	10.621041	0	0.632181
160 160 100	2.924854	0	0.899632	10.768936	0	0.618209
160 160 -100	3.047248	0	0.907908	10.915764	0	0.604139
12 1	3.171552	0	0.915554	11.061467	0	0.589983
2	3.297718	0	0.922570	11.205991	0	0.575753
160 160 -100	3.425696	0	0.928953	11.349278	0	0.561462
-160 160 -100	3.555438	0	0.934706	11.491274	0	0.547121
13 1	3.686893	0	0.939828	11.631924	0	0.532743
161	3.820011	0	0.944321	11.771174	0	0.518340

15924555 0 -0.010745
15944548 0 -0.007903
15961478 0 -0.005494
15975339 0 -0.003519
15986125 0 -0.001981
15993832 0 -0.000881
15998458 0 -0.000220
16000000 0 0.000000
15 1
161
0.000000 32 0.000000
0.001542 32 0.027865
0.006168 32 0.055494
0.013875 32 0.082883
0.024661 32 0.110027
0.038522 32 0.136923
0.055452 32 0.163563
0.075445 32 0.189942
0.098493 32 0.216053
0.124587 32 0.241889
0.153718 32 0.267440
0.185873 32 0.292700
0.221041 32 0.317658
0.259207 32 0.342306
0.300358 32 0.366632
0.344477 32 0.390628
0.391548 32 0.414281
0.441552 32 0.437581
0.494469 32 0.460516
0.550281 32 0.483075
0.608964 32 0.505246
0.670496 32 0.527017
0.734855 32 0.548375
0.802014 32 0.569308
0.871948 32 0.589805
0.944630 32 0.609852
1.020032 32 0.629438
1.098125 32 0.648550
1.178879 32 0.667177
1.262262 32 0.685306
1.348243 32 0.702927
1.436788 32 0.720029
1.527864 32 0.736699
1.621435 32 0.752628
1.717465 32 0.768107
1.815916 32 0.783024
1.916752 32 0.797372
2.019933 32 0.811141
2.125420 32 0.824323
2.233171 32 0.836912
2.343146 32 0.848899
2.455301 32 0.860280
2.569594 32 0.871048
2.685980 32 0.881199
2.804416 32 0.890728
2.924854 32 0.899632
3.047248 32 0.907908
3.171552 32 0.915554
3.297718 32 0.922570
3.425696 32 0.928953
3.555438 32 0.934706
3.686893 32 0.939828
3.820011 32 0.944321
3.954741 32 0.948188
4.091030 32 0.951432
4.228826 32 0.954057
4.368076 32 0.956067
4.508726 32 0.957468
4.650722 32 0.958266
4.794009 32 0.958466

4.938533 32 0.958077
5.084236 32 0.957106
5.231064 32 0.955562
5.378959 32 0.953453
5.527864 32 0.950789
5.677723 32 0.947580
5.828476 32 0.943836
5.980067 32 0.939569
6.132437 32 0.934789
6.285527 32 0.929508
6.439277 32 0.923739
6.593630 32 0.917493
6.748524 32 0.910783
6.903901 32 0.903623
7.059701 32 0.896025
7.215863 32 0.888002
7.372327 32 0.879569
7.529034 32 0.870739
7.685921 32 0.861525
7.842930 32 0.851942
8.000000 32 0.842004
8.157070 32 0.831724
8.314079 32 0.821117
8.470966 32 0.810197
8.627673 32 0.798978
8.784137 32 0.787473
8.940299 32 0.775697
9.096099 32 0.763664
9.251476 32 0.751388
9.406370 32 0.738882
9.560723 32 0.726159
9.714473 32 0.713235
9.867563 32 0.700121
10.019933 32 0.686832
10.171524 32 0.673381
10.322277 32 0.659780
10.472136 32 0.646042
10.621041 32 0.632181
10.768936 32 0.618209
10.915764 32 0.604139
11.061467 32 0.589983
11.205991 32 0.575753
11.349278 32 0.561462
11.491274 32 0.547121
11.631924 32 0.532743
11.771174 32 0.518340
11.908970 32 0.503922
12.045259 32 0.489503
12.179989 32 0.475093
12.313107 32 0.460704
12.444562 32 0.446347
12.574304 32 0.432034
12.702282 32 0.417776
12.828448 32 0.403585
12.952752 32 0.389470
13.075146 32 0.375445
13.195584 32 0.361518
13.314020 32 0.347703
13.430406 32 0.334009
13.544699 32 0.320447
13.656854 32 0.307029
13.766829 32 0.293765
13.874580 32 0.280666
13.980067 32 0.267743
14.083248 32 0.255006
14.184084 32 0.242466
14.282535 32 0.230134
14.378565 32 0.218021
14.472136 32 0.206136
14.563212 32 0.194489

14.651757 32 0.183092
14.737738 32 0.171955
14.821121 32 0.161087
14.901875 32 0.150498
14.979968 32 0.140198
15.055370 32 0.130196
15.128052 32 0.120502
15.197986 32 0.111126
15.265145 32 0.102075
15.329504 32 0.093360
15.391036 32 0.084988
15.449719 32 0.076967
15.505531 32 0.069306
15.558448 32 0.062013
15.608452 32 0.055094
15.655523 32 0.048558
15.699642 32 0.042410
15.740793 32 0.036657
15.778959 32 0.031305
15.814127 32 0.026359
15.846282 32 0.021826
15.875413 32 0.017710
15.901507 32 0.014015
15.924555 32 0.010745
15.944548 32 0.007903
15.961478 32 0.005494
15.975339 32 0.003519
15.986125 32 0.001981
15.993832 32 0.000881
15.998458 32 0.000220
16.000000 32 0.000000
16 1
161
0.000000 32 0.000000
0.001542 32 -0.027865
0.006168 32 -0.055494
0.013875 32 -0.082883
0.024661 32 -0.110027
0.038522 32 -0.136923
0.055452 32 -0.163563
0.075445 32 -0.189942
0.098493 32 -0.216053
0.124587 32 -0.241889
0.153718 32 -0.267440
0.185873 32 -0.292700
0.221041 32 -0.317658
0.259207 32 -0.342306
0.300358 32 -0.366632
0.344477 32 -0.390628
0.391548 32 -0.414281
0.441552 32 -0.437581
0.494469 32 -0.460516
0.550281 32 -0.483075
0.608964 32 -0.505246
0.670496 32 -0.527017
0.734855 32 -0.548375
0.802014 32 -0.569308
0.871948 32 -0.589805
0.944630 32 -0.609852
1.020032 32 -0.629438
1.098125 32 -0.648550
1.178879 32 -0.667177
1.262262 32 -0.685306
1.348243 32 -0.702927
1.436788 32 -0.720029
1.527864 32 -0.736699
1.621435 32 -0.752628
1.717465 32 -0.768107
1.815916 32 -0.783024
1.916752 32 -0.797372

2.019933 32 -0.811141
 2.125420 32 -0.824323
 2.233171 32 -0.836912
 2.343146 32 -0.848899
 2.455301 32 -0.860280
 2.569594 32 -0.871048
 2.685980 32 -0.881199
 2.804416 32 -0.890728
 2.924854 32 -0.899632
 3.047248 32 -0.907908
 3.171552 32 -0.915554
 3.297718 32 -0.922570
 3.425696 32 -0.928953
 3.555438 32 -0.934706
 3.686893 32 -0.939828
 3.820011 32 -0.944321
 3.954741 32 -0.948188
 4.091030 32 -0.951432
 4.228826 32 -0.954057
 4.368076 32 -0.956607
 4.508726 32 -0.957468
 4.650722 32 -0.958266
 4.794009 32 -0.958466
 4.938533 32 -0.958077
 5.084236 32 -0.957106
 5.231064 32 -0.955562
 5.378959 32 -0.953453
 5.527864 32 -0.950789
 5.677723 32 -0.947580
 5.828476 32 -0.943836
 5.980067 32 -0.939569
 6.132437 32 -0.934789
 6.285527 32 -0.929508
 6.439277 32 -0.923739
 6.593630 32 -0.917493
 6.748524 32 -0.910783
 6.903901 32 -0.903623
 7.059701 32 -0.896025
 7.215863 32 -0.888002
 7.372327 32 -0.879569
 7.529034 32 -0.870739
 7.685921 32 -0.861525
 7.842930 32 -0.851942
 8.000000 32 -0.842004
 8.157070 32 -0.831724
 8.314079 32 -0.821117
 8.470966 32 -0.810197
 8.627673 32 -0.798978
 8.784137 32 -0.787473
 8.940299 32 -0.775697
 9.096099 32 -0.763664
 9.251476 32 -0.751388
 9.406370 32 -0.738882
 9.560723 32 -0.726159
 9.714473 32 -0.713235
 9.867563 32 -0.700121
 10.019933 32 -0.686832
 10.171524 32 -0.673381
 10.322277 32 -0.659780
 10.472136 32 -0.646042
 10.621041 32 -0.632181
 10.768936 32 -0.618209
 10.915764 32 -0.604139
 11.061467 32 -0.589983
 11.205991 32 -0.575753
 11.349278 32 -0.561462
 11.491274 32 -0.547121
 11.631924 32 -0.532743
 11.771174 32 -0.518340
 11.908970 32 -0.503922

12.045259 32 -0.489503
 12.179989 32 -0.475093
 12.313107 32 -0.460704
 12.444562 32 -0.446347
 12.574304 32 -0.432034
 12.702282 32 -0.417776
 12.828448 32 -0.403585
 12.952752 32 -0.389470
 13.075146 32 -0.375445
 13.195584 32 -0.361518
 13.314020 32 -0.347703
 13.430406 32 -0.334009
 13.544699 32 -0.320447
 13.656854 32 -0.307029
 13.766829 32 -0.293765
 13.874580 32 -0.280666
 13.980067 32 -0.267743
 14.083248 32 -0.255006
 14.184084 32 -0.242466
 14.282535 32 -0.230134
 14.378565 32 -0.218021
 14.472136 32 -0.206136
 14.563212 32 -0.194489
 14.651757 32 -0.183092
 14.737738 32 -0.171955
 14.821121 32 -0.161087
 14.901875 32 -0.150498
 14.979968 32 -0.140198
 15.055370 32 -0.130196
 15.128052 32 -0.120502
 15.197986 32 -0.111126
 15.265145 32 -0.102075
 15.329504 32 -0.093360
 15.391036 32 -0.084988
 15.449719 32 -0.076967
 15.505531 32 -0.069306
 15.558448 32 -0.062013
 15.608452 32 -0.055094
 15.655523 32 -0.048558
 15.699642 32 -0.042410
 15.740793 32 -0.036657
 15.778959 32 -0.031305
 15.814127 32 -0.026359
 15.846282 32 -0.021826
 15.875413 32 -0.017710
 15.901507 32 -0.014015
 15.924555 32 -0.010745
 15.944548 32 -0.007903
 15.961478 32 -0.005494
 15.975339 32 -0.003519
 15.986125 32 -0.001981
 15.993832 32 -0.000881
 15.998458 32 -0.000220
 16.000000 32 0.000000
 17 1
 2
 0 0 0
 0 144 0
 18 1
 2
 16 0 0
 16 144 0
 19 1
 2
 16 144 0
 16 24 0
 20 1
 2
 16 24 0
 16 32 0

21 1
 55
 12.000000 144 0.494308997
 12.045259 144 0.489503001
 12.179989 144 0.475093031
 12.313107 144 0.460704012
 12.444562 144 0.446347363
 12.574304 144 0.432034431
 12.702282 144 0.417776497
 12.828448 144 0.403584782
 12.952752 144 0.389470453
 13.075146 144 0.375444624
 13.195584 144 0.361518361
 13.314020 144 0.347702684
 13.430406 144 0.334008569
 13.544699 144 0.320446949
 13.656854 144 0.307028714
 13.766829 144 0.293764709
 13.874580 144 0.280665734
 13.980067 144 0.267742539
 14.083248 144 0.255005822
 14.184084 144 0.242466224
 14.282535 144 0.230134319
 14.378565 144 0.218020612
 14.472136 144 0.206135553
 14.563212 144 0.19448941
 14.651757 144 0.183092492
 14.737738 144 0.171954906
 14.821121 144 0.161086662
 14.901875 144 0.150497635
 14.979968 144 0.140197555
 15.055370 144 0.130195989
 15.128052 144 0.12050233
 15.197986 144 0.111125777
 15.265145 144 0.102075327
 15.329504 144 0.093359749
 15.391036 144 0.084987577
 15.449719 144 0.076967086
 15.505531 144 0.069306282
 15.558448 144 0.062012879
 15.608452 144 0.055094287
 15.655523 144 0.048557594
 15.699642 144 0.04240955
 15.740793 144 0.036656553
 15.778959 144 0.031304631
 15.814127 144 0.026359429
 15.846282 144 0.021826198
 15.875413 144 0.017709775
 15.901507 144 0.014014579
 15.924555 144 0.010744594
 15.944548 144 0.007903359
 15.961478 144 0.005493962
 15.975339 144 0.003519031
 15.986125 144 0.001980723
 15.993832 144 0.000880725
 15.998458 144 0.000220242
 16.000000 144 0.000000
 22 1
 2
 12 144 0.494308997
 12 24 0.494308997
 23 1
 55
 12.000000 24 0.494308997
 12.045259 24 0.489503001
 12.179989 24 0.475093031
 12.313107 24 0.460704012
 12.444562 24 0.446347363
 12.574304 24 0.432034431
 12.702282 24 0.417776497

12.828448 24 0.403584782
 12.952752 24 0.389470453
 13.075146 24 0.375444624
 13.195584 24 0.361518361
 13.314020 24 0.347702684
 13.430406 24 0.334008569
 13.544699 24 0.320446949
 13.656854 24 0.307028714
 13.766829 24 0.293764709
 13.874580 24 0.280665734
 13.980067 24 0.267742539
 14.083248 24 0.255005822
 14.184084 24 0.242466224
 14.282535 24 0.230134319
 14.378565 24 0.218020612
 14.472136 24 0.20613553
 14.563212 24 0.19448941
 14.651757 24 0.183092492
 14.737738 24 0.171954906
 14.821121 24 0.161086662
 14.901875 24 0.150497635
 14.979968 24 0.140197555
 15.055370 24 0.130195989
 15.128052 24 0.12050233
 15.197986 24 0.111125777
 15.265145 24 0.102075327
 15.329504 24 0.093359749
 15.391036 24 0.084987577
 15.449719 24 0.076967086
 15.505531 24 0.069306282
 15.558448 24 0.062012879
 15.608452 24 0.055094287
 15.655523 24 0.048557594
 15.699642 24 0.04240955
 15.740793 24 0.036665653
 15.778959 24 0.031304631
 15.814127 24 0.026359429
 15.846282 24 0.021826198
 15.875413 24 0.017709775
 15.901507 24 0.014014579
 15.924555 24 0.010744594
 15.944548 24 0.007903359
 15.961478 24 0.005493962
 15.975339 24 0.003519031
 15.986125 24 0.001980723
 15.993832 24 0.000880725
 15.998458 24 0.000220242
 16.000000 24 0.000000
 24 1
 55
 12.000000 14.4 -0.494309
 12.045259 14.4 -0.489503
 12.179989 14.4 -0.475093
 12.313107 14.4 -0.460704
 12.444562 14.4 -0.446347
 12.574304 14.4 -0.432034
 12.702282 14.4 -0.417776
 12.828448 14.4 -0.403585
 12.952752 14.4 -0.389470
 13.075146 14.4 -0.375445
 13.195584 14.4 -0.361518
 13.314020 14.4 -0.347703
 13.430406 14.4 -0.334009
 13.544699 14.4 -0.320447
 13.656854 14.4 -0.307029
 13.766829 14.4 -0.293765
 13.874580 14.4 -0.280666
 13.980067 14.4 -0.267743
 14.083248 14.4 -0.255006
 14.184084 14.4 -0.242466

14.282535 14.4 -0.230134
 14.378565 14.4 -0.218021
 14.472136 14.4 -0.206136
 14.563212 14.4 -0.194489
 14.651757 14.4 -0.183092
 14.737738 14.4 -0.171955
 14.821121 14.4 -0.161087
 14.901875 14.4 -0.150498
 14.979968 14.4 -0.140198
 15.055370 14.4 -0.130196
 15.128052 14.4 -0.120502
 15.197986 14.4 -0.111126
 15.265145 14.4 -0.102075
 15.329504 14.4 -0.093360
 15.391036 14.4 -0.084988
 15.449719 14.4 -0.076967
 15.505531 14.4 -0.069306
 15.558448 14.4 -0.062013
 15.608452 14.4 -0.055094
 15.655523 14.4 -0.048558
 15.699642 14.4 -0.042410
 15.740793 14.4 -0.036657
 15.778959 14.4 -0.031305
 15.814127 14.4 -0.026359
 15.846282 14.4 -0.021826
 15.875413 14.4 -0.017710
 15.901507 14.4 -0.014015
 15.924555 14.4 -0.010745
 15.944548 14.4 -0.007903
 15.961478 14.4 -0.005494
 15.975339 14.4 -0.003519
 15.986125 14.4 -0.001981
 15.993832 14.4 -0.000881
 15.998458 14.4 -0.000220
 16.000000 14.4 0.000000
 25 1
 2
 12 14.4 -0.494308997
 12 24 -0.494308997
 26 1
 55
 12.000000 24 -0.494309
 12.045259 24 -0.489503
 12.179989 24 -0.475093
 12.313107 24 -0.460704
 12.444562 24 -0.446347
 12.574304 24 -0.432034
 12.702282 24 -0.417776
 12.828448 24 -0.403585
 12.952752 24 -0.389470
 13.075146 24 -0.375445
 13.195584 24 -0.361518
 13.314020 24 -0.347703
 13.430406 24 -0.334009
 13.544699 24 -0.320447
 13.656854 24 -0.307029
 13.766829 24 -0.293765
 13.874580 24 -0.280666
 13.980067 24 -0.267743
 14.083248 24 -0.255006
 14.184084 24 -0.242466
 14.282535 24 -0.230134
 14.378565 24 -0.218021
 14.472136 24 -0.206136
 14.563212 24 -0.194489
 14.651757 24 -0.183092
 14.737738 24 -0.171955
 14.821121 24 -0.161087
 14.901875 24 -0.150498
 14.979968 24 -0.140198

15.055370 24 -0.130196
 15.128052 24 -0.120502
 15.197986 24 -0.111126
 15.265145 24 -0.102075
 15.329504 24 -0.093360
 15.391036 24 -0.084988
 15.449719 24 -0.076967
 15.505531 24 -0.069306
 15.558448 24 -0.062013
 15.608452 24 -0.055094
 15.655523 24 -0.048558
 15.699642 24 -0.042410
 15.740793 24 -0.036657
 15.778959 24 -0.031305
 15.814127 24 -0.026359
 15.846282 24 -0.021826
 15.875413 24 -0.017710
 15.901507 24 -0.014015
 15.924555 24 -0.010745
 15.944548 24 -0.007903
 15.961478 24 -0.005494
 15.975339 24 -0.003519
 15.986125 24 -0.001981
 15.993832 24 -0.000881
 15.998458 24 -0.000220
 16.000000 24 0.000000
 27 1
 108
 0.000000 14.4 0.000000
 0.001542 14.4 0.027865
 0.006168 14.4 0.055494
 0.013875 14.4 0.082883
 0.024661 14.4 0.110027
 0.038522 14.4 0.136923
 0.055452 14.4 0.163563
 0.075445 14.4 0.189942
 0.098493 14.4 0.216053
 0.124587 14.4 0.241889
 0.153718 14.4 0.267440
 0.185873 14.4 0.292700
 0.221041 14.4 0.317658
 0.259207 14.4 0.342306
 0.300358 14.4 0.366632
 0.344477 14.4 0.390628
 0.391548 14.4 0.414281
 0.441552 14.4 0.437581
 0.494469 14.4 0.460516
 0.550281 14.4 0.483075
 0.608964 14.4 0.505246
 0.670496 14.4 0.527017
 0.734855 14.4 0.548375
 0.802014 14.4 0.569308
 0.871948 14.4 0.589805
 0.944630 14.4 0.609852
 1.020032 14.4 0.629438
 1.098125 14.4 0.648550
 1.178879 14.4 0.667177
 1.262262 14.4 0.685306
 1.348243 14.4 0.702927
 1.436788 14.4 0.720029
 1.527864 14.4 0.736599
 1.621435 14.4 0.752628
 1.717465 14.4 0.768107
 1.815916 14.4 0.783024
 1.916752 14.4 0.797372
 2.019933 14.4 0.811141
 2.125420 14.4 0.824323
 2.233171 14.4 0.836912
 2.343146 14.4 0.848899
 2.455301 14.4 0.860280

2.569594 14.4 0.871048
 2.685980 14.4 0.881199
 2.804416 14.4 0.890728
 2.924854 14.4 0.899632
 3.047248 14.4 0.907908
 3.171552 14.4 0.915554
 3.297718 14.4 0.922570
 3.425696 14.4 0.928953
 3.555438 14.4 0.934706
 3.686893 14.4 0.939828
 3.820011 14.4 0.944321
 3.954741 14.4 0.948188
 4.091030 14.4 0.951432
 4.228826 14.4 0.954057
 4.368076 14.4 0.956067
 4.508726 14.4 0.957468
 4.650722 14.4 0.958266
 4.794009 14.4 0.958466
 4.938533 14.4 0.958077
 5.084236 14.4 0.957106
 5.231064 14.4 0.955562
 5.378959 14.4 0.953453
 5.527864 14.4 0.950789
 5.677723 14.4 0.947580
 5.828476 14.4 0.943836
 5.980067 14.4 0.939569
 6.132437 14.4 0.934789
 6.285527 14.4 0.929508
 6.439277 14.4 0.923739
 6.593630 14.4 0.917493
 6.748524 14.4 0.910783
 6.903901 14.4 0.903623
 7.059701 14.4 0.896025
 7.215863 14.4 0.888002
 7.372327 14.4 0.879569
 7.529034 14.4 0.870739
 7.685921 14.4 0.861525
 7.842930 14.4 0.851942
 8.000000 14.4 0.842004
 8.157070 14.4 0.831724
 8.314079 14.4 0.821117
 8.470966 14.4 0.810197
 8.627673 14.4 0.798978
 8.784137 14.4 0.787473
 8.940299 14.4 0.775697
 9.096099 14.4 0.763664
 9.251476 14.4 0.751388
 9.406370 14.4 0.738882
 9.560723 14.4 0.726159
 9.714473 14.4 0.713235
 9.867563 14.4 0.700121
 10.019933 14.4 0.686832
 10.171524 14.4 0.673381
 10.322277 14.4 0.659780
 10.472136 14.4 0.646042
 10.621041 14.4 0.632181
 10.768936 14.4 0.618209
 10.915764 14.4 0.604139
 11.061467 14.4 0.589983
 11.205991 14.4 0.575753
 11.349278 14.4 0.561462
 11.491274 14.4 0.547121
 11.631924 14.4 0.532743
 11.771174 14.4 0.518340
 11.908970 14.4 0.503922
 12.000000 14.4 0.494309
 28 1
 108
 0.000000 14.4 0.000000
 0.001542 14.4 -0.027865

0.006168 14.4 -0.055494
 0.013875 14.4 -0.082883
 0.024661 14.4 -0.110027
 0.038522 14.4 -0.136923
 0.055452 14.4 -0.163563
 0.075445 14.4 -0.189942
 0.098493 14.4 -0.216053
 0.124587 14.4 -0.241889
 0.153718 14.4 -0.267440
 0.185873 14.4 -0.292700
 0.221041 14.4 -0.317658
 0.259207 14.4 -0.342306
 0.300358 14.4 -0.366632
 0.344477 14.4 -0.390628
 0.391548 14.4 -0.414281
 0.441552 14.4 -0.437581
 0.494469 14.4 -0.460516
 0.550281 14.4 -0.483075
 0.608964 14.4 -0.505246
 0.670496 14.4 -0.527017
 0.734855 14.4 -0.548375
 0.802014 14.4 -0.569308
 0.871948 14.4 -0.589805
 0.944630 14.4 -0.609852
 1.020032 14.4 -0.629438
 1.098125 14.4 -0.648550
 1.178879 14.4 -0.667177
 1.262262 14.4 -0.685306
 1.348243 14.4 -0.702927
 1.436788 14.4 -0.720029
 1.527864 14.4 -0.736599
 1.621435 14.4 -0.752628
 1.717465 14.4 -0.768107
 1.815916 14.4 -0.783024
 1.916752 14.4 -0.797372
 2.019933 14.4 -0.811141
 2.125420 14.4 -0.824323
 2.233171 14.4 -0.836912
 2.343146 14.4 -0.848899
 2.455301 14.4 -0.860280
 2.569594 14.4 -0.871048
 2.685980 14.4 -0.881199
 2.804416 14.4 -0.890728
 2.924854 14.4 -0.899632
 3.047248 14.4 -0.907908
 3.171552 14.4 -0.915554
 3.297718 14.4 -0.922570
 3.425696 14.4 -0.928953
 3.555438 14.4 -0.934706
 3.686893 14.4 -0.939828
 3.820011 14.4 -0.944321
 3.954741 14.4 -0.948188
 4.091030 14.4 -0.951432
 4.228826 14.4 -0.954057
 4.368076 14.4 -0.956067
 4.508726 14.4 -0.957468
 4.650722 14.4 -0.958266
 4.794009 14.4 -0.958466
 4.938533 14.4 -0.958077
 5.084236 14.4 -0.957106
 5.231064 14.4 -0.955562
 5.378959 14.4 -0.953453
 5.527864 14.4 -0.950789
 5.677723 14.4 -0.947580
 5.828476 14.4 -0.943836
 5.980067 14.4 -0.939569
 6.132437 14.4 -0.934789
 6.285527 14.4 -0.929508
 6.439277 14.4 -0.923739
 6.593630 14.4 -0.917493

6.748524 14.4 -0.910783
 6.903901 14.4 -0.903623
 7.059701 14.4 -0.896025
 7.215863 14.4 -0.888002
 7.372327 14.4 -0.879569
 7.529034 14.4 -0.870739
 7.685921 14.4 -0.861525
 7.842930 14.4 -0.851942
 8.000000 14.4 -0.842004
 8.157070 14.4 -0.831724
 8.314079 14.4 -0.821117
 8.470966 14.4 -0.810197
 8.627673 14.4 -0.798978
 8.784137 14.4 -0.787473
 8.940299 14.4 -0.775697
 9.096099 14.4 -0.763664
 9.251476 14.4 -0.751388
 9.406370 14.4 -0.738882
 9.560723 14.4 -0.726159
 9.714473 14.4 -0.713235
 9.867563 14.4 -0.700121
 10.019933 14.4 -0.686832
 10.171524 14.4 -0.673381
 10.322277 14.4 -0.659780
 10.472136 14.4 -0.646042
 10.621041 14.4 -0.632181
 10.768936 14.4 -0.618209
 10.915764 14.4 -0.604139
 11.061467 14.4 -0.589983
 11.205991 14.4 -0.575753
 11.349278 14.4 -0.561462
 11.491274 14.4 -0.547121
 11.631924 14.4 -0.532743
 11.771174 14.4 -0.518340
 11.908970 14.4 -0.503922
 12.000000 14.4 -0.494309
 29 1
 108
 0.000000 24 0.000000
 0.001542 24 0.027865
 0.006168 24 0.055494
 0.013875 24 0.082883
 0.024661 24 0.110027
 0.038522 24 0.136923
 0.055452 24 0.163563
 0.075445 24 0.189942
 0.098493 24 0.216053
 0.124587 24 0.241889
 0.153718 24 0.267440
 0.185873 24 0.292700
 0.221041 24 0.317658
 0.259207 24 0.342306
 0.300358 24 0.366632
 0.344477 24 0.390628
 0.391548 24 0.414281
 0.441552 24 0.437581
 0.494469 24 0.460516
 0.550281 24 0.483075
 0.608964 24 0.505246
 0.670496 24 0.527017
 0.734855 24 0.548375
 0.802014 24 0.569308
 0.871948 24 0.589805
 0.944630 24 0.609852
 1.020032 24 0.629438
 1.098125 24 0.648550
 1.178879 24 0.667177
 1.262262 24 0.685306
 1.348243 24 0.702927
 1.436788 24 0.720029

1.527864 24 0.736599
1.621435 24 0.752628
1.717465 24 0.768107
1.815916 24 0.783024
1.916752 24 0.797372
2.019933 24 0.811141
2.125420 24 0.824323
2.233171 24 0.836912
2.343146 24 0.848899
2.455301 24 0.860280
2.569594 24 0.871048
2.685980 24 0.881199
2.804416 24 0.890728
2.924854 24 0.899632
3.047248 24 0.907908
3.171552 24 0.915554
3.297718 24 0.922570
3.425696 24 0.928953
3.555438 24 0.934706
3.686893 24 0.939828
3.820011 24 0.944321
3.954741 24 0.948188
4.091030 24 0.951432
4.228826 24 0.954057
4.368076 24 0.956067
4.508726 24 0.957468
4.650722 24 0.958266
4.794009 24 0.958466
4.938533 24 0.958077
5.084236 24 0.957106
5.231064 24 0.955562
5.378959 24 0.953453
5.527864 24 0.950789
5.677723 24 0.947580
5.828476 24 0.943836
5.980067 24 0.939569
6.132437 24 0.934789
6.285527 24 0.929508
6.439277 24 0.923739
6.593630 24 0.917493
6.748524 24 0.910783
6.903901 24 0.903623
7.059701 24 0.896025
7.215863 24 0.888002
7.372327 24 0.879569
7.529034 24 0.870739
7.685921 24 0.861525
7.842930 24 0.851942
8.000000 24 0.842004
8.157070 24 0.831724
8.314079 24 0.821117
8.470966 24 0.810197
8.627673 24 0.798978
8.784137 24 0.787473
8.940299 24 0.775697
9.096099 24 0.763664
9.251476 24 0.751388
9.406370 24 0.738882
9.560723 24 0.726159
9.714473 24 0.713235
9.867563 24 0.700121
10.019933 24 0.686832
10.171524 24 0.673381
10.322277 24 0.659780
10.472136 24 0.646042
10.621041 24 0.632181
10.768936 24 0.618209
10.915764 24 0.604139
11.061467 24 0.589983
11.205991 24 0.575753

11.349278 24 0.561462
11.491274 24 0.547121
11.631924 24 0.532743
11.771174 24 0.518340
11.908970 24 0.503922
12.000000 24 0.494309
30 1
108
0.000000 24 0.000000
0.001542 24 -0.027865
0.006168 24 -0.055494
0.013875 24 -0.082883
0.024661 24 -0.110027
0.038522 24 -0.136923
0.055452 24 -0.163563
0.075445 24 -0.189942
0.098493 24 -0.216053
0.124587 24 -0.241889
0.153718 24 -0.267440
0.185873 24 -0.292700
0.221041 24 -0.317658
0.259207 24 -0.342306
0.300358 24 -0.366632
0.344477 24 -0.390628
0.391548 24 -0.414281
0.441552 24 -0.437581
0.494469 24 -0.460516
0.550281 24 -0.483075
0.608964 24 -0.505246
0.670496 24 -0.527017
0.734855 24 -0.548375
0.802014 24 -0.569308
0.871948 24 -0.589805
0.944630 24 -0.609852
1.020032 24 -0.629438
1.098125 24 -0.648550
1.178879 24 -0.667177
1.262262 24 -0.685306
1.348243 24 -0.702927
1.436788 24 -0.720029
1.527864 24 -0.736599
1.621435 24 -0.752628
1.717465 24 -0.768107
1.815916 24 -0.783024
1.916752 24 -0.797372
2.019933 24 -0.811141
2.125420 24 -0.824323
2.233171 24 -0.836912
2.343146 24 -0.848899
2.455301 24 -0.860280
2.569594 24 -0.871048
2.685980 24 -0.881199
2.804416 24 -0.890728
2.924854 24 -0.899632
3.047248 24 -0.907908
3.171552 24 -0.915554
3.297718 24 -0.922570
3.425696 24 -0.928953
3.555438 24 -0.934706
3.686893 24 -0.939828
3.820011 24 -0.944321
3.954741 24 -0.948188
4.091030 24 -0.951432
4.228826 24 -0.954057
4.368076 24 -0.956067
4.508726 24 -0.957468
4.650722 24 -0.958266
4.794009 24 -0.958466
4.938533 24 -0.958077
5.084236 24 -0.957106

5.231064 24 -0.955562
5.378959 24 -0.953453
5.527864 24 -0.950789
5.677723 24 -0.947580
5.828476 24 -0.943836
5.980067 24 -0.939569
6.132437 24 -0.934789
6.285527 24 -0.929508
6.439277 24 -0.923739
6.593630 24 -0.917493
6.748524 24 -0.910783
6.903901 24 -0.903623
7.059701 24 -0.896025
7.215863 24 -0.888002
7.372327 24 -0.879569
7.529034 24 -0.870739
7.685921 24 -0.861525
7.842930 24 -0.851942
8.000000 24 -0.842004
8.157070 24 -0.831724
8.314079 24 -0.821117
8.470966 24 -0.810197
8.627673 24 -0.798978
8.784137 24 -0.787473
8.940299 24 -0.775697
9.096099 24 -0.763664
9.251476 24 -0.751388
9.406370 24 -0.738882
9.560723 24 -0.726159
9.714473 24 -0.713235
9.867563 24 -0.700121
10.019933 24 -0.686832
10.171524 24 -0.673381
10.322277 24 -0.659780
10.472136 24 -0.646042
10.621041 24 -0.632181
10.768936 24 -0.618209
10.915764 24 -0.604139
11.061467 24 -0.589983
11.205991 24 -0.575753
11.349278 24 -0.561462
11.491274 24 -0.547121
11.631924 24 -0.532743
11.771174 24 -0.518340
11.908970 24 -0.503922
12.000000 24 -0.494309
31 1
2
0 144 0
0 24 0
32 1
2
0 24 0
0 32 0
Surface Components
1 1
2 2
-160 0 -100
160 0 -100
-160 0 100
160 0 100
2 1
2 2
160 160 100
-160 160 100
160 160 -100
-160 160 -100
3 1
2 2
-160 0 -100

160 0 -100	3.171552 0 0.915554	13.314020 0 0.347703
-160 160 -100	3.297718 0 0.922570	13.430406 0 0.334009
160 160 -100	3.425696 0 0.928953	13.544699 0 0.320447
4 1	3.555438 0 0.934706	13.656854 0 0.307029
2 2	3.686893 0 0.939828	13.766829 0 0.293765
-160 160 100	3.820011 0 0.944321	13.874580 0 0.280666
160 160 100	3.954741 0 0.948188	13.980067 0 0.267743
-160 0 100	4.091030 0 0.951432	14.083248 0 0.255006
160 0 100	4.228826 0 0.954057	14.184084 0 0.242466
5 1	4.368076 0 0.956067	14.282535 0 0.230134
2 2	4.508726 0 0.957468	14.378565 0 0.218021
-160 160 -100	4.650722 0 0.958266	14.472136 0 0.206136
-160 160 100	4.794009 0 0.958466	14.563212 0 0.194489
-160 0 -100	4.938533 0 0.958077	14.651757 0 0.183092
-160 0 100	5.084236 0 0.957106	14.737738 0 0.171955
6 1	5.231064 0 0.955562	14.821121 0 0.161087
2 2	5.378959 0 0.953453	14.901875 0 0.150498
160 0 -100	5.527864 0 0.950789	14.979968 0 0.140198
160 0 100	5.677723 0 0.947580	15.055370 0 0.130196
160 160 -100	5.828476 0 0.943836	15.128052 0 0.120502
160 160 100	5.980067 0 0.939569	15.197986 0 0.111126
7 1	6.132437 0 0.934789	15.265145 0 0.102075
161 2	6.285527 0 0.929508	15.329504 0 0.093360
0.000000 0 0.000000	6.439277 0 0.923739	15.391036 0 0.084988
0.001542 0 0.027865	6.593630 0 0.917493	15.449719 0 0.076967
0.006168 0 0.055494	6.748524 0 0.910783	15.505531 0 0.069306
0.013875 0 0.082883	6.903901 0 0.903623	15.558448 0 0.062013
0.024661 0 0.110027	7.059701 0 0.896025	15.608452 0 0.055094
0.038522 0 0.136923	7.215863 0 0.888002	15.655523 0 0.048558
0.055452 0 0.163563	7.372327 0 0.879569	15.699642 0 0.042410
0.075445 0 0.189942	7.529034 0 0.870739	15.740793 0 0.036657
0.098493 0 0.216053	7.685921 0 0.861525	15.778959 0 0.031305
0.124587 0 0.241889	7.842930 0 0.851942	15.814127 0 0.026359
0.153718 0 0.267440	8.000000 0 0.842004	15.846282 0 0.021826
0.185873 0 0.292700	8.157070 0 0.831724	15.875413 0 0.017710
0.221041 0 0.317658	8.314079 0 0.821117	15.901507 0 0.014015
0.259207 0 0.342306	8.470966 0 0.810197	15.924555 0 0.010745
0.300358 0 0.366632	8.627673 0 0.798978	15.944548 0 0.007903
0.344477 0 0.390628	8.784137 0 0.787473	15.961478 0 0.005494
0.391548 0 0.414281	8.940299 0 0.775697	15.975339 0 0.003519
0.441552 0 0.437581	9.096099 0 0.763664	15.986125 0 0.001981
0.494469 0 0.460516	9.251476 0 0.751388	15.993832 0 0.000881
0.550281 0 0.483075	9.406370 0 0.738882	15.998458 0 0.000220
0.608964 0 0.505246	9.560723 0 0.726159	16.000000 0 0.000000
0.670496 0 0.527017	9.714473 0 0.713235	0.000000 14.4 0.000000
0.734855 0 0.548375	9.867563 0 0.700121	0.001542 14.4 0.027865
0.802014 0 0.569308	10.019933 0 0.686832	0.006168 14.4 0.055494
0.871948 0 0.589805	10.171524 0 0.673381	0.013875 14.4 0.082883
0.944630 0 0.609852	10.322277 0 0.659780	0.024661 14.4 0.110027
1.020032 0 0.629438	10.472136 0 0.646042	0.038522 14.4 0.136923
1.098125 0 0.648550	10.621041 0 0.632181	0.055452 14.4 0.163563
1.178879 0 0.667177	10.768936 0 0.618209	0.075445 14.4 0.189942
1.262262 0 0.685306	10.915764 0 0.604139	0.098493 14.4 0.216053
1.348243 0 0.702927	11.061467 0 0.589983	0.124587 14.4 0.241889
1.436788 0 0.720029	11.205991 0 0.575753	0.153718 14.4 0.267440
1.527864 0 0.736599	11.349278 0 0.561462	0.185873 14.4 0.292700
1.621435 0 0.752628	11.491274 0 0.547121	0.221041 14.4 0.317658
1.717465 0 0.768107	11.631924 0 0.532743	0.259207 14.4 0.342306
1.815916 0 0.783024	11.771174 0 0.518340	0.300358 14.4 0.366632
1.916752 0 0.797372	11.908970 0 0.503922	0.344477 14.4 0.390628
2.019933 0 0.811141	12.045259 0 0.489503	0.391548 14.4 0.414281
2.125420 0 0.824323	12.179989 0 0.475093	0.441552 14.4 0.437581
2.233171 0 0.836912	12.313107 0 0.460704	0.494469 14.4 0.460516
2.343146 0 0.848899	12.444562 0 0.446347	0.550281 14.4 0.483075
2.455301 0 0.860280	12.574304 0 0.432034	0.608964 14.4 0.505246
2.569594 0 0.871048	12.702282 0 0.417776	0.670496 14.4 0.527017
2.685980 0 0.881199	12.828448 0 0.403585	0.734855 14.4 0.548375
2.804416 0 0.890728	12.952752 0 0.389470	0.802014 14.4 0.569308
2.924854 0 0.899632	13.075146 0 0.375445	0.871948 14.4 0.589805
3.047248 0 0.907908	13.195584 0 0.361518	0.944630 14.4 0.609852

1.020032 14.4 0.629438
1.098125 14.4 0.648550
1.178879 14.4 0.667177
1.262262 14.4 0.685306
1.348243 14.4 0.702927
1.436788 14.4 0.720029
1.527864 14.4 0.736599
1.621435 14.4 0.752628
1.717465 14.4 0.768107
1.815916 14.4 0.783024
1.916752 14.4 0.797372
2.019933 14.4 0.811141
2.125420 14.4 0.824323
2.233171 14.4 0.836912
2.343146 14.4 0.848899
2.455301 14.4 0.860280
2.569594 14.4 0.871048
2.685980 14.4 0.881199
2.804416 14.4 0.890728
2.924854 14.4 0.899632
3.047248 14.4 0.907908
3.171552 14.4 0.915554
3.297718 14.4 0.922570
3.425696 14.4 0.928953
3.555438 14.4 0.934706
3.686893 14.4 0.939828
3.820011 14.4 0.944321
3.954741 14.4 0.948188
4.091030 14.4 0.951432
4.228826 14.4 0.954057
4.368076 14.4 0.956067
4.508726 14.4 0.957468
4.650722 14.4 0.958266
4.794009 14.4 0.958466
4.938533 14.4 0.958077
5.084236 14.4 0.957106
5.231064 14.4 0.955562
5.378959 14.4 0.953453
5.527864 14.4 0.950789
5.677723 14.4 0.947580
5.828476 14.4 0.943836
5.980067 14.4 0.939569
6.132437 14.4 0.934789
6.285527 14.4 0.929508
6.439277 14.4 0.923739
6.593630 14.4 0.917493
6.748524 14.4 0.910783
6.903901 14.4 0.903623
7.059701 14.4 0.896025
7.215863 14.4 0.888002
7.372327 14.4 0.879569
7.529034 14.4 0.870739
7.685921 14.4 0.861525
7.842930 14.4 0.851942
8.000000 14.4 0.842004
8.157070 14.4 0.831724
8.314079 14.4 0.821117
8.470966 14.4 0.810197
8.627673 14.4 0.798978
8.784137 14.4 0.787473
8.940299 14.4 0.775697
9.096099 14.4 0.763664
9.251476 14.4 0.751388
9.406370 14.4 0.738882
9.560723 14.4 0.726159
9.714473 14.4 0.713235
9.867563 14.4 0.700121
10.019933 14.4 0.686832
10.171524 14.4 0.673381
10.322277 14.4 0.659780

10.472136 14.4 0.646042
10.621041 14.4 0.632181
10.768936 14.4 0.618209
10.915764 14.4 0.604139
11.061467 14.4 0.589983
11.205991 14.4 0.575753
11.349278 14.4 0.561462
11.491274 14.4 0.547121
11.631924 14.4 0.532743
11.771174 14.4 0.518340
11.908970 14.4 0.503922
12.045259 14.4 0.489503
12.179989 14.4 0.475093
12.313107 14.4 0.460704
12.444562 14.4 0.446347
12.574304 14.4 0.432034
12.702282 14.4 0.417776
12.828448 14.4 0.403585
12.952752 14.4 0.389470
13.075146 14.4 0.375445
13.195584 14.4 0.361518
13.314020 14.4 0.347703
13.430406 14.4 0.334009
13.544699 14.4 0.320447
13.656854 14.4 0.307029
13.766829 14.4 0.293765
13.874580 14.4 0.280666
13.980067 14.4 0.267743
14.083248 14.4 0.255006
14.184084 14.4 0.242466
14.282535 14.4 0.230134
14.378565 14.4 0.218021
14.472136 14.4 0.206136
14.563212 14.4 0.194489
14.651757 14.4 0.183092
14.737738 14.4 0.171955
14.821121 14.4 0.161087
14.901875 14.4 0.150498
14.979968 14.4 0.140198
15.055370 14.4 0.130196
15.128052 14.4 0.120502
15.197986 14.4 0.111126
15.265145 14.4 0.102075
15.329504 14.4 0.093360
15.391036 14.4 0.084988
15.449719 14.4 0.076967
15.505531 14.4 0.069306
15.558448 14.4 0.062013
15.608452 14.4 0.055094
15.655523 14.4 0.048558
15.699642 14.4 0.042410
15.740793 14.4 0.036657
15.778959 14.4 0.031305
15.814127 14.4 0.026359
15.846282 14.4 0.021826
15.875413 14.4 0.017710
15.901507 14.4 0.014015
15.924555 14.4 0.010745
15.944548 14.4 0.007903
15.961478 14.4 0.005494
15.975339 14.4 0.003519
15.986125 14.4 0.001981
15.993832 14.4 0.000881
15.998458 14.4 0.000220
16.000000 14.4 0.000000
8 1
161 2
0.000000 14.4 0.000000
0.001542 14.4 -0.027865
0.006168 14.4 -0.055494

0.013875 14.4 -0.082883
0.024661 14.4 -0.110027
0.038522 14.4 -0.136923
0.055452 14.4 -0.163563
0.075445 14.4 -0.189942
0.098493 14.4 -0.216053
0.124587 14.4 -0.241889
0.153718 14.4 -0.267440
0.185873 14.4 -0.292700
0.221041 14.4 -0.317658
0.259207 14.4 -0.342306
0.300358 14.4 -0.366632
0.344477 14.4 -0.390628
0.391548 14.4 -0.414281
0.441552 14.4 -0.437581
0.494469 14.4 -0.460516
0.550281 14.4 -0.483075
0.608964 14.4 -0.505246
0.670496 14.4 -0.527017
0.734855 14.4 -0.548375
0.802014 14.4 -0.569308
0.871948 14.4 -0.589805
0.944630 14.4 -0.609852
1.020032 14.4 -0.629438
1.098125 14.4 -0.648550
1.178879 14.4 -0.667177
1.262262 14.4 -0.685306
1.348243 14.4 -0.702927
1.436788 14.4 -0.720029
1.527864 14.4 -0.736599
1.621435 14.4 -0.752628
1.717465 14.4 -0.768107
1.815916 14.4 -0.783024
1.916752 14.4 -0.797372
2.019933 14.4 -0.811141
2.125420 14.4 -0.824323
2.233171 14.4 -0.836912
2.343146 14.4 -0.848899
2.455301 14.4 -0.860280
2.569594 14.4 -0.871048
2.685980 14.4 -0.881199
2.804416 14.4 -0.890728
2.924854 14.4 -0.899632
3.047248 14.4 -0.907908
3.171552 14.4 -0.915554
3.297718 14.4 -0.922570
3.425696 14.4 -0.928953
3.555438 14.4 -0.934706
3.686893 14.4 -0.939828
3.820011 14.4 -0.944321
3.954741 14.4 -0.948188
4.091030 14.4 -0.951432
4.228826 14.4 -0.954057
4.368076 14.4 -0.956067
4.508726 14.4 -0.957468
4.650722 14.4 -0.958266
4.794009 14.4 -0.958466
4.938533 14.4 -0.958077
5.084236 14.4 -0.957106
5.231064 14.4 -0.955562
5.378959 14.4 -0.953453
5.527864 14.4 -0.950789
5.677723 14.4 -0.947580
5.828476 14.4 -0.943836
5.980067 14.4 -0.939569
6.132437 14.4 -0.934789
6.285527 14.4 -0.929508
6.439277 14.4 -0.923739
6.593630 14.4 -0.917493
6.748524 14.4 -0.910783

13.874580 0 -0.280666
 13.980067 0 -0.267743
 14.083248 0 -0.255006
 14.184084 0 -0.242466
 14.282535 0 -0.230134
 14.378565 0 -0.218021
 14.472136 0 -0.206136
 14.563212 0 -0.194489
 14.651757 0 -0.183092
 14.737738 0 -0.171955
 14.821121 0 -0.161087
 14.901875 0 -0.150498
 14.979968 0 -0.140198
 15.055370 0 -0.130196
 15.128052 0 -0.120502
 15.197986 0 -0.111126
 15.265145 0 -0.102075
 15.329504 0 -0.093360
 15.391036 0 -0.084988
 15.449719 0 -0.076967
 15.505531 0 -0.069306
 15.558448 0 -0.062013
 15.608452 0 -0.055094
 15.655523 0 -0.048558
 15.699642 0 -0.042410
 15.740793 0 -0.036657
 15.778959 0 -0.031305
 15.814127 0 -0.026359
 15.846282 0 -0.021826
 15.875413 0 -0.017710
 15.901507 0 -0.014015
 15.924555 0 -0.010745
 15.944548 0 -0.007903
 15.961478 0 -0.005494
 15.975339 0 -0.003519
 15.986125 0 -0.001981
 15.993832 0 -0.000881
 15.998458 0 -0.000220
 16.000000 0 0.000000
 9 1
 108 2
 0.000000 144 0.000000
 0.001542 144 0.027865
 0.006168 144 0.055494
 0.013875 144 0.082883
 0.024661 144 0.110027
 0.038522 144 0.136923
 0.055452 144 0.163563
 0.075445 144 0.189942
 0.098493 144 0.216053
 0.124587 144 0.241889
 0.153718 144 0.267440
 0.185873 144 0.292700
 0.221041 144 0.317658
 0.259207 144 0.342306
 0.300358 144 0.366632
 0.344477 144 0.390628
 0.391548 144 0.414281
 0.441552 144 0.437581
 0.494469 144 0.460516
 0.550281 144 0.483075
 0.608964 144 0.505246
 0.670496 144 0.527017
 0.734855 144 0.548375
 0.802014 144 0.569308
 0.871948 144 0.589805
 0.944630 144 0.609852
 1.020032 144 0.629438
 1.098125 144 0.648550
 1.178879 144 0.667177

1.262262 144 0.685306
 1.348243 144 0.702927
 1.436788 144 0.720029
 1.527864 144 0.736599
 1.621435 144 0.752628
 1.717465 144 0.768107
 1.815916 144 0.783024
 1.916752 144 0.797372
 2.019933 144 0.811141
 2.125420 144 0.824323
 2.233171 144 0.836912
 2.343146 144 0.848899
 2.455301 144 0.860280
 2.569594 144 0.871048
 2.685980 144 0.881199
 2.804416 144 0.890728
 2.924854 144 0.899632
 3.047248 144 0.907908
 3.171552 144 0.915554
 3.297718 144 0.922570
 3.425696 144 0.928953
 3.555438 144 0.934706
 3.686893 144 0.939828
 3.820011 144 0.944321
 3.954741 144 0.948188
 4.091030 144 0.951432
 4.228826 144 0.954057
 4.368076 144 0.956067
 4.508726 144 0.957468
 4.650722 144 0.958266
 4.794009 144 0.958466
 4.938533 144 0.958077
 5.084236 144 0.957106
 5.231064 144 0.955562
 5.378959 144 0.953453
 5.527864 144 0.950789
 5.677723 144 0.947580
 5.828476 144 0.943836
 5.980067 144 0.939569
 6.132437 144 0.934789
 6.285527 144 0.929508
 6.439277 144 0.923739
 6.593630 144 0.917493
 6.748524 144 0.910783
 6.903901 144 0.903623
 7.059701 144 0.896025
 7.215863 144 0.888002
 7.372327 144 0.879569
 7.529034 144 0.870739
 7.685921 144 0.861525
 7.842930 144 0.851942
 8.000000 144 0.842004
 8.157070 144 0.831724
 8.314079 144 0.821117
 8.470966 144 0.810197
 8.627673 144 0.798978
 8.784137 144 0.787473
 8.940299 144 0.775697
 9.096099 144 0.763664
 9.251476 144 0.751388
 9.406370 144 0.738882
 9.560723 144 0.726159
 9.714473 144 0.713235
 9.867563 144 0.700121
 10.019933 144 0.686832
 10.171524 144 0.673381
 10.322277 144 0.659780
 10.472136 144 0.646042
 10.621041 144 0.632181
 10.768936 144 0.618209

10.915764 144 0.604139
 11.061467 144 0.589983
 11.205991 144 0.575753
 11.349278 144 0.561462
 11.491274 144 0.547121
 11.631924 144 0.532743
 11.771174 144 0.518340
 11.908970 144 0.503922
 12.000000 144 0.494309
 0.000000 24 0.000000
 0.001542 24 0.027865
 0.006168 24 0.055494
 0.013875 24 0.082883
 0.024661 24 0.110027
 0.038522 24 0.136923
 0.055452 24 0.163563
 0.075445 24 0.189942
 0.098493 24 0.216053
 0.124587 24 0.241889
 0.153718 24 0.267440
 0.185873 24 0.292700
 0.221041 24 0.317658
 0.259207 24 0.342306
 0.300358 24 0.366632
 0.344477 24 0.390628
 0.391548 24 0.414281
 0.441552 24 0.437581
 0.494469 24 0.460516
 0.550281 24 0.483075
 0.608964 24 0.505246
 0.670496 24 0.527017
 0.734855 24 0.548375
 0.802014 24 0.569308
 0.871948 24 0.589805
 0.944630 24 0.609852
 1.020032 24 0.629438
 1.098125 24 0.648550
 1.178879 24 0.667177
 1.262262 24 0.685306
 1.348243 24 0.702927
 1.436788 24 0.720029
 1.527864 24 0.736599
 1.621435 24 0.752628
 1.717465 24 0.768107
 1.815916 24 0.783024
 1.916752 24 0.797372
 2.019933 24 0.811141
 2.125420 24 0.824323
 2.233171 24 0.836912
 2.343146 24 0.848899
 2.455301 24 0.860280
 2.569594 24 0.871048
 2.685980 24 0.881199
 2.804416 24 0.890728
 2.924854 24 0.899632
 3.047248 24 0.907908
 3.171552 24 0.915554
 3.297718 24 0.922570
 3.425696 24 0.928953
 3.555438 24 0.934706
 3.686893 24 0.939828
 3.820011 24 0.944321
 3.954741 24 0.948188
 4.091030 24 0.951432
 4.228826 24 0.954057
 4.368076 24 0.956067
 4.508726 24 0.957468
 4.650722 24 0.958266
 4.794009 24 0.958466
 4.938533 24 0.958077

5.084236 24 0.957106
 5.231064 24 0.955562
 5.378959 24 0.953453
 5.527864 24 0.950789
 5.677723 24 0.947580
 5.828476 24 0.943836
 5.980067 24 0.939569
 6.132437 24 0.934789
 6.285527 24 0.929508
 6.439277 24 0.923739
 6.593630 24 0.917493
 6.748524 24 0.910783
 6.903901 24 0.903623
 7.059701 24 0.896025
 7.215863 24 0.888002
 7.372327 24 0.879569
 7.529034 24 0.870739
 7.685921 24 0.861525
 7.842930 24 0.851942
 8.000000 24 0.842004
 8.157070 24 0.831724
 8.314079 24 0.821117
 8.470966 24 0.810197
 8.627673 24 0.798978
 8.784137 24 0.787473
 8.940299 24 0.775697
 9.096099 24 0.763664
 9.251476 24 0.751388
 9.406370 24 0.738882
 9.560723 24 0.726159
 9.714473 24 0.713235
 9.867563 24 0.700121
 10.019933 24 0.686832
 10.171524 24 0.673381
 10.322277 24 0.659780
 10.472136 24 0.646042
 10.621041 24 0.632181
 10.768936 24 0.618209
 10.915764 24 0.604139
 11.061467 24 0.589983
 11.205991 24 0.575753
 11.349278 24 0.561462
 11.491274 24 0.547121
 11.631924 24 0.532743
 11.771174 24 0.518340
 11.908970 24 0.503922
 12.000000 24 0.494309
 10 1
 108 2
 0.000000 24 0.000000
 0.001542 24 -0.027865
 0.006168 24 -0.055494
 0.013875 24 -0.082883
 0.024661 24 -0.110027
 0.038522 24 -0.136923
 0.055452 24 -0.163563
 0.075445 24 -0.189942
 0.098493 24 -0.216053
 0.124587 24 -0.241889
 0.153718 24 -0.267440
 0.185873 24 -0.292700
 0.221041 24 -0.317658
 0.259207 24 -0.342306
 0.300358 24 -0.366632
 0.344477 24 -0.390628
 0.391548 24 -0.414281
 0.441552 24 -0.437581
 0.494469 24 -0.460516
 0.550281 24 -0.483075
 0.608964 24 -0.505246

0.670496 24 -0.527017
 0.734855 24 -0.548375
 0.802014 24 -0.569308
 0.871948 24 -0.589805
 0.944630 24 -0.609852
 1.020032 24 -0.629438
 1.098125 24 -0.648550
 1.178879 24 -0.667177
 1.262262 24 -0.685306
 1.348243 24 -0.702927
 1.436788 24 -0.720029
 1.527864 24 -0.736599
 1.621435 24 -0.752628
 1.717465 24 -0.768107
 1.815916 24 -0.783024
 1.916752 24 -0.797372
 2.019933 24 -0.811141
 2.125420 24 -0.824323
 2.233171 24 -0.836912
 2.343146 24 -0.848899
 2.455301 24 -0.860280
 2.569594 24 -0.871048
 2.685980 24 -0.881199
 2.804416 24 -0.890728
 2.924854 24 -0.899632
 3.047248 24 -0.907908
 3.171552 24 -0.915554
 3.297718 24 -0.922570
 3.425696 24 -0.928953
 3.555438 24 -0.934706
 3.686893 24 -0.939828
 3.820011 24 -0.944321
 3.954741 24 -0.948188
 4.091030 24 -0.951432
 4.228826 24 -0.954057
 4.368076 24 -0.956067
 4.508726 24 -0.957468
 4.650722 24 -0.958266
 4.794009 24 -0.958466
 4.938533 24 -0.958077
 5.084236 24 -0.957106
 5.231064 24 -0.955562
 5.378959 24 -0.953453
 5.527864 24 -0.950789
 5.677723 24 -0.947580
 5.828476 24 -0.943836
 5.980067 24 -0.939569
 6.132437 24 -0.934789
 6.285527 24 -0.929508
 6.439277 24 -0.923739
 6.593630 24 -0.917493
 6.748524 24 -0.910783
 6.903901 24 -0.903623
 7.059701 24 -0.896025
 7.215863 24 -0.888002
 7.372327 24 -0.879569
 7.529034 24 -0.870739
 7.685921 24 -0.861525
 7.842930 24 -0.851942
 8.000000 24 -0.842004
 8.157070 24 -0.831724
 8.314079 24 -0.821117
 8.470966 24 -0.810197
 8.627673 24 -0.798978
 8.784137 24 -0.787473
 8.940299 24 -0.775697
 9.096099 24 -0.763664
 9.251476 24 -0.751388
 9.406370 24 -0.738882
 9.560723 24 -0.726159

9.714473 24 -0.713235
 9.867563 24 -0.700121
 10.019933 24 -0.686832
 10.171524 24 -0.673381
 10.322277 24 -0.659780
 10.472136 24 -0.646042
 10.621041 24 -0.632181
 10.768936 24 -0.618209
 10.915764 24 -0.604139
 11.061467 24 -0.589983
 11.205991 24 -0.575753
 11.349278 24 -0.561462
 11.491274 24 -0.547121
 11.631924 24 -0.532743
 11.771174 24 -0.518340
 11.908970 24 -0.503922
 12.000000 24 -0.494309
 0.000000 14.4 0.000000
 0.001542 14.4 -0.027865
 0.006168 14.4 -0.055494
 0.013875 14.4 -0.082883
 0.024661 14.4 -0.110027
 0.038522 14.4 -0.136923
 0.055452 14.4 -0.163563
 0.075445 14.4 -0.189942
 0.098493 14.4 -0.216053
 0.124587 14.4 -0.241889
 0.153718 14.4 -0.267440
 0.185873 14.4 -0.292700
 0.221041 14.4 -0.317658
 0.259207 14.4 -0.342306
 0.300358 14.4 -0.366632
 0.344477 14.4 -0.390628
 0.391548 14.4 -0.414281
 0.441552 14.4 -0.437581
 0.494469 14.4 -0.460516
 0.550281 14.4 -0.483075
 0.608964 14.4 -0.505246
 0.670496 14.4 -0.527017
 0.734855 14.4 -0.548375
 0.802014 14.4 -0.569308
 0.871948 14.4 -0.589805
 0.944630 14.4 -0.609852
 1.020032 14.4 -0.629438
 1.098125 14.4 -0.648550
 1.178879 14.4 -0.667177
 1.262262 14.4 -0.685306
 1.348243 14.4 -0.702927
 1.436788 14.4 -0.720029
 1.527864 14.4 -0.736599
 1.621435 14.4 -0.752628
 1.717465 14.4 -0.768107
 1.815916 14.4 -0.783024
 1.916752 14.4 -0.797372
 2.019933 14.4 -0.811141
 2.125420 14.4 -0.824323
 2.233171 14.4 -0.836912
 2.343146 14.4 -0.848899
 2.455301 14.4 -0.860280
 2.569594 14.4 -0.871048
 2.685980 14.4 -0.881199
 2.804416 14.4 -0.890728
 2.924854 14.4 -0.899632
 3.047248 14.4 -0.907908
 3.171552 14.4 -0.915554
 3.297718 14.4 -0.922570
 3.425696 14.4 -0.928953
 3.555438 14.4 -0.934706
 3.686893 14.4 -0.939828
 3.820011 14.4 -0.944321

3.954741 14.4 -0.948188
 4.091030 14.4 -0.951432
 4.228826 14.4 -0.954057
 4.368076 14.4 -0.956067
 4.508726 14.4 -0.957468
 4.650722 14.4 -0.958266
 4.794009 14.4 -0.958466
 4.938533 14.4 -0.958077
 5.084236 14.4 -0.957106
 5.231064 14.4 -0.955562
 5.378959 14.4 -0.953453
 5.527864 14.4 -0.950789
 5.677723 14.4 -0.947580
 5.828476 14.4 -0.943836
 5.980067 14.4 -0.939569
 6.132437 14.4 -0.934789
 6.285527 14.4 -0.929508
 6.439277 14.4 -0.923739
 6.593630 14.4 -0.917493
 6.748524 14.4 -0.910783
 6.903901 14.4 -0.903623
 7.059701 14.4 -0.896025
 7.215863 14.4 -0.888002
 7.372327 14.4 -0.879569
 7.529034 14.4 -0.870739
 7.685921 14.4 -0.861525
 7.842930 14.4 -0.851942
 8.000000 14.4 -0.842004
 8.157070 14.4 -0.831724
 8.314079 14.4 -0.821117
 8.470966 14.4 -0.810197
 8.627673 14.4 -0.798978
 8.784137 14.4 -0.787473
 8.940299 14.4 -0.775697
 9.096099 14.4 -0.763664
 9.251476 14.4 -0.751388
 9.406370 14.4 -0.738882
 9.560723 14.4 -0.726159
 9.714473 14.4 -0.713235
 9.867563 14.4 -0.700121
 10.019933 14.4 -0.686832
 10.171524 14.4 -0.673381
 10.322277 14.4 -0.659780
 10.472136 14.4 -0.646042
 10.621041 14.4 -0.632181
 10.768936 14.4 -0.618209
 10.915764 14.4 -0.604139
 11.061467 14.4 -0.589983
 11.205991 14.4 -0.575753
 11.349278 14.4 -0.561462
 11.491274 14.4 -0.547121
 11.631924 14.4 -0.532743
 11.771174 14.4 -0.518340
 11.908970 14.4 -0.503922
 12.000000 14.4 -0.494309
 11 1
 161 2
 0.000000 24 0.000000
 0.001542 24 0.027865
 0.006168 24 0.055494
 0.013875 24 0.082883
 0.024661 24 0.110027
 0.038522 24 0.136923
 0.055452 24 0.163563
 0.075445 24 0.189942
 0.098493 24 0.216053
 0.124587 24 0.241889
 0.153718 24 0.267440
 0.185873 24 0.292700
 0.221041 24 0.317658

0.259207 24 0.342306
 0.300358 24 0.366632
 0.344477 24 0.390628
 0.391548 24 0.414281
 0.441552 24 0.437581
 0.494469 24 0.460516
 0.550281 24 0.483075
 0.608964 24 0.505246
 0.670496 24 0.527017
 0.734855 24 0.548375
 0.802014 24 0.569308
 0.871948 24 0.589805
 0.944630 24 0.609852
 1.020032 24 0.629438
 1.098125 24 0.648550
 1.178879 24 0.667177
 1.262262 24 0.685306
 1.348243 24 0.702927
 1.436788 24 0.720029
 1.527864 24 0.736599
 1.621435 24 0.752628
 1.717465 24 0.768107
 1.815916 24 0.783024
 1.916752 24 0.797372
 2.019933 24 0.811141
 2.125420 24 0.824323
 2.233171 24 0.836912
 2.343146 24 0.848899
 2.455301 24 0.860280
 2.569594 24 0.871048
 2.685980 24 0.881199
 2.804416 24 0.890728
 2.924854 24 0.899632
 3.047248 24 0.907908
 3.171552 24 0.915554
 3.297718 24 0.922570
 3.425696 24 0.928953
 3.555438 24 0.934706
 3.686893 24 0.939828
 3.820011 24 0.944321
 3.954741 24 0.948188
 4.091030 24 0.951432
 4.228826 24 0.954057
 4.368076 24 0.956067
 4.508726 24 0.957468
 4.650722 24 0.958266
 4.794009 24 0.958466
 4.938533 24 0.958077
 5.084236 24 0.957106
 5.231064 24 0.955562
 5.378959 24 0.953453
 5.527864 24 0.950789
 5.677723 24 0.947580
 5.828476 24 0.943836
 5.980067 24 0.939569
 6.132437 24 0.934789
 6.285527 24 0.929508
 6.439277 24 0.923739
 6.593630 24 0.917493
 6.748524 24 0.910783
 6.903901 24 0.903623
 7.059701 24 0.896025
 7.215863 24 0.888002
 7.372327 24 0.879569
 7.529034 24 0.870739
 7.685921 24 0.861525
 7.842930 24 0.851942
 8.000000 24 0.842004
 8.157070 24 0.831724
 8.314079 24 0.821117

8.470966 24 0.810197
 8.627673 24 0.798978
 8.784137 24 0.787473
 8.940299 24 0.775697
 9.096099 24 0.763664
 9.251476 24 0.751388
 9.406370 24 0.738882
 9.560723 24 0.726159
 9.714473 24 0.713235
 9.867563 24 0.700121
 10.019933 24 0.686832
 10.171524 24 0.673381
 10.322277 24 0.659780
 10.472136 24 0.646042
 10.621041 24 0.632181
 10.768936 24 0.618209
 10.915764 24 0.604139
 11.061467 24 0.589983
 11.205991 24 0.575753
 11.349278 24 0.561462
 11.491274 24 0.547121
 11.631924 24 0.532743
 11.771174 24 0.518340
 11.908970 24 0.503922
 12.045259 24 0.489503
 12.179989 24 0.475093
 12.313107 24 0.460704
 12.444562 24 0.446347
 12.574304 24 0.432034
 12.702282 24 0.417776
 12.828448 24 0.403585
 12.952752 24 0.389470
 13.075146 24 0.375445
 13.195584 24 0.361518
 13.314020 24 0.347703
 13.430406 24 0.334009
 13.544699 24 0.320447
 13.656854 24 0.307029
 13.766829 24 0.293765
 13.874580 24 0.280666
 13.980067 24 0.267743
 14.083248 24 0.255006
 14.184084 24 0.242466
 14.282535 24 0.230134
 14.378565 24 0.218021
 14.472136 24 0.206136
 14.563212 24 0.194489
 14.651757 24 0.183092
 14.737738 24 0.171955
 14.821121 24 0.161087
 14.901875 24 0.150498
 14.979968 24 0.140198
 15.055370 24 0.130196
 15.128052 24 0.120502
 15.197986 24 0.111126
 15.265145 24 0.102075
 15.329504 24 0.093360
 15.391036 24 0.084988
 15.449719 24 0.076967
 15.505531 24 0.069306
 15.558448 24 0.062013
 15.608452 24 0.055094
 15.655523 24 0.048558
 15.699642 24 0.042410
 15.740793 24 0.036657
 15.778959 24 0.031305
 15.814127 24 0.026359
 15.846282 24 0.021826
 15.875413 24 0.017710
 15.901507 24 0.014015

15924555 24 0.010745
15944548 24 0.007903
15961478 24 0.005494
15975339 24 0.003519
15986125 24 0.001981
15993832 24 0.000881
15998458 24 0.000220
16.000000 24 0.000000
0.000000 32 0.000000
0.001542 32 0.027865
0.006168 32 0.055494
0.013875 32 0.082883
0.024661 32 0.110027
0.038522 32 0.136923
0.055452 32 0.163563
0.075445 32 0.189942
0.098493 32 0.216053
0.124587 32 0.241889
0.153718 32 0.267440
0.185873 32 0.292700
0.221041 32 0.317658
0.259207 32 0.342306
0.300358 32 0.366632
0.344477 32 0.390628
0.391548 32 0.414281
0.441552 32 0.437581
0.494469 32 0.460516
0.550281 32 0.483075
0.608964 32 0.505246
0.670496 32 0.527017
0.734855 32 0.548375
0.802014 32 0.569308
0.871948 32 0.589805
0.944630 32 0.609852
1.020032 32 0.629438
1.098125 32 0.648550
1.178879 32 0.667177
1.262262 32 0.685306
1.348243 32 0.702927
1.436788 32 0.720029
1.527864 32 0.736599
1.621435 32 0.752628
1.717465 32 0.768107
1.815916 32 0.783024
1.916752 32 0.797372
2.019933 32 0.811141
2.125420 32 0.824323
2.233171 32 0.836912
2.343146 32 0.848899
2.455301 32 0.860280
2.569594 32 0.871048
2.685980 32 0.881199
2.804416 32 0.890728
2.924854 32 0.899632
3.047248 32 0.907908
3.171552 32 0.915554
3.297718 32 0.922570
3.425696 32 0.928953
3.555438 32 0.934706
3.686893 32 0.939828
3.820011 32 0.944321
3.954741 32 0.948188
4.091030 32 0.951432
4.228826 32 0.954057
4.368076 32 0.956067
4.508726 32 0.957468
4.650722 32 0.958266
4.794009 32 0.958466
4.938533 32 0.958077
5.084236 32 0.957106

5.231064 32 0.955562
5.378959 32 0.953453
5.527864 32 0.950789
5.677723 32 0.947580
5.828476 32 0.943836
5.980067 32 0.939569
6.132437 32 0.934789
6.285527 32 0.929508
6.439277 32 0.923739
6.593630 32 0.917493
6.748524 32 0.910783
6.903901 32 0.903623
7.059701 32 0.896025
7.215863 32 0.888002
7.372327 32 0.879569
7.529034 32 0.870739
7.685921 32 0.861525
7.842930 32 0.851942
8.000000 32 0.842004
8.157070 32 0.831724
8.314079 32 0.821117
8.470966 32 0.810197
8.627673 32 0.798978
8.784137 32 0.787473
8.940299 32 0.775697
9.096099 32 0.763664
9.251476 32 0.751388
9.406370 32 0.738882
9.560723 32 0.726159
9.714473 32 0.713235
9.867563 32 0.700121
10.019933 32 0.686832
10.171524 32 0.673381
10.322277 32 0.659780
10.472136 32 0.646042
10.621041 32 0.632181
10.768936 32 0.618209
10.915764 32 0.604139
11.061467 32 0.589983
11.205991 32 0.575753
11.349278 32 0.561462
11.491274 32 0.547121
11.631924 32 0.532743
11.771174 32 0.518340
11.908970 32 0.503922
12.045259 32 0.489503
12.179989 32 0.475093
12.313107 32 0.460704
12.444562 32 0.446347
12.574304 32 0.432034
12.702282 32 0.417776
12.828448 32 0.403585
12.952752 32 0.389470
13.075146 32 0.375445
13.195584 32 0.361518
13.314020 32 0.347703
13.430406 32 0.334009
13.544699 32 0.320447
13.656854 32 0.307029
13.766829 32 0.293765
13.874580 32 0.280666
13.980067 32 0.267743
14.083248 32 0.255006
14.184084 32 0.242466
14.282535 32 0.230134
14.378565 32 0.218021
14.472136 32 0.206136
14.563212 32 0.194489
14.651757 32 0.183092
14.737738 32 0.171955

14.821121 32 0.161087
14.901875 32 0.150498
14.979968 32 0.140198
15.055370 32 0.130196
15.128052 32 0.120502
15.197986 32 0.111126
15.265145 32 0.102075
15.329504 32 0.093360
15.391036 32 0.084988
15.449719 32 0.076967
15.505531 32 0.069306
15.558448 32 0.062013
15.608452 32 0.055094
15.655523 32 0.048558
15.699642 32 0.042410
15.740793 32 0.036657
15.778959 32 0.031305
15.814127 32 0.026359
15.846282 32 0.021826
15.875413 32 0.017710
15.901507 32 0.014015
15.924555 32 0.010745
15.944548 32 0.007903
15.961478 32 0.005494
15.975339 32 0.003519
15.986125 32 0.001981
15.993832 32 0.000881
15.998458 32 0.000220
16.000000 32 0.000000
12 1
161 2
0.000000 32 0.000000
0.001542 32 -0.027865
0.006168 32 -0.055494
0.013875 32 -0.082883
0.024661 32 -0.110027
0.038522 32 -0.136923
0.055452 32 -0.163563
0.075445 32 -0.189942
0.098493 32 -0.216053
0.124587 32 -0.241889
0.153718 32 -0.267440
0.185873 32 -0.292700
0.221041 32 -0.317658
0.259207 32 -0.342306
0.300358 32 -0.366632
0.344477 32 -0.390628
0.391548 32 -0.414281
0.441552 32 -0.437581
0.494469 32 -0.460516
0.550281 32 -0.483075
0.608964 32 -0.505246
0.670496 32 -0.527017
0.734855 32 -0.548375
0.802014 32 -0.569308
0.871948 32 -0.589805
0.944630 32 -0.609852
1.020032 32 -0.629438
1.098125 32 -0.648550
1.178879 32 -0.667177
1.262262 32 -0.685306
1.348243 32 -0.702927
1.436788 32 -0.720029
1.527864 32 -0.736599
1.621435 32 -0.752628
1.717465 32 -0.768107
1.815916 32 -0.783024
1.916752 32 -0.797372
2.019933 32 -0.811141
2.125420 32 -0.824323

2.233171 32 -0.836912
2.343146 32 -0.848899
2.455301 32 -0.860280
2.569594 32 -0.871048
2.685980 32 -0.881199
2.804416 32 -0.890728
2.924854 32 -0.899632
3.047248 32 -0.907908
3.171552 32 -0.915554
3.297718 32 -0.922570
3.425696 32 -0.928953
3.555438 32 -0.934706
3.686893 32 -0.939828
3.820011 32 -0.944321
3.954741 32 -0.948188
4.091030 32 -0.951432
4.228826 32 -0.954057
4.368076 32 -0.956067
4.508726 32 -0.957468
4.650722 32 -0.958266
4.794009 32 -0.958466
4.938533 32 -0.958077
5.084236 32 -0.957106
5.231064 32 -0.955562
5.378959 32 -0.953453
5.527864 32 -0.950789
5.677723 32 -0.947580
5.828476 32 -0.943836
5.980067 32 -0.939569
6.132437 32 -0.934789
6.285527 32 -0.929508
6.439277 32 -0.923739
6.593630 32 -0.917493
6.748524 32 -0.910783
6.903901 32 -0.903623
7.059701 32 -0.896025
7.215863 32 -0.888002
7.372327 32 -0.879569
7.529034 32 -0.870739
7.685921 32 -0.861525
7.842930 32 -0.851942
8.000000 32 -0.842004
8.157070 32 -0.831724
8.314079 32 -0.821117
8.470966 32 -0.810197
8.627673 32 -0.798978
8.784137 32 -0.787473
8.940299 32 -0.775697
9.096099 32 -0.763664
9.251476 32 -0.751388
9.406370 32 -0.738882
9.560723 32 -0.726159
9.714473 32 -0.713235
9.867563 32 -0.700121
10.019933 32 -0.686832
10.171524 32 -0.673381
10.322277 32 -0.659780
10.472136 32 -0.646042
10.621041 32 -0.632181
10.768936 32 -0.618209
10.915764 32 -0.604139
11.061467 32 -0.589983
11.205991 32 -0.575753
11.349278 32 -0.561462
11.491274 32 -0.547121
11.631924 32 -0.532743
11.771174 32 -0.518340
11.908970 32 -0.503922
12.045259 32 -0.489503
12.179989 32 -0.475093

12.313107 32 -0.460704
12.444562 32 -0.446347
12.574304 32 -0.432034
12.702282 32 -0.417776
12.828448 32 -0.403585
12.952752 32 -0.389470
13.075146 32 -0.375445
13.195584 32 -0.361518
13.314020 32 -0.347703
13.430406 32 -0.334009
13.544699 32 -0.320447
13.656854 32 -0.307029
13.766829 32 -0.293765
13.874580 32 -0.280666
13.980067 32 -0.267743
14.083248 32 -0.255006
14.184804 32 -0.242466
14.282535 32 -0.230134
14.378565 32 -0.218021
14.472136 32 -0.206136
14.563212 32 -0.194489
14.651757 32 -0.183092
14.737738 32 -0.171955
14.821121 32 -0.161087
14.901875 32 -0.150498
14.979968 32 -0.140198
15.055370 32 -0.130196
15.128052 32 -0.120502
15.197986 32 -0.111126
15.265145 32 -0.102075
15.329504 32 -0.093360
15.391036 32 -0.084988
15.449719 32 -0.076967
15.505531 32 -0.069306
15.558448 32 -0.062013
15.608452 32 -0.055094
15.655523 32 -0.048558
15.699642 32 -0.042410
15.740793 32 -0.036657
15.778959 32 -0.031305
15.814127 32 -0.026359
15.846282 32 -0.021826
15.875413 32 -0.017710
15.901507 32 -0.014015
15.924555 32 -0.010745
15.944548 32 -0.007903
15.961478 32 -0.005494
15.975339 32 -0.003519
15.986125 32 -0.001981
15.993832 32 -0.000881
15.998458 32 -0.000220
16.000000 32 0.000000
0.000000 24 0.000000
0.001542 24 -0.027865
0.006168 24 -0.055494
0.013875 24 -0.082883
0.024661 24 -0.110027
0.038522 24 -0.136923
0.055452 24 -0.163563
0.075445 24 -0.189942
0.098493 24 -0.216053
0.124587 24 -0.241889
0.153718 24 -0.267440
0.185873 24 -0.292700
0.221041 24 -0.317658
0.259207 24 -0.342306
0.300358 24 -0.366632
0.344477 24 -0.390628
0.391548 24 -0.414281
0.441552 24 -0.437581

0.494469 24 -0.460516
0.550281 24 -0.483075
0.608964 24 -0.505246
0.670496 24 -0.527017
0.734855 24 -0.548375
0.802014 24 -0.569308
0.871948 24 -0.589805
0.944630 24 -0.609852
1.020032 24 -0.629438
1.098125 24 -0.648550
1.178879 24 -0.667177
1.262262 24 -0.685306
1.348243 24 -0.702927
1.436788 24 -0.720029
1.527864 24 -0.736599
1.621435 24 -0.752628
1.717465 24 -0.768107
1.815916 24 -0.783024
1.916752 24 -0.797372
2.019933 24 -0.811141
2.125420 24 -0.824323
2.233171 24 -0.836912
2.343146 24 -0.848899
2.455301 24 -0.860280
2.569594 24 -0.871048
2.685980 24 -0.881199
2.804416 24 -0.890728
2.924854 24 -0.899632
3.047248 24 -0.907908
3.171552 24 -0.915554
3.297718 24 -0.922570
3.425696 24 -0.928953
3.555438 24 -0.934706
3.686893 24 -0.939828
3.820011 24 -0.944321
3.954741 24 -0.948188
4.091030 24 -0.951432
4.228826 24 -0.954057
4.368076 24 -0.956067
4.508726 24 -0.957468
4.650722 24 -0.958266
4.794009 24 -0.958466
4.938533 24 -0.958077
5.084236 24 -0.957106
5.231064 24 -0.955562
5.378959 24 -0.953453
5.527864 24 -0.950789
5.677723 24 -0.947580
5.828476 24 -0.943836
5.980067 24 -0.939569
6.132437 24 -0.934789
6.285527 24 -0.929508
6.439277 24 -0.923739
6.593630 24 -0.917493
6.748524 24 -0.910783
6.903901 24 -0.903623
7.059701 24 -0.896025
7.215863 24 -0.888002
7.372327 24 -0.879569
7.529034 24 -0.870739
7.685921 24 -0.861525
7.842930 24 -0.851942
8.000000 24 -0.842004
8.157070 24 -0.831724
8.314079 24 -0.821117
8.470966 24 -0.810197
8.627673 24 -0.798978
8.784137 24 -0.787473
8.940299 24 -0.775697
9.096099 24 -0.763664

9.251476 24 -0.751388
9.406370 24 -0.738882
9.560723 24 -0.726159
9.714473 24 -0.713235
9.867563 24 -0.700121
10.019933 24 -0.686832
10.171524 24 -0.673381
10.322277 24 -0.659780
10.472136 24 -0.646042
10.621041 24 -0.632181
10.768936 24 -0.618209
10.915764 24 -0.604139
11.061467 24 -0.589983
11.205991 24 -0.575753
11.349278 24 -0.561462
11.491274 24 -0.547121
11.631924 24 -0.532743
11.771174 24 -0.518340
11.908970 24 -0.503922
12.045259 24 -0.489503
12.179989 24 -0.475093
12.313107 24 -0.460704
12.444562 24 -0.446347
12.574304 24 -0.432034
12.702282 24 -0.417776
12.828448 24 -0.403585
12.952752 24 -0.389470
13.075146 24 -0.375445
13.195584 24 -0.361518
13.314020 24 -0.347703
13.430406 24 -0.334009
13.544699 24 -0.320447
13.656854 24 -0.307029
13.766829 24 -0.293765
13.874580 24 -0.280666
13.980067 24 -0.267743
14.083248 24 -0.255006
14.184084 24 -0.242466
14.282535 24 -0.230134
14.378565 24 -0.218021
14.472136 24 -0.206136
14.563212 24 -0.194489
14.651757 24 -0.183092
14.737738 24 -0.171955
14.821121 24 -0.161087
14.901875 24 -0.150498
14.979968 24 -0.140198
15.055370 24 -0.130196
15.128052 24 -0.120502
15.197986 24 -0.111126
15.265145 24 -0.102075
15.329504 24 -0.093360
15.391036 24 -0.084988
15.449719 24 -0.076967
15.505531 24 -0.069306
15.558448 24 -0.062013
15.608452 24 -0.055094
15.655523 24 -0.048558
15.699642 24 -0.042410
15.740793 24 -0.036657
15.778959 24 -0.031305
15.814127 24 -0.026359
15.846282 24 -0.021826
15.875413 24 -0.017710
15.901507 24 -0.014015
15.924555 24 -0.010745
15.944548 24 -0.007903
15.961478 24 -0.005494
15.975339 24 -0.003519
15.986125 24 -0.001981

15.993832 24 -0.000881
15.998458 24 -0.000220
16.000000 24 0.000000
13 1
55 2
12.000000 14.4 0.494309
12.045259 14.4 0.489503
12.179989 14.4 0.475093
12.313107 14.4 0.460704
12.444562 14.4 0.446347
12.574304 14.4 0.432034
12.702282 14.4 0.417776
12.828448 14.4 0.403585
12.952752 14.4 0.389470
13.075146 14.4 0.375445
13.195584 14.4 0.361518
13.314020 14.4 0.347703
13.430406 14.4 0.334009
13.544699 14.4 0.320447
13.656854 14.4 0.307029
13.766829 14.4 0.293765
13.874580 14.4 0.280666
13.980067 14.4 0.267743
14.083248 14.4 0.255006
14.184084 14.4 0.242466
14.282535 14.4 0.230134
14.378565 14.4 0.218021
14.472136 14.4 0.206136
14.563212 14.4 0.194489
14.651757 14.4 0.183092
14.737738 14.4 0.171955
14.821121 14.4 0.161087
14.901875 14.4 0.150498
14.979968 14.4 0.140198
15.055370 14.4 0.130196
15.128052 14.4 0.120502
15.197986 14.4 0.111126
15.265145 14.4 0.102075
15.329504 14.4 0.093360
15.391036 14.4 0.084988
15.449719 14.4 0.076967
15.505531 14.4 0.069306
15.558448 14.4 0.062013
15.608452 14.4 0.055094
15.655523 14.4 0.048558
15.699642 14.4 0.042410
15.740793 14.4 0.036657
15.778959 14.4 0.031305
15.814127 14.4 0.026359
15.846282 14.4 0.021826
15.875413 14.4 0.017710
15.901507 14.4 0.014015
15.924555 14.4 0.010745
15.944548 14.4 0.007903
15.961478 14.4 0.005494
15.975339 14.4 0.003519
15.986125 14.4 0.001981
15.993832 14.4 0.000881
15.998458 14.4 0.000220
16.000000 14.4 0.000000
12.000000 24 0.494309
12.045259 24 0.489503
12.179989 24 0.475093
12.313107 24 -0.460704
12.444562 24 -0.446347
12.574304 24 -0.432034
12.702282 24 -0.417776
12.828448 24 -0.403585
12.952752 24 -0.389470
13.075146 24 -0.375445
13.195584 24 -0.361518
13.314020 24 -0.347703
13.430406 24 -0.334009
13.544699 24 -0.320447
13.656854 24 -0.307029
13.766829 24 -0.293765
13.874580 24 -0.280666
13.980067 24 -0.267743
14.083248 24 -0.255006
14.184084 24 -0.242466
14.282535 24 -0.230134
14.378565 24 -0.218021
14.472136 24 -0.206136

13.195584 24 0.361518
13.314020 24 0.347703
13.430406 24 0.334009
13.544699 24 0.320447
13.656854 24 0.307029
13.766829 24 0.293765
13.874580 24 0.280666
13.980067 24 0.267743
14.083248 24 0.255006
14.184084 24 0.242466
14.282535 24 0.230134
14.378565 24 0.218021
14.472136 24 0.206136
14.563212 24 0.194489
14.651757 24 0.183092
14.737738 24 0.171955
14.821121 24 0.161087
14.901875 24 0.150498
14.979968 24 0.140198
15.055370 24 0.130196
15.128052 24 0.120502
15.197986 24 0.111126
15.265145 24 0.102075
15.329504 24 0.093360
15.391036 24 0.084988
15.449719 24 0.076967
15.505531 24 0.069306
15.558448 24 0.062013
15.608452 24 0.055094
15.655523 24 0.048558
15.699642 24 0.042410
15.740793 24 0.036657
15.778959 24 0.031305
15.814127 24 0.026359
15.846282 24 0.021826
15.875413 24 0.017710
15.901507 24 0.014015
15.924555 24 0.010745
15.944548 24 0.007903
15.961478 24 0.005494
15.975339 24 0.003519
15.986125 24 0.001981
16.000000 24 0.000000
14 1
55 2
12.000000 24 -0.494309
12.045259 24 -0.489503
12.179989 24 -0.475093
12.313107 24 -0.460704
12.444562 24 -0.446347
12.574304 24 -0.432034
12.702282 24 -0.417776
12.828448 24 -0.403585
12.952752 24 -0.389470
13.075146 24 -0.375445
13.195584 24 -0.361518
13.314020 24 -0.347703
13.430406 24 -0.334009
13.544699 24 -0.320447
13.656854 24 -0.307029
13.766829 24 -0.293765
13.874580 24 -0.280666
13.980067 24 -0.267743
14.083248 24 -0.255006
14.184084 24 -0.242466
14.282535 24 -0.230134
14.378565 24 -0.218021
14.472136 24 -0.206136

14.563212 24 -0.194489
 14.651757 24 -0.183092
 14.737738 24 -0.171955
 14.821121 24 -0.161087
 14.901875 24 -0.150498
 14.979968 24 -0.140198
 15.055370 24 -0.130196
 15.128052 24 -0.120502
 15.197986 24 -0.111126
 15.265145 24 -0.102075
 15.329504 24 -0.093360
 15.391036 24 -0.084988
 15.449719 24 -0.076967
 15.505531 24 -0.069306
 15.558448 24 -0.062013
 15.608452 24 -0.055094
 15.655523 24 -0.048558
 15.699642 24 -0.042410
 15.740793 24 -0.036657
 15.778959 24 -0.031305
 15.814127 24 -0.026359
 15.846282 24 -0.021826
 15.875413 24 -0.017710
 15.901507 24 -0.014015
 15.924555 24 -0.010745
 15.944548 24 -0.007903
 15.961478 24 -0.005494
 15.975339 24 -0.003519
 15.986125 24 -0.001981
 15.993832 24 -0.000881
 15.998458 24 -0.000220
 16.000000 24 0.000000
 12.000000 14.4 -0.494309
 12.045259 14.4 -0.489503
 12.179989 14.4 -0.475093
 12.313107 14.4 -0.460704
 12.444562 14.4 -0.446347
 12.574304 14.4 -0.432034
 12.702282 14.4 -0.417776
 12.828448 14.4 -0.403585
 12.952752 14.4 -0.389470
 13.075146 14.4 -0.375445
 13.195584 14.4 -0.361518
 13.314020 14.4 -0.347703
 13.430406 14.4 -0.334009
 13.544699 14.4 -0.320447
 13.656854 14.4 -0.307029
 13.766829 14.4 -0.293765
 13.874580 14.4 -0.280666
 13.980067 14.4 -0.267743
 14.083248 14.4 -0.255006
 14.184084 14.4 -0.242466
 14.282535 14.4 -0.230134
 14.378565 14.4 -0.218021
 14.472136 14.4 -0.206136
 14.563212 14.4 -0.194489
 14.651757 14.4 -0.183092
 14.737738 14.4 -0.171955
 14.821121 14.4 -0.161087
 14.901875 14.4 -0.150498
 14.979968 14.4 -0.140198
 15.055370 14.4 -0.130196
 15.128052 14.4 -0.120502
 15.197986 14.4 -0.111126
 15.265145 14.4 -0.102075
 15.329504 14.4 -0.093360
 15.391036 14.4 -0.084988
 15.449719 14.4 -0.076967
 15.505531 14.4 -0.069306
 15.558448 14.4 -0.062013

15.608452 14.4 -0.055094
 15.655523 14.4 -0.048558
 15.699642 14.4 -0.042410
 15.740793 14.4 -0.036657
 15.778959 14.4 -0.031305
 15.814127 14.4 -0.026359
 15.846282 14.4 -0.021826
 15.875413 14.4 -0.017710
 15.901507 14.4 -0.014015
 15.924555 14.4 -0.010745
 15.944548 14.4 -0.007903
 15.961478 14.4 -0.005494
 15.975339 14.4 -0.003519
 15.986125 14.4 -0.001981
 15.993832 14.4 -0.000881
 15.998458 14.4 -0.000220
 16.000000 14.4 0.000000
 15 1
 161 15
 0.000000 32 0.000000
 0.001542 32 -0.027865
 0.006168 32 -0.055494
 0.013875 32 -0.082883
 0.024661 32 -0.110027
 0.038522 32 -0.136923
 0.05452 32 -0.163563
 0.075445 32 -0.189942
 0.098493 32 -0.216053
 0.124587 32 -0.241889
 0.153718 32 -0.267440
 0.185873 32 -0.292700
 0.221041 32 -0.317658
 0.259207 32 -0.342306
 0.300358 32 -0.366632
 0.344477 32 -0.390628
 0.391548 32 -0.414281
 0.441552 32 -0.437581
 0.494469 32 -0.460516
 0.550281 32 -0.483075
 0.608964 32 -0.505246
 0.670496 32 -0.527017
 0.734855 32 -0.548375
 0.802014 32 -0.569308
 0.871948 32 -0.589805
 0.944630 32 -0.609852
 1.020032 32 -0.629438
 1.098125 32 -0.648550
 1.178879 32 -0.667177
 1.262262 32 -0.685306
 1.348243 32 -0.702927
 1.436788 32 -0.720029
 1.527864 32 -0.736599
 1.621435 32 -0.752628
 1.717465 32 -0.768107
 1.815916 32 -0.783024
 1.916752 32 -0.797372
 2.019933 32 -0.811141
 2.125420 32 -0.824323
 2.233171 32 -0.836912
 2.343146 32 -0.848899
 2.455301 32 -0.860280
 2.569594 32 -0.871048
 2.685980 32 -0.881199
 2.804416 32 -0.890728
 2.924854 32 -0.899632
 3.047248 32 -0.907908
 3.171552 32 -0.915554
 3.297718 32 -0.922570
 3.425696 32 -0.928953
 3.555438 32 -0.934706

3.686893 32 -0.939828
 3.820011 32 -0.944321
 3.954741 32 -0.948188
 4.091030 32 -0.951432
 4.228826 32 -0.954057
 4.368076 32 -0.956067
 4.508726 32 -0.957468
 4.650722 32 -0.958266
 4.794009 32 -0.958466
 4.938533 32 -0.958077
 5.084236 32 -0.957106
 5.231064 32 -0.955562
 5.378959 32 -0.953453
 5.527864 32 -0.950789
 5.677723 32 -0.947580
 5.828476 32 -0.943836
 5.980067 32 -0.939569
 6.132437 32 -0.934789
 6.285527 32 -0.929508
 6.439277 32 -0.923739
 6.593630 32 -0.917493
 6.748524 32 -0.910783
 6.903901 32 -0.903623
 7.059701 32 -0.896025
 7.215863 32 -0.888002
 7.372327 32 -0.879569
 7.529034 32 -0.870739
 7.685921 32 -0.861525
 7.842930 32 -0.851942
 8.000000 32 -0.842004
 8.157070 32 -0.831724
 8.314079 32 -0.821117
 8.470966 32 -0.810197
 8.627673 32 -0.798978
 8.784137 32 -0.787473
 8.940299 32 -0.775697
 9.096099 32 -0.763664
 9.251476 32 -0.751388
 9.406370 32 -0.738882
 9.560723 32 -0.726159
 9.714473 32 -0.713235
 9.867563 32 -0.700121
 10.019933 32 -0.686832
 10.171524 32 -0.673381
 10.322277 32 -0.659780
 10.472136 32 -0.646042
 10.621041 32 -0.632181
 10.768936 32 -0.618209
 10.915764 32 -0.604139
 11.061467 32 -0.589983
 11.205991 32 -0.575753
 11.349278 32 -0.561462
 11.491274 32 -0.547121
 11.631924 32 -0.532743
 11.771174 32 -0.518340
 11.908970 32 -0.503922
 12.045259 32 -0.489503
 12.179989 32 -0.475093
 12.313107 32 -0.460704
 12.444562 32 -0.446347
 12.574304 32 -0.432034
 12.702282 32 -0.417776
 12.828448 32 -0.403585
 12.952752 32 -0.389470
 13.075146 32 -0.375445
 13.195584 32 -0.361518
 13.314020 32 -0.347703
 13.430406 32 -0.334009
 13.544699 32 -0.320447
 13.656854 32 -0.307029

13.766829 32 -0.293765
13.874580 32 -0.280666
13.980067 32 -0.267743
14.083248 32 -0.255006
14.184084 32 -0.242466
14.282535 32 -0.230134
14.378565 32 -0.218021
14.472136 32 -0.206136
14.563212 32 -0.194489
14.651757 32 -0.183092
14.737738 32 -0.171955
14.821121 32 -0.161087
14.901875 32 -0.150498
14.979968 32 -0.140198
15.055370 32 -0.130196
15.128052 32 -0.120502
15.197986 32 -0.111126
15.265145 32 -0.102075
15.329504 32 -0.093360
15.391036 32 -0.084988
15.449719 32 -0.076967
15.505531 32 -0.069306
15.558448 32 -0.062013
15.608452 32 -0.055094
15.655523 32 -0.048558
15.699642 32 -0.042410
15.740793 32 -0.036657
15.778959 32 -0.031305
15.814127 32 -0.026359
15.846282 32 -0.021826
15.875413 32 -0.017710
15.901507 32 -0.014015
15.924555 32 -0.010745
15.944548 32 -0.007903
15.961478 32 -0.005494
15.975339 32 -0.003519
15.986125 32 -0.001981
15.993832 32 -0.000881
15.998458 32 -0.000220
16.000000 32 0.000000
0.000000 32.000000 0.000000
0.001542 32.006201 -0.027166
0.006168 32.012349 -0.054103
0.013875 32.018443 -0.080805
0.024661 32.024483 -0.107269
0.038522 32.030468 -0.133490
0.055452 32.036396 -0.159462
0.075445 32.042266 -0.185180
0.098493 32.048076 -0.210636
0.124587 32.053825 -0.235824
0.153718 32.059511 -0.260735
0.185873 32.065132 -0.285361
0.221041 32.070686 -0.309694
0.259207 32.076170 -0.333723
0.300358 32.081583 -0.357440
0.344477 32.086923 -0.380834
0.391548 32.092186 -0.403894
0.441552 32.097371 -0.426610
0.494469 32.102475 -0.448970
0.550281 32.107494 -0.470964
0.608964 32.112428 -0.492579
0.670496 32.117272 -0.513803
0.734855 32.122025 -0.534626
0.802014 32.126683 -0.555035
0.871948 32.131244 -0.575017
0.944630 32.135705 -0.594562
1.020032 32.140063 -0.613656
1.098125 32.144316 -0.632290
1.178879 32.148461 -0.650449
1.262262 32.152495 -0.668124

1.348243 32.156416 -0.685304
1.436788 32.160221 -0.701976
1.527864 32.163909 -0.718131
1.621435 32.167476 -0.733759
1.717465 32.170920 -0.748849
1.815916 32.174239 -0.763392
1.916752 32.177432 -0.777380
2.019933 32.180496 -0.790804
2.125420 32.183429 -0.803656
2.233171 32.186230 -0.815929
2.343146 32.188898 -0.827616
2.455301 32.191430 -0.838711
2.569594 32.193826 -0.849209
2.685980 32.196085 -0.859105
2.804416 32.198206 -0.868395
2.924854 32.200187 -0.877076
3.047248 32.202029 -0.885145
3.171552 32.203730 -0.892599
3.297718 32.205291 -0.899439
3.425696 32.206712 -0.905663
3.555438 32.207992 -0.911271
3.686893 32.209131 -0.916264
3.820011 32.210131 -0.920645
3.954741 32.210992 -0.924415
4.091030 32.211714 -0.927578
4.228826 32.212298 -0.930137
4.368076 32.212745 -0.932097
4.508726 32.213057 -0.933463
4.650722 32.213234 -0.934240
4.794009 32.213279 -0.934436
4.938533 32.213192 -0.934056
5.084236 32.212976 -0.933110
5.231064 32.212633 -0.931604
5.378959 32.212163 -0.929548
5.527864 32.211570 -0.926951
5.677723 32.210856 -0.923822
5.828476 32.210023 -0.920172
5.980067 32.209074 -0.916012
6.132437 32.208010 -0.911352
6.285527 32.206835 -0.906203
6.439277 32.205551 -0.900579
6.593630 32.204161 -0.894489
6.748524 32.202668 -0.887948
6.903901 32.201075 -0.880967
7.059701 32.199384 -0.873560
7.215863 32.197599 -0.865738
7.372327 32.195723 -0.857517
7.529034 32.193758 -0.848908
7.685921 32.191707 -0.839925
7.842930 32.189575 -0.830582
8.000000 32.187364 -0.820893
8.157070 32.185076 -0.810871
8.314079 32.182716 -0.800530
8.470966 32.180286 -0.789884
8.627673 32.177789 -0.778946
8.784137 32.175229 -0.767729
8.940299 32.172609 -0.756249
9.096099 32.169931 -0.744517
9.251476 32.167199 -0.732549
9.406370 32.164417 -0.720356
9.560723 32.161586 -0.707953
9.714473 32.158710 -0.695353
9.867563 32.155792 -0.682568
10.019933 32.152835 -0.669612
10.171524 32.149841 -0.656498
10.322277 32.146815 -0.643238
10.472136 32.143758 -0.629845
10.621041 32.140674 -0.616331
10.768936 32.137565 -0.602710
10.915764 32.134434 -0.588992

11.061467 32.131284 -0.575191
11.205991 32.128117 -0.561318
11.349278 32.124937 -0.547385
11.491274 32.121746 -0.533404
11.631924 32.118547 -0.519386
11.771174 32.115341 -0.505344
11.908970 32.112133 -0.491288
12.045259 32.108925 -0.477230
12.179989 32.105718 -0.463181
12.313107 32.102516 -0.449153
12.444562 32.099322 -0.435157
12.574304 32.096137 -0.421202
12.702282 32.092964 -0.407302
12.828448 32.089806 -0.393466
12.952752 32.086665 -0.379706
13.075146 32.083544 -0.366031
13.195584 32.080445 -0.352454
13.314020 32.077371 -0.338985
13.430406 32.074324 -0.325634
13.544699 32.071306 -0.312413
13.656854 32.068320 -0.299331
13.766829 32.065369 -0.286399
13.874580 32.062454 -0.273629
13.980067 32.059578 -0.261030
14.083248 32.056744 -0.248612
14.184084 32.053954 -0.236387
14.282535 32.051210 -0.224364
14.378565 32.048514 -0.212554
14.472136 32.045869 -0.200967
14.563212 32.043278 -0.189613
14.651757 32.040742 -0.178502
14.737738 32.038264 -0.167644
14.821121 32.035845 -0.157048
14.901875 32.033489 -0.146724
14.979968 32.031197 -0.136683
15.055370 32.028971 -0.126932
15.128052 32.026814 -0.117481
15.197986 32.024728 -0.108340
15.265145 32.022714 -0.099516
15.329504 32.020774 -0.091019
15.391036 32.018912 -0.082857
15.449719 32.017127 -0.075037
15.505531 32.015422 -0.067569
15.558448 32.013799 -0.060458
15.608452 32.012260 -0.053713
15.655523 32.010805 -0.047340
15.699642 32.009437 -0.041346
15.740793 32.008157 -0.035737
15.778959 32.006966 -0.030520
15.814127 32.005866 -0.025699
15.846282 32.004857 -0.021279
15.875413 32.003941 -0.017266
15.901507 32.003119 -0.013663
15.924555 32.002391 -0.010475
15.944548 32.001759 -0.007705
15.961478 32.001223 -0.005356
15.975339 32.000783 -0.003431
15.986125 32.000441 -0.001931
15.993832 32.000196 -0.000859
15.998458 32.000049 -0.000215
16.000000 32.000000 0.000000
0 32 0
0.001542076 32.01209022 -0.025105591
0.00616771 32.02407792 -0.049998323
0.013875119 32.03596152 -0.074674868
0.02466133 32.04773912 -0.099131302
0.038522187 32.05940854 -0.123363113
0.055452344 32.07096735 -0.147365216
0.075445276 32.08241281 -0.171131958
0.098493275 32.09374194 -0.19465714

14 14 1
 15 15 1
 16 16 1
 17 17 1
 18 18 1
 19 19 1
 20 20 1
 21 21 1
 22 22 1
 23 23 1
 24 24 1
 25 25 1
 26 26 1
 27 27 1
 28 28 1
 29 29 1
 30 30 1
 31 31 1
 32 32 1
 Regions on Surfaces
 1 1 1
 6
 1 2 3 4 13 14
 2 2 1
 4
 12 11 10 9
 3 3 1
 4
 4 8 12 5
 4 4 1
 4
 6 10 7 2
 5 5 1
 4
 9 6 1 5
 6 6 1
 4
 3 7 11 8
 7 7 1
 5
 13 18 21 27 17
 8 8 1
 5
 14 17 28 24 18
 9 9 1
 4
 27 22 29 31
 10 10 1
 4
 28 31 30 25
 11 11 1
 5
 29 23 20 15 32
 12 12 1
 5
 30 32 16 20 26
 13 13 1
 4
 19 23 22 21
 14 14 1
 4
 24 25 26 19
 15 15 1
 2
 15 16

APPENDIX B-2

STARS-CFD Background Mesh Data File (*BACT.BAC*)

Background mesh — NACA 0012 w/Flap

4	1	0	9	6
1	1000	80	-1000	
	1	0	0	10
	0	1	0	10
	0	0	1	10
2	-1000	-1000	-1000	
	1	0	0	10
	0	1	0	10
	0	0	1	10
3	-1000	1000	-1000	
	1	0	0	10
	0	1	0	10
	0	0	1	10
4	8	80	1000	
	1	0	0	10
	0	1	0	10
	0	0	1	10
1	1	2	3	4

* Point Sources

* Line Sources

Leading Edge

0	0	0	.30	.50	1.00
0	32	0	.30	.50	1.00

Trailing Edge 1

16	0	0	.65	2.00	10.00
16	14.4	0	.65	2.00	10.00

Flap Trailing Edge

16	14.4	0	.65	2.00	10.00
16	24	0	.65	2.00	10.00

Trailing Edge 3

16	24	0	.65	2.00	10.00
16	32	0	.65	2.00	10.00

Airfoil Tip 1

0	32	0	.35	.50	1.00
---	----	---	-----	-----	------

4	33	0	.35	.50	1.00		
Airfoil Tip 2							
4	33	0	.35	.50	1.00		
12	32.5	0	.35	.50	1.00		
Airfoil Tip 3							
12	32.5	0	.25	.50	1.00		
16	32	0	.25	.50	1.00		
Top Beginning of Flap							
12	14.4	0.494309	.40	0.50	1.00		
12	24	0.494309	.40	0.50	1.00		
Bottom Beginning of Flap							
12	14.4	-0.494309	.40	0.50	1.00		
12	24	-0.494309	.40	0.50	1.00		
* Triangle Sources							
Airfoil Surface 1							
0	0	0	0.65	2.0	10.0		
16	0	0	0.65	2.0	10.0		
16	32	0	0.65	2.0	10.0		
Airfoil Surface 2							
16	32	0	0.65	2.0	10.0		
0	32	0	0.65	2.0	10.0		
0	0	0	0.65	2.0	10.0		
Flap Top Surface 1							
12		14.4	.494309	0.40	0.5	1.0	
12		24	.494309	0.40	0.5	1.0	
16.0		24	0	0.40	0.5	1.0	
Flap Top Surface 2							
12		14.4	.494309	0.40	0.5	1.0	
16		14.4	0	0.40	0.5	1.0	
16		24	0	0.40	0.5	1.0	
Flap Bottom Surface 1							
12		14.4	-.494309	0.40	0.5	1.0	
12		24	-.494309	0.40	0.5	1.0	
16		24	0	0.40	0.5	1.0	
Flap Bottom Surface 2							
12		14.4	-.494309	0.40	0.5	1.0	
16		14.4	0	0.40	0.5	1.0	
16		24	0	0.40	0.5	1.0	

APPENDIX B-3

STARS-CFD Boundary Condition File (*BACT.BCO*)

Boundary Condition File -- NACA 0012 "BACT" with Flap	24	4
15 32	25	0
Surface Regions	26	4
1 1	27	0
2 3	28	0
3 3	29	0
4 3	30	0
5 3	31	0
6 3	32	0
7 1		
8 1		
9 1		
10 1		
11 1		
12 1		
13 1		
14 1		
15 1		
Curve Segments		
1 0		
2 0		
3 0		
4 0		
5 0		
6 0		
7 0		
8 0		
9 0		
10 0		
11 0		
12 0		
13 4		
14 4		
15 4		
16 4		
17 0		
18 1		
19 1		
20 1		
21 4		
22 0		
23 4		

APPENDIX B-4

STARS-CFD Parameter Control File (*BACT.CONU*)

```
&control
nstep = 240,
nout = 6000,
ncycl = 40,
ncyci = 40,
nstage = 5,
cfl = 0.7,
nsmth = 2,
smofc = 0.2,
diss1 = 3.5,
diss2 = 3.5,
relax = 1.0,
mach = 0.77,
alpha = 0.0,
beta = 0.0,
restart = 1,
nlimit = 2,
lg = 1,
nite0 = 1,
nite1 = 1,
nite2 = 0,
tlr = 0.00001,
debug = .false.,
meshc = 1,
meshf = 1,
low = .false.,
cvt(1) = 1.0,
cvt(2) = 0.5,
cvt(3) = 0.0,
cvt(4) = 0.0,
wux = 0.0,
wuy = 0.0,
wuz = 1.0,
amplitude= 2.0,
freq = 1.0,
trans = .true.,
bulkvis = .false.,
pistonn_sol= .false.,
model_sol= .true.,
/
```

APPENDIX B-5

STARS-Unsteady Scalars File (*BACT.SCALARS*)

```
$ aeroelastic scalars data file
$ nr, ibc ( 0=full modes, 1=q(1) = 0.01, 2=q(nr+1)=0.01 )
  3, 2, 0.5, 10
  10, 1, 7, 8, 9, 10, 11, 12, 13, 14, 15
$ iread, iprint
  2, 1
$ dimensional parameters; mach-inf, rho-inf(slin/in^3), a-inf(in/s), gamma,   pinf
                                0.77  1.8924E-08      13165.2  1.4    0.0
$ shift factor and gravity constant
  1.0  1.0
$ flag, ffi,  ns,  ne
  2,  35.0,  5,  20
$ cfa, cfi
  1,  1
$ nterms, nsteps
  20,  2
$ na,  nb
  4,  11
```

APPENDIX B-6

Portion of STARS-Unsteady Arrays File (*BACT.ARRAYS*)

```
$ ARRAYS FILE FOR RUNNING UNSTEADY
$ nna, nela
  8814 17624
$ Frequency (hz)
  3.344
  5.207
  26.261
$ COMPLETE GENERALIZED STIFFNESS MATRIX
.223833E+03 .000000E+00 .000000E+00
.000000E+00 .109500E+02 .000000E+00
.000000E+00 .000000E+00 .109663E+04
$ COMPLETE GENERALIZED MASS MATRIX
.506670E+00 .405333E-01 .002880E+00
.123472E-04 .102350E-01 .573900E-05
.877300E-06 .573900E-05 .402803E-01
$ COMPLETE GENERALIZED DAMPING MATRIX
.298190E-01 .000000E+00 .000000E+00
.000000E+00 .669850E-03 .000000E+00
.000000E+00 .000000E+00 .000000E+00
$ AERO VECTORS
0.0000000000E+00 0.0000000000E+00 0.0000000000E+00
0.0000000000E+00 0.0000000000E+00 0.0000000000E+00
0.0000000000E+00 0.0000000000E+00 0.0000000000E+00
0.0000000000E+00 0.0000000000E+00 0.0000000000E+00
0.0000000000E+00 0.0000000000E+00 0.0000000000E+00
0.0000000000E+00 0.0000000000E+00 0.0000000000E+00
:
```